

---

**Structure, Function and Input Pathways of  
Motion-sensitive Visual Interneurons  
in *Drosophila melanogaster*.**

---

Bettina Schnell



München 2010



---

**Structure, Function and Input Pathways of  
Motion-sensitive Visual Interneurons  
in *Drosophila melanogaster*.**

---

Dissertation  
der Fakultät für Biologie  
der Ludwig-Maximilians-Universität  
München

vorgelegt von

Bettina Schnell  
aus Würzburg

München, 28. Oktober 2010

Erstgutachter

Prof. Dr. Alexander Borst

Zweitgutachter

Prof. Dr. Rainer Uhl

Tag der mündlichen Prüfung

15.12.2010





# Table of Contents

---

<b>I. Summary</b>	<b>11</b>
<b>II. Introduction</b>	<b>13</b>
1. Visually driven behavior	13
2. The correlation-type motion-detector	14
3. Structure and function of the visual system	16
4. Genetic tools	26
5. Goals and results	33
<b>III. Fluorescence Changes of Genetic Calcium Indicators and OGB-1 Correlated with Neural Activity and Calcium In Vivo and In Vitro</b>	<b>35</b>
1. Abstract	35
2. Introduction	36
3. Material and Methods	37
4. Results	46
Fig. 1	47
Fig. 2	50
Fig. 3	53
Fig. 4	55
Fig. 5	58
Fig. 6	60
Fig. 7	60
5. Discussion	61
6. Supplement	66
Fig. S1	67
Fig. S2	68
Fig. S3	69
7. Footnotes	70
8. References	71
<b>IV. Processing of Horizontal Optic Flow in Three Visual Interneurons of the <i>Drosophila</i> Brain</b>	<b>77</b>
1. Abstract	77
2. Introduction	78

3. Methods	79
4. Results	85
Fig. 1	85
Fig. 2	88
Fig. 3	90
Fig. 4	92
Fig. 5	93
Fig. 6	95
5. Discussion	96
6. Supplement	102
Supplementary Fig. 1	102
Supplementary Fig. 2	103
7. Acknowledgments	104
8. References	104
<b>V. ON- and OFF-Pathways in <i>Drosophila</i> Motion Vision</b>	<b>109</b>
1. Summary	109
2. Results and Discussion	110
Fig. 1	111
Fig. 2	113
Fig. 3	115
Fig. 4	117
Supplementary Fig.	120
4. Methods	121
5. References	124
<b>VI. Dscams affect dendritic shape, information processing and optomotor behavior in <i>Drosophila</i>.</b>	<b>127</b>
1. Summary	127
2. Introduction	127
3. Results	132
Fig. 1	133
Fig. 2	135
Fig. 3	138
Fig. 4	140
Fig. 5	144
4. Discussion	146
5. Experimental Procedures	153



6. References	159
<b>VII. Discussion</b>	<b>167</b>
1. Calcium imaging vs. electrophysiology	167
2. LPTCs and behavior	168
3. Manipulating neuronal circuits	171
4. Gap-junctions in the fly visual system	172
5. Implementation of the correlation-type motion detector	175
6. Similarities to vertebrates	177
7. LPTCs and Dscam	179
8. Outlook	180
<b>VIII. References</b>	<b>181</b>
<b>IX. Abbreviations</b>	<b>194</b>
<b>X. Curriculum Vitae</b>	<b>195</b>
<b>XI. Acknowledgments</b>	<b>197</b>



## I. Summary

Visual motion detection is of major importance for flies as they use the optic flow generated by their self-motion to control their course during flight. This so called optomotor behavior is thought to be controlled by a set of large-field motion-sensitive cells in the optic lobes called lobula plate tangential cells (LPTCs). LPTCs come in different variants and are tuned to different preferred directions. Their responses can be explained by assuming input from an array of local motion detectors of the correlation-type. In addition, they receive input from other LPTCs from both the ipsi- and the contralateral hemisphere. Response properties of LPTCs have been extensively described in large fly species. However, information about the presynaptic circuits that constitute the local motion detectors is still largely missing. Research on the fruit fly *Drosophila* promises to close this gap as it allows for combining physiological recordings from motion-sensitive cells with a genetic manipulation of the system. In that way the function of neurons too small for electrophysiological recordings can also be analyzed. Here, I provide important steps towards elucidating the cellular implementation of the correlation-type motion detector in the fly brain.

First, I tested different genetically encoded Calcium indicators (GECIs) expressed in LPTCs by stimulating the neurons with potassium chloride. These experiments revealed that GECIs are functional in LPTCs and might thus be useful for monitoring neuronal activity in the visual system.

Second, I described the response properties of HS (horizontal system) cells, a prominent subgroup of LPTCs in *Drosophila*. There are three HS cells per hemisphere, HSN, HSE and HSS. All of them are tuned to horizontal motion in a directionally selective way. I could show that their responses are indicative of correlation-type motion detectors providing input to them. In addition, they receive information from the contralateral side most likely via other LPTCs. HS cells not only have strongly overlapping dendritic trees in the lobula plate accounting for their large and overlapping receptive fields, but are also coupled electrically with each

## Summary

---

other. Extensive electrical connections can also be found to descending neurons in their output region in the central brain. This characterization of HS cells is important for two reasons: i) Their responses can be used as a read-out for the effects of manipulating the presynaptic motion detection circuitry in the fly by genetic techniques; ii) they can be correlated with behavioral reactions induced by horizontal motion to study how optomotor responses are controlled in the fly.

Third, I studied the input pathways to the LPTCs in the lamina, the first optic neuropile after the compound eye. From all lamina cells, L1 and L2 are the most prominent neurons and were previously shown to provide the major input to the motion detection circuits. By genetically restoring synaptic input to either one of the two pathways I revealed that these two types of cells indeed provide the major input to LPTCs. However, their functional specialization for light increments and light decrements, disclosed by blocking their synaptic output, could not be revealed in these experiments. As L1 and L2 turned out to be electrically coupled with each other restoring the input to only one cell type also restores the input to the other one.

Finally, I analyzed response properties of HS cells whose dendritic structure has been altered by overexpression of Dscam (Down syndrome cell adhesion molecule) during development. Dscam is a protein that comes in a large number of different isoforms and is thought to play a major role in self-recognition and thus proper dendritic and axonal branching. HS cells that misexpress a single isoform develop smaller and less overlapping dendritic trees in the lobula plate. These anatomical defects are accompanied by smaller receptive fields but otherwise normal motion responses.

All these experiments show that the combination of physiological and genetic tools is a promising approach for dissecting neural circuits and gaining new insights into information processing in the brain. Continuation of this approach will hopefully bridge the gap between neurons of the lamina and the lobula plate by revealing the local motion detectors in the intermediate neuropile, the medulla.

## II. Introduction

The fly visual system has for long fascinated many researchers, probably for two main reasons. One lies in its similarity, the other one in its difference to our own visual system. As for humans, vision is probably the most important sensory system for the fly. Visual information is essential for them to steer through the environment and perform complex, acrobatic flight maneuvers. On the other hand, just one look at their large compound eyes with the tiny underlying brain reveals that their visual system is organized quite differently from our own. Nevertheless one hopes that general principles of information processing can be revealed in the fly brain which might be common to all species relying on visual input.

Motion vision is one such fundamental task a visual system has to perform. It is not only essential for detecting moving objects that, for a fly, could be a predator or a potential mate, but also to deal with the constant motion of the surrounding world caused by one's own movements. The question of how motion is detected in the fly brain has challenged researchers since decades. However, only the recent development of physiological recording techniques in the small fruit fly together with the elaborate genetic toolset available in *Drosophila* has put a comprehensive answer within reach.

The goal of this work was to analyze the response properties of large-field motion-sensitive neurons in the fly brain and then use their responses as a read-out for the effects of genetic manipulations in the fly visual system.

The following will provide a small summary of motion detection in the fly and its underlying neuronal circuits as well as of the tools available in *Drosophila* to manipulate their function.

### **1. Visually driven behavior**

Flies rely heavily on vision to control their course during walking and flight. Out of the behavioral repertoire of the fly several basic, visually driven responses could be exploited to develop behavioral paradigms for studying properties of the underlying

neural circuits. For example, flies tend to walk or fly towards a source of light, a reaction called “positive phototaxis”. This behavior is wavelength dependent as flies exhibit e.g. a spectral preference for UV over green light (Schümperli, 1973).

In addition flies orient towards dark objects presented in their visual surround, a behavior called “object fixation” (Reichardt and Wenking, 1969; Wehner, 1972). These objects can be either stationary or move relative to the background.

Expanding stimuli can trigger two rather stereotyped behavioral reactions one being the landing response (Goodman, 1960; Borst, 1986), the other being an escape response caused by a dark looming object (Card and Dickinson, 2008).

However, the behavior studied by far the most is the optomotor response which is a reaction of flies to large-field motion (for review see Heisenberg and Wolf, 1984). It is generally assumed that flies use the optic flow, i.e the pattern of local motion vectors in their visual field, to obtain information about their self-motion. For example, if a fly rotates to the right around its vertical body axis, it would perceive the whole surround as rotating to the left. If the turn was not voluntarily initiated, the fly would react to this deviation from its course by turning to the left, thus stabilizing a straight flight path. This response can even be measured if the fly is not actually turning by presenting moving patterns to a stationary walking (Buchner, 1976) or flying fly (Fermi and Reichardt, 1963; Götz, 1964). In the latter case the readout for the intended turning response is either the produced force measured by a torque meter (Götz, 1964) or the difference in the stroke amplitude between both wings measured with a wing-beat analyzer (Götz, 1968; Götz, 1987). Both methods have been and are still being used extensively to study the dependence of this reaction on various stimulus parameters like the contrast, velocity and spatial layout of the presented pattern. By applying the analysis to mutant or transgenic flies, these paradigms can also be exploited to gain insights into the underlying neural circuits, as will be discussed later.

## **2. The correlation-type motion-detector**

Information about visual motion has to be computed by the brain from brightness changes perceived by the eye. Based on behavioral studies on the beetle *Clorophanus viridis*, a minimal algorithmic model was proposed (Hassenstein and

Reichardt, 1956; Reichardt, 1961), describing how the direction of motion could be computed by the brain (for review see Borst and Egelhaaf, 1989; Borst and Haag, 2002). This model, the correlation-type or elementary motion detector (EMD), basically relies on comparing the signals of two neighboring units after one of them has been delayed in time (see Fig. 1). The delay can be mathematically achieved by low-pass filtering the signal. This signal then has to interact in a non-linear way with the non-delayed signal of the neighboring unit, which is mathematically most easily done by a multiplication. This multiplication results in a maximal response to motion in one direction and in no or a weaker response to motion in any other direction or to a flickering stimulus. Full directional selectivity is obtained by subtracting the signals of two such detectors mirror symmetric to each other (Borst and Egelhaaf, 1990).

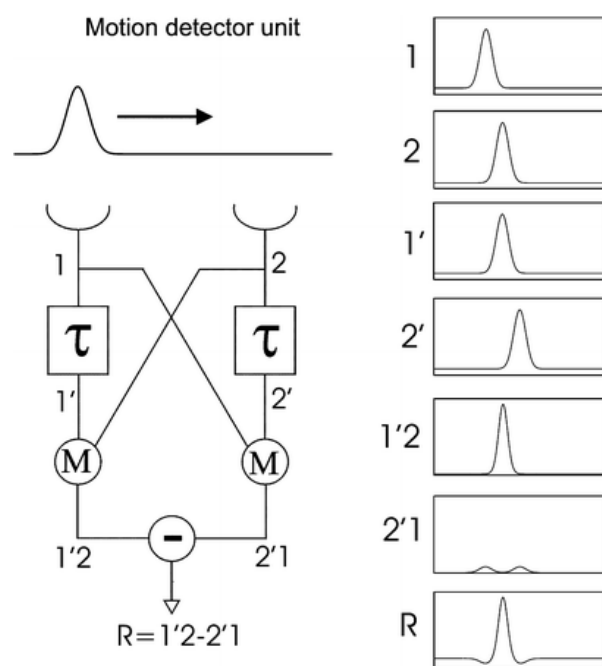


**Fig. 1: The Reichardt detector.**

According to this model, the direction of motion is detected by multiplying the signals from two neighboring receptors after one of them has been delayed in time. Doing that twice in a mirror-symmetrical way and subtracting the resulting signals from each other results in a directional-selective output signal (R).

Abundant behavioral and physiological evidence suggests that this detector is somehow implemented in the fly brain (from Borst and Haag, 2002.)

This model makes certain predictions, which are fulfilled in the optomotor response of the beetle. The major prediction of this model is that its output depends on the velocity and the spatial layout of a pattern such that it is maximal for a certain temporal frequency, i.e. the frequency with which the brightness varies at one sampling point. This condition was later also shown to be fulfilled in the optomotor

## Introduction

---

response of the fruit fly (Götz, 1964; Buchner, 1976) and the responses of large motion-sensitive cells in different fly species (for review see Borst et al., 2010).

Thus, it is generally assumed that the correlation-type motion detector is somehow implemented in the fly brain. However, the model is purely algorithmic and does not make any statement about underlying neuronal structures and mechanisms. In addition, the model by Hassenstein and Reichardt only explains how the local motion direction is computed. For course control a fly has to analyze the optic flow of large parts of the visual surround and thus has to look at the output of many such motion detectors. Whereas it is still an open question how the correlation-type motion detector is implemented in the fly brain, a lot is known about neurons involved in the latter task. These neurons are located in a part of the optic lobe, the so-called lobula plate (see Fig. 2).

### 3. Structure and function of the visual system

The visual system of *Drosophila* is composed of two compound eyes with their underlying optic lobes. In addition, there are three dorsally located ocelli and a few extraretinal photoreceptors in the so called eyelets (Yasuyama and Meinertzhagen, 1999).

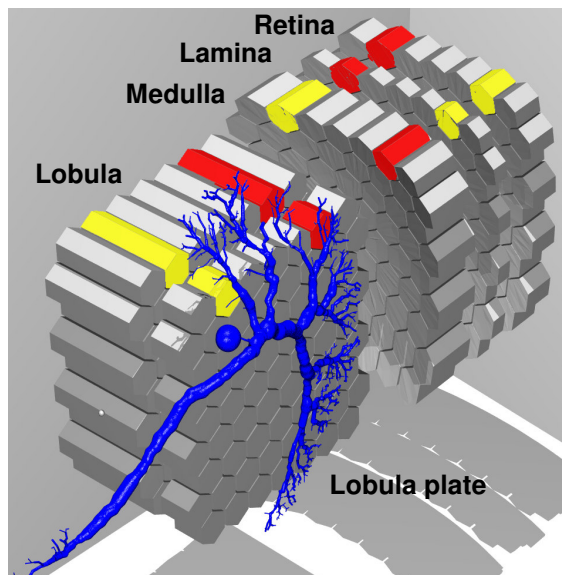


**Fig. 2: Scheme of the fly optic lobe.**

The optic lobe underlying the retina is composed of the lamina, the medulla, the lobula and the lobula plate and is organized retinotopically. This means that the spatial relationship between different columns (depicted e.g. in red and yellow) is preserved throughout the neuropile, although the whole representation gets inverted by two optic chiasmata (between lamina and medulla, and medulla and lobula plate). In the lobula plate, tangential cells (blue) integrate the information from many columns (from Borst and Haag, 2002).

The optic lobes in turn consist of three distinct neuropiles, which from distal to proximal are the lamina, the medulla and the lobula complex, the latter being further divided into the lobula and the lobula plate. Generally the optic lobe can be



viewed as a stack of retinotopically organized maps, where neighboring columns represent neighboring points in space (see Fig. 2). In addition, there are large-field tangential neurons that extend their dendrites over many such columns.

Concerning the functional involvement in motion detection the lobula plate is the best studied optic neuropile, so it will be described first.

### 3.1 Lobula plate

A distinct feature of the lobula plate is the set of large tangential cells (LPTCs) it contains (Hausen, 1984). In large fly species, like *Calliphora* and *Musca*, these cells are easily accessible for electrophysiological recordings and thus have been studied in greatest detail since the 1970s (e.g. Hengstenberg et al., 1982; Hausen, 1982; Hausen, 1976). In general LPTCs have large receptive fields and respond to motion in a directionally selective way: They are excited by motion in one and inhibited by motion in the opposite direction.

LPTCs can be divided into several subclasses, based on their preferred direction of motion (horizontal or vertical), their response mode (graded or spiking), their projection area (ipsi- or heterolateral) or their preference for either small- or large-field motion (for review see Borst and Haag, 2002). HS and VS cells are major output neurons of the lobula plate and respond to horizontal and vertical motion, respectively, with graded membrane potential changes. H1-4 and V1 neurons are heterolateral spiking neurons projecting either to the contralateral lobula plate or to its output region and confer contralateral sensitivity to other LPTCs like HS cells. CH cells, of which there are two per hemisphere in *Calliphora* (dCH and vCH), are similar to HS cells, but they are both, pre- and postsynaptic in the lobula plate. All these neurons respond strongest to large field motion. In addition, there are several types of figure detection (Fd) cells that respond preferentially to small moving objects irrespective of background motion (Egelhaaf, 1985).

LPTCs receive their input either via many columnar neurons that synapse onto their large dendritic trees, from other LPTCs or both (see Fig. 3). Detailed analyses of their receptive fields revealed that they are tuned to specific optic flow fields and thus well suited for computing information about self-motion of the fly (Krapp and Hengstenberg, 1996; Wertz et al., 2009).

## Introduction

In addition, the receptive fields of VS cells were found to be much larger than predicted by the extent of their dendritic trees, which lead to the discovery of electrical connections between neighboring VS cells (Haag and Borst, 2004; Farrow et al., 2005). These connections make responses of VS cells to naturalistic stimuli more reliable (Cuntz et al., 2007). Electrical connections were among others also found between HS and CH cells (Haag and Borst, 2005) and between VS cells and V1 (Haag and Borst, 2008) (see Fig. 3).

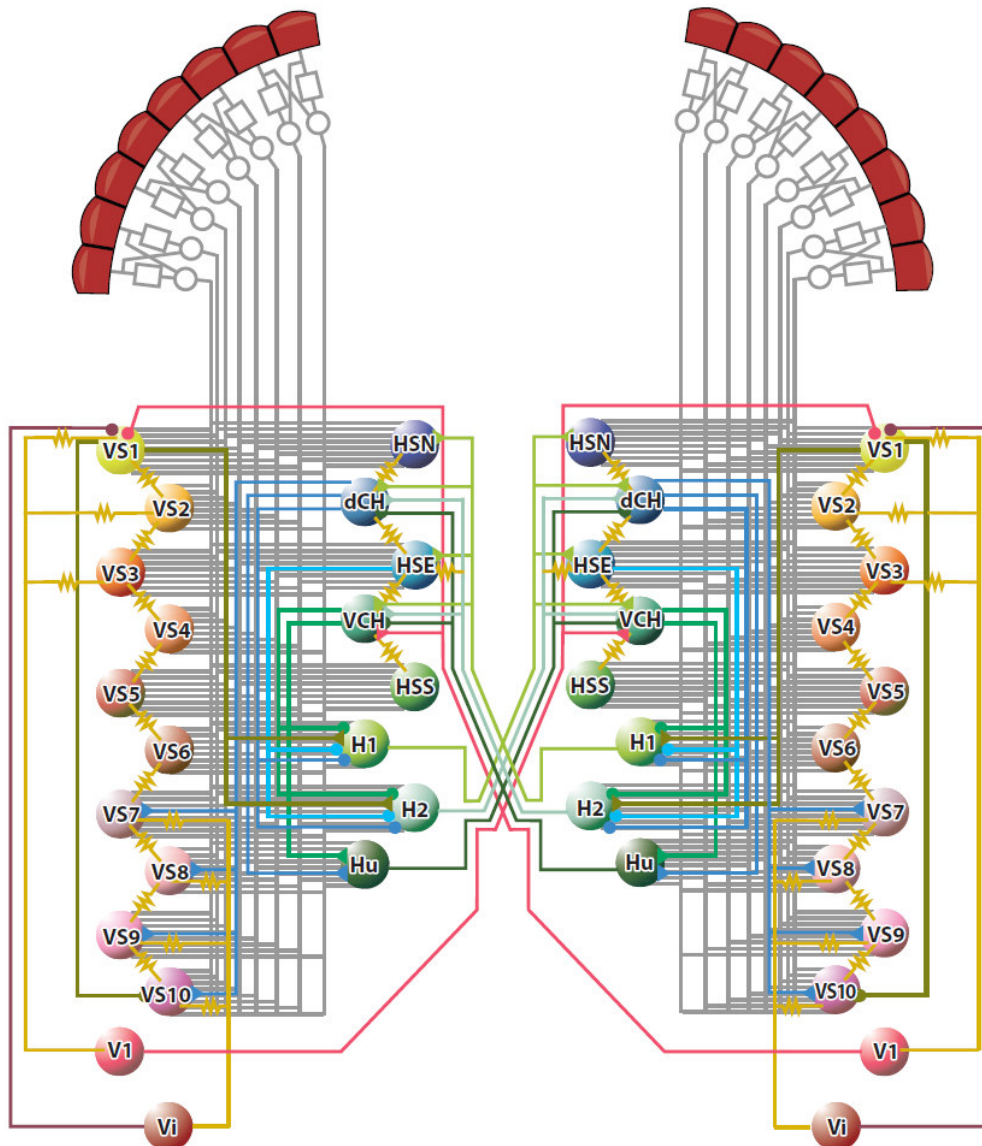


**Fig. 3: LPTC network in the lobula plate.**

Besides receiving input from columnar elementary motion detectors (depicted in grey), LPTCs form an extensive network among each other. Connections can be found between ipsi- as well as contralateral cells and are realized via electrical (indicated as yellow resistors) or chemical synapses (inhibitory synapses depicted as circles, excitatory synapses as triangles) (from Borst et al., 2010).

These findings on LPTCs are based on work done in the blowfly *Calliphora*. In *Drosophila* LPTCs were until recently only described anatomically (Heisenberg et al., 1978; Fischbach and Dittrich, 1989; Scott et al., 2002). However, the first patch clamp recordings from VS cells in the fruit fly performed in our lab revealed that they have similar response properties and connections as their counterparts in *Calliphora* (Joesch et al., 2008).

Response properties of LPTCs like the optomotor response described above are in agreement with correlation-type motion detectors providing input to them. Most likely, the subtraction stage takes place on their dendrites (Single et al. 1997) as these were shown to receive excitatory cholinergic as well as inhibitory GABAergic input (Brotz and Borst, 1996; Raghu et al., 2007; Raghu et al., 2009) (see Fig. 4). Possible input pathways will be discussed in the following.

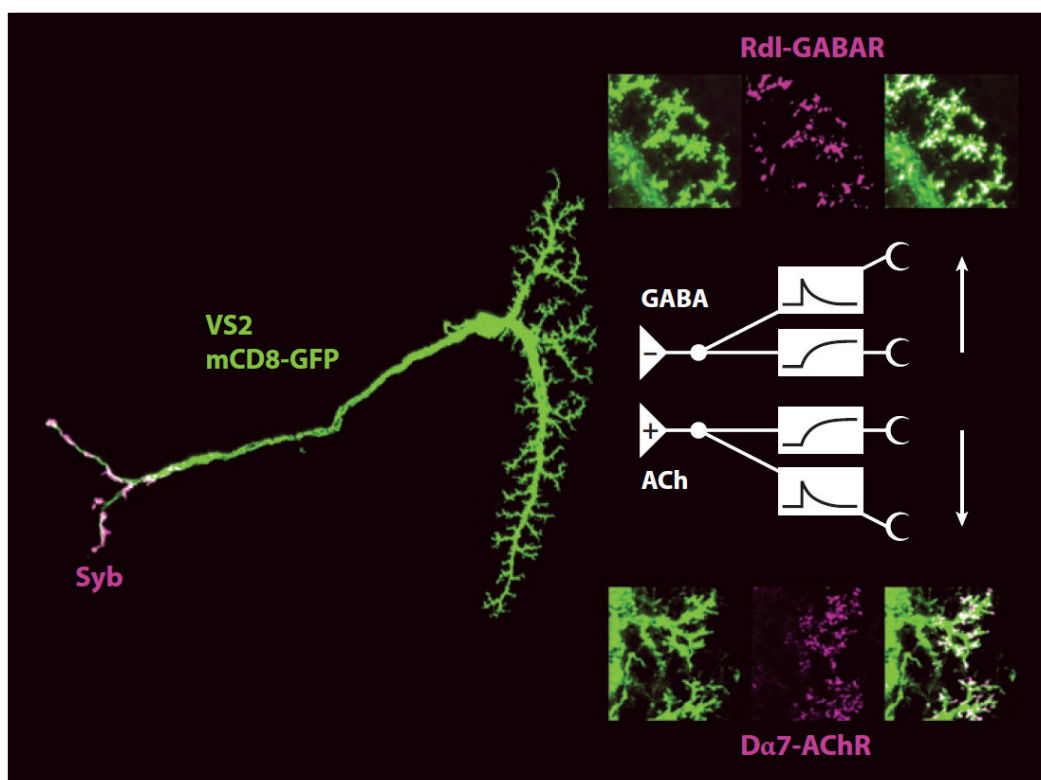


**Fig. 4: Columnar input to LPTCs.**

A VS2 cell from *Drosophila* is depicted in green with the output synapses labeled in magenta by expression of DsRed-tagged synaptobrevin. The localization of DsRed-labeled transmitter receptors (Rdl for GABA and D $\alpha$ 7 for ACh) on the dendrites (magnifications shown to the right) suggests that LPTCs receive cholinergic as well as GABAergic input. Thus, the subtraction postulated by the Reichardt detector (scheme depicted to the right) is most likely performed on the dendrites of LPTCs in the lobula plate (from Borst et al., 2010 based on Raghu et al., 2007; 2009).

### 3.2 Retina

In *Drosophila*, each compound eye is composed of about 750 ommatidia. Each of these ommatidia contains 8 microvillar photoreceptors with a rhabdomere as their light-capturing structure. In photoreceptors R1-6 Rhodopsin 1 (Rh1) is the light-absorbing pigment (O'Tousa et al., 1985), which is most sensitive in the UV and green range. R7 and R8 are arranged as a tandem in the center of the ommatidium and contain Rhodopsins with different absorption spectra and can thus mediate color vision (Cook and Desplan, 2001).

To enhance signal-to-noise ratio at low light intensities without sacrificing spatial resolution flies possess a neuronal superposition eye (Kirschfeld, 1973): Six photoreceptors R1-6 from six different ommatidia but with parallel optical axes, thus looking at the same point in space, converge onto the same postsynaptic neurons. Concomitantly, all photoreceptors of one ommatidium except for R7 and R8 have different optical axes and thus look at different points in space. A prerequisite for this to work is that the divergence angle between the rhabdomeres of one ommatidium corresponds to the interommatidial angle, which is actually the case (Kirschfeld, 1967). One prediction from this building principle is that one ommatidium should be sufficient for motion detection based on the comparison between neighboring image points. Sequentially stimulating single rhabdomeres of only one ommatidium could indeed elicit significant responses in LPTCs (Riehle and Franceschini, 1984) and even optomotor responses (Kirschfeld, 1972) in the fly.

Light responses of fly photoreceptors have been studied in detail using intracellular recordings. In contrast to vertebrate photoreceptors they depolarize upon illumination with extremely fast kinetics (Hardie, 2001) and release histamine as neurotransmitter.

Different studies have established R1-6 as major players in motion detection being both necessary and sufficient for this task (Heisenberg and Buchner, 1977; Yamaguchi et al., 2008). R7 and R8 in turn are involved in color vision and influence spectral preferences in the fly (Gao et al., 2008; Yamaguchi et al., 2010). Their axons bypass the next optic neuropile, the lamina, which is thus exclusively dedicated to the processing of achromatic stimuli.

### 3.3 Lamina

The axons of the photoreceptors R1-6 project to the lamina. On their way, they sort out according to the neuronal superposition principle described above, such that the six photoreceptors from different ommatidia looking at the same point in space terminate in the same substructure called lamina cartridge (Braitenberg, 1967). Each lamina cartridge thus represents one image pixel and is also called neuro-ommatidium.

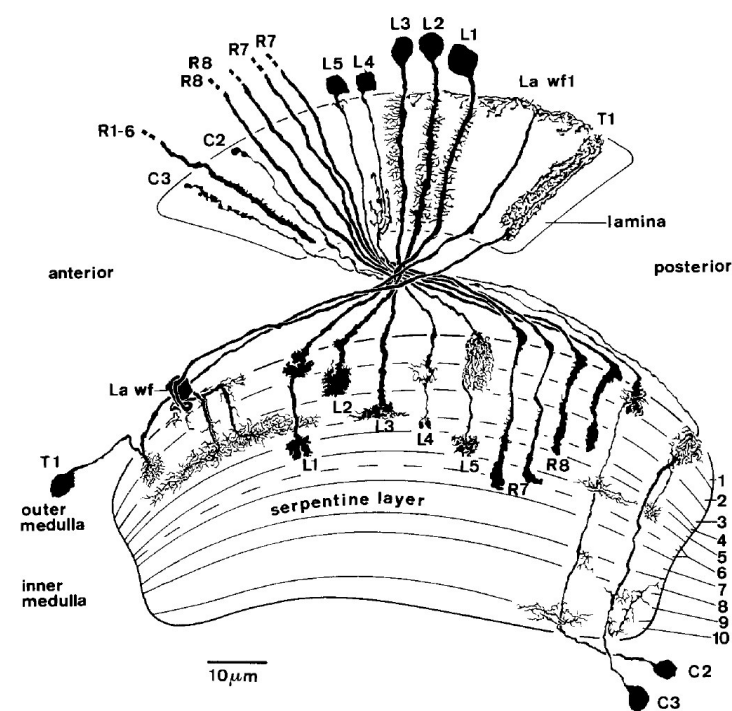


**Fig. 5: Neurons of the lamina with their terminals in the medulla.**

Each neuronal type usually occurs once per lamina cartridge and column in the medulla. Photoreceptors R1-6 make direct synaptic contact with L1, L2, L3 and amacrine cells (not shown) in the lamina and indirectly provide input to L4, L5 and T1. Anatomical reconstructions are based on Golgi stainings (from Fischbach and Dittrich, 1989).

In one cartridge, the photoreceptors make contact with several postsynaptic neurons. All types of lamina neurons (see Fig. 5) and their synaptic connections have been comprehensively described (Meinertzhagen and O'Neil, 1991). The two most prominent postsynaptic partners of R1-6 are the lamina monopolar cells L1 and L2 located in the center of the cartridge. Of all lamina cells L1 and L2 have the largest diameter and receive the most synaptic input from R1-6 on their radial dendrites (Meinertzhagen and Sorra, 2001). L2, but not L1, provides feedback synapses onto the photoreceptor terminals. From the other lamina monopolar cells L3-5, only L3 receives direct input from photoreceptor cells. L3 is located between R5 and R6 and extends its dendrites to only one side. As it receives less synaptic input from R1-6 and is thus presumably less light-sensitive, and as it projects to the same layer in the medulla as R8, it is thought to be involved in color vision (Anderson and Laughlin,

## Introduction

---

2000). L4 extends two collaterals to two neighboring cartridges located more laterally, where it synapses onto L2 and L4. In its own cartridge it makes reciprocal connections with L2. It was also reported to be rarely postsynaptic to amacrine cell processes as is L5, which otherwise does not seem to form synaptic connections in the lamina. The processes of amacrine cells, also called  $\alpha$ -fibers, intercalate between the photoreceptor terminals to which they are postsynaptic. Amacrine cells typically form a horizontal network distally to the lamina and extend processes into several cartridges. There they are presynaptic to  $\beta$ -fibers, which run adjacent to  $\alpha$ -processes between the photoreceptor axons. All  $\beta$ -fibers of one cartridge form a basket-like structure belonging to one T1-neuron.

Consequently, in the lamina the information from the photoreceptors is split into several pathways. L1, L2, L3 and the amacrine cell are directly postsynaptic to photoreceptors, whereas L4, L5 and T1 only receive indirect input. Except for the amacrine cells, all these neurons project to the next neuropile, the medulla, where they terminate in different layers. In addition, the two feedback neurons C2 and C3 project from the medulla back to the lamina. The lamina tangential cells (LamTan) with processes in several cartridges complete the set of lamina neurons.

Concerning their function, much less is known about the different types of neurons. Intracellular recordings have been performed from L1, L2 and L3 in big flies. These neurons were all shown to hyperpolarize in response to light. Since the photoreceptors depolarize in response to light, the synapses between photoreceptors and lamina monopolar cells have to invert the sign of the response. This is indeed the case, as the neurotransmitter of photoreceptor cells is histamine, which gates chloride channels in the postsynaptic neurons (Hardie, 1989). This histamine-gated chloride channel is encoded by a gene called *ort* or *hisCIA* (Witte et al., 2002; Zheng et al., 2002; Gengs et al., 2002), which is strongly expressed by L1, L2 and L3 as well as by neurons postsynaptic to R7 and R8 in the medulla. Another histamine receptor is encoded by the gene *hisCIB*, which was found to be mainly expressed in glia cells in the lamina (Pantazis et al., 2008). L1 and L2 have a resting potential of around -40mV (Hardie and Weckström, 1990) and respond to light with a strong transient hyperpolarizing peak that decays quickly to resting level or to a smaller sustained response depending on the level of light adaptation and the

intensity of the stimulus (Järvilehto and Zettler, 1973). L3 has lower resting potentials, a larger sustained response and produces a pronounced depolarizing peak at light-off (Hardie and Weckström, 1990). This depolarization was also measured in L1 and L2 in larger flies, but not in *Drosophila* so far. However, many studies did not discriminate between the different types of LMCs recorded from, so it is difficult to draw conclusions about differences in their response properties. L1 and L2 were found to have smaller receptive fields than photoreceptors (Järvilehto and Zettler, 1973) suggesting that they receive lateral inhibition. One study reported that this inhibition is more pronounced in L2 than in L1 (Laughlin and Osorio, 1989). Feedback synapses from L2 back to the photoreceptors were claimed to be involved in light adaptation in *Drosophila* (Nikolaev et al., 2009; Zheng et al., 2006).

In addition, few studies, in which extracellular recordings were obtained from the chiasm between lamina and medulla, described units with different responses to light (Arnett, 1972) like on- and off- and sustaining units. However, these responses could not be attributed to certain cell types so far.

The obvious separation of signals into different channels in the lamina has led to wide speculations about their functional role especially concerning L1 and L2. As the lamina has to provide input into the motion detection circuitry it was speculated that L1 and L2 might constitute the two arms of the correlation-type motion detector or, alternatively, feed into the two half-detectors with opposite preferred direction (Braitenberg and Hauser-Holschuh, 1972). Another study doubted that they are involved in motion detection at all (Coombe et al., 1989).

More recent studies that combined new genetic tools for blocking or rescuing specific lamina pathways with behavioral readouts in *Drosophila* provided first evidence for a functional specialization of these pathways for different behaviors (Rister et al., 2007; Katsov and Clandinin, 2008). The major conclusion was that L1 and L2 are key players in motion detection, being both necessary and sufficient for this task (Rister et al., 2007). T1 also seems to feed into the motion detection circuitry, being however of minor importance. Concerning a functional specialization of L1 and L2, the picture becomes more diffuse. One study found a specialization of L1 for back-to-front and of L2 for front-to-back motion at low contrasts and a higher sensitivity of L2 at low contrasts and low light intensities (Rister et al., 2007). The

other study claimed a different involvement of the two channels in mediating translatory and rotatory motion responses in walking flies (Katsov and Clandinin, 2008). While L3 is supposed to be involved in color-vision and L4 was speculated to play a major role in motion detection (Zhu et al., 2009), detailed knowledge about computations performed by the lamina is still largely lacking. Whereas it is obvious that one of the major tasks of the lamina is to enhance the signal-to-noise ratio by pooling the output from several photoreceptors, not much is known about how visual information is otherwise preprocessed in the lamina and about the functional role of the different lamina cell types.

### 3.4 Medulla

The second optic neuropile, the medulla, is a layered structure that can be divided in an outer and inner part separated by the serpentine layer. The lamina monopolar cells L1-5, as well as T1 send their axons through the outer optic chiasm and terminate in the outer medulla. There they can be easily discriminated by their characteristic arborizations in different layers (Fischbach and Dittrich, 1989). The terminals of L1, for example, occupy layers M1 and M5, whereas L2 and T1 both have only one arborization in layer M2.

Whereas the connectivity in the lamina is well-described, far less is known about connections between neurons of the medulla. A major reason is that the medulla is far more complex with at least 60 different types of columnar and tangential neurons in *Drosophila*. All these cells are well described anatomically in *Drosophila* (Fischbach and Dittrich, 1989) and in *Musca* (Strausfeld, 1976). The columnar neurons of the medulla can be subdivided into different groups based on their projections to other neuropiles (see Fig. 6). The transmedullary (Tm) cells extend through the whole medulla and terminate in different layers in the lobula. The terminals of TmY cells bifurcate and send axons to both the lobula and the lobula plate. The medulla intrinsic (Mi) neurons in contrast are restricted to the medulla as are the amacrine cells, of which the Dm cells occupy the distal and the Pm cells the proximal part. All these neurons have characteristic arborizations in several layers and cell bodies that are located distally between lamina and medulla. In addition, there are several types of T-cells whose cell bodies are located posterior to the



medulla and the lobula plate and that project from the medulla either to the lobula plate or to the lobula.

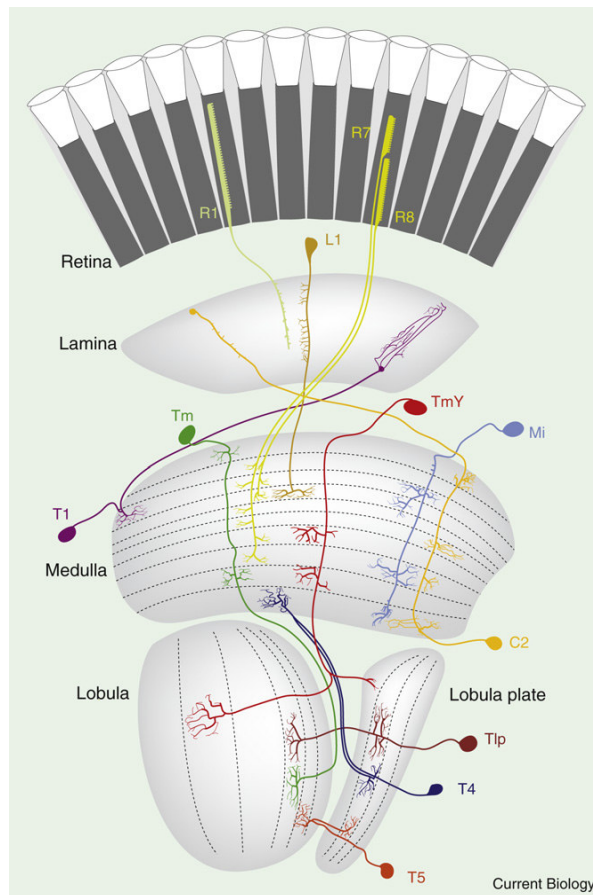


**Fig. 6: Neurons of the optic lobe.**

Whereas photoreceptors R7 and R8 project directly to the medulla, input from R1-6 is relayed there via lamina neurons. From the medulla, the information is further transmitted to the lobula and lobula plate via different types of Tm, TmY and T neurons. Mi cells in contrast are confined to the medulla. All these neurons can be identified based on their arborizations in different layers of the medulla.

T5 and Tlp neurons interconnect the lobula and lobula plate. T4 and T5 come in four different variants projecting to one of four different layers of the lobula plate dedicated to processing motion of a certain direction (from Borst, 2009).

Thus far, synaptic connections between medulla neurons were mainly inferred from their arborization patterns based on the assumption that neurons that occupy the same layer most likely form synapses with each other (Bausenwein et al., 1992). Only recently an EM study shed first light onto the synaptic connections between lamina and medulla cells in the outer medulla (Takemura et al., 2008). Interestingly this study revealed that L1 and L2 have indeed different postsynaptic partners, suggesting a separation between the two channels. L1, however, does provide input to L2 via C2 and C3. L5 is reciprocally connected with L1. T1 is somehow enigmatic as no output synapses of this cell could be found in the lamina and the medulla. As in the lamina, L4 is associated with L2 in the medulla, providing input to the same postsynaptic neuron, and sending collaterals to neighboring columns.

Based on arborization patterns and few electrophysiological recordings, two pathways were proposed relaying information from L1 and L2 to the lobula plate and being involved in motion detection (Bausenwein et al., 1992; Douglass and

Strausfeld, 1995; Douglass and Strausfeld, 1996). The first one is via L1, Mi1 and T4, the second one via L2, Tm1 and T5. T4 and T5 connect the most proximal layer of the medulla and the outer layer of the lobula, respectively, with the lobula plate. Both T4 and T5 come in four different variants that project to four different layers in the lobula plate. As these layers are dedicated to the processing of motion in different directions, it was speculated that T4 and T5 likely provide this directional selective input. One study showed indeed a synaptic connection between a T4 neuron and an HS cell (Strausfeld and Lee, 1991). However, due to their small size only few electrophysiological recordings could be obtained from medulla neurons (Devoe and Ockleford, 1976; Gilbert et al., 1991; Douglass and Strausfeld, 1995; Douglass and Strausfeld, 1996). Therefore, their function still remains unknown. Some further evidence that the proposed pathways are involved in motion detection comes from 2-Deoxyglucose labeling (Buchner et al., 1984; Bausenwein and Fischbach, 1992). Stimulating the fly with motion of a certain direction indeed led to labeling of those layers in the medulla, lobula and lobula plate, where neurons of the above mentioned two pathways have their arborizations.

However, how the correlation-type motion detector is implemented in the fly brain, i.e. which neurons take part in motion processing and how, is still unclear. The combination of all the genetic techniques available in *Drosophila* in combination with newly established physiological techniques promises to shed new light on that question.

### **4. Genetic tools**

*Drosophila* has been the model organism of geneticists for over 100 years. Therefore, a vast set of elaborate genetic tools is available for manipulating neuronal circuits (for review see Luo et al., 2008). Physiological techniques or behavioral assays can then be used as readout for the effects of the manipulation. In addition Calcium imaging allows for directly monitoring neuronal activity in a population of neurons. These tools will be discussed in the following.

#### 4.1 Gal4-UAS-system

The first and most important step is to genetically target specific neurons of interest. The introduction of the Gal4-UAS-system, a transcriptional control system from yeast, into *Drosophila* genetics (Brand and Perrimon, 1993) has revolutionized the field in this regard. Gal4 is a transcriptional activator that binds to the UAS sequence and activates expression of any downstream transgene. A selective expression of Gal4 in only specific cells can be achieved by either cloning it downstream of a known promoter or by introducing it randomly into the genome, where it comes under control of endogenous enhancers depending on its insertion site (Rubin and Spradling, 1982). By screening a large number of these random-insertion lines (e.g. Hayashi et al., 2002) one can select those that show expression in the cells one is interested in. The huge advantage of this system is first, that it boosts expression of the transgene, and second, its combinatorial character. Once the expression pattern of a Gal4 line is established, this line can be used to drive a variety of effector genes by combining it with the respective UAS lines. The UAS line thus determines what transgene is expressed and the Gal4 line where it is expressed. The temporal expression pattern solely reflects the activity of the promoter controlling transcription of Gal4. Further temporal control can be achieved with a temperature sensitive Gal80 (Gal80<sup>ts</sup>). Gal80 binds to and inhibits Gal4. Gal80<sup>ts</sup>, however, becomes inactive above 30°C, thus allowing to activate transgene expression by subjecting flies to a temperature shift (McGuire et al., 2003). Another method is to introduce a stop codon flanked by FRT sites in front of the transgene. These FRT sites are recognized by a flippase that removes the stop codon and thus enables transgene expression. If the flippase is under the control of a heat shock promoter, its activity can again be induced by a temperature shift.

One disadvantage of the Gal4 system is that most of the lines are relatively unspecific showing not only expression in the neurons of interest, but also in a variety of other cell types. However, there are several techniques available with which to narrow down the population of affected neurons (see Fig. 7). Gal80 expressed in a different but overlapping cell population is one possibility. Another combinatorial approach is the split-Gal4 system, where the DNA-binding and the

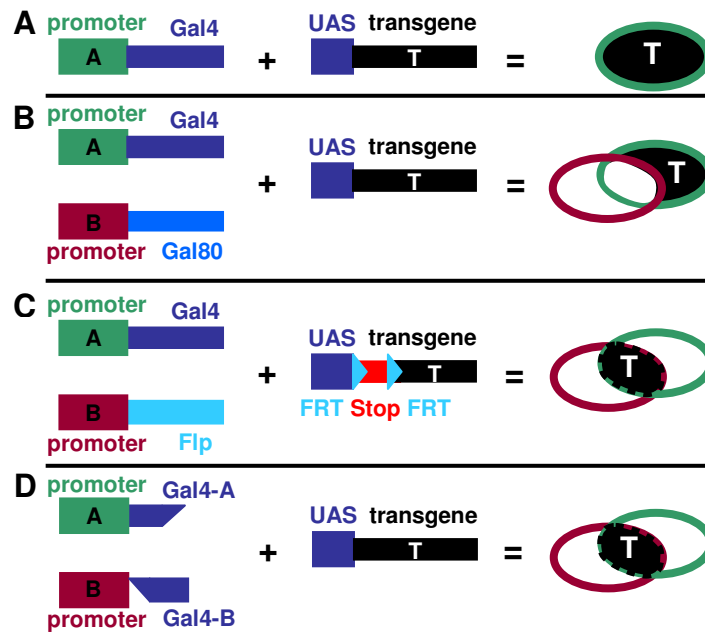


**Fig. 7: Variants of the Gal4-UAS-system.** (A) In its original version the expression pattern of a transgene T (green ellipse) is determined by the promoter and enhancer fragments controlling the expression of Gal4 (promoter A). (B) This pattern can be restricted by expressing Gal80, which inhibits Gal4, in an overlapping cell population defined by promoter B (red ellipse). (C) By introducing a stop codon flanked by FRT sites in front of the transgene, its expression occurs only in cells expressing Gal4 (controlled by promoter A) and a flippase (controlled by promoter B), which removes the stop codon. (D) Another combinatorial approach is the split-Gal4 systems, where two parts of the Gal4 gene are under control of two different promoters. Only in cells, where both are active, expression of the transgene occurs (after Luo et al., 2008).

transcriptional-activation domain of the Gal4 gene are under the control of two different promoters (Luan et al., 2006). Only in those cells where both promoters are active, a functional Gal4 protein is formed and transcription occurs. Alternatively, with the MARCM technique single cell clones can be obtained by mitotic recombination (Lee and Luo, 1999). However, the recombination event might occur only rarely and results in only low expression levels, so that this approach is only feasible for studying cell anatomy and loss of gene function.

The most recent and largest-scale approach for obtaining specific Gal4 lines is to bring the Gal4 gene under control of every single enhancer element identified in the fly genome (Pfeiffer et al., 2008). These constructs are introduced into the fly using a site-specific integration system to obtain comparable expression levels. The hope is that the expression patterns of these lines will be restricted to only one or a view cell

types. Another advantage of this approach is its flexibility. The specificity of these lines is only determined by the inserted enhancer fragments and not by the insertion site. Therefore, the Gal4 gene can easily be replaced by any other transgene (e.g. to generate Gal80 or split-Gal4 lines) without altering the expression pattern.

### 4.2 Labeling cells

To analyze the expression pattern of a Gal4 line one usually uses marker genes like the green fluorescent protein (GFP) for labeling the cells (Brand, 1995). This marker usually stays in the cytosol, but can be equipped with certain tags leading to its insertion at other places of the cell. For example, mCD8-GFP targets the protein to the cell membrane. Visualizing cells does not only allow for studying their anatomy, but also to make them easier accessible for electrophysiological recordings. In *Drosophila* patch clamp recordings are performed from the somata (Wilson et al., 2004), so a GFP derivative highlighting the somata proved especially useful (Joesch et al., 2008).

### 4.3 Calcium indicators

Columnar neurons in *Drosophila* are hardly accessible with electrophysiological techniques due to their small size. Therefore, genetically encoded Calcium indicators (GECIs) are a promising tool for analyzing their function. They can be targeted to specific cell populations and allow for recording their activity without much external interference. GECIs signal changes in the intracellular Calcium concentration, an indirect measure for neuronal activity and synaptic transmission, with a change in fluorescence. GECIs are derivatives of GFP and come in two variants (for review see Mank and Griesbeck, 2008). Single-chromophore indicators like GCaMPs increase their fluorescence upon binding of Calcium (e.g. Nakai et al., 2001). Ratiometric indicators in contrast consist of two fluorophores with different spectral characteristics (e.g. YFP and CFP) interlinked by a Calcium-binding domain like calmodulin or troponinC (Miyawaki et al., 1997; Heim et al., 2007). Calcium binding leads to a conformational change that alters the probability of FRET (fluorescence resonance energy transfer) between the two fluorophores i.e. the emitted light of one fluorophore excites the other fluorophore. Thus, the fluorescence signal of CFP

decreases and that of YFP increases, so that their ratio can be used as a measure for the intracellular Calcium concentration. The main advantage of ratiometric indicators is that they are less sensitive to motion artifacts, whereas single-chromophore indicators usually lead to larger fluorescence signals (Reiff et al., 2005). The sensitivity of GECIs, however, is still low in comparison with synthetic dyes and electrophysiological recordings, thus necessitating further improvement.

### 4.4 Blocking neurons

Insights about the function of a neuron can not only be obtained by monitoring its activity, but also by manipulating its function and studying the phenotypic consequences.

A number of tools are available that block neuronal activity at different levels.

Firstly, mutations can be introduced that interfere with normal cell function. For example, mutations in genes necessary for the development or function of fly photoreceptors allowed for studying their involvement in optomotor behavior (Heisenberg and Buchner, 1977; Strauss et al., 2001; Yamaguchi et al., 2008). This approach can be further elaborated by combining it with the Gal4-UAS-system, which can be used for restoring the affected gene in only a subset of the neurons involved (Rister et al., 2007; Gao et al., 2008). However, this method is only feasible in the rare cases, where the function of a gene is well-described and restricted to only a few cell types. In these cases, this approach represents a good possibility for interfering with neuronal activity in a highly specific way.

Secondly, transgenes can be introduced that are detrimental to cell function and that act at different levels (for a comparison of different tools see Thum et al., 2006). Toxins from bacteria (like Diphtheria toxin, Kunes and Steller, 1991) or plants (like RicinA, Moffat et al., 1992), for example, interfere with protein synthesis and can thus be used for cell ablation. To prevent expression during development and obtain viable flies, their expression often has to be made conditional using Gal80<sup>ts</sup> or the flippase technique (see above). A milder way for interfering with neuronal function is to block synaptic transmission. Expression of TNT, which cleaves synaptobrevin and thus blocks synaptic vesicle release (Sweeney et al., 1995), is one way for doing that. However, it does not work in all types of neurons and can cause developmental

defects (Rister and Heisenberg, 2006; Thum et al., 2006). Another tool is *shibire<sup>ts</sup>*, a temperature sensitive dynamin. *Shibire<sup>ts</sup>* acts in a dominant-negative fashion and blocks endocytosis thus leading to a depletion of synaptic vesicles at the restrictive temperature (Chen et al., 1991; Kitamoto, 2001). In addition it also seems to act on the cytoskeleton making its effects not fully reversible (Gonzalez-Bellido et al., 2009). Morphological defects in some neuronal types even occur at the permissive temperature and thus have to be controlled for. The main advantage of *shibire<sup>ts</sup>* is nevertheless that it allows for a fast block in adult animals, so developmental effects can be largely circumvented.

In addition to synaptic transmission also the excitability of neurons can be manipulated e.g. by an inward-rectifying K-channel (Kir), whose overexpression hyperpolarizes and shunts the neuron thus blocking the generation of action potentials (Johns et al., 1999). However, its effects on interneurons responding with graded potential changes, which widely occur in the visual system of *Drosophila*, are not well described.

### 4.5 Dscam

*Drosophila* neurons often exhibit complex morphologies (Fischbach and Dittrich, 1989), suggesting a tight interrelation between anatomy and function. To study that relation one can manipulate signaling molecules involved in dendritic branching during development like the Dscams (Downs Syndrom Cell Adhesion Molecules) (Schmucker et al., 2000). There are four Dscam genes in *Drosophila*, Dscam1-4, all belonging to the immunoglobulin superfamily. They have similar extracellular domains containing ten immunoglobulin and six fibronectin type III repeats, but different cytoplasmic tails (Millard et al., 2007). Dscam1, referred to as Dscam in the following, is remarkable in so far, as at least 38 016 different protein isoforms can be derived from it by alternative splicing (Schmucker et al., 2000) (see Fig. 8). These isoforms differ in Ig2, Ig3 and Ig7 (encoded by exons 4, 6 and 9, respectively) and possess one of two alternative transmembrane domains (encoded by exon 17). Most isoforms bind to each other in a homophilic way, strongly preferring identical isoforms over even similar ones (Wojtowicz et al., 2007; Wojtowicz et al., 2004). Swapping certain structural elements between isoforms (Wojtowicz et al., 2007) and

## Introduction

X-ray crystallography revealing the structure of parts of the extracellular domain (Meijers et al., 2007) have shed first light at how these specific interactions might be achieved.

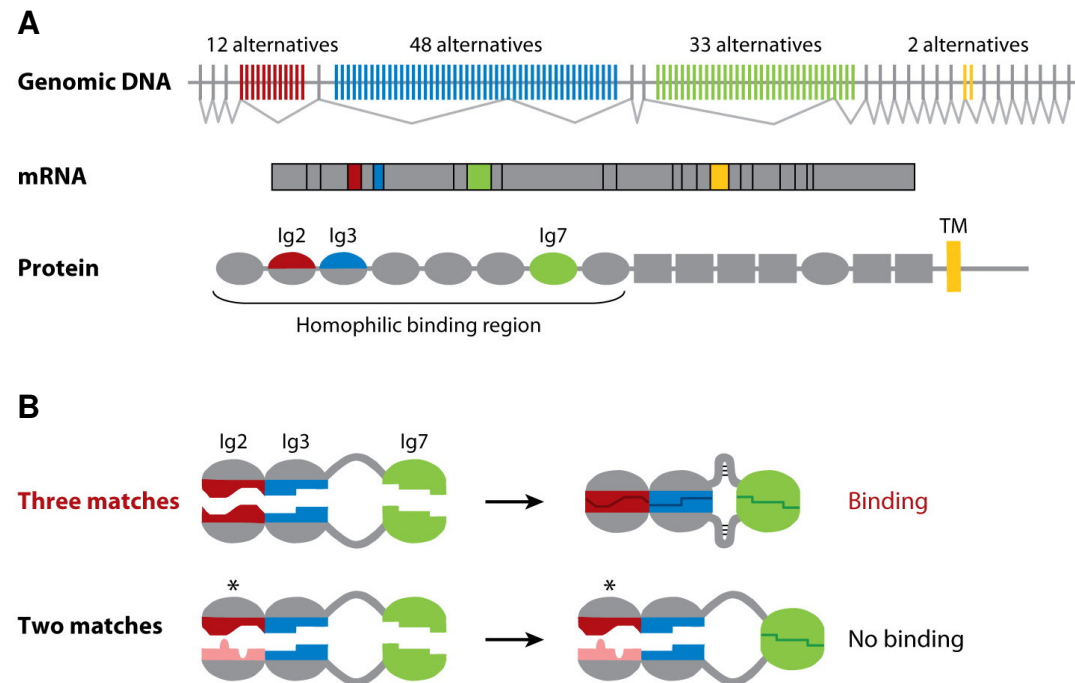


**Fig. 8: The Dscam gene and homophilic binding.**

(A) By alternative splicing of four variable exons, over 38 016 different Dscam mRNAs and protein isoforms can be generated differing in three of the Ig domains and in the transmembrane domain. (B) These isoforms bind homophilically to each other in a very specific manner. A mismatch in only one domain already excludes binding in most cases (Hattori et al., 2008).

The vast number of different possible isoforms has since its first discovery led to the speculation that Dscam might play an important role in neuronal wiring providing neurons with a unique surface code. By single-cell RT-PCR it could indeed be shown that neurons express non-overlapping sets of between 10-50 different isoforms (Neves et al., 2004) allowing them to discriminate between themselves and others.

The role of Dscam in different aspects of neuronal wiring has been extensively studied. It acts e.g. as a guidance receptor in Bolwig's nerve (Schmucker et al., 2000), is necessary for axonal extension in mechanosensory neurons (Chen et al., 2006) and sister-branch segregation in mushroom body (Wang et al., 2002; Hattori et al., 2007) and mechanosensory neurons (Hughes et al., 2007; Matthews et al., 2007; Soba et al., 2007). Based on these findings it was proposed that a major function of Dscam is



to mediate self-recognition and -avoidance by homophilic binding and subsequent repulsion. Ectopic avoidance between different, usually overlapping neurons can be induced by overexpressing single Dscam isoform in them. In addition, it was shown that several thousand different isoforms are required to provide each neuron with a unique Dscam code and to assure proper branching patterns (Chen et al., 2006; Hattori et al., 2009).

The function of Dscam has so far only been described at the anatomical level. Whether and how far an altered morphology also influences the function of a neuron is unclear. Several different approaches allow manipulating the Dscam system for such a structure-function analysis. First, one can try to remove Dscam completely from single or populations of neurons. This, however, is complicated by the fact that a complete null-mutation is lethal. This problem can be circumvented by generating single null-mutant cell clones using the MARCM technique or by using a UAS-flippase in combination with a modified Dscam gene that contains FRT-sites flanking essential parts of the gene. Second, one can reduce isoform variability by replacing the wild-type Dscam gene with one lacking some of the alternative exons. Finally, one can overexpress single Dscam isoforms in populations of neurons using the Gal4-UAS-system. The newly established physiological techniques as well as behavioral paradigms can then be used to test for an altered function of those neurons affected by the manipulation.

### **5. Goals and results**

The major goal of this work was to advance our understanding of how motion information is computed in the fly brain. To this end I combined physiological techniques with genetic manipulation in *Drosophila melanogaster*. First I characterized different Calcium indicators in lobula plate tangential cells by stimulating the neurons with a high potassium concentration (Chapter III). In that way, it could be shown that these indicators are indeed functional in neurons of the fly visual system.

Second, I performed whole-cell recordings from a subset of LPTCs, the HS cells, and analyzed their response properties, receptive fields and electrical connectivity (Chapter IV). As these neurons are thought to underlie optomotor behavior elicited

## Introduction

---

by horizontal motion, this is an important step towards understanding how this behavior is controlled by the fly brain. In addition, response properties of these cells can be used as readout for the effects of genetically manipulating the presynaptic circuitry.

This was done in the third project, where the lamina pathways providing input to the motion detection circuitry were analyzed by blocking or rescuing their function while recording from LPTCs (Chapter V). My approach was to restore the histamine receptor encoded by *ort* in only L1 or L2 in an *ort*-null mutant background, such that only one of the two pathways should be functional. It appeared, however, that these cells are electrically coupled so that restoring input to one channel automatically also restores the other channel. Consequently, rescuing synaptic input to either L1 or L2 always lead to wild-type motion responses, whereas blocking their chemical output using *shibire*<sup>ts</sup> (experiments performed by M. Jösch) revealed that both pathways are specialized for processing information about brightness increments and decrements, respectively.

Finally, I analyzed how the altered morphology of HS cells overexpressing a single *Dscam* isoform affects their responses to motion stimuli (Chapter VI). As was shown in the second study, HS cells have largely overlapping dendritic trees and receptive fields and in addition are coupled electrically with each other. These findings lead to the speculation that by overexpressing a single *Dscam* isoform in all HS cells tiling between these neurons might be induced. Overexpression of one specific isoform indeed lead to HS cells with smaller dendritic trees and thus, reduced coverage of the lobula plate and reduced overlap between neighboring cells. Concomitantly, these cells had smaller receptive fields, meaning that they receive no or less input from those areas no longer covered by their dendrites.

### III. Fluorescence Changes of Genetic Calcium Indicators and OGB-1 Correlated with Neural Activity and Calcium In Vivo and In Vitro

Thomas Hendel, Marco Mank, Bettina Schnell, Oliver Griesbeck, Alexander Borst, and Dierk F. Reiff

This chapter was published in the Journal of Neuroscience in 2008.

#### 1. Abstract

Recent advance in the design of genetically encoded calcium indicators (GECIs) has further increased their potential for direct measurements of activity in intact neural circuits. However, a quantitative analysis of their fluorescence changes ( $\Delta F$ ) *in vivo* and the relationship to the underlying neural activity and changes in intracellular calcium concentration ( $\Delta[\text{Ca}^{2+}]_i$ ) has not been given. We used two-photon microscopy, microinjection of synthetic  $\text{Ca}^{2+}$  dyes and *in vivo* calibration of Oregon-Green-BAPTA-1 (OGB-1) to estimate  $[\text{Ca}^{2+}]_i$  at rest and  $\Delta[\text{Ca}^{2+}]_i$  at different action potential frequencies in presynaptic motoneuron boutons of transgenic *Drosophila* larvae. We calibrated  $\Delta F$  of eight different GECIs *in vivo* to neural activity,  $\Delta[\text{Ca}^{2+}]_i$ , and  $\Delta F$  of purified GECI protein at similar  $\Delta[\text{Ca}^{2+}]_i$  *in vitro*. Yellow Cameleon 3.60 (YC3.60), YC2.60, D3cpv, and TN-XL exhibited twofold higher maximum  $\Delta F$  compared with YC3.3 and TN-L15 *in vivo*. Maximum  $\Delta F$  of GCaMP2 and GCaMP1.6 were almost identical. Small  $\Delta[\text{Ca}^{2+}]_i$  were reported best by YC3.60, D3cpv, and YC2.60. The kinetics of  $\Delta[\text{Ca}^{2+}]_i$  was massively distorted by all GECIs, with YC2.60 showing the slowest kinetics, whereas TN-XL exhibited the fastest decay. Single spikes were only reported by OGB-1; all GECIs were blind for  $\Delta[\text{Ca}^{2+}]_i$  associated with single action potentials. YC3.60 and D3cpv tentatively reported spike doublets. *In vivo*, the  $K_D$  (dissociation constant) of all GECIs was shifted toward lower values, the Hill coefficient was changed, and the maximum  $\Delta F$  was reduced. The latter could be

attributed to resting  $[Ca^{2+}]_i$  and the optical filters of the equipment. These results suggest increased sensitivity of new GECIs but still slow on rates for calcium binding.

### **2. Introduction**

The rapid development of fluorescent genetic probes [for review, see Miesenböck and Kevrekidis (2005) and Kleinfeld and Griesbeck (2005)] might soon allow routine recordings of activity in intact neural circuits and long-term studies in intact and behaving animals. Moreover, genetic probes promise to overcome the spatial limitations of electrode recordings by monitoring large ensembles of functionally related neurons (Fiala et al., 2002; Ng et al., 2002; Higashijima et al., 2003; Wang et al., 2003) as well as small subcellular compartments (Guerrero et al., 2005; Reiff et al., 2005). Whereas intracellular and extracellular electrode recordings report changes in membrane and field potential, respectively, genetic probes usually translate a change in ion concentration into changes in the fluorescence of green fluorescent protein (GFP) variants (Miyawaki, 2005). The kinetics of this translation process and the interplay with parameters of the cell at rest determine whether biological signals can be discerned from noise.

Direct assessment of membrane potential has been promised by several genetic probes (Siegel and Isacoff, 1997; Sakai et al., 2001; Ataka and Pieribone, 2002; Guerrero et al., 2002), but small fluorescence changes ( $\Delta F$ ) or slow kinetics prevented their successful application *in vivo*. On the other hand, synaptopHluorin (Miesenböck et al., 1998) successfully provided a fluorescent readout of slow changes in the net equilibrium of presynaptic vesicle release and recycling (Ng et al., 2002; Bozza et al., 2004; Shang et al., 2007). However, experiments in neurons of nematodes (Suzuki et al., 2003; Clark et al., 2007), fruit flies (Fiala et al., 2002; Reiff et al., 2002; Wang et al., 2003, 2004; Suh et al., 2004; Marella et al., 2006), zebrafish (Higashijima et al., 2003), and mice (Hasan et al., 2004; Díez-García et al., 2005; Heim et al., 2007) suggest that genetically encoded calcium indicators (GECIs) report spatial and temporal dynamics of neural activity with somewhat higher accuracy. Yet, they still suffer from rather small  $\Delta F$ , poor signal-to-noise ratio (SNR), a capricious relationship to neural activity, slow kinetics, and changes in the dissociation constant ( $K_D$ ) *in vivo* (Hasan et al., 2004; Pologruto et al., 2004; Reiff et al., 2005). Most

importantly, no faithful calibration of  $\Delta F$ , the underlying neural activity, and change in intracellular calcium concentration ( $\Delta[\text{Ca}^{2+}]_i$ ) has been given for different GEClS in similar neurons *in vivo* so far.

We injected synthetic calcium indicators into subcellular compartments in *Drosophila* and calibrated  $\Delta F$  of Oregon-Green-BAPTA-1 (OGB-1) *in situ* (Maravall et al., 2000). This allowed us to estimate  $[\text{Ca}^{2+}]_i$  at rest and to convert  $\Delta F$  of OGB-1 to  $\Delta[\text{Ca}^{2+}]_i$  at known rates of sustained neuronal activity when  $[\text{Ca}^{2+}]_i$  is at steady state. The amplitude of these fluorescence changes at steady state is not influenced by buffering of calcium by the indicator and thus independent of indicator concentration (see Discussion). Following this approach,  $\Delta F$  of eight different GEClS was correlated to  $\Delta[\text{Ca}^{2+}]_i$  at similar activity rates and to  $\Delta F$  of purified GECl protein *in vitro*. In addition, the capacity of the GEClS to report transient changes in neural activity was analyzed. This way we analyzed Yellow Cameleon 3.3 (YC3.3) (Griesbeck et al., 2001), YC3.60, YC2.60 (Nagai et al., 2004), D3cpv (Palmer et al., 2006), TN-L15 (Heim and Griesbeck, 2004), TN-XL (Mank et al., 2006), GCaMP1.6 (GC1.6) (Ohkura et al., 2005), and GCaMP2 (Díez-García et al., 2005; Tallini et al., 2006) by two-photon laser-scanning microscopy (2PLSM) (Denk et al., 1990) in presynaptic boutons of transgenic *Drosophila* larvae and describe what these recent indicators can tell us about neural activity *in vivo* and what they still cannot.

### **3. Material and Methods**

#### **Flies and genetics**

Using the Gal4/UAS system (Brand and Perrimon, 1993), we directed expression of GEClS or monomeric DsRed (mDsRed) to the nervous system of flies. UAS-GECl flies carried cDNA for each GECl under UAS control as described by Reiff et al. (2005). Flies expressing YC3.3 (Griesbeck et al., 2001), GC1.6 (Ohkura et al., 2005), and TN-L15 (Heim and Griesbeck, 2004) were described by Reiff et al. (2005); TN-XL flies were described by Mank et al. (2006). For YC3.60, YC2.60 (Nagai et al., 2004), D3cpv (Palmer et al., 2006), and GCaMP2 (Tallini et al., 2006) new transgenic lines were generated.

We crossed 10 female, virgin  $elav^{C155}$ -Gal4 (Lin and Goodman, 1994) flies to five male UAS-GECl flies. For experiments, we collected female, third-instar larval offspring.

Where double heterozygous flies showed insufficient expression levels for imaging experiments, offspring was back-crossed to UAS-GECl or *elav*<sup>C155</sup>-Gal4 flies to yield flies homozygous for one or both transgenes. All animals were raised at 25°C on standard corn meal medium supplemented with yeast.

Transgenic flies were created by P-element-mediated germline transfection (Spradling and Rubin, 1982) in white<sup>-</sup> genetic background (*w*<sup>-</sup>, "Bayreuth" flies kindly provided by Christian Lehner, University of Bayreuth, Bayreuth, Germany). Stocks were established from hatching flies as described previously (Reiff et al., 2005). All fly strains used appeared normal in locomotion and neuromuscular junction (NMJ) gross morphology; however, this was not systematically addressed.

cDNAs for YC3.60 (provided by Atsushi Miyawaki, RIKEN Brain Science Institute, Wako City, Saitama, Japan) and TN-XL (provided by Marco Mank and Oliver Griesbeck, Max Planck Institute of Neurobiology, Martinsried, Germany) were amplified by PCR, adding *NotI* restriction sites to 3' and 5' ends, and inserted into the *NotI* site of the multicloning site of pUAST (Brand and Perrimon, 1993). Orientation of the insertion was controlled by sequencing.

D3cpv was provided in pcDNA3 in *Bam*HI and *Eco*RI sites (by Maz Hasan, Max Planck Institute for Experimental Medicine, Heidelberg, Germany). An upstream His tag with *NotI* site at the 5' end was inserted between *Hind*III and *Bam*HI. A *NotI/NotI* fragment (including His tag and D3cpv) was then extracted and cloned into pUAST. Orientation and sequence were confirmed.

YC2.60 was generated by subcloning YC3.60 into pRSETb. PCR with primers GGCTACATCAGCGCTGCTGAATTACGTCACGTCATGACAAACC and GGTTTGTCATGACGTGACGTAATTCAGCAGCGCTGATGTAGCC were used to introduce two base exchanges (CAG to GAA), leading to the E104Q amino acid exchange in calmodulin as described by Nagai et al. (2004).

pUAST-GCaMP2 (Tallini et al., 2006) was generated by isolating a *Bgl*II/*NotI* fragment containing GCaMP2 preceded by His repeats from pN1 (provided by Junichi Nakai, RIKEN Brain Science Institute, Wako-shi, Saitama, Japan) and inserting this fragment between the *Bgl*II and *NotI* sites of pUAST.

UAS-mDsRed flies used for the injection of synthetic  $\text{Ca}^{2+}$  sensors were kindly provided by Gaia Tavosanis (Max Planck Institute of Neurobiology, Martinsreid, Germany).

### **GECIs**

We compared ratiometric GECIs and single-chromophore indicators in their fluorescence responses to different activity levels in presynaptic boutons of the larval *Drosophila* NMJ. The GECIs are based on a  $\text{Ca}^{2+}$ -binding protein fused to one or two different GFP variants.  $\text{Ca}^{2+}$  binding induces a conformational change in the binding protein(s) that leads either to enhanced fluorescent resonance energy transfer (FRET) (in ratiometric indicators) or to a higher ratio of deprotonated/protonated forms of the chromophore. The deprotonated and protonated forms are represented by the long-wavelength peak (490 nm) and the short-wavelength peak (375 nm) of GFP emission, respectively (Tsien, 1998). Thus, increase in  $\text{Ca}^{2+}$  increases the long-wavelength emission in GCaMPs. Specific constituents and basic properties of the GECIs included in this study are summarized in Table 1.

### **Physiology and optical imaging**

The larval preparation and solutions have been described previously (Macleod et al., 2002; Reiff et al., 2005). Unless stated otherwise, HL6 with 7 mM L-glutamate and 1.5 mM  $\text{Ca}^{2+}$  at pH 7.2 was used for superfusion of preparations and filling of electrodes. L-Glutamate effectively blocks postsynaptic muscle contractions at concentrations  $\geq 5$  mM without influencing presynaptic  $\text{Ca}^{2+}$  dynamics. In brief, late third-instar larvae were pinned to the bottom of a recording chamber with Sylgard lining and cut open along the dorsal midline using buckled scissors (Frohnhäuser); fat body, gut, and big trachea were removed. Segmental nerves were severed, and the ventral nerve cord (vnc) and brain were removed. Larval NMJs were recorded at muscle 6/7 in abdominal segments 2, 3, or 4. Presynaptic boutons were stimulated by placing the cut end of a segmental nerve into a suction electrode. We induced action potentials (APs) by applying voltage pulses (5.5 V, 0.3 ms) to the nerve (Iso-Stim 01-D; NPI Electronic). Pulses were applied at frequencies of 160, 80, 40, 20, 10, and 0 Hz, respectively, over a period of 2 s. Sequence of stimulus frequencies was altered

pseudorandomly. Recording time was 8 s (12 s for YC2.60 because of slow decay time constant of the  $\text{Ca}^{2+}$  response) (see Figs. 2, 3), and stimulus period was 2 s starting after 2 s. The interval between individual recordings was 1 min at least.

We imaged individual boutons using a custom-built 2P microscope [design kindly provided by Winfried Denk, Max Planck Institute for Medical Research, Heidelberg, Germany (Wachowiak et al., 2004)], which allows for wide-field or 2P imaging through the same objective [63x/0.90 numerical aperture (NA) for GECIs, 40x/0.80 NA for OGB-1 and Magnesium Green (Invitrogen), water-immersion, IR Achromplan; Zeiss]. Wide-field illumination used a 150 W mercury arc lamp housed in a lamp house and power supply from Opti-Quip (models 770 and 1600) with optical filters [450/50 excitation, 480 long-pass (LP) dichroic, and 510/50 emission for yellow fluorescent protein (YFP) and cyan fluorescent protein (CFP); 565/30 excitation, 585 LP dichroic, and 620/60 emission for mDsRed; all optical filters and dichroic mirrors by AHF]. The epifluorescence condenser was coupled to the microscope head containing tube lens, mirrors, and step motors to move the objective in three dimensions while the optical path was kept nearly constant (steering: Sutter MP285). Emitted light was projected onto the chip (1040 x 1392 pixels) of a CCD camera (Cool Snap HQ and MetaView software; Visitron Systems). Switch from wide-field to 2P microscopy involved moving of two mirrors. 2P fluorescence was excited by a mode-locked Ti:Sapphire laser (<100 fs, 80 MHz, 700–1000 nm; pumped by a 10 W Millennia laser; both Tsunami; Spectraphysics). Laser intensity was held constant at 6–15 mW for GECIs and at 45 mW for OGB-1 and Magnesium Green to minimize photobleaching and allow sufficient SNR (Patterson and Piston, 2000). Ratiometric GECIs were excited at 830 nM, GCaMPs at 920–930 nM, and OGB-1 and Magnesium Green at 950 nM. An emission filter (700 SP) was inserted in front of a cassette of two photomultiplier tubes, allowing simultaneous recording of different wavelengths of light. The photomultiplier tubes were equipped with bandpass dichroic mirrors (485/40 for CFP; 535/30 for YFP; 510/50 for GCaMPs, OGB-1, and Magnesium Green; and 620/60 for DsRed). Image acquisition was controlled by custom software [CfNT, written by R. Stepnoski (Bell Labs, Murray Hill, NJ) and M. Müller (Max Planck Institute for Medical Research, Heidelberg, Germany)].



Ca<sup>2+</sup> signals were recorded at 64 x 64 pixel resolution at 8 Hz frame rate or at 1 x 64 pixel line scans at 500 Hz, respectively. Experiments were controlled by custom software [written in Delphi (Borland) by J. Haag (Max Planck Institute of Neurobiology, Martinsried, Germany)] using an analog-to-digital converter (DAS-1602/12; Computerboards). All data were analyzed using custom software written in IDL (RSI).

### Data analysis

Further data evaluation and signal processing was done in Matlab R2006b (MathWorks) software and Origin 7.5 (Additive).

*Single-chromophore indicators.* For background subtraction, a homogeneous region neighboring individual boutons was selected, and its intensity was subtracted from the intensity of the bouton. (For line scans, a time-averaged mean intensity next to each bouton was subtracted as background.) Bleach correction of individual bouton intensity traces was done by deleting the stimulation period before fitting a single-exponential function to each trace and subtracting the resulting function from the original fluorescence trace. From the corrected data for each bouton, fractional fluorescence changes ( $\Delta F/F$ ) were calculated by subtracting the average intensity measured before stimulus onset (average of nine control frames =  $F_{\text{ctrl}}$ ) from the fluorescence in each image  $F_t$  of a series and subsequently dividing the difference by  $F_{\text{ctrl}}$ . (For line scans, the average of the first 240 lines was used as  $F_{\text{ctrl}}$ .)

*Double-chromophore indicators.* The ratio of fluorescence values from both channels was calculated after background subtraction and bleach correction. The resulting trace was processed as described above to yield relative changes in the fluorescence ratio ( $\Delta R/R$ ).

*SNR.* SNR was calculated for each bouton as the ratio of the mean  $\Delta R/R$  or  $\Delta F/F$  from five frames around peak amplitude and the corresponding SD. Presented values represent mean SNRs of all boutons measured at one stimulus protocol. (For line scans, amplitudes and SNR were calculated separately for each stimulus event within individual recordings. Then all SNR values from all four trials were averaged). The  $\Delta$  [Ca<sup>2+</sup>]<sub>i</sub> and frequency of action potentials ( $f_{\text{AP}}$ ) leading to SNR = 2 were interpolated

by fitting experimental results to sigmoidal functions in semilogarithmic plots (concentration log-scaled, SNR linear).

### Two-photon guided dye injection

Sharp electrodes ( $R \sim 100 \text{ M}\Omega$ ; Science Products) were made on a standard puller (P-97; Sutter Instruments) and backfilled with OGB-1 or Magnesium Green, respectively (10 mM dye, in 0.5 M KCl and 2 M KAc). Photomultipliers of the 2PLSM were equipped with red (620/60 nm) and green (535/50 nm; AHF) bandpass filters for simultaneous dual-channel recording of monomeric DsRed and synthetic calcium dyes (red channel: axon terminals at larval NMJs; green channel: dye-filled electrode tip/loaded boutons). Excitation was adjusted to 980 nm for dye injection and 950 nm for recordings. Pressure was applied to the electrode to provide a minimal efflux from the tip and to avoid  $\text{Ca}^{2+}$  diffusion into the electrode. Injections were mostly done into boutons, occasionally into axons. The injection electrode was steered with electronic manipulator units (Luigs and Neumann Feinmechanik). Membrane potentials were between  $-20$  and  $-55$  mV; NMJs displaying lower membrane potentials did not show  $\text{Ca}^{2+}$  responses after dye injection. Dye concentration reached a plateau after 20 min (data not shown). Concentration in NMJs was unknown. However,  $\Delta F/F$  amplitudes at steady-state  $\text{Ca}^{2+}$  are independent of indicator concentration, and thus different experiments were pooled. In contrast, time constants and SNR of fluorescence signals are affected by dye concentration. The presented time constants and SNRs represent an average over different concentrations in an experimentally realistic range.

### Calcium measurements in NMJs

We used a method that allows intracellular  $\text{Ca}^{2+}$  measurements without wavelength ratioing described by Maravall et al. (2000). Briefly this method relies on a known  $K_D$  for the given indicator, *in situ* measurements of  $R_f = F_{\max}/F_{\min}$ , and linear  $[\text{Ca}^{2+}]/\text{stimulus}$  relationship of the system under observation. It provides resting  $[\text{Ca}^{2+}]$  by

$$\frac{[\text{Ca}^{2+}]_0}{K_D} = \frac{(1 - R_f^{-1})}{\Delta F_{\max}} - R_f^{-1},$$

and  $\Delta[\text{Ca}^{2+}]$  for a given steady-state response as follows:

$$\frac{\Delta[\text{Ca}^{2+}]}{K_D} = \frac{F_{max}}{F_0} (1 - R_f^{-1}) \frac{\Delta F}{(\Delta F_{max} - \Delta F) \Delta F_{max}}$$

where  $[\text{Ca}^{2+}]_0$  is intracellular  $[\text{Ca}^{2+}]$  at rest,  $F_0$  is fluorescence at rest, and

$$\Delta F = \frac{F_+ - F_{ctrl}}{F_{ctrl}}.$$

See Maravall et al. (2000) for details.  $K_D$  of OGB-1 was determined in the cuvette as 240 nM, in good accordance with values in the literature.

$F_{min}$  was determined by bath applying BAPTA-AM (200  $\mu\text{M}$ ; Invitrogen) in HL6 with zero  $[\text{Ca}^{2+}]$ . Using transgenic animals expressing YC2.60, we determined effective concentrations and exposure times for *in situ*  $\text{Ca}^{2+}$  buffering with BAPTA-AM (data not shown). Standard HL6 with glutamate and 1.5 mM  $[\text{Ca}^{2+}]$  was exchanged with HL6 with glutamate, zero  $[\text{Ca}^{2+}]$ , 1 mM EGTA, and 130  $\mu\text{M}$  BAPTA-AM. Diffusion of AM esters was allowed for 30 min before washout with HL6. Earlier washout led to incomplete intracellular  $\text{Ca}^{2+}$  buffering. After washout, residual  $\text{Ca}^{2+}$  responses were recorded that were markedly slowed down (data not shown), representing an effect of BAPTA-AM at low concentration. After 30 min, no response to any stimulus was noticeable, and  $F_{min}$  could be determined.

*In vivo*  $K_D$  values represent the  $[\text{Ca}^{2+}]$  and stimulus frequency at half-maximum fluorescence changes. Hill coefficients were derived from fitting experimental results to a model for the Hill coefficient:

$$R = \frac{f^n}{K_D^n + f^n}$$

where  $R$  is the experimental response,  $f$  is the stimulus frequency,  $n$  is the Hill coefficient, and  $K_D$  is the half-maximum stimulus frequency.

### Protein expression and purification

For cuvette determination of  $\text{Ca}^{2+}$  binding curves, GECl cDNAs were subcloned into the pRSETB vector (Invitrogen), which is optimized for protein expression using the T7 expression system and carries a 6xhis-tag 5' of the multiple cloning site. Protein expression was achieved using the *Escherichia coli* strain BL-21 (Invitrogen). Induction of protein expression took place at an  $\text{OD}_{600}$  of 0.6–0.8 with 0.5 mM IPTG (isopropyl- $\beta$ -D-thiogalactoside) for 2–3 h at 37°C. His-tagged protein was bound to a

Ni-NTA-Sepharose column by shaking for 2 h at 4°C. After washing the column with 10 ml of protein wash buffer (containing 10 mM imidazole), GECl protein was eluted by competitively displacing it with a high concentration of imidazole (150 mM).

### **Spectroscopic determination of $K_D$ values**

For determination of  $K_D$  values, freshly purified protein was used. For titration, a prewarmed (room temperature) titration kit (Calcium Calibration Buffer Kit with Magnesium #1, C3721; Invitrogen) was applied as follows. Two stock solutions were prepared: zero calcium: mix 1 ml of zero calcium buffer with 1 volume of protein solution [ $\sim 0.2$ – $1 \mu\text{M}$  protein, directly into the cuvette (Hellma Precision Cells Quartz Suprasil, type 101-QS/10 mm path)]. High calcium: mix 5.4 ml of  $39.8 \mu\text{M}$  free calcium buffer with 5.4 volumes of protein solution.

Subsequently, the zero calcium stock was put into the fluorescence spectrophotometer (Cary Eclipse fluorometer; Varian) to determine a baseline spectrum. Excitation wavelength for a CFP/YFP-FRET pair was 432 nm. Emission was determined in the range from 450 to 600 nm (all bandwidths 5 nm). Excitation wavelength for GC1.6 was 470 nm. Emission was determined in the range from 470 to 600 nm (all bandwidths, 5 nm). Excitation wavelength for OGB-1 was 475 nm (bandwidth, 10 nm). Emission was determined in the range from 490 to 600 nm (bandwidths, 5 nm).

Adjustment of free  $[\text{Ca}^{2+}]$  was achieved by reciprocal dilution (replacing same amount of zero  $[\text{Ca}^{2+}]$  buffer with the  $[\text{Ca}^{2+}]$  stock) to the desired concentrations. Zero, 0.065, 0.100, 0.225, 0.350, 0.600, 0.850, 1.35, 1.73, 2.85, 4.87, 7.37, 14.9, 29.9, and  $39.8 \mu\text{M}$  free  $[\text{Ca}^{2+}]$  were used as reference points to determine the  $K_D$  value for GECl (for OGB-1 concentrations were 0, 0.017, 0.038, 0.065, 0.1, 0.15, 0.225, 0.351, 0.602, 1.35, and  $39.8 \mu\text{M}$  free  $[\text{Ca}^{2+}]$ ). Calculation of the volumes that had to be replaced was according to the manufacturer's manual.

After measuring the spectra, the  $\Delta R/R$  at distinct  $[\text{Ca}^{2+}]$  was calculated as follows:

$$\Delta R/R = \frac{R_x - R_{Rest}}{R_{Rest}} * 100$$

with  $R_x$  = Ratio of YFP/CFP intensities at  $[Ca^{2+}] = x$  and  $R_{Rest} = 0.065 \mu M$ . For OGB-1 and GC1.6,  $\Delta F/F$  was determined analogously. To make cuvette measurements comparable with *in vivo* data acquired at the 2PLSM, two corrections were made:

(1) we calculated  $\Delta R/R$  using  $R_{Rest}$  at  $0.065 \mu M$ . This deviation from real resting  $[Ca^{2+}]_i$  ( $\sim 31$  nM) has negligible influence on resulting  $\Delta R/R$  for GC1.6 and TN-XL. For YC3.60, D3cpv, and OGB-1, however, this influence had to be considered (because of the steep slope of the titration curve close to zero  $[Ca^{2+}]_i$ ).  $R_x$  for a hypothetical  $Ca^{2+}$  level of 31 nM was interpolated for the titration of these GECIs, and this value was used as  $R_{Rest}$ . For OGB-1, a titration value was measured at 38 nM and used for  $R_{Rest}$ . (2) We mimicked bandpass filters by integrating the emission intensities from 465 to 505 nm for CFP, from 520 to 550 nm for YFP and 510–560 nm for OGB-1 and GC1.6. We measured a titration curve of a purified GECI protein at the two-photon microscope in aqueous solution as described for cuvette measurements and found that this bandpass correction leads to a maximum difference in  $\Delta R/R$  under both imaging conditions of only 3.7%. Extraction of the  $K_D$  values was done by sigmoidal fits to the dose–response curves (logarithmic  $[Ca^{2+}]$  vs  $\Delta R/R$ , normalized to  $39.8 \mu M [Ca^{2+}]$ ).

**Table 1.** Characteristics of GECIs and OGB-1 *in vivo* and *in vitro*

Probe	GFP variants <sup>a</sup>	functional sensor <sup>b</sup>	hill coefficient		$K_D$		max change		$\tau$ rise <sup>e</sup> (40Hz) <sup>k</sup>	$\tau$ decay <sup>f</sup> (40Hz) <sup>k</sup>
			<i>in vitro</i> <sup>c</sup>	<i>in vivo</i> <sup>d</sup>	<i>in vitro</i> <sup>e</sup>	<i>in vivo</i> <sup>f</sup>	<i>in vitro</i> <sup>g</sup>	<i>in vivo</i> <sup>h</sup>		
YC3.3	ECFP/ Citrine	CaM/ M13	-	2.50	-	0.47 $\mu M$	-	67 %	1.41 s	1.05 s
			-		(1.5 $\mu M$ )	38 Hz	(100 %)			
YC3.60	ECFP/ cpVenus	CaM/M13 E104Q	2.24 (1.7)	1.67	0.63 $\mu M$ (0.25 $\mu M$ )	0.36 $\mu M$ 30 Hz	346 % (560 %)	136 %	0.82 s	0.73 s
YC2.60	ECFP/ cpVenus	CaM/ M13	-	1.84	-	0.40 $\mu M$	-	194 %	0.88 s <sup>k</sup>	3.91 s <sup>k</sup>
			(2.4)		(0.04 $\mu M$ )	32 Hz	(560 %)			
D3cpv	ECFP/ cpVenus	CaM/M13 redesigned	0.63 (0.74)	0.96	0.66 $\mu M$ (0.53 $\mu M$ )	0.49 $\mu M$ 41 Hz	190 % (530 %)	90 %	0.36 s <sup>k</sup>	1.84 s <sup>k</sup>
TN-L15	ECFP/ Citrine	csTnC	1.29 (0.89)	2.59	0.72 $\mu M$ (1.2 $\mu M$ )	0.36 $\mu M$ 30 Hz	82 % (140 %)	60 %	0.81 s	1.49 s
TN-XL	ECFP/ cpCitrine	csTnC mut <sup>l</sup>	1.90 (1.7)	2.74	2.20 $\mu M$ (2.5 $\mu M$ )	0.77 $\mu M$ 65 Hz	252 % (400 %)	106 %	0.59 s	0.20 s
GC1.6	cpEGFP	CaM/M13	-	2.34	-	0.64 $\mu M$	-	162 %	1.38 s	0.45 s
			(3.8)		(0.15 $\mu M$ )	54 Hz	(490 %)			
OGB-1	-	Bapta	0.97	1.48	0.24 $\mu M$ (0.17 $\mu M$ )	0.26 $\mu M$ 21 Hz	11 (14)	316 %	0.17 s <sup>k</sup>	0.41 s <sup>k</sup>

<sup>a</sup>"GFP variants" lists the chromophores used in each indicator. cp, Circular permuted variant; EGFP, enhanced YFP; ECFP, enhanced CFP. <sup>b</sup>"Functional sensor" indicates the Ca<sup>2+</sup> binding and interaction moieties. CaM, Calmodulin; csTnC, chicken skeletal muscle troponin C. Hill coefficients are listed for <sup>c</sup>cuvette measurements (Fig. 4) and <sup>d</sup>*in vivo* measurements (Fig. 3).  $K_D$  values shown represent <sup>e</sup>cuvette measurements (Fig. 4) and <sup>f</sup>*in vivo* data (Fig. 3), respectively. Max. change represents  $(\Delta R/R)_{\max}$  or  $(\Delta F/F)_{\max}$  in <sup>g</sup>cuvette (uncorrected spectrophotometer measurements) for  $[Ca^{2+}] = 39.8 \mu M$  and <sup>h</sup>amplitudes at 160 Hz *in vivo* (2PLSM measurements) as shown in Figure 4. <sup>i</sup> $\tau_{\text{rise}}$  and <sup>j</sup> $\tau_{\text{decay}}$  were determined from single-exponential fits to rise and decay phases of indicator responses to 40 Hz. <sup>k</sup>20 Hz for YC2.60, D3cpv, and OGB-1. These values represent the properties of both the indicator and the specific fly lines. Values in parentheses represent literature values from original publications as cited in the text. <sup>l</sup>Four mutations within the C-terminal lobe of troponin C altered Mg<sup>2+</sup> and Ca<sup>2+</sup> binding properties.

### 4. Results

In a first series of experiments, neural activity was evoked at known rates ( $f_{AP}$ ), and the relationship to  $\Delta F$  exhibited by OGB-1 and  $\Delta[Ca^{2+}]_i$  was quantified. These recordings as well as all other live recording experiments were done in presynaptic boutons of transgenic *Drosophila* larvae. Thus, we had to develop a protocol for the injection of synthetic calcium indicators into targeted neuronal compartments in *Drosophila*.

#### Two-photon guided dye injection into genetically labeled presynaptic boutons

We used sharp quartz electrodes to inject the green synthetic Ca<sup>2+</sup> indicators OGB-1 and Magnesium Green into presynaptic boutons labeled in red by transgenic expression of mDsRed (see Materials and Methods). Injected boutons and axons were of 2–5 and 1  $\mu m$  diameter, respectively (Fig. 1A–C). Fluorescence was excited at 980 nm and visualized by dual-channel 2PLSM (Denk et al., 1990; Wachowiak et al., 2004). This allowed guidance of the dye-filled electrode tip toward boutons and axons and dye loading by current injection (Fig. 1B,C). A similar strategy has previously been described for patch electrodes and large cell bodies (Margrie et al., 2003; Komai et al., 2006). Twenty minutes after removal of the electrode dye concentration reached a plateau (data not shown). At that point, we began our experiments. The axon was stimulated with trains of action potentials at different frequencies (0–160 Hz). Figure 1D shows intensity changes of OGB-1 (raw data) in several boutons stimulated at 160 Hz (stimulation from  $t = 2\text{--}4$  s).

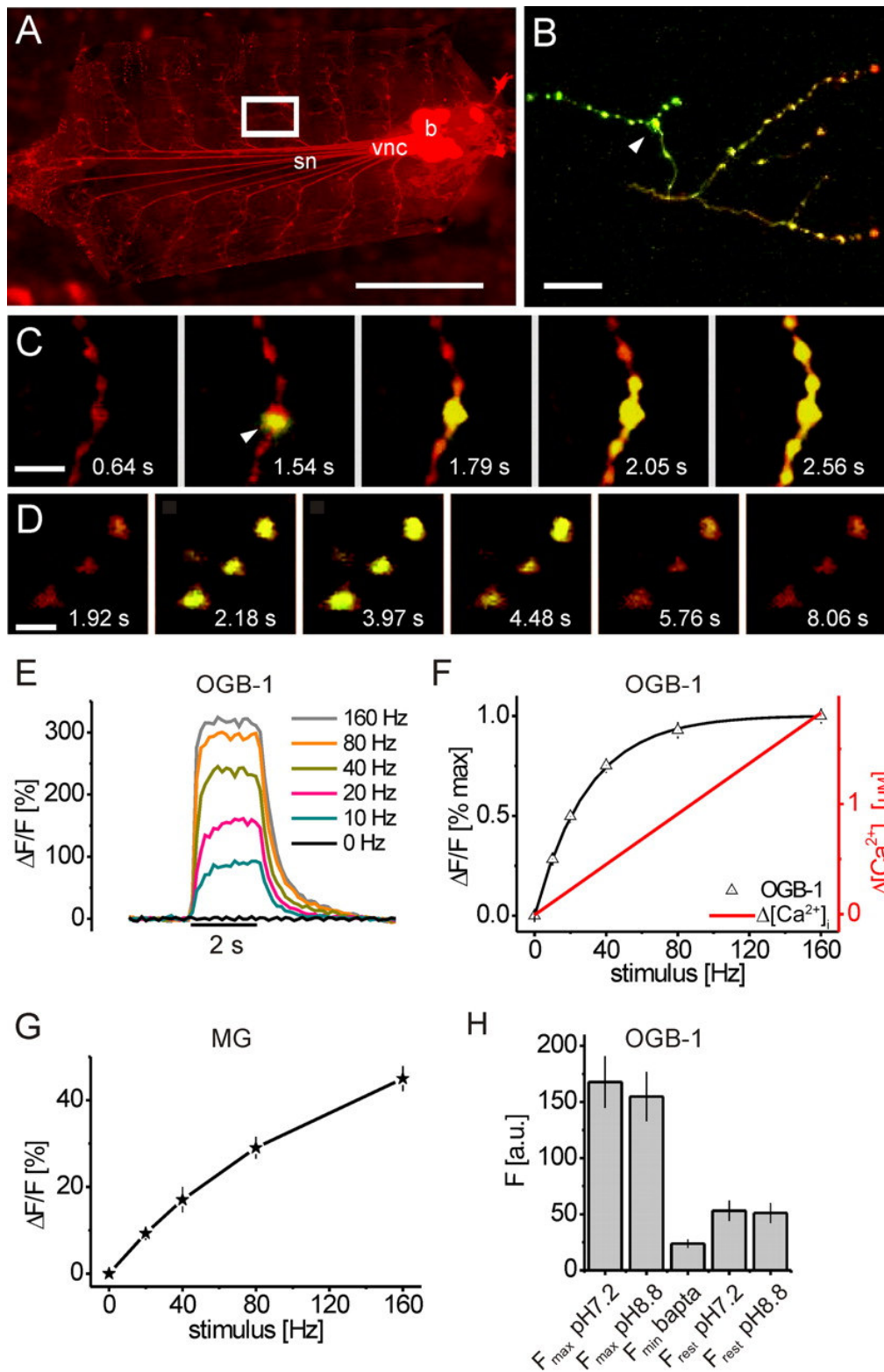


**Fig. 1:** *In vivo* cross-calibration of OGB-1 fluorescence changes, neural activity, and  $\Delta[Ca^{2+}]_i$ . **A**, A transgenic *Drosophila* larva expressing monomeric DsRed (elavC155-gal4 $\rightarrow$ UAS-mDsRed) in all neurons has been prepared for recording. For imaging experiments, the brain was removed and severed nerve ends were placed into a suction electrode for electrical stimulation. OGB-1 was injected into presynaptic boutons using sharp electrodes (white box in **A**, close-up in **B–D**) and 2PLSM imaging

[image: incident fluorescence light microscopy; brain (b), vnc, segmental nerves (sn)]. **B–D**, 2P excitation and graphic overlay of simultaneously recorded mDsRed (red) and OGB-1 (green) fluorescence. **B**, One minute after injection of the synthetic calcium indicator OGB-1 (green), intense green fluorescence is visible near the injection site (white arrowhead). **C**, Zoom-in during the 2PLSM-controlled injection of OGB-1 into a single bouton (white arrowhead): rapid filling and initial diffusion of OGB-1 along the axonal branch is visible (electrode barely visible). **D**, Fluorescence changes of OGB-1 (raw data) in response to a train of APs. Time points of frames are indicated; stimulation: 80 Hz from  $t = 2$  to  $t = 4$  s. **E**,  $\Delta F/F$  of OGB-1 in boutons evoked by trains of APs at different frequencies plotted as a function of time ( $f_{AP} = 0$ –160 Hz;  $n = 17, 30, 32, 32, 31,$  and  $30$  boutons). **F**, Cross-calibration of OGB-1 fluorescence changes (black triangles, extracted from the data in **E**; black line represents a hyperbolic fit) to neural activity ( $f_{AP}$ ) and  $\Delta[Ca^{2+}]_i$  (red trace) *in situ*.  $\Delta F/F$  and  $\Delta[Ca^{2+}]_i$  are plotted as a function of  $f_{AP}$ . OGB-1 exhibited fluorescence saturation at 160 Hz stimulation, and  $\Delta[Ca^{2+}]_i$  increased linearly up to 160 Hz. Determination of  $F_{max}$  and  $F_{min}$  (see **H**) allowed conversion of the fluorescence changes into an estimate of changes in  $[Ca^{2+}]_i$ . **G**, Calcium influx increases approximately linearly with the frequency of action potentials in presynaptic boutons. Steady-state amplitude and SNR of fractional fluorescence changes are plotted as a function of stimulus frequency. Magnesium Green (MG) responses increased almost linearly with stimulus intensity ( $15 < n < 24$ ). **H**, Determination of  $F_{max}$  and  $F_{min}$  of OGB-1 *in situ*.  $F_{max}$  was reached at 160 Hz stimulation; there was no further increase when raising the extracellular pH from 7.2 to 8.8 ( $p \approx 0.5$ ;  $n = 11$ ).  $F_{min}$  was reached in HL6 with zero  $[Ca^{2+}]_i$  by buffering of  $[Ca^{2+}]_i$  by excess BAPTA-AM, which reduced the resting fluorescence  $F_{rest}$  to  $F_{min}$  ( $F_{min}^{BAPTA}$  vs  $F_{rest}$  pH7.2,  $p < 0.01$ ;  $n = 11$ ).  $F_{rest}$  was unaffected by the extracellular pH ( $F_{rest}$  pH7.2 vs  $F_{rest}$  pH8.8,  $p \approx 0.5$ ;  $n = 11$ ). Imaging frame rate was 8 Hz throughout. Scale bars: **A**, 1 mm; **B**, 20  $\mu$ m; **C**, 10  $\mu$ m; **D**, 5  $\mu$ m. Calibration: **E**, 2 s.

Baseline fluorescence was reached again  $\approx 2$  s after the offset of the stimulus.  $\Delta F/F$  of OGB-1 at all stimulation frequencies is summarized in Figure 1, **E** and **F**. The OGB-1 response saturates with increasing  $f_{AP}$  (Fig. 1**F**, black triangles), whereas responses recorded with Magnesium Green exhibited an almost linear increase in  $\Delta F/F$  over the same stimulus range (Fig. 1**G**). The fast kinetics of the Magnesium Green responses (data not shown) and linear increase in amplitude can be explained by low  $Ca^{2+}$  affinity ( $K_D \approx 6 \mu$ M; Invitrogen), whereas the saturation curve of OGB-1 (Fig. 1**E,F**) reflects high  $Ca^{2+}$  affinity ( $K_D = 170$  nM; Invitrogen) (Table 1). Notably, the approximately linear increase of the Magnesium Green response suggests that the calcium concentration reached in presynaptic boutons is a linear function of  $f_{AP}$  up to 160 Hz.



### Estimation of intracellular calcium

We used *in situ* fluorescence saturation of OGB-1 to estimate  $[Ca^{2+}]_i$  (Maravall et al., 2000). Assuming a linear stimulus ( $f_{AP}$ )– $[Ca^{2+}]_i$  relationship, as suggested by the response of the low-affinity  $Ca^{2+}$  indicator Magnesium Green (see above),  $[Ca^{2+}]_i$  at rest and  $\Delta[Ca^{2+}]_i$  at steady state during stimulus trains can be calculated from the fluorescence response of OGB-1. This translation of OGB-1 fluorescence changes into  $[Ca^{2+}]_i$  after Equations 1 and 2 requires knowledge of the following parameters *in situ*: (1)  $K_D$ , (2) maximum  $\Delta F/F$  evoked by neural activity, (3)  $F_{max}$ , and (4)  $F_{min}$ . (1) The  $K_D$  for OGB-1 was determined as 240 nM at 22°C in the cuvette, which is in good accordance with our *in vivo* OGB-1 measurements (see Fig. 4F, Table 1). (2) For  $(\Delta F/F)_{max}$  *in situ*, complete saturation of the OGB-1 fluorescence response was estimated from fitting a hyperbolic function  $y = y_0 \times [Ca]/([Ca] + K_D)$  to the data points (Fig. 1F), where  $y_0$  is the asymptotic fluorescence value. The measured response at 160 Hz stimulation was ~99% of this value (318%  $\Delta F/F$ ) (Figs. 1F, 4F). (3) For  $F_{max}$ , we confirmed that OGB-1 fluorescence *in situ* cannot be further increased by stimulating at 160 Hz and extracellular pH 8.8 (Fig. 1H). Increasing the extracellular pH increases the intracellular  $Ca^{2+}$  accumulation at steady state (Lnenicka et al., 2006) because  $Ca^{2+}$  extrusion from presynaptic boutons in *Drosophila* NMJs is mainly achieved by a  $Ca^{2+}/H^+$  exchanger. In supplemental Figure 1A, we demonstrate this effect using GC1.6-expressing boutons. Stimulation at 40 Hz reversibly increased  $\Delta F/F$  to ~80%  $\Delta F/F$  at pH 8.8, which is a threefold increase compared with pH 7.2. The baseline fluorescence showed no significant increase (data not shown), suggesting that increased  $\Delta F/F$  of GC1.6 is not caused by a shift in the intracellular pH (Ohkura et al., 2005). For OGB-1, however,  $\Delta F/F$  at 160 Hz could not be further increased at pH 8.8 (Fig. 1H), indicating that OGB-1 was saturated with  $Ca^{2+}$  at this  $f_{AP}$  *in situ* and extracellular pH 7.2, as suggested by the saturation curve (Fig. 1F). Thus, the fluorescence at 160 Hz represents the true  $F_{max}$  and could be used to calculate  $(\Delta F/F)_{max}$ . (4)  $F_{min}$  was determined by creating an intracellular environment of effectively zero  $[Ca^{2+}]_i$  using extracellular solution of zero  $[Ca^{2+}]_i$  together with the cell-permeable  $Ca^{2+}$  chelator BAPTA-AM (130  $\mu$ M) (Fig. 1H) (see Materials and Methods). Using Equation 1, we determined  $[Ca^{2+}]_{i\text{ Rest}} = 31$  nM. Equation 2 gave  $\Delta[Ca^{2+}]_{i\text{ 10Hz}} = 92$  nM and  $\Delta[Ca^{2+}]_{i\text{ 20Hz}} = 229$  nM. A linear fit (Fig. 1F, red line) resulted in

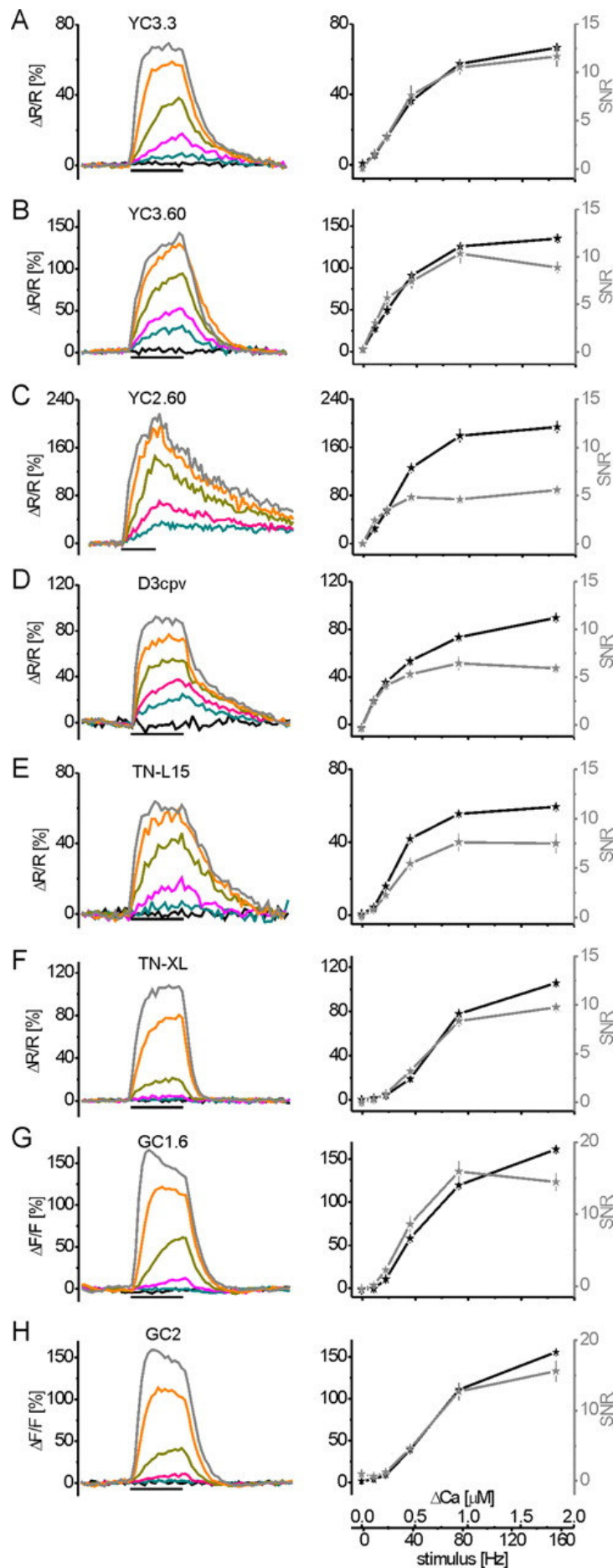


**Fig. 2:** GECl fluorescence changes at sustained neural activity and  $\Delta[\text{Ca}^{2+}]_i$ . Transgenic flies were engineered to allow the expression of eight different GECl *in vivo*. Fluorescence changes were analyzed at presynaptic terminals of the larval NMJ, similar to the experiment in Figure 1 [2 s stimulus period indicated by the black bar underneath the recording traces;  $f_{AP} = 0$  (black), 10 (blue), 20 (purple), 40 (green), 80 (orange), and 160 (gray) Hz]. **A**, YC3.3; **B**, YC3.60; **C**, YC2.60; **D**, D3cpv; **E**, TN-L15; **F**, TN-XL; **G**, GC1.6; **H**, GC2. To the left, mean fractional fluorescence changes ( $\Delta R/R$  for all dual-chromophore indicators and  $\Delta F/F$  for GC1.6 and GC2) of a large number of experiments are plotted as a function of time (for  $n$ , see Results). To the right, the maximum fluorescence change (black trace) and SNR (gray trace) calculated at steady state are plotted as a function of the stimulus frequency and the corresponding  $\Delta[\text{Ca}^{2+}]_i$ , respectively (for conversion of fluorescence changes to  $\Delta[\text{Ca}^{2+}]_i$  via OGB-1, see Fig. 1). Images were recorded at 8 Hz frame rate for 8 s (12 s for YC2.60; note different time scale of stimulus bar).

estimates of  $\Delta[\text{Ca}^{2+}]_i$  at steady state for each of the applied stimuli: 0.11  $\mu\text{M}/10$  Hz, 0.22  $\mu\text{M}/20$  Hz, 0.45  $\mu\text{M}/40$  Hz, 0.91  $\mu\text{M}/80$  Hz, and 1.82  $\mu\text{M}/160$  Hz. The obtained high  $\Delta[\text{Ca}^{2+}]_i$  at high action potential frequencies is in accordance with the slightly sublinear increase of the Magnesium Green response (Fig. 1G). At these concentrations, a slightly sublinear increase of the response is predicted by the law of mass action and can be explained by beginning sublinear binding of  $\text{Ca}^{2+}$  to the indicator as  $[\text{Ca}^{2+}]_i$  approaches  $0.5 \times K_D$  (Yasuda et al., 2004).

### **GECIs *in vivo*: cross-calibration of steady-state fluorescence changes, neural activity, and $\Delta[\text{Ca}^{2+}]_i$**

Experimental evidence (Pologruto et al., 2004; Reiff et al., 2005) suggests that, in general, available GECIs suffer from low-sensitivity, low-SNR, nonlinear concentration dependence with unusual supralinear and sublinear regimes and slow binding kinetics. These features influence whether and how a given GECI reports transient and fast  $\Delta[\text{Ca}^{2+}]_i$  and whether  $\Delta[\text{Ca}^{2+}]_i$  falls into the dynamic range of the indicator.

In the following experiments, nerves were stimulated at 0–160 Hz as described for OGB-1 (Fig. 1). Fluorescence changes of eight different GECIs were recorded in presynaptic boutons of transgenic animals and plotted as a function of time (Fig. 2, left). The stimulus-evoked fractional fluorescence changes at the end of 2 s stimulus trains represent steady-state conditions. Other than during dynamic calcium concentration changes, at steady state the amplitude of an indicator's fluorescence change is independent of indicator concentration (see Discussion). Thus, amplitudes and SNR of fractional fluorescence changes were extracted at steady state and related to neural activity and  $\Delta[\text{Ca}^{2+}]_i$  (Fig. 2, right) as determined in the OGB-1 experiments (Fig. 1F). Time constants for the rise and decay were derived from single-exponential functions fitted to the respective phase of the 40 Hz response unless a given indicator showed saturation at this frequency. In these cases (OGB-1, D3cpv, and YC2.60), the 20 Hz responses were analyzed (see Discussion). Data represent mean  $\pm$  SEM. The eight GECIs performed as follows [summaries are given in Table 1 and supplemental Table 1].

YC3.3 (Fig. 2A): The dependence of SNR on  $[Ca^{2+}]_i$  is shown in Figure 3B. The lowest  $f_{AP}$  that still yielded fluorescence changes with an SNR > 2 was 20 Hz. Fitting these data allowed us to interpolate the minimum  $\Delta[Ca^{2+}]_i$  or  $f_{AP}$  at which a SNR of 2 would be reached. For YC3.3, this was the case at  $\Delta[Ca^{2+}]_i \sim 140$  nM/13 Hz (Fig. 3C). We observed a linear increase in the response up to 40 Hz and beginning saturation above.  $(\Delta R/R)_{max}$  was  $66.6 \pm 0.9\%$ , and the half-maximum  $\Delta R/R$ , corresponding to the  $K_D$ , was reached at  $\sim 38$  Hz or  $0.47 \mu M [Ca^{2+}]_i$  *in vivo* (Fig. 3A). Rise and decay displayed time constants of 1.41 and 1.05 s, respectively (Fig. 3D, Table 1) ( $48 < n < 63$ ).

YC3.60 (Fig. 2B) showed a fivefold higher  $\Delta R/R$  at 10 Hz stimulation compared with YC3.3 and the highest SNR of all GECIs (SNR > 3) at this frequency. SNR of 2 was reached at  $\Delta[Ca^{2+}]_i \sim 80$  nM/8 Hz (Fig. 3B,C).  $\Delta R/R$  increased linearly up to 40 Hz, and  $f_{AP} > 40$  Hz led to a sublinear increase in the signal amplitude with  $(\Delta R/R)_{max} = 135.8 \pm 4.4\%$ . The half-maximum response corresponds to  $\sim 30$  Hz stimulation or a  $K_D$  of  $0.36 \mu M$  *in vivo* (Fig. 3A). Rise and decay displayed time constants of 0.82 and 0.73 s, respectively (Fig. 3D, Table 1) ( $33 < n < 71$ ).

YC2.60 (Fig. 2C): A SNR of 2 was reached at  $\Delta[Ca^{2+}]_i \sim 100$  nM/9 Hz (Fig. 3B,C).  $\Delta R/R$  increased linearly up to 40 Hz. At 80 and 160 Hz, amplitudes increased sublinearly with  $(\Delta R/R)_{max} = 193.8 \pm 9.7\%$ , and the half-maximum response corresponds to  $\sim 32$  Hz or a  $K_D$  of  $0.40 \mu M$  *in vivo* (Fig. 3A). Responses of comparable size had previously not been reported for any ratiometric GECI *in vivo*. The response amplitudes may still be slightly underestimated, because a plateau was not fully reached after 2 s stimulation. However, SNR did not increase linearly (see Discussion), and the slow kinetics is disadvantageous for most experiments. A fit to the decay of the 20 Hz response showed a time constant of 5.24 s for the decay (single exponentials could not be fit to the rise) (Fig. 3D, Table 1) ( $29 < n < 30$ ).

D3cpv (Fig. 2D) is a reengineered variant of YC, whose sites of interaction with wild-type calmodulin were eliminated (see Discussion). SNR of 2 was reached at  $\Delta[Ca^{2+}]_i \sim 100$  nM/9 Hz (Fig. 3B,C).  $\Delta R/R$  increased sublinearly when frequencies exceeded 20 Hz and reached  $(\Delta R/R)_{max} = 89.7 \pm 3.9\%$ . The half-maximum response is reached at  $\sim 41$  Hz, reflecting a  $K_D$  of  $0.49 \mu M$  *in vivo* (Fig. 3A). Rise and decay of the 20 Hz

responses displayed time constants of 0.68 and 1.96 s, respectively (Fig. 3D, Table 1) ( $48 < n < 56$ ).

TN-L15 (Fig. 2E) uses the same chromophores as YC3.3 but troponin C as calcium binding moiety. SNR of 2 was reached at  $\Delta[\text{Ca}^{2+}]_i \approx 200 \text{ nM}/18 \text{ Hz}$  (Fig. 3B,C).  $\Delta R/R$  increased about linearly up to 40 Hz with  $(\Delta R/R)_{\text{max}} = 59.5 \pm 2.3\%$ . The half-maximum response is reached at  $\sim 30 \text{ Hz}$  or a  $K_D$  of  $0.36 \mu\text{M}$   $[\text{Ca}^{2+}]$  *in vivo* (Fig. 3A). Rise and decay displayed time constants 0.81 and 1.49 s, respectively (Fig. 3D, Table 1) ( $27 < n < 30$ ).

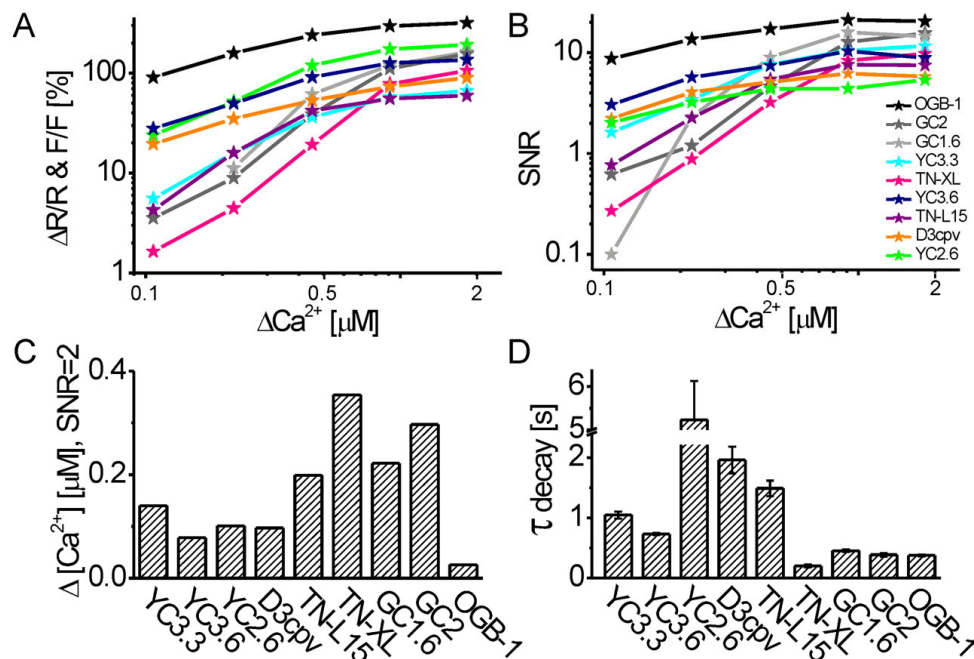


**Fig. 3:** Summary of the *in vivo* quantification of GECI and OGB-1 fluorescence changes at steady state. **A**, **B**, Side-by-side comparison of maximum fractional fluorescence changes (**A**) and SNR (**B**) plotted as a function of  $\Delta[\text{Ca}^{2+}]_i$  (logarithmic x- and y-axes). **C**,  $\Delta[\text{Ca}^{2+}]_i$  necessary to elicit a fractional fluorescence change with SNR of 2 under our recording conditions. **D**, Time constants for the decay of the fluorescence change, determined after 40 Hz stimulation (20 Hz for YC2.60, D3cpv, and OGB-1). Parameters in **A–C** were analyzed at steady state; OGB-1 data are from Figure 1, and GECI data are from Figure 2.

TN-XL (Fig. 2F) exhibited pronounced supralinear behavior at lower activity rates. SNR of 2 was reached at  $\Delta[\text{Ca}^{2+}]_i \approx 350 \text{ nM}/31 \text{ Hz}$  (Fig. 3B,C). Higher activity rates rapidly evoked a sublinear increase.  $(\Delta R/R)_{\text{max}}$  was  $105.9 \pm 2.7\%$ , and the half-maximum response corresponds to  $\sim 65 \text{ Hz}$  or a  $K_D$  of  $0.77 \mu\text{M}$  *in vivo* (Fig. 3A). TN-XL

responses showed time constants of 0.59 s for the rise and the fastest decay time constant of all GECIs with 0.20 s (Fig. 3D, Table 1) ( $48 < n < 87$ ).

GC1.6 (Fig. 2G): This single-chromophore GECI in our study exhibited  $\Delta F/F$  with SNR of 2 at  $\Delta[Ca^{2+}]_i \approx 220$  nM/20 Hz (Fig. 3B,C).  $\Delta F/F$  increased supralinearly with stimulus intensity up to 40 Hz and sublinearly above.  $(\Delta F/F)_{\max}$  was  $161.6 \pm 13.1\%$ , and the highest maximum SNR of all GECIs in this study was reached at 80 Hz ( $15.9 \pm 1.5$ ) (Fig. 3B). The half-maximum response was reached at  $\sim 54$  Hz or a  $K_D$  of  $0.64 \mu M$  *in vivo* (Fig. 3A). Time constants of 40 Hz responses were 1.38 s for the rise and 0.45 s for the decay (Fig. 3D, Table 1) ( $42 < n < 52$ ).

Finally, we generated UAS-GCaMP2 (Tallini et al., 2006; Díez-García et al., 2007) flies that carried the full cDNA (including his-tag) under control of the UAS. Live imaging with these GCaMP2-expressing flies was hardly possible because of the low baseline fluorescence of the indicator (Mao et al., 2008). Only 3 of  $\sim 50$  fly strains gave rise to high enough expression that it could be detected *in vivo* when animals were homozygous for both Gal4 and UAS-GCaMP2. The fractional fluorescence changes recorded with GC2 mostly mimicked those exhibited by GC1.6 (Fig. 2G). However, an SNR of 2 was only reached at stimulus frequencies  $> 20$  Hz ( $\Delta[Ca^{2+}]_i \approx 300$  nM/27 Hz) (Fig. 3B,C).  $\Delta F/F$  increased supralinearly with stimulus intensity up to 20 Hz, then linearly up to 80 Hz.  $(\Delta F/F)_{\max}$  was  $155.7 \pm 4.2\%$  with an SNR of  $15.6 \pm 1.5$  (Fig. 3A,B). This corresponds to a  $K_D$  of  $0.75 \mu M$  *in vivo* ( $\sim 63$  Hz), which is close to the  $K_D$  of GC1.6. Time constants of 40 Hz responses were 0.63 s for the rise and 0.38 s for the decay (Fig. 3D, Table 1) ( $30 < n < 58$ ).

### ***In vitro* versus *in vivo* response characteristics of GECIs at steady state**

We assessed the influence of the cellular environment on the signaling properties of the GECIs and OGB-1. We measured fluorescence changes at defined  $\Delta[Ca^{2+}]_i$  exhibited by purified GECI protein in the cuvette of a spectrophotometer and compared it to our measurements *in vivo* (Fig. 4). Two corrections were applied to the cuvette data to allow this comparison: first, the bandpass filters in the detection pathway of the 2PLSM were mimicked; and second, baseline  $[Ca^{2+}]_i$  *in vivo* was taken into consideration (see Materials and Methods). Because fluorescence changes of single and dual wavelength indicators are both expressed as changes relative to

baseline fluorescence,  $[Ca^{2+}]$  at baseline limits the maximum fluorescence change and the signaling capacity of an indicator, in particular for low- $K_D$  indicators (see Discussion).

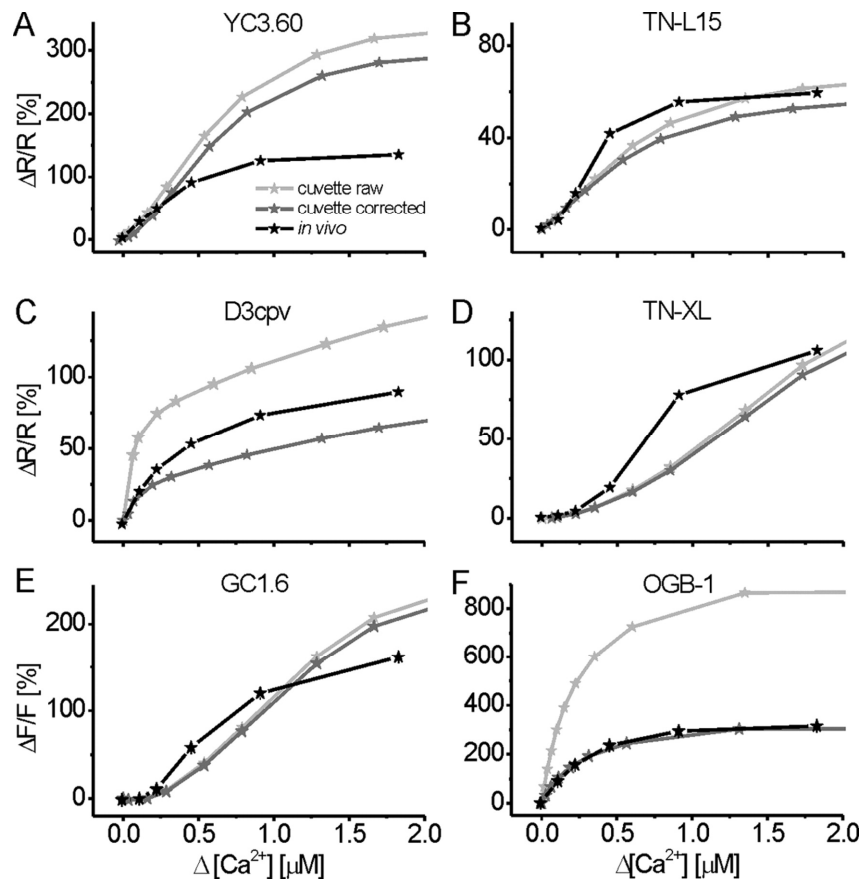


**Fig. 4:** *In vivo* versus *in vitro*: quantitative comparison of fractional fluorescence changes of GECIs and OGB-1 at steady state. GECI and OGB-1 fluorescence changes were analyzed at the end of stimulus trains in presynaptic boutons of transgenic larvae (black traces) and compared with the purified protein and OGB-1 in solution in the cuvette. **A**, YC3.60; **B**, TN-L15; **C**, D3cpv; **D**, TN-XL; **E**, GC1.6; **F**, OGB-1. Fractional fluorescence changes ( $\Delta R/R$  and  $\Delta F/F$ ) *in vivo* (black traces) are compared with *in vitro*  $\Delta R/R$  and  $\Delta F/F$  calculated from spectrophotometer data either directly (light gray traces) or after applying corrections (dark gray traces; see Materials and Methods). Correction was done for the resting calcium concentration and the width of the bandpass filters in the detection pathway of the 2PLSM. Both corrections significantly reduce  $F_{max}$ , which is most obvious for the synthetic indicator OGB-1 (**F**). Applying these corrections, the fluorescence change of OGB-1 *in vivo* matches perfectly the one observed *in vitro*. All GECIs show significant deviations of *in vivo* from *in vitro* (**A–E**), the origin of which remains to be investigated. However, the applied corrections cancel out effects of the applied imaging conditions, and the remaining differences between GECIs probably represent interactions with the chemical environment.

Thus, both corrections reduce the magnitude of the fluorescence responses (Fig. 4). This effect can be seen for all GECIs (Fig. 4A–E) and OGB-1 (Fig. 4F) by comparing uncorrected (light gray traces) with corrected (dark gray traces) spectrophotometer data. Most importantly, deviations of the corrected spectrophotometer data from the data acquired in presynaptic boutons (Fig. 4, black traces) can likely be attributed to interactions of the indicator with the intracellular environment (see Discussion).

At low  $\Delta[\text{Ca}^{2+}]_i$ , YC3.60 showed rather similar response properties *in vitro* and *in vivo* (compare Figs. 2B, 4A). YC3.60 was identified as most promising GECI in this study for the detection of low rates of activity or small  $\Delta[\text{Ca}^{2+}]_i$ . However, above  $0.25 \mu\text{M} \Delta[\text{Ca}^{2+}]_i$  ( $f_{\text{AP}} > 20 \text{ Hz}$ ), the large fluorescence changes *in vitro* were not retained *in vivo* (Fig. 4A). However, Figure 4A indicates a relatively large dynamic range (notice the linear scaling of the x-axis in Fig. 4) over which neural activity is reported about linearly (up to  $\Delta[\text{Ca}^{2+}]_i$  of  $0.4 \mu\text{M}/40 \text{ Hz}$ ). Such linear regimes with high signaling capacity were less pronounced in D3cpv, TN-L15, and TN-XL (Fig. 4B–D): D3cpv saturated more quickly, whereas the troponin-C-based GECIs exhibited more complex binding curves *in vivo* with supralinear and sublinear regimes. Interestingly, these three indicators showed larger  $\Delta R/R$  *in vivo* (black curves) than *in vitro* (dark gray curves) when  $\Delta[\text{Ca}^{2+}]_i$  exceeded  $0.25 \mu\text{M}$  (Fig. 4B–D). Also, GC1.6 responses exhibited complex  $\text{Ca}^{2+}$ -binding dynamics (Fig. 4E), and at  $\Delta[\text{Ca}^{2+}]_i > 1 \mu\text{M}$ , the observed GC1.6 responses were smaller *in vivo*. However, *in vivo* responses higher than *in vitro* were observed within a certain range ( $0.2 < \Delta[\text{Ca}^{2+}]_i < 1 \mu\text{M}$ ). The mechanistic interpretations of these findings remain to be given. The comparison of OGB-1 between the cuvette and *in vivo* (Fig. 4F) convincingly demonstrates that the applied methods are suitable to make significant statements on calcium indicator properties *in vivo* and *in vitro*: the applied corrections reduced the original *in vitro*  $\Delta F/F$  of OGB-1 (light gray trace) as expected, and the obtained curve (dark gray trace) matches the *in vivo* data (black trace) over the full range of  $\Delta[\text{Ca}^{2+}]_i$ . The maximum fluorescence change is thus identical under both conditions. However, because the calibration was done using OGB-1 *in vitro*, effects of the cellular environment on the  $K_D$  of OGB-1 may be hidden (see Discussion).

From the data described so far, the  $K_D$  value and the Hill coefficient of the different GECIs were calculated (supplemental Fig. 1B,C; Table 1). For all GECIs that we



measured under both conditions, the  $K_D$  was significantly decreased *in vivo* (supplemental Fig. 1B). Moreover, the differences in the  $K_D$  values of the individual GECIs were less pronounced *in vivo*. Thus, as a rule of thumb, the *in vivo*  $K_D$  of GECIs appears to be shifted toward higher affinity compared with our *in vitro* calibration [with YC2.60 and GC2 being the only exception, because they were not calibrated in cuvettes in our lab, and the *in vitro*  $K_D$  values were taken from literature (Nagai et al., 2004; Tallini et al., 2006)]. For the Hill coefficient (supplemental Fig. 1C), the picture is slightly more complex. However, there is a systematic change too. *In vivo*, the Hill coefficient of GECIs based on wild-type calmodulin (GC1.6, YC2.60, and YC3.60; no data available on YC3.3) is decreased. This finding is in line with  $[Ca^{2+}]$ -dependent interactions of GECI proteins with native wild-type proteins: at higher  $[Ca^{2+}]$  concentrations, such interactions are favored, interfering with GECI function. In contrast, D3cpv and the troponin-C-based indicators TN-L15 and TN-XL showed higher Hill coefficients *in vivo*, indicative of increased cooperativity of calcium binding to the indicator.

#### **Fluorescence changes of GECIs and OGB-1 in response to short $Ca^{2+}$ transients *in vivo***

The combination of concentration, sensitivity, and speed of the fluorescence transition kinetics determines how well transient calcium fluctuations can be resolved by a fluorescent indicator. The favorable combination of backward binding rate ( $K_b$ ) and forward binding rate ( $K_f$ ) allows some synthetic  $Ca^{2+}$  indicators to report neuronal activity with single action potential resolution (Schiller et al., 1995; Helmchen et al., 1996, 1997; Maravall et al., 2000). In contrast, cytosolic GECIs were reported to lack sufficient SNR and  $Ca^{2+}$  binding kinetics to report individual APs (Pologruto et al., 2004; Reiff et al., 2005) (but see Díez-García et al., 2007). We assessed the capacity of cytosolic GECIs and OGB-1 to signal a transient increase in  $[Ca^{2+}]_i$  in presynaptic boutons of transgenic *Drosophila* by 2PLSM fluorescence recordings at high temporal resolution.

In a first set of experiments, we chose TN-XL for its fast decay time constant (Fig. 3D) and evoked APs at 10, 20, and 40 Hz over a period of 4 s. The power spectra of the fractional fluorescence changes did in no case reveal significant peaks corresponding

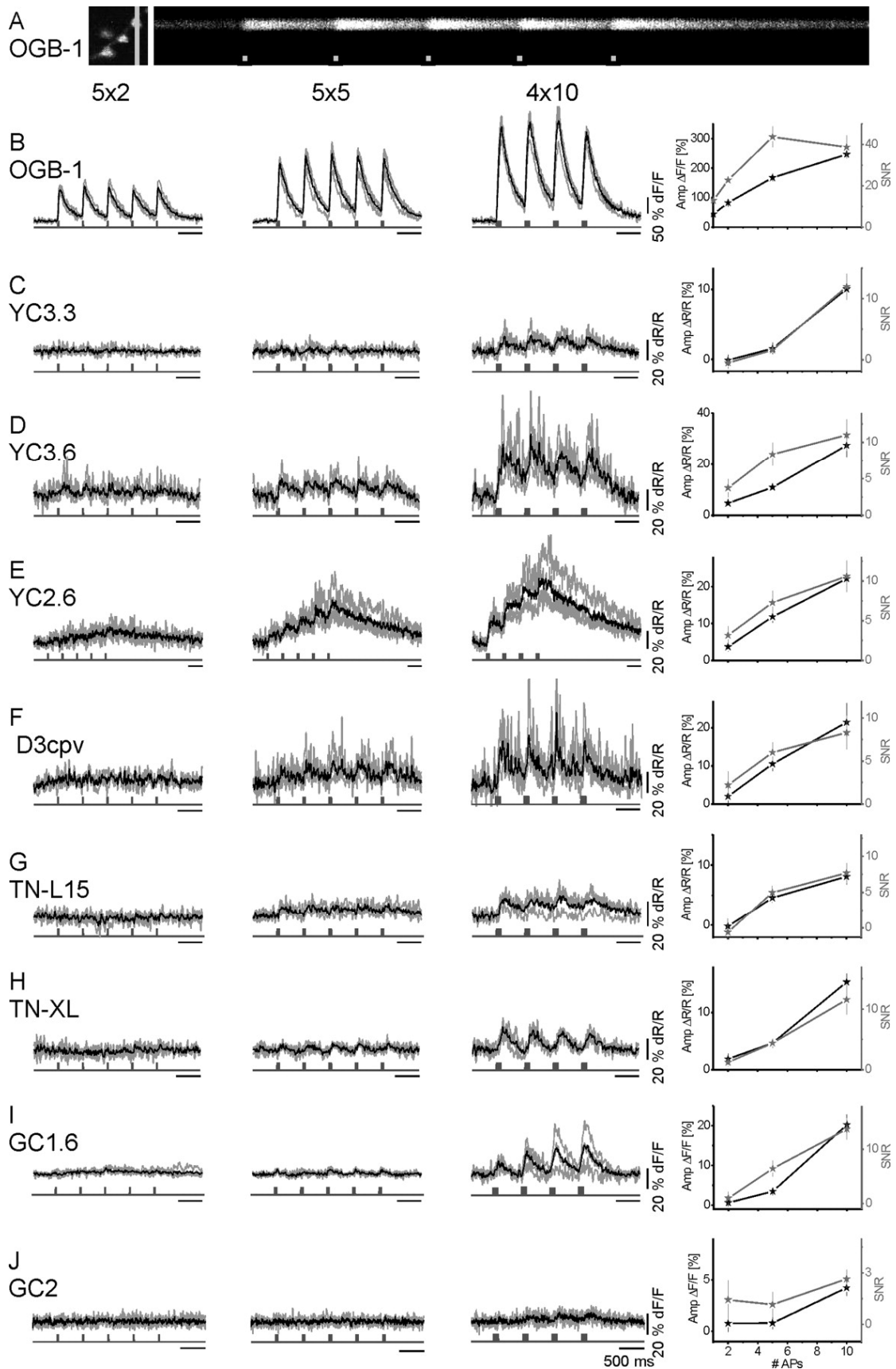


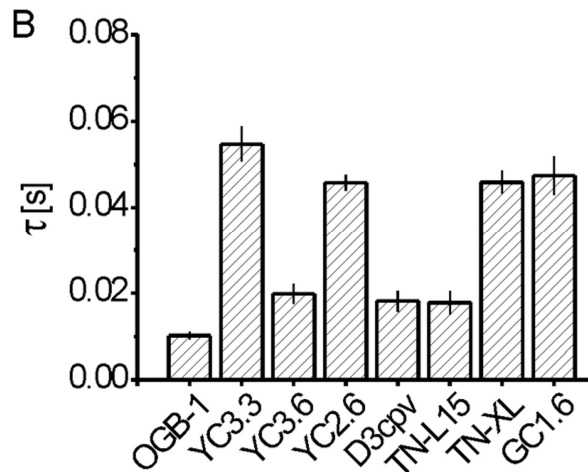
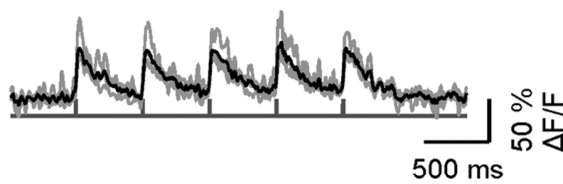
**Fig. 5:** *In vivo* comparison of fluorescence transients of GECIs and OGB-1 in response to short AP volleys. GECIs and OGB-1 fluorescence changes were recorded in response to biologically more realistic stimuli. Nerves were stimulated with short AP

sequences. **A**, 2PLSM recording in line-scan mode at an acquisition rate of 500 Hz. Left, Close-up of a small branch of a larval NMJ showing several boutons labeled with OGB-1. Position of the line scan is indicated by the light gray line. Right, Raw line-scan data show transient fluorescence increases evoked by calcium influx during AP volleys (light gray squares, 5 APs at 100 Hz/volley; x-axis represents time). Calibration, 200 ms. **B–J**, OGB-1 (**B**) and GECI (**C–J**) recording traces. AP volleys were spaced by 500 ms. Within a volley, APs were elicited at 100 Hz in packs of 2, 5, and 10 APs per volley (first, second, and third columns, respectively). Shown are four individual recording traces from different boutons (gray) and their mean (black). The maximum amplitude of the mean fluorescence response is plotted against the number of APs per volley (mean  $\pm$  SEM). In addition, the average SNR of single responses to single AP volleys is plotted. Only OGB-1 reliably reported single APs (SNR of  $>15$ ; see **B** and supplemental Fig. 3A, supplemental Table 1).

to the action potential frequency (supplemental Fig. 2A). Similar measurements in OGB-1 filled boutons revealed clear stimulus-related peaks for 10 and 20 Hz experiments (supplemental Fig. 2B,C), whereas individual APs at 40 Hz and higher activity rates were masked by the rather slow time constant for the fluorescence decay of OGB-1 (supplemental Fig. 2D). Next, we evoked brief volleys of 2, 5, and 10 APs (Fig. 5) (APs separated by 10 ms, volleys by 500 ms). OGB-1 reported even single action potentials with  $43.6 \pm 2.5\%$   $\Delta F/F$  and SNR  $> 15$  (Fig. 6A). Volleys of 2, 5, and 10 APs were reported with increasing  $\Delta F/F$  and SNR (Fig. 5B). SNRs were calculated for each individual burst and given as the average of all bursts from the four traces. In contrast to OGB-1, no GECI responded to transient  $\Delta[Ca^{2+}]_i$  associated with single spikes. Spike doublets were reported with SNR  $> 3$  only by YC3.60 and YC2.60. D3cpv provided SNR of 2.2. Only YC3.3 and GC2 failed to report volleys of five APs. Volleys of 10 APs were reported by all GECIs, although with widely differing amplitudes, SNRs, and rise times (Figs. 5C–J, 6B; supplemental Table 1).

In a last series of experiments, we expressed GECIs in tangential neurons of the optic lobe of adult flies and recorded fluorescence changes in response to bath-applied high-KCl solution (Fig. 7). All GECIs exhibited fluorescence changes under these conditions. However, the fluorescence responses elicited by the rather strong stimulation with 100 mM KCl were relatively small. This might be explained by only small  $\Delta[Ca^{2+}]_i$  in the analyzed neurons and/or high rates of neural activity at rest and resulting high levels of baseline  $[Ca^{2+}]_i$  before KCl application.

A OGB-1 5x1 AP



the exception of YC2.60. The latter may be because of very high protein concentration. Time constants were determined for data from  $t = 0$  to the peak of the response to the first volley fit by a single-exponential function.

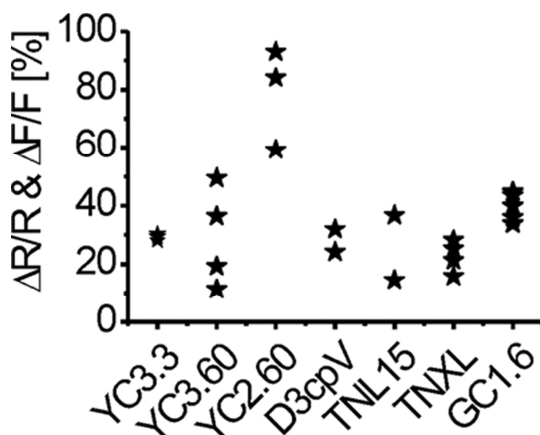


**Fig. 7:** GECI responses in the adult CNS *in vivo*. All GECIs reproducibly exhibited fluorescence changes in the CNS of adult *Drosophila* flies. GECIs were expressed in a subset of large tangential neurons (and few unknown interneurons) of the optic lobe (genotype, DB331-Gal4→UAS-GECI). Details of the preparation were given by Joesch et al. (2008). In short, a young female fly was glued to a holder and its head was bent down such that its back side faced upward. The back side of the

head was opened up to expose the caudal optic lobes with GECI-expressing neurons. The preparation was covered with Ringer's solution and imaged for 33 s using wide-field epifluorescence microscopy. During the experiment, the external potassium concentration was raised to 100 mM. Fluorescence responses were recorded at somata and axons of the large tangential cells. Each data point represents the maximum fluorescence change recorded in one animal. Before calculation of the fractional fluorescence changes, motion artifacts were reduced by alignment of the sequential images. DB331-Gal4 flies were a generous gift from Reinhard Stocker, University of Fribourg, Fribourg, Switzerland.

Nevertheless, the result suggests that our experimental findings in larval motoneurons can be generalized to neurons in the CNS of adult flies (Jayaraman and Laurent, 2007). However, these experiments do not allow a more quantitative analysis of GECI signaling properties in terms of amplitudes and kinetics.

## 5. Discussion

The advent of optical recording with genetic probes triggered a renaissance for systemic neuroscience in invertebrates and in particular in *Drosophila*, in which genetic probes can be combined with circuit-breaking genetic tools (Marella et al., 2006; Holmes et al., 2007). Hence, we used *Drosophila* neurons as a testing ground to compare eight different GECIs *in vivo* that can similarly be applied to neurons in vertebrates.

Meaningful optical recordings rely on the faithful interpretation of fluorescence changes with respect to the underlying neural activity and  $[Ca^{2+}]_i$ . This relationship has been reported to be notoriously difficult to interpret when using GECIs (Hasan et al., 2004; Pologruto et al., 2004; Reiff et al., 2005; Jayaraman and Laurent, 2007; Tay et al., 2007). At best, fluctuations in  $[Ca^{2+}]_i$  represent a low-pass filtered version of fluctuations in the membrane potential. The  $\Delta[Ca^{2+}]_i$  is then reported by GECI signals with rather small amplitude and low SNR that, depending on the GECI concentration and  $K_D$  value, become further distorted. Thus, the spatial and temporal relationship between neural activity and GECI signals is far from trivial, which will be discussed here.

### Steady state

In Calcium imaging studies, fluorescence changes are commonly expressed as changes relative to baseline  $(F_t - F_0)/F_0$  ( $F_0$  is fluorescence at baseline, and  $F_t$  is fluorescence at time  $t$ ). Thus,  $[Ca^{2+}]_i$  at baseline reduces  $(\Delta F/F)_{\max}$  and the signaling capacity of the indicator by increasing  $F_0$ . The signaling capacity is highest within the dynamic range of an indicator where  $\Delta[Ca^{2+}]_i$  is reported by a linear increase in  $\Delta F$  of maximum magnitude. Thus, the dynamic range of the indicator should ideally match the regime of expected  $\Delta[Ca^{2+}]_i$  that are superimposed on a given  $[Ca^{2+}]_i$  at baseline. Furthermore, the rate constants for binding and unbinding of Calcium to the

indicator must be fast enough to allow detection of short  $\Delta[\text{Ca}^{2+}]_i$  transients [Borst and Abarbanel (2007), their Equation 10], and indicators should exhibit bright fluorescence and large  $\Delta F$  to provide a good SNR. Following these guidelines, we can rank the eight GECIs for their capability to report  $\Delta[\text{Ca}^{2+}]_i$  at steady state and thus to report different rates of sustained neural activity (Yasuda et al., 2004).

In presynaptic boutons of *Drosophila*,  $\Delta[\text{Ca}^{2+}]_i$  of 10–11 nM/AP were superimposed on  $[\text{Ca}^{2+}]_i$  at rest of 31 nM (Fig. 1). Small  $\Delta[\text{Ca}^{2+}]_i$  were reported best by YC3.60 (Fig. 3C), and higher  $\Delta[\text{Ca}^{2+}]_i$  fell within the broad dynamic range of this indicator (Fig. 4A, black trace). Also D3cpv reported small  $\Delta[\text{Ca}^{2+}]_i$  quite well but showed a narrow dynamic range. YC2.60 provided fluorescence changes of magnitude similar to YC3.60 (Figs. 2, 4), but lower SNR (for discussion of SNR, see below). YC3.3, TN-L15, TN-XL, GC1.6, and GC2 did not allow detection of small  $\Delta[\text{Ca}^{2+}]_i$  from baseline. Nevertheless, the large maximum fluorescence change and high SNR in GCaMPs and TN-XL and their  $K_D$  makes these GECIs valuable indicators to address large  $\Delta[\text{Ca}^{2+}]_i$  or medium  $\Delta[\text{Ca}^{2+}]_i$  superimposed on high  $[\text{Ca}^{2+}]_i$  at rest. However, their capricious  $\text{Ca}^{2+}$ -binding dynamics (Fig. 4), with sublinear and supralinear regimes (Pologruto et al., 2004; Reiff et al., 2005), and the increase in  $\Delta F/F$  with repetition of AP volleys (Fig. 5) have to be taken into account.

### SNR

The calculated SNR values do only partially represent an endogenous property of the indicator (see below). The SNR is also dependent on all parameters of the imaging setup (e.g., laser intensity, pixel dwell time, photon noise, and collection efficiency), on the imaged volume, and on the indicator concentration (SNR depends on the square root of the number of detected photons). The only of these variables that we could neither hold constant nor measure was the concentration of the GECIs in boutons *in vivo*, a problem that will be faced by most experimenters, too. Instead we aimed for a high expression level of each GECI *in vivo* using constant copy numbers for Gal4 and the UAS-GECI (see Materials and Methods), which probably comes closest to the strategy typically used in *in vivo* imaging experiments that involve GECIs. Thus, the given SNR values represent useful landmarks that reflect the mixed properties of the GECI (see below) and a given fly strain, i.e., expression level.

It has to be noted that the indicator concentration influences in addition how fast steady state is achieved inside a bouton (see below). But it does not influence the level of this steady state (including  $[Ca^{2+}]_{i \text{ Rest}}$ ), which is an exclusive function of the driving forces for Calcium influx and efflux (Borst and Abarbanel, 2007).

### Signal kinetics

So far, we have mostly considered the nondynamic features of  $\Delta F$  when Calcium influx and efflux are in equilibrium and the concentration of Calcium-bound-indicator is constant. However, GECIs should ideally report individual APs with sufficient SNR in a quantitative manner (Wallace et al., 2008; Mao et al., 2008). This property is limited by the concentration of the indicator and the forward and backward binding rates that define the  $K_D$  as  $K_D = K_b/K_f$  (Schiller et al., 1995; Tank et al., 1995; Helmchen et al., 1996, 1997; Maravall et al., 2000; Borst and Abarbanel, 2007). A high indicator concentration slows down the time constant of the fluorescence signal and thus reduces the magnitude of the fluorescence response during a single AP. Also, in experiments using long stimulus trains (Figs. 2, 3D), the indicator concentration can affect the time constants of the rise and decay. However, exemplary calculations for the two GECIs TN-L15 and TN-XL show that their kinetics are dominated by their binding rates and are largely independent of the indicator concentration (supplemental Fig. 3). Whatever the reason for the given kinetics might be, i.e., binding rates or indicator concentration, time constants close to those presented here can be expected if GECIs are expressed at a level that enables *in vivo* imaging.

In addition, the rise and decay time in these experiments is affected by indicator saturation. If the steady state  $[Ca^{2+}]$  is far below the  $K_D$  of an indicator, the system is linear and the time constants for the rise and the decay are equal. If the steady-state Calcium concentration approaches the  $K_D$  of an indicator or even exceeds it, the rise will appear faster and the decay slower compared with the linear case (Borst and Abarbanel, 2007). We thus analyzed time constants from steady-state responses in the linear regime of the indicators (20 and 40 Hz stimuli).

### Transient neural activity

OGB-1 allowed the detection of a single AP with an average SNR > 15 (Figs. 5B, 6A). No GECI allowed the detection of single spikes. Volleys of two APs were tentatively

reported by YC3.60, YC2.60, and D3cpv (Fig. 5; supplemental Table 1). Significant further improvements leading to GECIs with faster reaction kinetics and very high  $K_D$  are required, in particular when tagged GECIs and the assessment of short-lived, large  $\Delta[\text{Ca}^{2+}]_i$  in spatially restricted microdomains are considered (Schneeggenburger and Neher, 2005). The recently achieved rapid fluorescence decay of TN-XL *in vivo* ( $\tau_{\text{TN-XL}} = 200$  ms;  $\tau_{\text{OGB-1}} = 380$  ms) (Fig. 3D) and differences in  $K_f$  of two to three orders of magnitude (Miyawaki et al., 1997; Naraghi, 1997) suggest that Calcium binding can be further modified in future GECIs. The low sensitivity and short decay time of TN-XL and the failure of the high-sensitivity GECIs YC3.60, YC2.60, and D3cpv to report  $\Delta[\text{Ca}^{2+}]_i$  associated with single spikes suggest that the on rate of Calcium binding to GECIs is the current bottleneck for the detection of fast Calcium transients.

A further difficulty in the detection of  $\Delta[\text{Ca}^{2+}]_i$  associated with a single AP arises from the large volume ( $\sim 2\text{--}70 \mu\text{m}^3$ ) of type 1b boutons (Hoang and Chiba, 2001) that causes small-volume-averaged  $\Delta[\text{Ca}^{2+}]_i$  compared with boutons of  $\sim 0.04 \mu\text{m}^3$  in the mouse brain (Schikorski and Stevens, 1997). Such differences might explain why GC2 came close to the detection of single APs when large populations of fibers and boutons were imaged simultaneously in the mouse cerebellum (Díez-García et al., 2007).

### **Ratiometric and single-chromophore GECIs**

Ratiometric analysis reduces motion artifacts and eliminates correlated noise in the two monitored signals, whereas uncorrelated noise can be increased, in particular under photon-limited conditions (then, a single-chromophore GECI might provide lower noise). In CFP/YFP pairs, the FRET efficiency can reach up to 98% (Shimozono et al., 2006). Then, the denominator in the emission ratio  $r = \text{YFP}/\text{CFP}$  approaches zero, which gives rise to noise and low SNR as in YC2.60 (Figs. 2, 3). Single-chromophore GCaMPs showed the highest SNR of all GECIs at high  $\Delta[\text{Ca}^{2+}]_i$  (SNR > 15).

### ***In vivo* versus *in vitro***

Shortcomings of GECIs *in vivo* have been attributed to interactions of the GECIs calmodulin and the calmodulin-binding peptide (Hasan et al., 2004) with cellular calmodulin [10–100  $\mu\text{M}$  (Xia and Storm, 2005)] and calmodulin-regulated proteins



(Mori et al., 2004). Complementary modification of the relevant interaction sites within the binding interface of calmodulin and M13 (Palmer et al., 2006), or replacement of calmodulin-M13 by troponin C (Heim and Griesbeck, 2004; Mank et al., 2006), should reduce such interactions. Our comparison of *in vivo* and *in vitro* responses supports the relevance of such interactions. GECIs that use wild-type calmodulin-M13 (YC3.60 and GC1.6) showed reduced  $\Delta F_{\max}$  and a reduced Hill coefficient *in vivo*, whereas  $\Delta F_{\max}$  of troponin-C-based GECIs and D3cpv was retained, and the Hill coefficients were increased *in vivo* (Fig. 4; supplemental Fig. 1B,C).

### **Injection of synthetic dyes in *Drosophila* and $[Ca^{2+}]_i$ estimation**

*Drosophila* is a classic model organism for studies on learning and memory (Quinn et al., 1974) and their underlying molecular mechanisms (Lin and Goodman, 1994). More recently, GECIs are increasingly used to study information processing in intact neural circuits of the *Drosophila* brain. Thus, we expect that the described dye injection into genetically labeled neurons is highly useful for the calibration of other neurons too.

Our calibration produced results that are in good accordance with previous work at the *Drosophila* NMJ (Macleod et al., 2004). Because we took the  $K_D$  of OGB-1 from our *in vitro* calibration, factors that influence indicator performance, such as the ionic strength, osmolarity, pH, and protein environment differed from the *in vivo* situation. This may lead to an underestimation of the *in vivo*  $K_D$  for OGB-1 (Thomas et al., 2000). Assuming a twofold higher *in vivo*  $K_D$  of OGB-1 compared with our measurement in the cuvette would result in a twofold increase of  $[Ca^{2+}]_i$  both at rest and at steady state during prolonged stimulation, as well as twofold higher *in vivo*  $K_D$  values of the GECIs. Earlier measurements of  $[Ca^{2+}]_{i \text{ Rest}}$  suggest that this is rather unlikely (Macleod et al., 2004).

### **Concluding remarks**

Since the first prototypic GECIs were published (Miyawaki et al., 1997; Nakai et al., 2001), GECIs have been improved with respect to bright fluorescence, increased FRET efficiency, decreased FRET at resting  $[Ca^{2+}]_i$ , reduced magnesium sensitivity,  $K_D$ , and response time constants. Still all GECIs exhibit low fluorescence and quantum

yield compared with synthetic indicators. Thus, to yield sufficient SNR, more molecules per volume are needed, which increases the external buffer capacity. This is even more the case because a single GECI molecule binds up to four  $\text{Ca}^{2+}$  ions, which in addition may cause higher-order reaction kinetics. The latter becomes evident when  $\Delta F$  is rather "loosely" related to activity and  $[\text{Ca}^{2+}]_i$ . Some of these aspects were improved in YC3.60 and D3cpv, making these indicators most sensitive for the detection of small  $[\text{Ca}^{2+}]_i$  and low rates of activity. Most importantly, those improvements were largely retained *in vivo*. GECIs such as GCaMPs and TN-XL, with their particular  $K_D$ , Hill coefficient, and fluorescence time course, are suitable for different experimental demands. Thus, selecting a particular GECI by matching its *in vivo* properties to the expected  $[\text{Ca}^{2+}]_i$  of the experimental system provides a promising way to decipher changes in neuronal activity in intact organisms.

## 6. Supplement

Stimulus	YC3.3	YC3.60	YC2.60	D3cpv	TN-L15	TN-XL	GCaMP1.6
10Hz, 2s amp	5.6± 0.5	27.9± 2.9	25.1± 2.9	20.1± 2.2	4.3± 1.2	1.6± 0.5	-0.4± 1.3
SNR	1.6± 0.2	3.0± 0.4	2.4± 0.4	2.4± 0.2	0.8± 0.2	0.3± 0.1	0.1± 0.3
20Hz, 2s amp	15.9± 0.4	49.7± 3.1	54.5± 5.3	35.4± 1.8	16.0± 2.0	4.5± 0.6	11.2± 1.2
SNR	3.4± 0.2	5.7± 0.7	3.5± 0.3	4.1± 0.3	2.3± 0.3	0.9± 0.1	2.3± 0.2
40Hz, 2s amp	36.2± 0.9	90.9± 5.2	125.7± 8.1	53.4± 2.3	41.9± 2.7	19.3± 1.2	61.7± 4.4
SNR	7.6± 1.0	7.4± 0.8	4.8± 0.4	5.3± 0.4	5.4± 0.6	3.2± 0.2	8.6± 1.1
80Hz, 2s amp	57.4± 1.0	125.9± 4.1	179.0± 11.6	73.4± 3.0	55.7± 1.8	77.9± 3.9	119.9± 4.8
SNR	10.5± 0.7	10.4± 1.0	4.6± 0.4	6.5± 0.7	7.6± 0.9	8.3± 0.6	15.9± 1.5
160Hz, 2s amp	66.6± 0.9	135.8± 4.4	193.9± 9.7	89.7± 3.9	59.5± 2.3	105.9± 2.7	161.6± 13.1
SNR	11.7± 1.1	8.9± 0.6	5.6± 0.4	5.9± 0.3	7.5± 1.0	9.8± 0.5	14.4± 1.2
2ap, 100Hz							
amp	-0.1± 0.8	4.7± 4.6	3.7± 1.3	2.0± 2.4	-0.9± 1.0	1.9± 1.0	0.6± 0.5
SNR	-0.6± 1.0	3.7± 1.3	3.2± 1.2	2.2± 1.6	0.2± 1.0	1.2± 0.7	1.0± 1.2
5ap, 100Hz							
amp	1.5± 0.9	10.9± 1.4	11.8± 1.6	10.5± 1.9	5.9± 0.9	4.7± 0.6	3.5± 0.4
SNR	1.6± 0.8	8.4± 1.6	7.3± 1.5	6.0± 1.2	8.3± 2.3	4.4± 0.8	6.4± 1.4
10ap, 100Hz							
amp	10.0± 1.5	27.4± 1.3	22.2± 2.5	21.4± 5.1	9.5± 1.1	15.3± 1.5	20.2± 2.6
SNR	12.0± 2.1	11.0± 2.2	10.6± 2.0	8.3± 2.0	9.5± 2.8	11.5± 2.5	13.7± 2.0

**Table S1: Summary of amplitude and SNR of fluorescence changes at steady state and during transient activity.** Stimulus protocols are indicated in the column to the left and are described in more detail in the text. In each cell the first line indicates the peak amplitude of the fluorescence change  $\pm$  SEM in %  $\Delta R/R$  and %  $\Delta F/F$  for GCaMPs, respectively. Second line indicates SNR. Data are represented in Fig. 2, 3 & 5.

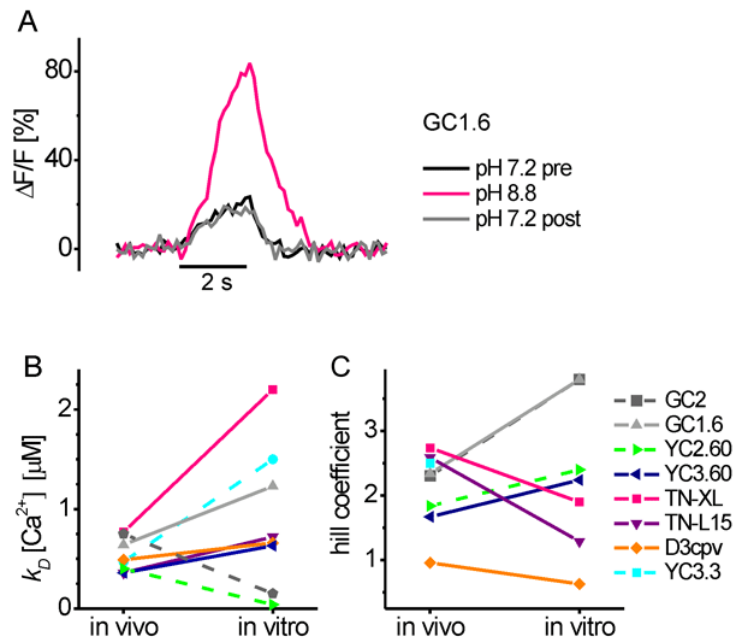


**Fig. S1: (A) Effect of extracellular pH on the Ca<sup>2+</sup>/H<sup>+</sup> exchanger.** A GC1.6 expressing NMJ was stimulated at 40 Hz. At this frequency the evoked  $\Delta$  [Ca]<sub>i</sub> are within the linear regime of GC1.6 (Fig. 2 G). Presynaptic boutons showed fractional fluorescence changes of  $19 \pm 2$  %  $\Delta F/F$  at pH 7.2 that increased to  $71 \pm 3$  %  $\Delta F/F$  at pH 8.8. This effect was fully reversible when returning to pH 7.2 again ( $17 \pm 4$  %  $\Delta F/F$ ;  $n=15$  GC1.6 expressing boutons). **(B) KD and (C) Hill-coefficient of GECIs *in vivo* and *in vitro*.** **(B)** The *in vivo* KDs of all GECIs were determined from our experiments in the *Drosophila* larva. The *in vitro* KDs were determined in cuvette measurements for all GECIs but YC2.6, YC3.3 and GC2 (dashed lines), whose *in vitro* KDs were taken from literature. Differences between the KD values of the individual GECIs *in vitro* appear to be smaller *in vivo*. Moreover, the data suggest a shift of the KD towards lower calcium concentrations *in vivo*. Only for YC2.6 and GC2, that were both not calibrated *in vitro* in our lab, the reverse seems to be true. However, it is very likely that an *in vitro* calibration of GC2 under our conditions would have revealed a much higher KD close to the one of GC1.6. **(C)** Hill-coefficients of all GECIs. The results suggest that indicators based on wild-type calmodulin (GCaMPs, YC2.60 and YC3.60) possess a lower Hill-coefficient *in vivo* as compared to *in vitro* (YC2.60 and GC2 data taken from literature, no *in vitro* data on YC3.3 available). In contrast, Hill coefficients seem to be increased *in vivo* in GECIs employing calcium binding moieties other than wild-type calmodulin (TN-L15, TN-XL and D3cpv). See also Table 1.

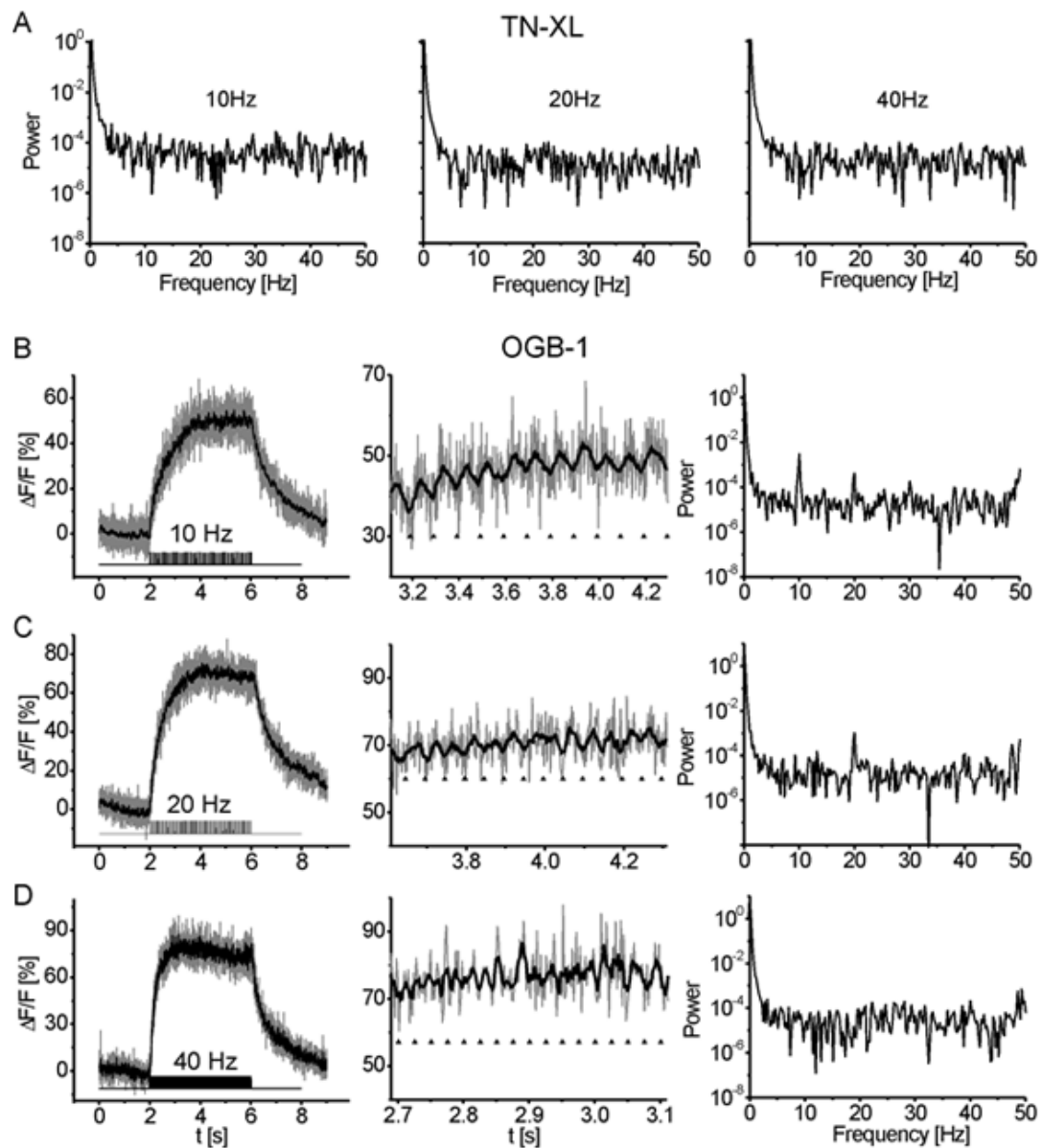


**Fig. S2: Power spectra of fluorescence recordings from TN-XL and OGB-1 during trains of action potentials.** Nerves were stimulated with trains of APs at indicated frequencies over a period of 4 s. Boutons were imaged in line scan mode at 500 Hz sampling rate. **(A)** Power spectra of the recorded fluorescence from boutons expressing TN-XL revealed no sign of the stimulus frequency. **(B)** Power spectra of OGB-1 fluorescence from injected boutons showed stimulus related peaks at 10 Hz and **(C)** 20 Hz. **(D)** No sign of the stimulus frequency at 40 Hz AP frequency. In B-D the left panels show the fractional fluorescence changes of OGB-1 plotted as a function of time. The middle column shows a blow up of these traces. Triangles under the fluorescence trace indicate APs. The right panels show the power spectra of the fractional fluorescence changes recorded during the stimulation period.

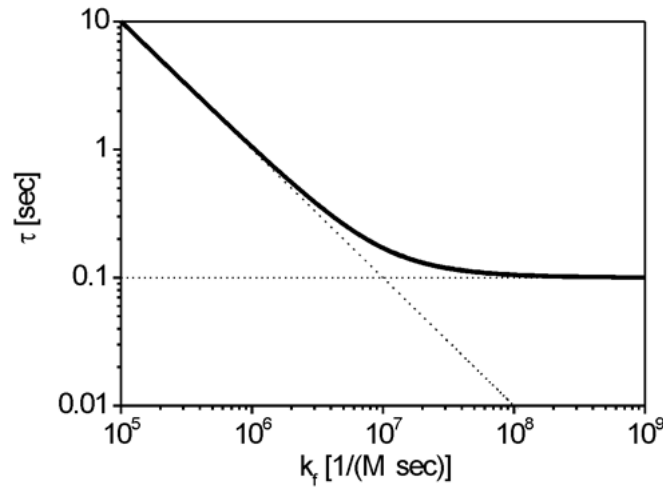


**Fig. S3:** Indicator kinetics are determined by (a) the intrinsic binding rates of the indicator and (b) the concentration of the indicator. Here we show for two of the indicators, i.e. TN-L15 and TN-XL where the binding rates are known, that the time-constants shown in Figure 3 D are largely independent of the indicator concentration. The exact relationship between the time-constants for rise and decay, the binding rates and indicator concentration is given by eq (14) and Figure 1 B in Borst and Abarbanel (2007) for the linear case, i.e. Calcium concentrations much smaller than the  $K_D$  of the indicator. There, one can see that the time-constants for rise and decay are equal and represent the sum of the two exponentials. Concentrating on the exponential with the larger time constant which dominates this process, we can reformulate eq (10) from Borst and Abarbanel (2007) such that we fix the  $K_D$  value and substitute  $k_b$  by  $K_D$  times  $k_f$ . Using  $y_{\max}$  as the total free and bound indicator concentration,  $\gamma$  as the extrusion rate (in 1/sec),  $k_f$  as the forward binding rate (in 1/(M sec)),  $k_b$  as the backward binding rate (1/sec) and finally  $K_D = k_b/k_f$  as the dissociation constant, we obtain:

$$(1) \quad \tau = \frac{1}{2\gamma K_D k_f} \left[ k_f (K_D + y_{\max}) + \gamma + \sqrt{(k_f (K_D + y_{\max}) + \gamma)^2 - 4\gamma K_D k_f} \right]$$

For large forward rates  $k_f$  we obtain:

$$(2) \quad \lim_{k_f \rightarrow \infty} \tau = \frac{1}{2\gamma K_D k_f} [2k_f (K_D + y_{\max})] = \frac{1}{\gamma} \left( 1 + \frac{y_{\max}}{K_D} \right);$$

This is the minimum time-constant that can be reached given a certain pump rate of the cell (i.e. its intrinsic parameter), the respective  $K_D$  value of the indicator and the indicator concentration  $y_{\max}$ .

For small forward rates  $k_f$ , the time-constant is approximated by:

$$(3) \quad \lim_{k_f \rightarrow 0} \tau = \frac{1}{K_D k_f} = \frac{1}{k_b};$$

We can thus define a corner rate  $k_{f, \text{corner}}$ .

$$(4) \quad k_{f, \text{corner}} = \frac{\gamma}{K_D + y_{\max}}$$

For  $k_f$  values smaller than this corner rate, the time constant is only determined by  $k_f$  and the  $K_D$  value of the indicator, i.e.  $1/k_b$  (eq 3). For larger  $k_f$  values, the time constant is no longer dependent on  $k_f$  but only determined by the total indicator concentration and the  $K_D$  value of the indicator (eq 2).

In the example plot, the corner rate  $k_{f, \text{corner}}$  is  $10^7/(\text{M sec})$ .

Parameters are:  $\gamma_{\text{max}} = 10^{-6} \text{ M}$ ,  $\gamma = 20 \text{ Hz}$ , and  $K_D = 10^{-6} \text{ M}$ .

The question now is in which regime the various GECIs fall. For two of them, we determined the binding rates  $k_f$  and  $k_b$  in the cuvette. We find the following values:

TN-L15:  $K_D = 0.71 \cdot 10^{-6} \text{ M}$ ,  $k_b = 0.81/\text{sec}$ ,  $k_f = 1.1 \cdot 10^6/(\text{M sec})$ .

TN-XL:  $K_D = 2.20 \cdot 10^{-6} \text{ M}$ ,  $k_b = 5.56/\text{sec}$ ,  $k_f = 2.5 \cdot 10^6/(\text{M sec})$ .

For the regime where the indicator concentration does not play a role, we expect the decay time constant to be roughly equal to  $1/k_b$  (eq 3).

TN-L15:  $\tau = 1/k_b = 1.23 \text{ sec}$

TN-XL:  $\tau = 1/k_b = 0.18 \text{ sec}$ .

The decay time-constants we have measured at the NMJ (see Fig. 3 D) amount to:

TN-L15:  $\tau_{\text{decay}} = 1.49 \text{ sec}$

TN-XL:  $\tau_{\text{decay}} = 0.20 \text{ sec}$ .

These values are close to our expectation for negligible indicator concentration. For these two indicator lines, we can therefore safely assume that an indicator concentration around  $10^{-6} \text{ Mol}$  would have a small (TN-L15) or almost no (TN-XL) influence at all on the kinetics of the signal. In fact, when solving eq (1) for  $\gamma_{\text{max}}$ , we find the following approximate indicator concentrations:

TN-L15:  $\gamma_{\text{max}} = 3.0 \cdot 10^{-6} \text{ M}$

TN-XL:  $\gamma_{\text{max}} = 0.5 \cdot 10^{-6} \text{ M}$ .

## 7. Footnotes

This work was supported by the Max Planck Society and a Human Frontier Science Program grant to K. Ito, A.B., and B. Nelson. We thank Atsushi Miyawaki and Roger Tsien for providing DNA; Katrin Deininger, Wolfgang Essbauer, Alexandra Ihring, Maximilian Joesch, and Christian Theile for experimental help; and Winfried Denk for the design and initial help on the 2P microscope.

## 8. References

Ataka K, Pieribone VA (2002) A genetically targetable fluorescent probe of channel gating with rapid kinetics. *Biophys J* 82:509–516.

Borst A, Abarbanel HD (2007) Relating a calcium indicator signal to the unperturbed calcium concentration time-course. *Theor Biol Med Model* 4:7.

Bozza T, McGann JP, Mombaerts P, Wachowiak M (2004) In vivo imaging of neuronal activity by targeted expression of a genetically encoded probe in the mouse. *Neuron* 42:9–21.

Brand AH, Perrimon N (1993) Targeted gene expression as a means of altering cell fates and generating dominant phenotypes. *Development* 118:401–415.

Clark DA, Gabel CV, Gabel H, Samuel ADT (2007) Temporal activity patterns in thermosensory neurons of freely moving *Caenorhabditis elegans* encode spatial thermal gradients. *J Neurosci* 27:6083–6090.

Denk W, Strickler JH, Webb WW (1990) Two-photon laser scanning fluorescence microscopy. *Science* 248:73–76.

Díez-García J, Matsushita S, Mutoh H, Nakai J, Ohkura M, Yokoyama J, Dimitrov D, Knöpfel T (2005) Activation of cerebellar parallel fibers monitored in transgenic mice expressing a fluorescent Ca<sup>2+</sup> indicator protein. *Eur J Neurosci* 22:627–635.

Díez-García J, Akemann W, Knöpfel T (2007) In vivo calcium imaging from genetically specified target cells in mouse cerebellum. *Neuroimage* 34:859–869.

Fiala A, Spall T, Diegelmann S, Eisermann B, Sachse S, Devaud JM, Buchner E, Galizia CG (2002) Genetically expressed cameleon in *Drosophila melanogaster* is used to visualize olfactory information in projection neurons. *Curr Biol* 12:1877–1884.

Griesbeck O, Baird GS, Campbell RE, Zacharias DA, Tsien RY (2001) Reducing the environmental sensitivity of yellow fluorescent protein. Mechanism and applications. *J Biol Chem* 276:29188–29194.

Guerrero G, Siegel MS, Roska B, Loots E, Isacoff EY (2002) Tuning FlaSh: redesign of the dynamics, voltage range, and color of the genetically encoded optical sensor of membrane potential. *Biophys J* 83:3607–3618.

Guerrero G, Reiff DF, Agarwal G, Ball RW, Borst A, Goodman CS, Isacoff EY (2005) Heterogeneity in synaptic transmission along a *Drosophila* larval motor axon. *Nat Neurosci* 8:1188–1196.

Hasan MT, Friedrich RW, Euler T, Larkum ME, Giese G, Both M, Duebel J, Waters J, Bujard H, Griesbeck O, Tsien RY, Nagai T, Miyawaki A, Denk W (2004) Functional fluorescent Ca<sup>2+</sup> indicator proteins in transgenic mice under TET control. *PLoS Biol* 2:e163.

Heim N, Griesbeck O (2004) Genetically encoded indicators of cellular calcium dynamics based on troponin C and green fluorescent protein. *J Biol Chem* 279:14280–14286.

Heim N, Garaschuk O, Friedrich MW, Mank M, Milos RI, Kovalchuk Y, Konnerth A, Griesbeck O (2007) Improved calcium imaging in transgenic mice expressing a troponin C-based biosensor. *Nat Methods* 4:127–129.

Helmchen F, Imoto K, Sakmann B (1996) Ca<sup>2+</sup> buffering and action potential-evoked Ca<sup>2+</sup> signaling in dendrites of pyramidal neurons. *Biophys J* 70:1069–1081.

Helmchen F, Borst JG, Sakmann B (1997) Calcium dynamics associated with a single action potential in a CNS presynaptic terminal. *Biophys J* 72:1458–1471.

Higashijima S, Masino MA, Mandel G, Fetcho JR (2003) Imaging neuronal activity during *zebrafish* behavior with a genetically encoded calcium indicator. *J Neurophysiol* 90:3986–3997.

Hoang B, Chiba A (2001) Single-cell analysis of *Drosophila* larval neuromuscular synapses. *Dev Biol* 229:55–70.

Holmes TC, Sheeba V, Mizrak D, Rubovszky B, Dahdal D (2007) Circuit-breaking and behavioral analysis by molecular genetic manipulation of neural activity in *Drosophila*. In: *Invertebrate neurobiology* (North G, Greenspan RJ, eds), pp 19–52. Cold Spring Harbor, New York: Cold Spring Harbor Laboratory.

Jayaraman V, Laurent G (2007) Evaluating a genetically encoded optical sensor of neural activity using electrophysiology in intact adult fruit flies. *Front Neural Circuits* 1:3.

Joesch M, Plett J, Borst A, Reiff DF (2008) Response properties of motion-sensitive visual interneurons in the lobula plate of *Drosophila melanogaster*. *Curr Biol* 18:368–374.

Kleinfeld D, Griesbeck O (2005) From art to engineering? The rise of in vivo mammalian electrophysiology via genetically targeted labeling and nonlinear imaging. *PLoS Biol* 3:e355.

Komai S, Denk W, Osten P, Brecht M, Margrie TW (2006) Two-photon targeted patching (TPTP) in vivo. *Nat Protoc* 1:647–652.

Lin DM, Goodman CS (1994) Ectopic and increased expression of Fasciclin II alters motoneuron growth cone guidance. *Neuron* 13:507–523.



Lnenicka GA, Grizzaffi J, Lee B, Rumpal N (2006)  $\text{Ca}^{2+}$  dynamics along identified synaptic terminals in *Drosophila* larvae. *J Neurosci* 26:12283–12293.

Macleod GT, Hegström-Wojtowicz M, Charlton MP, Atwood HL (2002) Fast calcium signals in *Drosophila* motor neuron terminals. *J Neurophysiol* 88:2659–2663.

Macleod GT, Marin L, Charlton MP, Atwood HL (2004) Synaptic vesicles: test for a role in presynaptic calcium regulation. *J Neurosci* 24:2496–2505.

Mank M, Reiff DF, Heim N, Friedrich MW, Borst A, Griesbeck O (2006) A FRET-based calcium biosensor with fast signal kinetics and high fluorescence change. *Biophys J* 90:1790–1796.

Mao T, O'Connor DH, Scheuss V, Nakai J, Svoboda K (2008) Characterization and subcellular targeting of GCaMP-type genetically-encoded calcium indicators. *PLoS ONE* 3:e1796.

Maravall M, Mainen ZF, Sabatini BL, Svoboda K (2000) Estimating intracellular calcium concentrations and buffering without wavelength ratioing. *Biophys J* 78:2655–2667.

Marella S, Fischler W, Kong P, Asgarian S, Rueckert E, Scott K (2006) Imaging taste responses in the fly brain reveals a functional map of taste category and behavior. *Neuron* 49:285–295.

Margrie TW, Meyer AH, Caputi A, Monyer H, Hasan MT, Schaefer AT, Denk W, Brecht M (2003) Targeted whole-cell recordings in the mammalian brain in vivo. *Neuron* 39:911–918.

Miesenböck G, Kevrekidis IG (2005) Optical imaging and control of genetically designated neurons in functioning circuits. *Annu Rev Neurosci* 28:533–563.

Miesenböck G, De Angelis DA, Rothman JE (1998) Visualizing secretion and synaptic transmission with pH-sensitive green fluorescent proteins. *Nature* 394:192–195.

Miyawaki A (2005) Innovations in the imaging of brain functions using fluorescent proteins. *Neuron* 48:189–199.

Miyawaki A, Llopis J, Heim R, McCaffery JM, Adams JA, Ikura M, Tsien RY (1997) Fluorescent indicators for  $\text{Ca}^{2+}$  based on green fluorescent proteins and calmodulin. *Nature* 388:882–887.

Mori MX, Erickson MG, Yue DT (2004) Functional stoichiometry and local enrichment of calmodulin interacting with  $\text{Ca}^{2+}$  channels. *Science* 304:432–435.

Nagai T, Yamada S, Tominaga T, Ichikawa M, Miyawaki A (2004) Expanded dynamic range of fluorescent indicators for  $\text{Ca}^{2+}$  by circularly permuted yellow fluorescent proteins. *Proc Natl Acad Sci U S A* 101:10554–10559.

Nakai J, Ohkura M, Imoto K (2001) A high signal-to-noise Ca<sup>2+</sup> probe composed of a single green fluorescent protein. *Nat Biotechnol* 19:137–141.

Naraghi M (1997) T-jump study of calcium binding kinetics of calcium chelators. *Cell Calcium* 22:255–268.

Ng M, Roorda RD, Lima SQ, Zemelman BV, Morcillo P, Miesenböck G (2002) Transmission of olfactory information between three populations of neurons in the antennal lobe of the fly. *Neuron* 36:463–474.

Ohkura M, Matsuzaki M, Kasai H, Imoto K, Nakai J (2005) Genetically encoded bright Ca<sup>2+</sup> probe applicable for dynamic Ca<sup>2+</sup> imaging of dendritic spines. *Anal Chem* 77:5861–5869.

Palmer AE, Giacomello M, Kortemme T, Hires SA, Lev-Ram V, Baker D, Tsien RY (2006) Ca<sup>2+</sup> indicators based on computationally redesigned calmodulin-peptide pairs. *Chem Biol* 13:521–530.

Patterson GH, Piston DW (2000) Photobleaching in two-photon excitation microscopy. *Biophys J* 78:2159–2162.

Pologruto TA, Yasuda R, Svoboda K (2004) Monitoring neural activity and [Ca<sup>2+</sup>] with genetically encoded Ca<sup>2+</sup> indicators. *J Neurosci* 24:9572–9579.

Quinn WG, Harris WA, Benzer S (1974) Conditioned behavior in *Drosophila melanogaster*. *Proc Natl Acad Sci U S A* 71:708–712.

Reiff DF, Thiel PR, Schuster CM (2002) Differential regulation of active zone density during long-term strengthening of *Drosophila* neuromuscular junctions. *J Neurosci* 22:9399–9409.

Reiff DF, Ihring A, Guerrero G, Isacoff EY, Joesch M, Nakai J, Borst A (2005) *In vivo* performance of genetically encoded indicators of neural activity in flies. *J Neurosci* 25:4766–4778.

Sakai R, Repunte-Canonigo V, Raj CD, Knöpfel T (2001) Design and characterization of a DNA-encoded, voltage-sensitive fluorescent protein. *Eur J Neurosci* 13:2314–2318.

Schikorski T, Stevens CF (1997) Quantitative ultrastructural analysis of hippocampal excitatory synapses. *J Neurosci* 17:5858–5867.

Schiller J, Helmchen F, Sakmann B (1995) Spatial profile of dendritic calcium transients evoked by action potentials in rat neocortical pyramidal neurones. *J Physiol* 487:583–600.

Schneggenburger R, Neher E (2005) Presynaptic calcium and control of vesicle fusion. *Curr Opin Neurobiol* 15:266–274.

Shang Y, Claridge-Chang A, Sjulson L, Pypaert M, Miesenböck G (2007) Excitatory local circuits and their implications for olfactory processing in the fly antennal lobe. *Cell* 128:601–612.

Shimozono S, Hosoi H, Mizuno H, Fukano T, Tahara T, Miyawaki A (2006) Concatenation of cyan and yellow fluorescent proteins for efficient resonance energy transfer. *Biochemistry* 45:6267–6271.

Siegel MS, Isacoff EY (1997) A genetically encoded optical probe of membrane voltage. *Neuron* 19:735–741.

Spradling AC, Rubin GM (1982) Transposition of cloned P elements into *Drosophila* germ line chromosomes. *Science* 218:341–347.

Suh GS, Wong AM, Hergarden AC, Wang JW, Simon AF, Benzer S, Axel R, Anderson DJ (2004) A single population of olfactory sensory neurons mediates an innate avoidance behaviour in *Drosophila*. *Nature* 431:854–859.

Suzuki H, Kerr R, Bianchi L, Frøkjær-Jensen C, Slone D, Xue J, Gerstbrein B, Driscoll M, Schafer WR (2003) In vivo imaging of *C. elegans* mechanosensory neurons demonstrates a specific role for the MEC-4 channel in the process of gentle touch sensation. *Neuron* 39:1005–1017.

Tallini YN, Ohkura M, Choi BR, Ji G, Imoto K, Doran R, Lee J, Plan P, Wilson J, Xin HB, Sanbe A, Gulick J, Mathai J, Robbins J, Salama G, Nakai J, Kotlikoff MI (2006) Imaging cellular signals in the heart in vivo: cardiac expression of the high-signal Ca<sup>2+</sup> indicator GCaMP2. *Proc Natl Acad Sci U S A* 103:4753–4758.

Tank DW, Regehr WG, Delaney KR (1995) A quantitative analysis of presynaptic calcium dynamics that contribute to short-term enhancement. *J Neurosci* 15:7940–7952.

Tay LH, Griesbeck O, Yue DT (2007) Live-cell transforms between Ca<sup>2+</sup> transients and FRET responses for a troponin-C-based Ca<sup>2+</sup> sensor. *Biophys J* 93:4031–4040.

Thomas D, Tovey SC, Collins TJ, Bootman MD, Berridge MJ, Lipp P (2000) A comparison of fluorescent Ca<sup>2+</sup> indicator properties and their use in measuring elementary and global Ca<sup>2+</sup> signals. *Cell Calcium* 28:213–223. Tsien RY (1998) The green fluorescent protein. *Annu Rev Biochem* 67:509–544.

Wachowiak M, Denk W, Friedrich RW (2004) Functional organization of sensory input to the olfactory bulb glomerulus analyzed by two-photon calcium imaging. *Proc Natl Acad Sci U S A* 101:9097–9102.

Wang JW, Wong AM, Flores J, Vosshall LB, Axel R (2003) Two-photon calcium imaging reveals an odor-evoked map of activity in the fly brain. *Cell* 112:271–282.

Wang Y, Guo HF, Pologruto TA, Hannan F, Hakker I, Svoboda K, Zhong Y (2004) Stereotyped odor-evoked activity in the mushroom body of *Drosophila* revealed by green fluorescent protein-based Ca<sup>2+</sup> imaging. *J Neurosci* 24:6507–6514.

Wallace DJ, Meyer zum Alten Borgloh S, Astori S, Yang Y, Bausen M, Kügler S, Palmer AE, Tsien RY, Sprengel R, Kerr JN, Denk W, Hasan MT (2008) Single-spike detection *in vitro* and *in vivo* with a genetic Ca<sup>2+</sup> sensor. *Nat Methods*, in press.

Xia Z, Storm DR (2005) The role of calmodulin as a signal integrator for synaptic plasticity. *Nat Rev Neurosci* 6:267–276.

Yasuda R, Nimchinsky EA, Scheuss V, Pologruto TA, Oertner TG, Sabatini BL, Svoboda K (2004) Imaging calcium concentration dynamics in small neuronal compartments. *Sci STKE* 2004:p15.

## IV. Processing of Horizontal Optic Flow in Three Visual Interneurons of the *Drosophila* Brain

B. Schnell, M. Joesch, F. Forstner, S. V. Raghu, H. Otsuna, K. Ito, A. Borst and D. F. Reiff

This chapter was published in the Journal of Neurophysiology in 2010.

### 1. Abstract

Motion vision is essential for navigating through the environment. Due to its genetic amenability, the fruit fly *Drosophila* has been serving for a lengthy period as a model organism for studying optomotor behavior as elicited by large-field horizontal motion. However, the neurons underlying the control of this behavior have not been studied in *Drosophila* so far. Here we report the first whole cell recordings from three cells of the horizontal system (HSN, HSE, and HSS) in the lobula plate of *Drosophila*. All three HS cells are tuned to large-field horizontal motion in a direction-selective way; they become excited by front-to-back motion and inhibited by back-to-front motion in the ipsilateral field of view. The response properties of HS cells such as contrast and velocity dependence are in accordance with the correlation-type model of motion detection. Neurobiotin injection suggests extensive coupling among ipsilateral HS cells and additional coupling to tangential cells that have their dendrites in the contralateral hemisphere of the brain. This connectivity scheme accounts for the complex layout of their receptive fields and explains their sensitivity both to ipsilateral and to contralateral motion. Thus the main response properties of *Drosophila* HS cells are strikingly similar to the responses of their counterparts in the blowfly *Calliphora*, although we found substantial differences with respect to their dendritic structure and connectivity. This long-awaited functional characterization of HS cells in *Drosophila* provides the basis for the future dissection of optomotor behavior and the underlying neural circuitry by combining genetics, physiology, and behavior.

### **2. Introduction**

Flies rely heavily on visual motion information to navigate safely through the environment (Borst and Haag 2002). Once airborne, they use the characteristic flow fields caused by their self-motion to correct for deviations from a straight flight path. The precision and reliability of these so-called optomotor responses, combined with the small size of their brain, make flies an ideal organism to study the underlying neural circuitry (Chan et al. 1998; Egelhaaf et al. 2003; Frye and Dickinson 2001; Götz 1964; Heisenberg et al. 1978).

Detailed anatomical maps describing the cell types of the optic lobes (Fischbach and Dittrich 1989; Scott et al. 2002; Strausfeld 1976) are at hand. In the blowfly *Calliphora*, about 60 motion sensitive neurons, the so-called lobula plate tangential cells (LPTCs), extract information about large- and small-field motion from the optic flow. Some LPTCs synapse directly onto descending neurons to ultimately control head movement and locomotion (Chan et al. 1998; Gilbert et al. 1995; Gronenberg and Strausfeld 1990).

To analyze neuronal function different approaches were pursued in large and small flies. In *Calliphora* the response properties of LPTCs have been characterized in greatest detail by intracellular recording (Borst and Haag 2002). Among them, cells of the vertical system (VS) respond preferentially to vertical motion (Hengstenberg et al. 1982) and motion elicited by rotation around an axis in the horizontal plane of the animal (Krapp et al. 1998). Horizontal system (HS) cells respond to translation (Hausen 1982a,b) and rotational motion around the vertical axis of the fly (Krapp et al. 2001). Their tuning to specific optic flow fields can be explained by dendritic input from opposing arrays of local motion detectors built from columnar elements (Borst and Egelhaaf 1990; Joesch et al. 2008; Raghu et al. 2007, 2009; Single and Borst 1998) as well as input from other LPTCs (Elyada et al. 2009; Farrow et al. 2005, 2006; Haag and Borst 2004, 2007, 2008).

In *Drosophila*, mainly genetic techniques have been used to disrupt parts of the circuitry and to compare the behavior of wild-type and mutant flies (Götz 1964, 1965; Heisenberg 1972; Heisenberg and Buchner 1977). This approach also allows one to study the functional role of small columnar neurons in the medulla

presynaptic to LPTCs that could not be recorded electrically so far. In large flies some example recordings (Douglass and Strausfeld 1995, 1996, 2003; Gilbert and Strausfeld 1991) of a small number of the about 50 different columnar neurons could be obtained. Yet, their small size and the low feasibility of this approach did not provide an exhaustive picture of the cellular mechanisms of visual motion detection in the medulla of dipteran flies.

Recent studies on the behavior of wild-type (Duistermars et al. 2007; Fry et al. 2009; Mronz and Lehmann 2008; Tammero et al. 2004) and transgenic *Drosophila* with certain types of columnar neurons blocked (Katsov and Clandinin 2008; Rister et al. 2007; Zhu et al. 2009) provided new insights into motion vision and optomotor behavior. However, these studies also revealed the limitations of behavioral experiments as read-out for the functional role of a specific class of neurons. Moreover, the interpretation of such studies in *Drosophila* relies heavily on physiological data from large flies because only one functional description of LPTCs in *Drosophila* is available so far (Joesch et al. 2008).

We close this gap by characterizing the response properties of the three HS cells in *Drosophila* that are supposed to mediate yaw-turning behavior. We show that their dendritic structure and connectivity to other LPTCs are different compared with those of large flies. Nevertheless, their complex receptive fields, contrast dependence, and velocity tuning corroborate findings on HS cells in *Calliphora*. HS cells in *Drosophila* are similarly tuned to rotational large-field horizontal motion and match the predictions of a correlation-type model of visual motion detection.

### **3. Methods**

#### **Flies**

Flies were raised on standard cornmeal-agar medium with a 12-h light/12-h dark cycle, 25°C, and 60% humidity. We used female experimental flies, 1 day after eclosion. The line NP 0282 (established by the NP consortium; for screening see Otsuna and Ito 2006) expresses Gal4 in two of the three HS cells (HSN and HSE, Fig. 1A) and in unidentified neurons of the central brain. UAS-mCD8-GFP was used to highlight entire cells and UAS-mCD8-TN-XL-8aa (Joesch et al. 2008) was used to predominantly label cell bodies.

### Visually guided whole cell recording

Patch-clamp recordings were performed as described previously (Joesch et al. 2008). Flies were anesthetized on ice and waxed on a Plexiglas holder. The head was bent down to expose the caudal backside of the head and the extended proboscis was fixed. Aluminum foil with a hole of about 1–2 mm sustained by a ring-shaped metal holder was placed on top of the fly and separated the upper wet part (covered with Ringer solution; Wilson et al. 2004) of the preparation from the lower dry part. Water-immersion optics was used from above; visual patterns (see following text) were presented to dry and fully intact compound eyes. A small window was cut into the backside of the head, and during mild protease treatment (protease XIV, E.C.3.4.24.31, P-5147; Sigma–Aldrich; 2 mg/ml, max 4 min), the neurolemma was partially digested and the main tracheal branches and fat body were removed. The protease was rinsed off carefully and replaced by Ringer solution. A saline jet was generated with a Ringer-filled electrode to remove the extracellular matrix and to expose the HS cell somata for recording.

Genetically labeled green fluorescent HS cell somata were approached with a patch electrode filled with a red fluorescent dye (intracellular solution; Wilson and Laurent 2005) containing an additional 5 mM Spermine (S-2876, Sigma–Aldrich) and 30 mM Alexa Fluor 568–hydrazide-Na (A-10441, Molecular Probes) adjusted to pH = 7.3). Recordings were established under visual control with a x40 water-immersion objective (LumplanF, Olympus), a Zeiss microscope (Axiotech Vario 100, Zeiss, Oberkochen, Germany), fluorescence excitation (100-W fluorescence lamp, heat filter, neutral-density filter OD 0.3; all from Zeiss), and a dual-band filter set (EGFP/DsRed, Chroma Technology, Bellows FallsVT). During the recordings, the fluorescence excitation was shut off to prevent blinding of the fly. Patch electrodes of 6- to 8-M $\Omega$  resistance (thin wall, filament, 1.5 mm; WPI, Sarasota, FL) were pulled on a Sutter- P97 (Sutter Instrument, Novato, CA). A reference electrode (Ag-AgCl) was immersed in the extracellular saline (pH 7.3, 1.5 mM CaCl<sub>2</sub>, no sucrose). Signals were recorded on a BA-1S Bridge Amplifier (npi electronics, Tamm, Germany), low-pass filtered at 3 kHz, and digitized at 10 kHz via a D/A converter (PCI-DAS6025, Measurement Computing, Norton, MA) with Matlab (version 7.3.0.267, The MathWorks, Natick, MA). After the recording, several images of each Alexa-filled



LPTC were taken at different depths along the z-axis (HQ-filter set Alexa-568, Chroma Technology) with a charge-coupled device (CCD) camera (Spot Pursuit 1.4 Megapixel; Visitron Systems, Puchheim, Germany).

### **Immunohistochemistry**

Female flies were dissected 3 to 5 days after eclosion. Their brains were removed and fixed in 4% paraformaldehyde for 30 min at room temperature. Subsequently, the brains were washed for 45–60 min in PBT [phosphate-buffered saline (pH 7.2) including 1% Triton X-100]. For antibody staining, the samples were incubated in PBT including 2% normal goat serum (Sigma–Aldrich, G9023) for 1 h at room temperature followed by incubation with primary antibodies (1:200, overnight at 4°C). Primary antibodies were removed by several washing steps (5 x 20 min in PBT) and secondary antibodies were added (1:200, overnight at 4°C). The samples were further washed with PBT (3 x 20 min) followed by final washing steps in PBS (3 x 20 min). The stained brains were mounted in Vectashield (Vector Laboratories, Burlingame, CA) and analyzed by confocal microscopy (see following text). The following primary and secondary antibodies were used: Alexa Fluor 488 rabbit anti-GFP-IgG (A-21311, Molecular Probes), mouse anti-Dlg (4F3, Developmental Studies Hybridoma Bank), and Alexa Fluor 594 goat anti-mouse IgG (A11005, Molecular Probes).

### **Intracellular dye filling**

Flies expressing mCD8-GFP driven by G73 were decapitated. The cut heads were fixed in a layer of two-component glue (UHU Plus; UHU, Baden, Germany), with the compound eyes looking downward into the glue. After hardening of the glue (~2 min) the specimen were covered with Ringer solution and the cuticle at the back side of the fly's head was removed with sharp needles (Neolus, Gx3/4 in. 0.4 x 20 mm). This procedure allowed direct access to the brain. The main tracheal branches were removed. Dye fillings were performed using quartz electrodes (QF 100-60-10; Sutter Instrument) pulled on a laser puller (P-2000; Sutter Instrument). Electrodes were filled with a 10 mM Alexa Fluor 594 solution (A10442; Invitrogen, Karlsruhe, Germany) and backfilled with 2 M KAc/0.5 M KCl solution. Impaled cells were loaded

by negative current pulses for a few seconds. Subsequently, the brains were fixed in 4% paraformaldehyde for 15 min.

### **Confocal microscopy and reconstruction**

Serial optical sections were taken at 0.5  $\mu\text{m}$  intervals with 1024 x 1024 pixel resolution using confocal microscopes (Leica TCSNT) and oil-immersion x40 (numerical aperture [NA] = 1.25) or x63 (NA = 1.4) Plan-Apochromat objectives. The individual confocal stacks were analyzed using Image J (National Institutes of Health, Bethesda, MD) software. The size, contrast, and brightness of the resulting images were adjusted with Photoshop CS (Adobe Systems, San Jose, CA).

Cells were manually traced using previously described custom-written software (Cuntz et al. 2008), resulting in detailed cylinder models. Lobula plate volumes were reconstructed manually by outlining their outer borders in each slice and sampling surface meshes. Cylinder and volume models were visualized using the Blender animation system (<http://www.blender.org>).

### **Neurobiotin staining**

HS cells were targeted and perfused with patch electrodes as described earlier. Neurobiotin (2–4%; Vector Labs) was added to the intracellular solution. Neurobiotin and Alexa Fluor 568 were coinjected via  $\pm 0.2$  nA current pulses for  $\leq 10$  min. For initial identification, the perfused individual HS cell was imaged with the fluorescence microscope and CCD camera as described earlier. Staining against Neurobiotin with Streptavidin–Alexa Fluor 568 conjugate (1:100, Invitrogen) was performed as described earlier, except that whole fly heads were fixed in 4% paraformaldehyde (2 h) before dissection in PBS. Perfusion of a single HS cell never resulted in more than one Alexa Fluor 568–filled cell. Only after labeling of Neurobiotin with Streptavidin–Alexa Fluor 568 conjugate did other cells light up. The second red label was used to prevent spectral overlap with the green fluorescence of genetically labeled neurons.

### Visual stimulation

For visual stimulation a custom-built light-emitting diode (LED) arena was used based on the open-source information of the Dickinson Laboratory (<http://www.dickinson.caltech.edu/PanelsPage>). Our arena consists of 15 x 8 TA08-81GWA dot matrix displays (Kingbright, Walnut, CA), each harboring 8 x 8 individual green (568-nm) LEDs, covering 170° in azimuth and 85° in elevation of the fly's visual field, with an angular resolution of about 1.4° between adjacent LEDs. The arena is capable of frame rates above 600 frames/s, with 16 intensity levels. To measure the velocity tuning, patterns were generated in which four consecutive frames were used to define one image. This resulted in 64 equidistant intensity levels available per pixel. Each dot matrix display is controlled by an ATmega644 microcontroller (Atmel, San Jose, CA) that obtains pattern information from one central ATmega128-based main controller board, which in turn reads in pattern information from a compact flash memory card. For achieving high frame rates with a system of this size, each panel controller was equipped with an external AT45DB041B flash memory chip for local pattern buffering. Matlab was used for programming and generation of the patterns as well as for sending the serial command sequences via RS-232 to the main controller board and local buffering. The luminance range of the stimuli was 0–8 cd/m<sup>2</sup>.

Large-field stimuli covered the whole extent of the arena. To study direction-selectivity, sine gratings of four different orientations (spatial wavelength: 42.5° for the horizontal, 45° for the vertical, and 32° for the diagonal patterns) moving in eight different directions at a temporal frequency of 1 Hz were presented.

For the velocity tuning, two sine gratings of either 22.4 or 44.8° spatial wavelength were presented moving at nine different angular velocities corresponding to temporal frequencies of 0.1 to 5 Hz. The sequence of velocities was changed during experiments.

To study contrast dependence, a square-wave grating of 34° spatial wavelength moved at a constant angular velocity of 34°/s, corresponding to a temporal frequency of 1 Hz. Contrast was calculated as  $(I_{\max} - I_{\min}) / (I_{\max} + I_{\min})$ . With the 16 intensity levels of the LEDs, seven pattern contrasts could be obtained ranging from

100% to 6.7% at the same mean luminance. To obtain a lower contrast of 3.3%, four consecutive image frames were used to define one image as described earlier.

The square-wave grating (spatial wavelength:  $22.4^\circ$ ; angular velocity:  $22.4^\circ/\text{s}$ ) used for either ipsilateral or contralateral stimulation covered about  $56^\circ$  in azimuth and  $85^\circ$  in elevation and was displaced by  $\pm 15^\circ$  relative to frontal gaze.

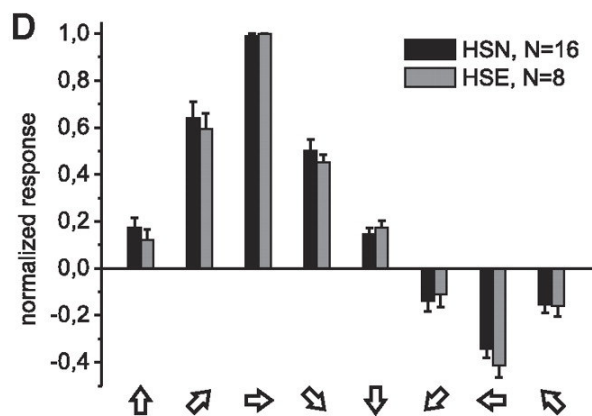
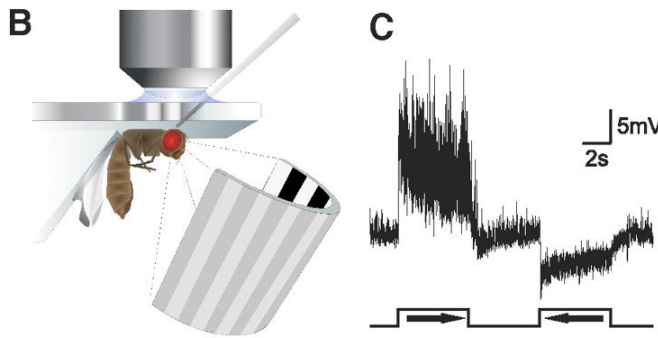
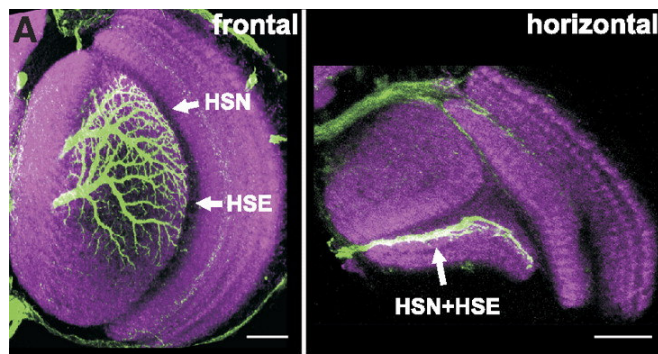
The local response characteristics of HS cells were determined using a previously described stimulus (Nordström et al. 2008; Wertz et al. 2009). A small bar of  $5.6^\circ$  length and  $1.4^\circ$  width was moved horizontally from the contra- to the ipsilateral side and back again at different elevations or vertically downward and upward at different positions along the azimuth. For both the vertical and horizontal stimuli an area of about  $145^\circ$  along the azimuth and  $85^\circ$  of elevation was covered. A typical response trace for the horizontal and the vertical local stimulus is shown in Supplemental Fig. S2.

### **Data analysis**

Data were acquired and analyzed with the data acquisition and analysis toolboxes of Matlab. Receptive fields were calculated by binning the responses of single HS cells to horizontal stimulation ( $\sim 5.6^\circ$  elevation and  $\sim 5.6^\circ$  azimuth) and subtracting the mean response during null direction from the mean response during preferred direction (PD) motion. The receptive fields of all HS cells of a certain type were averaged, smoothed by convolving them with a  $3 \times 3$  kernel approximating an isotropic Gaussian function, and normalized to maximal value.

The horizontal and vertical sensitivity components for the vector fields were calculated locally and used to calculate a single local vector for each region that results in the shown vector fields. Importantly, it was recently shown that these x- and y-components are fully sufficient to determine the local orientation tuning and directional preference of the cell (Wertz et al. 2009).

To analyze the velocity dependence the mean response of the first 500 ms after the onset of PD motion was taken. In all other cases the mean over the whole stimulus duration was calculated. The mean potential during 500 ms before stimulus onset was used as a baseline and subtracted from this response.



response of an HSN cell plotted against time. A vertical sine grating ( $\lambda = 42.5^\circ$ ) moving horizontally (temporal frequency = 1 Hz) elicits a directionally selective response. Large-field rotation with an ipsilateral front-to-back component (preferred direction [PD]) elicits a strong depolarization. Motion in the opposite direction (null direction [ND]) elicits a strong hyperpolarization of the membrane potential. Small, fast membrane fluctuations increase in size during PD motion. **D**: directional tuning. Plotted is the mean response amplitude during 5-s grating motion (same stimulus as in C) in 4 different orientations and a total of 8 different directions. HSN and HSE respond strongest to horizontal motion. Error bars indicate SE.

#### 4. Results

Based on anatomical similarity to the three horizontally sensitive LPTCs in blowflies (Hausen 1982a,b), the horizontal system of *Drosophila* has been proposed to consist of the three giant output neurons HSN, HSE, and HSS (Fischbach and Dittrich 1989; Heisenberg et al. 1978). The dendrites of these cells reside in a thin anterior layer of

the lobula plate (Fig. 1A), where they cover the dorsal, middle, and ventral parts of this retinotopically organized neuropile, respectively (Heisenberg et al. 1978; Scott et al. 2002). Their axons project centrally to the lateral protocerebrum, where they are supposed to synapse onto descending neurons (Eckert and Meller 1981; Haag et al. 2007) and thus to control optomotor turning responses induced by horizontal optic flow.

We performed *in vivo* whole cell recordings from the somata of HS cells and characterized their response properties during large-field visual motion (Fig. 1B). In the first series of experiments reproducible recordings from identified cells were enabled using the NP 0282 Gal4 driver line. At the level of the lobula plate, NP 0282 specifically labels HSN and HSE (Fig. 1A). Despite the lack of HSS, NP 0282 was chosen to express a green fluorescent marker that highlights the soma (Joesch et al. 2008) of HSN and HSE under the fluorescence microscope. The recording electrode was visualized by adding a red fluorescent dye to the electrode solution, which allowed directing the electrode under visual guidance toward the green cell bodies. During the recording, the cells became perfused with the red dye and the recorded signals could be assigned to the specific cell type. In these recordings, HS cells exhibited a resting membrane potential of about  $-55$  mV (corrected for liquid junction potential) and an input resistance of  $100$ – $200$  M $\Omega$  ( $n = 25$ ). At rest, all recorded HS cells showed small and rapid spontaneous membrane fluctuations of high frequency (Fig. 1C).

### **HSN and HSE are tuned to horizontal motion in a direction-selective way**

When stimulated with a large-field sine grating (spatial wavelength =  $42.5^\circ$ ) moving front-to-back in front of the ipsilateral eye (including an area of back-to-front motion in the contralateral eye), HS cells canonically exhibited a graded depolarization superimposed by spikelike events (Fig. 1C). Motion in the opposite direction led to a hyperpolarization of the membrane potential and a reduction of the fast spikelike events. Presentation of sine gratings moving in four different orientations and a total of eight different directions revealed a strong directional tuning of both HSN and HSE (black and gray bars, respectively, Fig. 1D) to large-field horizontal motion, similar to

their counterparts in *Calliphora*. Ipsilateral front-to-back motion elicited the strongest activation (preferred direction [PD]) and back-to-front motion the strongest inhibition (null direction [ND]). Typically, ND responses were smaller in amplitude than PD responses. Diagonal motion led to weaker responses and almost no responses were elicited by vertical motion in either direction. Thus HS cells in *Drosophila* are tuned to large-field horizontal motion in a directional-selective way.

### **HS cell responses suggest input from correlation-type motion detectors**

According to the correlation-type model for elementary motion detection (Borst and Egelhaaf 1989; Reichardt 1961), motion information is extracted from the retinal image by a multiplicative interaction of luminance signals from two neighboring receptors after delaying one of them in time. Large-field directional selectivity of LPTCs can then arise from spatial integration of input from two arrays of such detectors, one excitatory and the other inhibitory, that compute local motion information with opposite preferred direction (Joesch et al. 2008; Raghu et al. 2007, 2009; Single and Borst 1998; Single et al. 1997). The output of such a correlation-type model has certain features that we tested for in HS cell responses. These features are the appearance of a velocity optimum (Reichardt 1961) (Fig. 2A), the linear dependence of this velocity optimum on the spatial wavelength of the moving grating (Fig. 2B), the dependence of the response on the magnitude of contrast (Buchner 1984) (Fig. 2C), and the independence of the sign of contrast (Egelhaaf and Borst 1992) (Fig. 2D). To characterize the velocity dependence of HS cells in response to PD motion, we presented sine gratings of 22 or 44° spatial wavelength (Fig. 2A, inset) at nine different velocities (Fig. 2A). For both patterns the HS cell response increased nonlinearly, exhibited a maximum response at an angular velocity of 22 and 44°/s, respectively, and declined at higher velocities (Fig. 2A). For both patterns this resulted in a maximal response at around 1 Hz (velocity [deg/s] divided by spatial wavelength [deg]), which represents the so-called temporal frequency optimum, a hallmark of the correlation-type detector model (Fig. 2B).

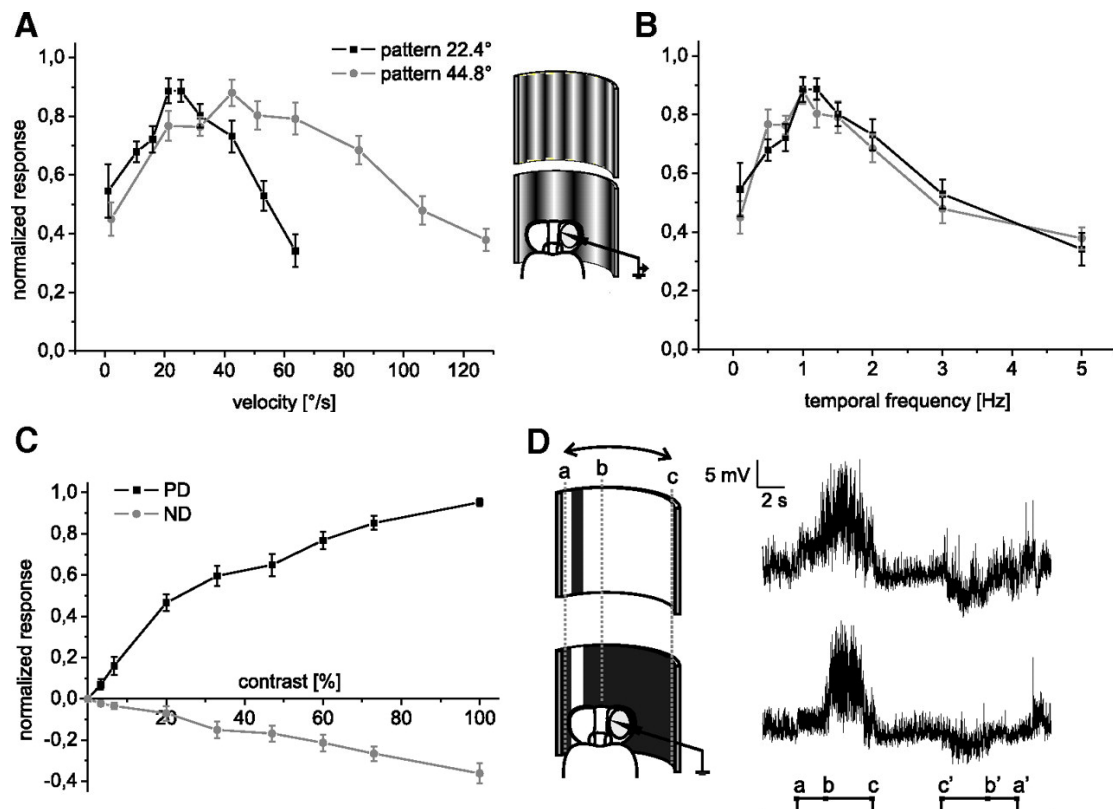


**Fig. 2:** HSN and HSE responses match the predictions of a correlation-type motion detector. **A:** velocity dependence. Two sine gratings of different spatial wavelength ( $\lambda = 22.4^\circ$ ,  $\lambda = 44.8^\circ$ ) moving at 9 different velocities elicited a velocity optimum that depended on the spatial wavelength of the pattern. Plotted is the mean response during the first 500 ms after onset of PD motion, normalized to the maximal response for each fly ( $n = 10$  for each grating; error bar: SE). **B:** constant temporal frequency optimum of 1 Hz. Same data as in A plotted against the temporal frequency ( $tf = \text{velocity}/\lambda$ ). **C:** contrast dependence. Square-wave gratings ( $\lambda = 34^\circ$ ) of different contrast moving in PD or ND ( $tf = 1$  Hz) were presented. Plotted is the mean response during 5 s of motion normalized to the maximal response of each HS cell. Response amplitudes increase with contrast, but exhibit saturation ( $n = 19$ ; error bars: SE). **D:** independence of the sign of contrast. Example trace of an HS cell responding to a light bar on a dark background and a dark bar on a light background moving in PD and ND (width of the bar:  $8.5^\circ$ , maximal contrast). The direction of motion is reported by the membrane potential independent of the sign of contrast.  $a$ ,  $b$ , and  $c$  and  $a'$ ,  $b'$ , and  $c'$  mark the time points at which the bar occupied the respective positions on the arena (see inset). Note that HS cells respond to motion on the contralateral side ( $a$  to  $b$  and  $b'$  to  $a'$ ) as well. Ipsilateral motion elicited stronger responses ( $b$  to  $c$  and  $c'$  to  $b'$ ).

The dependence of the response on the magnitude of contrast was shown by presenting square-wave gratings (spatial wavelength:  $34^\circ$ ) of different contrasts, ranging from 3.3 to 100%, that were moving at a constant velocity of  $34^\circ/\text{s}$  (Fig. 1C).



For both PD and ND motion the response amplitudes increased with pattern contrast and PD responses saturated at higher contrast (Fig. 2C). Furthermore, the correlation-type motion detector reports the direction of movement independent of the sign of contrast. In accordance with this prediction, a moving dark bar on a light background or a moving light bar on a dark background evoked depolarizing PD responses for front-to-back motion and hyperpolarizing ND responses for back-to-front motion (Fig. 2D). In these experiments a still bar was presented to the contralateral field of view, began to move at time a, entered the ipsilateral field of view at time b, continued its way and stopped at a lateral position at time c. From there it moved back by reversing the sequence c', b', and a' (Fig. 2D). Regressive motion of the bar through the contralateral visual field of view elicited a depolarizing response, although it was smaller than that caused by ipsilateral progressive motion (see following text). Taken together, the response properties of HS cells are indicative of presynaptic computations according to the correlation-type model of motion detection.

### **HS cells of one hemisphere have strongly overlapping, binocular receptive fields**

The environment, as scanned by the ipsilateral compound eye, is mapped retinotopically onto the columnar elements that are supposed to provide the synaptic input to the giant HS cell dendrites in the lobula plate (Braitenberg 1970; Strausfeld 1984). As a consequence of this layout, the position and the branching pattern of an HS cell within the lobula plate (Fig. 3A) should be predictive of its ipsilateral receptive field (Hausen 1982a,b). To analyze the dendritic structure of all three HS cells in detail we filled HSS of one hemisphere with a red fluorescent dye in three flies, in which HSN and HSE were labeled with green fluorescent protein (GFP), and reconstructed their dendritic trees from confocal image stacks (Supplemental Fig. S1, Fig. 3A). The dendrites of HSN, HSE, and HSS cover dorsal, equatorial, and ventral parts of the lobula plate, where they occupy on average 70, 90, and 75% of the total area, respectively. The overlap of their dendritic spanning fields is extremely large (Fig. 3B); HSE covers about 90% of HSN and about 80% of HSS. A dendritic branch of HSE reaches close to the dorsal-most boundary of HSN (Fig. 3A). Even HSN and HSS dendrites overlap to about 20%. Any deviation of the receptive

field from this anatomical map can possibly be attributed to input from neurons other than the columnar ones.

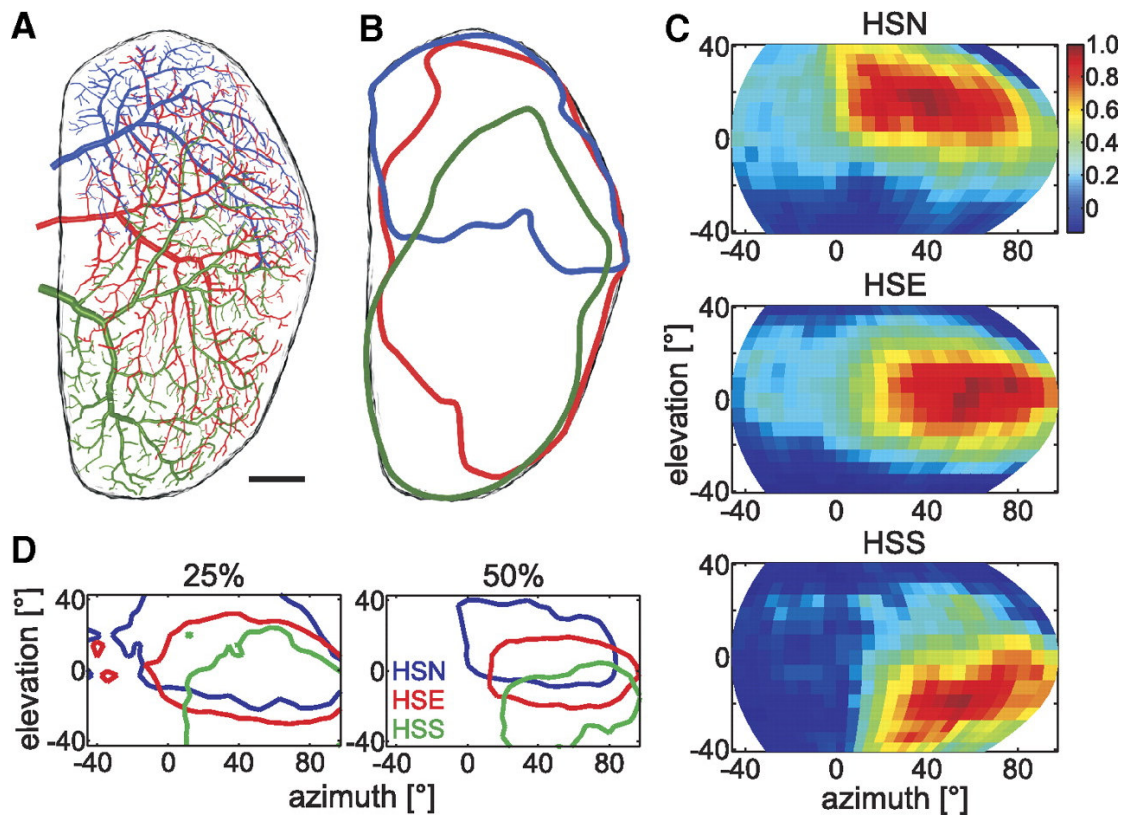


**Fig. 3:** Dendritic structure and receptive fields of HSN, HSE, and HSS.

**A:** reconstruction of the dendritic arborization of HSN (blue), HSE (red), and HSS (green) in the lobula plate from confocal image stacks (HSN and HSE were GFP-labeled and HSS was filled with Alexa Fluor 594). Scale bar: 20  $\mu\text{m}$ . **B:** outline of the dendritic spanning field of HSN (blue), HSE (red), and HSS (green) from A. In particular the spanning fields of HSE and HSS cover large parts of the lobula plate and the dendrites of all 3 HS cell dendrites overlap extensively. **C:** receptive fields of HSN, HSE, and HSS. Plotted are response amplitudes (PD–ND) elicited by a small bar moving horizontally at different elevations normalized to the maximal response. HSN, HSE, and HSS are most responsive to motion at positions covered by their own dendritic trees in the lobula plate (that is more dorsal for HSN, equatorial for HSE, and more ventral for HSS). HSN and HSE additionally respond to contralateral motion. All HSS responses were recorded from cells ( $n = 5$ ) without GFP expression and all HSN responses from genetically labeled cells ( $n = 7$ ). Data for HSE are from unlabeled ( $n = 4$ ) and GFP-labeled ( $n = 4$ ) cells. **D:** overlap of the receptive fields. The amount of overlap between the receptive fields of HSN (blue), HSE (red), and HSS (green) was estimated by applying a threshold of 50 or 25% of the maximal response in C. For both thresholds the receptive fields of all 3 HS cells intersect in the equatorial area. Compare with the overlap of the dendritic trees in B.

In the course of our experiments we occasionally recorded from genetically unlabeled HS cells in different genotypes that represented control situations and identified the recorded cells by filling them with the red fluorescent dye of the electrode solution. The recordings of these cells were indistinguishable from our previous recordings of genetically labeled HSE and HSN and included recordings from HSS cells that were not highlighted by the Gal4-driver in the previous experiments. We analyzed the receptive fields of genetically labeled and unlabeled HSN, HSE, and HSS cells, respectively, by presenting a small vertical bar (5.6° high and 1.4° wide) moving horizontally at different positions subtending 145° along the azimuth and about 85° of elevation (see Methods; Nordström et al. 2008; Wertz et al. 2009). A typical response trace recorded during such an experiment is shown in Supplemental Fig. S2. The relatively large membrane potential fluctuations in response to this local motion stimulus suggest a rather unexpected (Borst and Haag 1996) short electrotonic distance from the dendrite to the recorded soma or, alternatively, active processes that enhance signal propagation (Gouwens and Wilson 2009). However, these results and the presence of small excitatory postsynaptic potentials in all recordings suggest that even potential unitary events propagate well to the soma.

We binned the response within a time window that corresponded to motion of about 5.6° along the azimuth and plotted the normalized response amplitudes (PD – ND) in false color code against the position of the bar on the arena (Fig. 3C). Because the arena is curved only in the horizontal direction, the size of the bar as stated earlier is valid for only the equatorial position and appeared slightly smaller to the fly in the dorsal and ventral parts of the visual field. Our analysis revealed that HSN, HSE, and HSS cells in *Drosophila* have large receptive fields that cover at their largest extent over 60° of elevation. HS cells are most sensitive to motion at positions corresponding to their dendritic trees in the lobula plate, which is dorsal for HSN, equatorial for HSE, and ventral for HSS (Fig. 3, A and C). In contrast to *Calliphora* (Hausen 1982b), however, HSE in *Drosophila* seems to be maximally sensitive in the lateral visual field and not in the frontal one.

To estimate the amount of overlap between the receptive fields of HSN, HSE, and HSS, a threshold of either 25 or 50% of the maximal response was set. The areas where the responses of HSN, HSE, or HSS exceeded the threshold were encircled in

blue, red, and green, respectively (Fig. 3D). If a threshold of 25% is used, the receptive fields of HSN and HSS overlap strongly with that of HSE. The receptive field of HSN reaches almost as far ventrally as that of HSE and that of HSS nearly as far dorsally as that of HSE. In an equatorial area extending  $\leq 40^\circ$  in the dorsoventral axis the receptive fields of all three HS cells overlap. Even if a threshold of 50% is used, there is a small equatorial region where the receptive fields of all three HS cells intersect. The huge overlap of the receptive fields of HSN, HSE, and HSS corresponds in part to the overlap of their dendrites stated earlier. However, the dorsoventral extension of the receptive field of HSE seems to be somewhat smaller than expected from its dendritic spanning field (compare Fig. 3, B, C, and D). One explanation might be that we miss signals from remote dendrites due to recording from the soma and thus underestimate the size of the receptive field. In contrast, the lack of dendritic branches of HSN in the ventral area indicates that the ventral extension of the receptive field of HSN cannot be explained by direct input to the dendrite alone (compare Fig. 3, B and D).

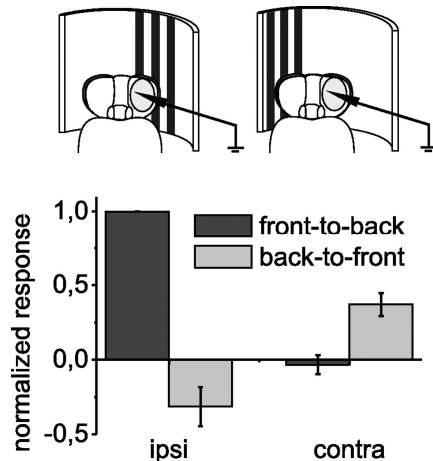


**Fig. 4:** Sensitivity to contralateral motion. Square-wave gratings ( $\lambda = 22.4^\circ$ ) were presented in either the contra- or the ipsilateral visual field as shown in the schematic drawing (sparing the frontal region of binocular overlap). Contralateral back-to-front motion elicited a weak depolarization of the membrane potential in HS cells and a strong depolarization in response to ipsilateral front-to-back motion ( $n = 6$ ; error bar: SE).

Another interesting feature of the receptive fields of HSN and HSE is their sensitivity to contralateral motion (Hausen 1982a; Krapp et al. 2001) (Fig. 4). We presented moving square-wave gratings in either the ipsilateral or the contralateral part of the visual field to investigate this in further detail. The pattern covered about  $56^\circ$  in azimuth and  $85^\circ$  in elevation. To prevent stimulation of the area of binocular overlap, which consists of three vertical rows of ommatidia (Heisenberg and Wolf

1984), the pattern was displaced by  $\pm 15^\circ$  with respect to the frontal gaze of the fly (Fig. 4). Motion in front of the ipsilateral eye elicited canonical PD and ND responses i.e., a depolarization for front-to-back and a hyperpolarization for back-to-front motion. Contralateral back-to-front motion, however, elicited a robust depolarization, whereas contralateral front-to-back motion did not elicit a noticeable response.

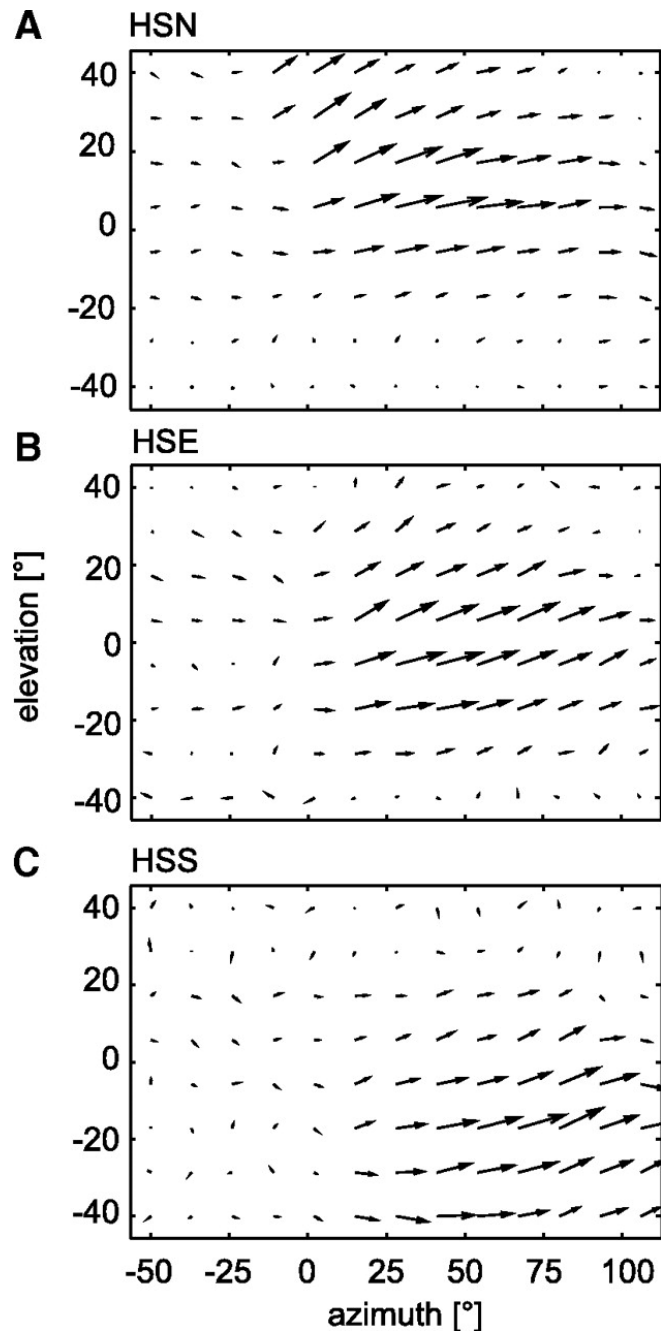


**Fig. 5:** Vector fields of HSN (**A**), HSE (**B**), and HSS (**C**). Local preferred direction and response strength of all 3 HS cells are indicated by the orientation and lengths of the motion vectors (arrows). Vectors were calculated by subtracting PD and ND responses to small bars moving either horizontally or vertically at different positions (compare Fig. 3). Similar to HSN and HSE the maximum sensitivity in the ventral receptive field of HSS corresponds to the area occupied by its dendritic tree in the lobula plate (not shown). Like the other HS cells, HSS responds mainly to horizontal motion. However, all HS cells show a slight sensitivity to upward motion in mostly the center of their receptive field. All responses from HSS ( $n = 6$ ) and HSE ( $n = 9$ ) were recorded from unlabeled cells. HSN vector maps were calculated from the local responses of labeled ( $n = 4$ ) and unlabeled cells ( $n = 1$ ).

Thus HSN and HSE are tuned to rotational panoramic motion stimuli as they arise from rotation of the animal around the vertical body axis. Importantly, their sensory input is not confined to the retinotopically organized columnar neurons that impinge onto their dendritic tree.

We characterized the receptive fields in further detail by presenting a local bar moving vertically in addition to the horizontally moving bar as shown earlier (see Methods; Nordström et al. 2008; Wertz et al. 2009). From the responses to local horizontal and vertical motion, we calculated response vectors that indicate by their orientation the local preferred direction and by their length, the strength of the response. Motion vectors calculated this way were recently shown to be identical to resulting motion vectors calculated from periodic gratings that drifted in many different orientations and directions (Wertz et al. 2009). All local vectors together constitute the optic flow field of a given HS cell (Fig. 5). All three HS cells exhibited a slight vertical sensitivity. HSN (Fig. 5A) and, to a weaker extent HSE (Fig. 5B), depolarize in response to upward motion in the frontodorsal and frontoequatorial parts of their receptive fields. HSS shows a similar sensitivity to upward motion in a more ventrolateral position (Fig. 5C).

### **Dye-coupling suggests that HS cells are part of a network of electrically coupled neurons**

In *Calliphora*, complex receptive fields of VS and HS cells arise from electric coupling to other LPTCs and descending neurons (Cuntz et al. 2007; Haag and Borst 2004). Injection of Neurobiotin, a molecule sufficiently small to pass Innexin-based gap junctions, and double recording revealed that neurons that allow the spread of Neurobiotin are indeed electrically coupled in *Calliphora* (Haag and Borst 2005).

We investigated whether this also holds true for HS cells in *Drosophila*. For that purpose, Neurobiotin was added to the intracellular solution in the recording electrode. GFP-labeled HSN or HSE cells were filled via their somata. We used patch electrodes instead of sharp electrodes to avoid unspecific labeling that might be caused by brief penetration of other neurons. Perfusion with Alexa-568 allowed for immediate identification of the recorded neuron. Later, the spread of Neurobiotin was detected by staining with Streptavidin-coupled Alexa-568 (Joesch et al. 2008).

Because the initially perfused free Alexa-568 never stained other cells except the injected one, we concluded that fluorescence after Streptavidin–Alexa-568 labeling in other cells is due to direct or indirect coupling via electrical synapses to the recorded cell (Fig. 6).

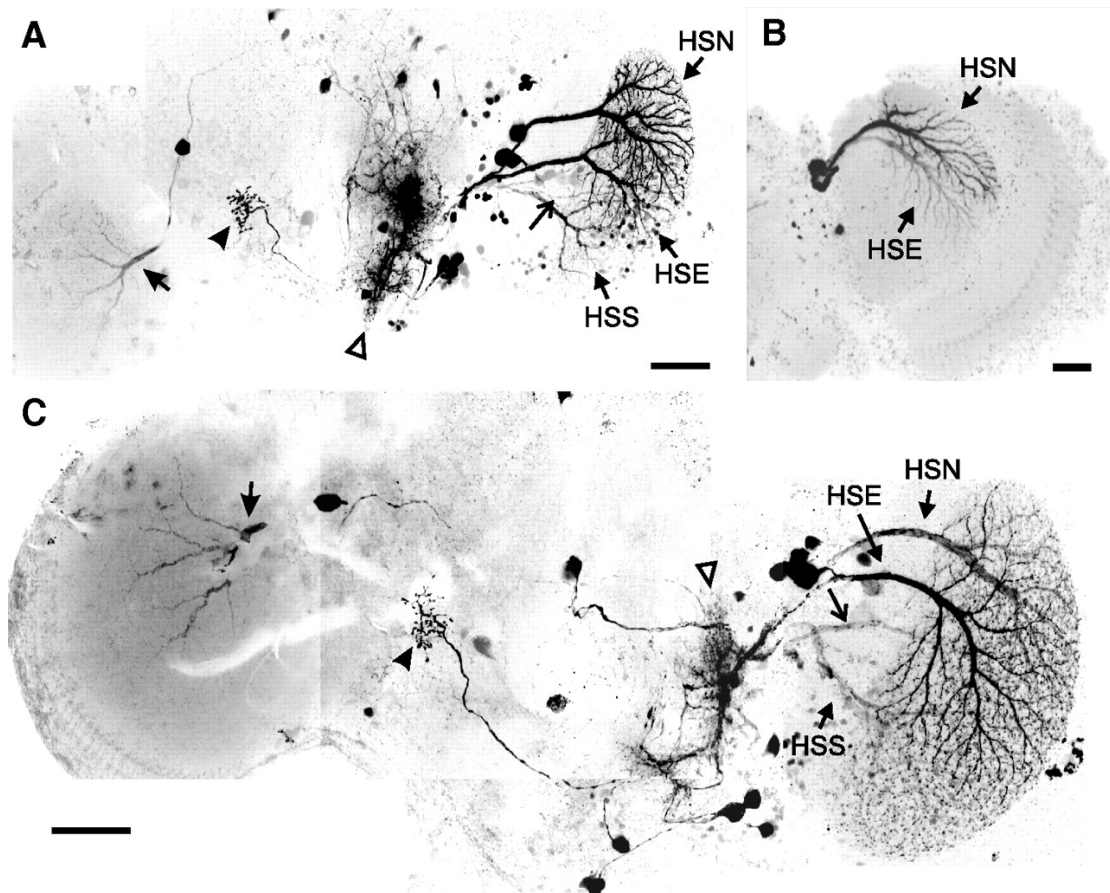


**Fig. 6:** Spread of Neurobiotin within the HS circuitry. The spread of Neurobiotin, which can pass through Innexin junctions, provides indirect evidence for electric coupling among HS and other cells. Neurobiotin was injected into either HSN (A and B) or HSE (C) and visualized with Streptavidin coupled to a red fluorescent dye. Costaining was detected in neighboring HS cells (named in A to C), unidentified ipsilateral descending neurons (open triangle), cells projecting to the contralateral protocerebrum where HS cell axons terminate (arrowheads in A and C), contralateral lobula plate tangential cells (LPTCs; filled arrows in A and C), and occasionally in unidentified fibers in the same lobula plate (open arrows in A and C). The figure shows composite images of maximum intensity projections of confocal image stacks taken from neighboring regions of the brain. Scale bars: 50 μm.

When we injected Neurobiotin into either HSN (Fig. 6, A and B) or HSE (Fig. 6C), one or both of the remaining ipsilateral HS cells were typically labeled. In contrast to similar experiments in *Calliphora*, no CH cells were found to be colabeled (Haag and Borst 2005). From this observation we conclude that HS cells in *Drosophila* are

directly or indirectly coupled with each other. Nevertheless, we observed additional staining in fibers other than the three HS cells in the same lobula plate (Fig. 6, A and C). Unfortunately, the staining was too weak to enable unequivocal identification of these processes. In these cases the arborization of an LPTC in the contralateral lobula plate was also labeled (filled arrows in Fig. 6, A and C) that might belong to the unidentified ipsilateral processes mentioned earlier. This cell represents a likely candidate neuron to provide contralateral input to HS cells (Figs. 2, 3, and 4). In addition, HS cells were extensively dye-coupled to descending neurons (open triangles in Fig. 6, A and C) that could not be identified individually. One frequently labeled neuron has a prominent arborization on the contralateral side and probably connects the output region of HS cells of both hemispheres (arrowhead in Fig. 6, A and C). Taken together, our findings suggest that HS cells are part of a complicated network of electrically coupled neurons. This network comprises descending neurons, ipsilateral HS cells, and LPTCs from the same and the contralateral hemisphere so far unidentified in *Drosophila*. The columnar input to the ipsilateral dendrite and the electric coupling to the LPTC network are likely sufficient to account for the wide receptive fields and rotational tuning of HS cells.

### **5. Discussion**

*Drosophila* reacts to horizontally drifting retinal images with compensatory yaw-torque responses to stabilize straight-flight segments (Heisenberg and Wolf 1984). The giant HS cells in the lobula plate are thought to play a key role in the control of this behavior, although their exact role remains elusive. Patch-clamp recordings in *Drosophila* were only established recently (Wilson et al. 2004) and physiological data from *Drosophila* HS cells were not available so far. We used the Gal4/UAS-system (Brand and Perrimon 1993) to fluorescently label two of the three HS cells, HSN and HSE, which allowed for the investigation of their basic anatomy (Figs. 1 and 3) and targeting for reliable recordings from their somata (Figs. 1–3); neighboring HSS cells were recorded and filled without the use of genetic labeling (Figs. 3 and 5). In *Drosophila*, whole cell recordings are so far feasible only from the soma. They allow for reliable and stable recordings for  $\leq 1$  h. We describe the response characteristics



of all three giant neurons of the HS system in *Drosophila*, their directional selective output, receptive field organization, and network interactions.

### **Basic response properties of *Drosophila* HS cells**

Concerning their basic response properties, we found that HS cells in *Drosophila* are largely similar to their counterparts in *Calliphora* (Hausen 1982a,b). They respond to horizontal motion with graded membrane potential changes in a directional-selective way (Fig. 1). Their responses are indicative of input from elementary motion detectors of the correlation type (Fig. 2) because they are independent of the sign of contrast and exhibit a velocity optimum that linearly depends on the spatial wavelength of the moving periodic grating. Such a dependence results in a single temporal frequency optimum and is a characteristic feature of presynaptic computations according to the correlation-type detector model (Borst and Egelhaaf 1989; Reichardt 1961). The temporal frequency optimum of 1 Hz (Fig. 2B) precisely matches the results from our previous account on *Drosophila* VS cells (Joesch et al. 2008) and findings from H1 cells in *Calliphora* (Haag et al. 2004). However, recordings from HS cells in *Calliphora* resulted in higher values of 2–5 Hz (Hausen 1982b), suggesting slight differences between the two fly species. The quadratic dependence of the response on the contrast predicted by a correlation-type detector model is generally found only in the low-contrast range (Buchner 1984). However, a detailed and satisfying analysis of the low-contrast regime cannot be performed using our LED arena. At higher contrasts, the responses saturate (Fig. 2C), probably due to a gain control mechanism in elementary motion detectors. The cellular implementation of these motion detectors is still an open question in the field.

### **Anatomical layout of HS cell dendrites and receptive fields**

The image of the environment is represented by retinotopically organized columnar maps in the optic lobes (Braitenberg 1970; Strausfeld 1976, 1984). Within this arrangement, the dendrite of each of the HS cells occupies about 40–45% of the lobula plate in *Calliphora* (Hausen 1982a), but 70–90% in *Drosophila*. In *Calliphora*,

the dendrites of HSN and HSS overlap to some extent with those of HSE, but not with each other. In *Drosophila*, in contrast, we find an area in the lobula plate, where all three cells overlap (Fig. 3A). Thus the overlap is much larger in *Drosophila* (Heisenberg et al. 1978) than that in *Calliphora*. In both cases female flies were studied to exclude sex-specific differences. Such differences in LPTC anatomy and number between different dipteran species have been described and were linked to differences in flight style and behavior (Buschbeck and Strausfeld 1997; Nordström et al. 2008).

The areas covered by the dendrites of HSN, HSE, and HSS correspond to the centers of large dorsal, equatorial, and ventral receptive fields, respectively. Yet, the ipsilateral receptive field of HSN significantly exceeds the area occupied by its dendrite in the lobula plate (Fig. 3). In addition, HSN and HSE are both sensitive to contralateral motion. These receptive fields of HS cells can be explained by assuming 1) dendritic input from local motion detectors, 2) electric coupling to neighboring HS cells, and 3) input from contralateral neurons tuned to regressive motion. The evidence for this input organization is discussed in the following text.

**IPSILATERAL COLUMNAR INPUT.** The excitatory and inhibitory responses of HS cells suggest that *Drosophila* HS cells receive input from two types of elementary motion detectors with opposite preferred direction (Borst and Egelhaaf 1990; Borst et al. 1995; Single and Borst 1998). Further evidence for this scheme comes from the localization of excitatory cholinergic and inhibitory GABAergic synapses on the dendritic tips of VS and HS cells in *Drosophila* (Raghu et al. 2007, 2009) and the simultaneous integration of excitatory and inhibitory input with separate reversal potentials during grating motion (Joesch et al. 2008).

The retinotopic arrangement of the detectors is further supported by our finding that HS cells respond to local motion stimuli with a strong preference for horizontal motion. Moreover, gradual changes in local PD with a bias to upward motion were observed in the dorsofrontal (HSN and HSE) and ventrolateral (HSS) margins of the receptive field (Fig. 5). Sensitivity to vertical motion in parts of the receptive field was also reported for HS cells in *Calliphora* and was attributed to the arrangement of the ommatidial lattice in the corresponding parts of the eye (Hausen 1982b). Most

likely this holds also true for *Drosophila* (Heisenberg and Wolf 1984). Neurobiotin did not spread from HS cells to vertically sensitive LPTCs in *Drosophila* (Fig. 6), although connections between HSN and lateral VS cells were reported in *Calliphora* (Haag and Borst 2005). However, in *Calliphora* these connections are supplied via the dCH cell (Haag and Borst 2007) and CH cells could not be found in *Drosophila* so far.

**COUPLING TO NEIGHBORING HS CELLS.** In flies, electrical connectivity schemes based on Neurobiotin coupling were previously shown to be in accordance with data obtained from double recordings (Fan et al. 2005; Haag and Borst 2005). Because our Neurobiotin injections resulted in highly reproducible patterns of stained cells, we conclude that it is a useful tool for studying direct or indirect electrical coupling. However, dye-coupling alone does not allow one to draw conclusions about the strength and functional significance of these connections.

Direct electric coupling between neighboring HS cells or via descending neurons is suggested by the spread of Neurobiotin (Fig. 6) and provides the most plausible explanation for the observed broad ipsilateral receptive field of HSN (Fig. 3). A similar ipsilateral coupling has been found in the VS cell network in *Drosophila* (Joesch et al. 2008) and within and between the HS and VS system of *Calliphora* (Farrow et al. 2005; Haag and Borst 2004, 2007). In the VS system of *Calliphora* lateral connections are thought to be responsible for the large receptive fields and thus the robustness of the response against inhomogeneous contrast distribution in the visual scene (Cuntz et al. 2007). However, HS cells in *Calliphora* are coupled to each other only indirectly via the dorsal and ventral CH cell (Cuntz et al. 2003; Haag and Borst 2002), which, by this way, receive graded input from HS cells. In response to large-field motion, CH cells in turn inhibit so-called figure-detection neurons, thereby tuning them to small-field motion (Cuntz et al. 2003; Egelhaaf 1985; Haag and Borst 2002; Warzecha et al. 1993). It is unclear how *Drosophila* solves this problem.

The fact that CH cells were never detected in our experiments matches their absence in any of the Gal4 screens and any of the detailed anatomical descriptions reported so far in *Drosophila* (Fischbach and Dittrich 1989). The weakly stained fibers next to HS cells (Fig. 6) in the ipsilateral lobula plate could not be identified due to their

weak Neurobiotin labeling. The very strong and reliable coupling of HS and CH cells in *Calliphora* makes it unlikely that these weakly stained fibers represent the processes of *Drosophila* CH cells; rather, they could belong to the heterolateral projecting neurons (see following text).

INPUT FROM NEURONS WITH CONTRALATERAL RECEPTIVE FIELDS. In addition to two sources of ipsilateral input, we found sensitivity to contralateral back-to-front motion in HSN and HSE. The heterolateral projecting LPTCs detected after Neurobiotin injection (Fig. 5, A and C) are good candidates to provide this input. They might correspond to either H1 or H2, two heterolateral spiking neurons that provide input to contralateral HS cells in *Calliphora* (Haag and Borst 2001; Hausen 1982a,b; Horstmann et al. 2000). Both cells have their dendrites in the contralateral lobula plate, where they respond to back-to-front motion with an increase in spike frequency. The axonal arborization of H1 is in the ipsilateral lobula plate. H2 axons project to the output region of HS cells in the ipsilateral protocerebrum, where they make electric contacts with HS cells. Due to the many other labeled cells and relatively weak labeling of the heterolateral neurons we could not determine whether Neurobiotin labeled H1, H2, or a third cell type. As in *Calliphora* (Götz and Buchner 1978; Hausen 1982a,b; Hausen and Wehrhahn 1989; Reichardt and Egelhaaf 1988), HSS in *Drosophila* does not respond to motion in the contralateral visual field.

Ultimately, navigation and course control in flies rely on the analysis of optic flow. Neurons that contribute to the underlying computations possess wide dendritic fields and further increase their receptive fields by connections to functionally related ipsilateral and contralateral neurons. Our data suggest that this principle is retained in the HS system of *Drosophila*, but it remains to be analyzed how the observed differences to *Calliphora* translate into differences in optomotor behavior.

### **Behavioral relevance**

HS cells are supposed to be key players for the control of optomotor turning responses elicited by horizontal motion. This notion is mostly based on the observation that electrical responses of HS cells in *Calliphora* and optomotor torque

responses in *Musca* and *Drosophila* show a similar dependence on spatial features of moving visual stimuli (Götz and Buchner 1978; Hausen 1982a,b; Hausen and Wehrhahn 1989; Reichardt and Egelhaaf 1988). In addition, elimination of the HS system in *Musca* by laser ablation (Geiger and Nässel 1981) and the *omb* mutation in *Drosophila* [largely missing HS cells and many other LPTCs and columnar neurons absent (*omb*; Heisenberg et al. 1978)] led to severe deficits in the execution of optomotor yaw responses.

We found that HSN and HSE in *Drosophila* are tuned to binocular rotational motion around the vertical body axis (Figs. 3 and 4). Their responses exhibit a similar dependence on features of the stimulus as optomotor yaw-torque responses, in particular a temporal frequency optimum of about 1 Hz (Fig. 2, A and B) (Buchner 1984; Götz 1964). Thus our experiments corroborate their functional contribution to compensatory turning behavior. This consent, however, is somewhat questioned by recently published behavioral experiments that report an optimum response between 5 and 10 Hz (Duistermars et al. 2007; Fry et al. 2009). At this frequency, however, HS cell responses (Fig. 2) and previously measured yaw-torque (Götz 1964) were reduced to less than half of the maximal response. It remains speculative whether this discrepancy can be attributed to differences in the stimulus presentation.

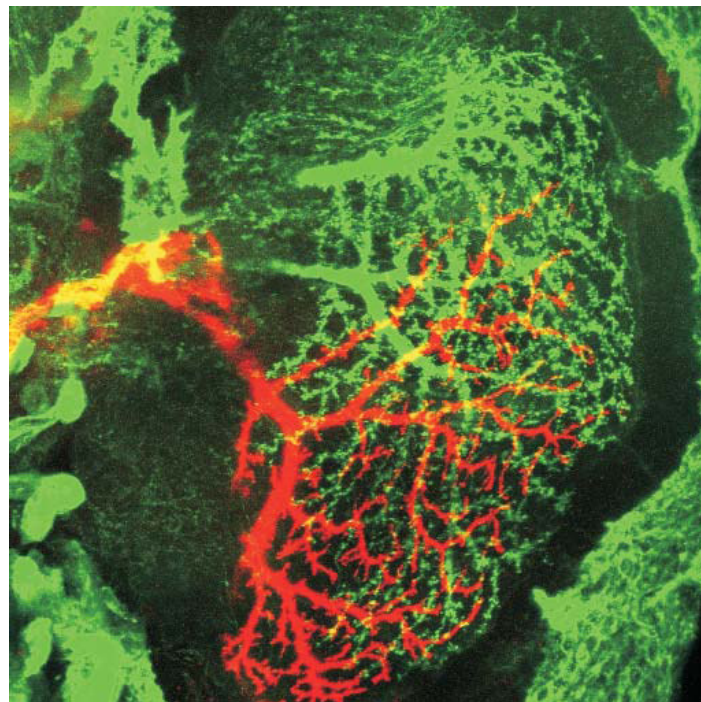
Further measurements are required to investigate whether HS cells in *Drosophila* also encode information about the structure of the visual surround during translational motion, as is suggested from experiments in blowflies (Boeddeker and Egelhaaf 2005; Kern et al. 2005). Also, lateral expansion stimuli need to be analyzed because they were reported to elicit larger optomotor responses than rotational ones (Duistermars et al. 2007; Tammero et al. 2004). In summary, HS cell output very likely feeds into multisensory neural circuits that control different behaviors of the fly (Frye and Dickinson 2001, 2004).

### **Concluding remarks**

HS cells in *Drosophila* and large dipteran flies have largely similar response properties despite substantial differences in the organization of the neural circuitry for the detection of horizontal optic flow. Their responses are indicative of a

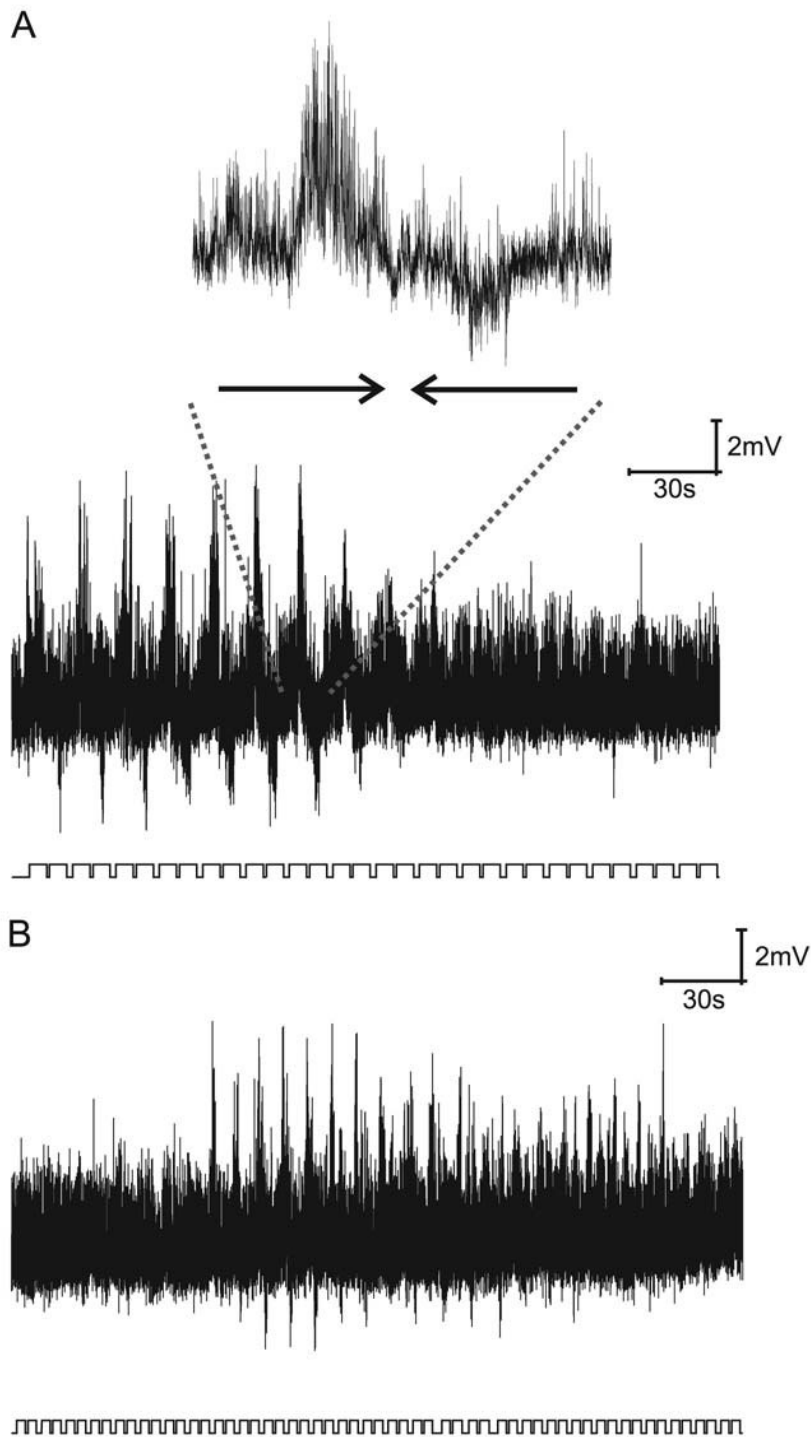
correlation-type motion detector model. The overlap and relative size of ipsilateral HS cell dendrites are larger in *Drosophila*. CH cells, which link the HS and VS systems in *Calliphora* and are key elements of a circuitry dedicated to the detection of small moving objects, were not found in *Drosophila*. In addition, *Drosophila* HS cells exhibit a somewhat lower temporal frequency optimum than that of their counterparts in *Calliphora*. These differences might reflect adaptations to different lifestyles, given that the basic response properties of large-field motion-sensitive neurons seem to match differences in flight style (O'Carroll et al. 1996). Our functional and anatomical characterization of the HS cell circuitry in *Drosophila* can now serve to dissect 1) the presynaptic motion detection circuitry and 2) the exquisite control mechanism of compensatory optomotor responses by combining genetic manipulation of neuronal function with physiological recording and behavioral analysis.

### 6. Supplement



#### **Supplementary Fig. 1: Anatomy of all three HS-cells.**

The Gal4-line NP0282 drives expression of the green fluorescent marker mCD8-GFP in HSN and HSE. HSS was labeled by injection of the red fluorescent dye Alexa Fluor 594 into its axon. This image was generated by collapsing a confocal image stack used for the reconstruction shown in Fig. 3A.



**Supplementary Fig. 2: Analysis of the receptive fields of HS-cells.**

Recording traces of an HSN-cell in response to a local motion stimulus. (A) A small vertical bar ( $1.4^\circ$  by  $5.6^\circ$ ) was moving alternately in preferred and null direction at different elevations from dorsal to ventral eliciting depolarizing and hyperpolarizing deflections of the membrane potential. These deflections are largest in the dorsal field of view (beginning of the trace) and absent in the most ventral area (end of the trace). Upward deflections of the lower trace indicate times at which the bar was moving. (B) Same as A only that a horizontal bar is moving alternately downward and upward at consecutive positions along the azimuth from contralateral to ipsilateral.

### 7. Acknowledgments

We thank W. Essbauer, C. Theile, and the Max Planck Institute workshop for excellent technical support; J. Plett for the design of the LED arena; R. Schorner for artwork; and J. Haag, E. Buchner, and the other members of the Borst department for discussion.

### 8. References

- Boeddeker N and Egelhaaf M.** A single control system for smooth and saccade-like pursuit in blowflies. *Journal of experimental biology* 208: 1563-1572, 2005.
- Borst A and Egelhaaf M.** Principles of visual motion detection. *Trends Neurosci* 12: 297-306, 1989.
- Borst A and Egelhaaf M.** Direction selectivity of fly motion-sensitive neurons is computed in a two-stage process. *Proc Natl Acad Sci USA* 87: 9363-9367, 1990.
- Borst A, Egelhaaf M and Haag J.** Mechanisms of dendritic integration underlying gain control in fly motion-sensitive interneurons. *J Computat Neurosci* 2: 5-18, 1995.
- Borst A and Haag J.** The intrinsic electrophysiological characteristics of fly lobula plate tangential cells :I. Passive membrane properties. *J Computat Neurosci* 3: 313-336, 1996.
- Borst A and Haag J.** Neural networks in the cockpit of the fly. *J Comp Physiol A Neuroethol Sens Neural Behav Physiol* 188: 419-437, 2002.
- Braitenberg V.** Ordnung und Orientierung der Elemente im Sehsystem der Fliege. *Kybernetik* 7: 235-242, 1970.
- Brand AH and Perrimon N.** Targeted gene expression as a means of altering cell fates and generating dominant phenotypes. *Development* 118: 401-15, 1993.
- Buchner E.** Behavioural analysis of spatial vision in insects. In: Photoreception and vision in invertebrates, edited by Ali MA. New York, London: Plenum Press, 1984, p. 561-621.
- Buschbeck EK and Strausfeld NJ.** The relevance of neural architecture to visual performance: phylogenetic conservation and variation in dipteran visual systems. *J Comp Neurol* 383: 282-304, 1997.
- Chan WP, Prete F and Dickinson MH.** Visual input to the efferent control system of a fly's "gyroscope". *Sci* 280: 289-292, 1998.
- Cuntz H, Forstner F, Haag J and Borst A.** The morphological identity of insect dendrites. *PLoS Comput Biol* 4: e1000251, 2008.
- Cuntz H, Haag J and Borst A.** Neural image processing by dendritic networks. *Proc Natl Acad Sci U S A* 100: 11082-11085, 2003.



**Cuntz H, Haag J, Forstner F, Segev I and Borst A.** Robust coding of flow-field parameters by axo-axonal gap junctions between fly visual interneurons. *Proc Natl Acad Sci U S A* 104: 10229-10233, 2007.

**Douglass JK and Strausfeld NJ.** Visual motion detection circuits in flies: peripheral motion computation by identified small-field retinotopic neurons. *J Neurosci* 15: 5596-5611, 1995.

**Douglass JK and Strausfeld NJ.** Visual motion - detection circuits in flies : parallel direction -and non-direction-sensitive pathways between the medulla and lobula plate. *J Neurosci* 16: 4551-4562, 1996.

**Douglass JK and Strausfeld NJ.** Anatomical organization of retinotopic motion-sensitive pathways in the optic lobes of flies. *Microsc Res Tech* 62: 132-150, 2003.

**Duistermars BJ, Chow DM, Condro M and Frye MA.** The spatial, temporal and contrast properties of expansion and rotation flight optomotor responses in *Drosophila*. *J Exp Biol* 210: 3218-3227, 2007.

**Eckert H and Meller K.** Synaptic structures of identified, motion-sensitive interneurons in the brain of the fly, *Phaenicia*. *Verh Dtsch Zool Ges* 1981: 179, 1981.

**Egelhaaf M.** On the neuronal basis of figure-ground discrimination by relative motion in the visual system of the fly. II. Figure-Detection Cells, a new class of visual interneurons. *Biol Cybern* 52: 195-209, 1985.

**Egelhaaf M, Boddeker N, Kern R, Kretzberg J, Lindemann JP and Warzecha AK.** Visually guided orientation in flies: case studies in computational neuroethology. *J Comp Physiol A Neuroethol Sens Neural Behav Physiol* 189: 401-409, 2003.

**Egelhaaf M and Borst A.** Are there separate ON and OFF channels in fly motion vision? *Vis Neurosci* 8: 151-164, 1992.

**Elyada YM, Haag J and Borst A.** Different receptive fields in axons and dendrites underlie robust coding in motion-sensitive neurons. *Nat Neurosci* 12: 327-332, 2009.

**Farrow K, Borst A and Haag J.** Sharing receptive fields with your neighbors: tuning the vertical system cells to wide field motion. *J Neurosci* 25: 3985-3993, 2005.

**Farrow K, Haag J and Borst A.** Nonlinear, binocular interactions underlying flow field selectivity of a motion-sensitive neuron. *Nat Neurosci* 9: 1312-1320, 2006.

**Fischbach KF and Dittrich APM.** The optic lobe of *Drosophila melanogaster*. I. A Golgi analysis of wild-type structure. *Cell Tissue Res* 258: 441-475, 1989.

**Fry SN, Rohrseitz N, Straw AD and Dickinson MH.** Visual control of flight speed in *Drosophila melanogaster*. *J Exp Biol* 212: 1120-1130, 2009.

**Frye MA and Dickinson MH.** Fly flight: a model for the neural control of complex behavior. *neuron* 32: 385-388, 2001.

**Frye MA and Dickinson MH.** Closing the loop between neurobiology and flight behavior in *Drosophila*. *Curr Opin Neurobiol* 14: 729-736, 2004.

**Geiger G and Nässel DR.** Visual orientation behaviour of flies after selective laser beam ablation of interneurons. *Nature* 293: 398-399, 1981.

**Gilbert C, Gronenberg W and Strausfeld NJ.** Oculomotor control in calliphorid flies: head movements during activation and inhibition of neck motor neurons corroborate neuroanatomical predictions. *J Comp Neurol* 361: 285-297, 1995.

**Gilbert C and Strausfeld NJ.** The functional organization of male-specific visual neurons in flies. *J Comp Physiol A* 169: 395-411, 1991.

**Götz KG.** Optomotorische Untersuchungen des visuellen Systems einiger Augenmutanten der Fruchtfliege *Drosophila*. *Kybernetik* 2: 77-92, 1964.

**Götz KG.** Die optischen Übertragungseigenschaften der Komplexaugen von *Drosophila*. *Kybernetik* 2: 215-221, 1965.

**Götz KG and Buchner E.** Evidence for one-way movement detection in the visual system of *Drosophila*. *Biol Cybern* 31: 243-248, 1978.

**Gouwens NW and Wilson RI.** Signal propagation in *Drosophila* central neurons. *J Neurosci* 29: 6239-6249, 2009.

**Gronenberg W and Strausfeld NJ.** Descending neurons supplying the neck and flight motor of diptera: Physiological and anatomical characteristics. *J Comp Neurol* 302: 973-991, 1990.

**Haag J and Borst A.** Recurrent network interactions underlying flow-field selectivity of visual interneurons. *J Neurosci* 21: 5685-5692, 2001.

**Haag J and Borst A.** Dendro-dendritic interactions between motion-sensitive large-field neurons in the fly. *J Neurosci* 22: 3227-3233, 2002.

**Haag J and Borst A.** Neural mechanism underlying complex receptive field properties of motion-sensitive interneurons. *Nat Neurosci* 7: 628-634, 2004.

**Haag J and Borst A.** Dye-coupling visualizes networks of large-field motion-sensitive neurons in the fly. *J Comp Physiol A Neuroethol Sens Neural Behav Physiol* 191: 445-454, 2005.

**Haag J and Borst A.** Reciprocal inhibitory connections within a neural network for rotational optic-flow processing. *Front Neurosci* 1: 111-121, 2007.

**Haag J and Borst A.** Electrical coupling of lobula plate tangential cells to a heterolateral motion-sensitive neuron in the fly. *J Neurosci* 28: 14435-14442, 2008.

**Haag J, Denk W and Borst A.** Fly motion vision is based on Reichardt detectors regardless of the signal-to-noise ratio. *Proc Natl Acad Sci U S A* 101: 16333-16338, 2004.

**Haag J, Wertz A and Borst A.** Integration of lobula plate output signals by DNOVS1, an identified premotor descending neuron. *J Neurosci* 27: 1992-2000, 2007.

**Hausen K.** Motion sensitive interneurons in the optomotor system of the fly. I. The Horizontal Cells: Structure and signals. *Biol Cybern* 45: 143-156, 1982a.

**Hausen K.** Motion sensitive interneurons in the optomotor system of the fly. II. The Horizontal Cells: Receptive field organization and response characteristics. *Biol Cybern* 46: 67-79, 1982b.

- Hausen K and Wehrhahn C.** Neural circuits mediating visual flight control in flies. I. Quantitative comparison of neural and behavioral response characteristics. *J Neurosci* 9: 3828-3836, 1989.
- Heisenberg M.** Comparative Behavioral Studies on 2 Visual Mutants of *Drosophila*. *J Comp Physiol* 80: 119-127, 1972.
- Heisenberg M and Buchner E.** The role of retinula cell types in visual behavior of *Drosophila melanogaster*. *J Comp Physiol* 117: 127-162, 1977.
- Heisenberg M and Wolf R.** *Vision in Drosophila*. Berlin, Heidelberg, New York, Tokyo: Springer, 1984.
- Heisenberg M, Wonneberger R and Wolf R.** Optomotor-blind (H31) - a *Drosophila* mutant of the lobula plate giant neurons. *J Comp Physiol* 124: 287-296, 1978.
- Hengstenberg R, Hausen K and Hengstenberg B.** The number and structure of giant vertical cells (VS) in the lobula plate of the blowfly *Calliphora erythrocephala*. *J Comp Physiol A* 149: 163-177, 1982.
- Horstmann W, Egelhaaf M and Warzecha AK.** Synaptic interaction increase optic flow specificity. *Eur J Neurosci* 12: 2157-2165, 2000.
- Joesch M, Plett J, Borst A and Reiff DF.** Response properties of motion-sensitive visual interneurons in the lobula plate of *Drosophila melanogaster*. *Current Biology* 18: 1-7, 2008.
- Katsov AY and Clandinin TR.** Motion processing streams in *Drosophila* are behaviorally specialized. *Neuron* 59: 322-335, 2008.
- Kern R, van Hateren JH, Michaelis C, Lindemann JP and Egelhaaf M.** Function of a fly motion-sensitive neuron matches eye movements during free flight. *PLoS Biol* 3: e171, 2005.
- Krapp HG, Hengstenberg B and Hengstenberg R.** Dendritic structure and receptive-field organization of optic flow processing interneurons in the fly. *J Neurophysiol* 79: 1902-1917, 1998.
- Krapp HG, Hengstenberg R and Egelhaaf M.** Binocular contributions to optic flow processing in the fly visual system. *J Neurophysiol* 85: 724-734, 2001.
- Mronz M and Lehmann FO.** The free-flight response of *Drosophila* to motion of the visual environment. *J Exp Biol* 211: 2026-2045, 2008.
- Nordstrom K, Barnett PD, Moyer dM, I, Brinkworth RS and O'Carroll DC.** Sexual dimorphism in the hoverfly motion vision pathway. *Curr Biol* 18: 661-667, 2008.
- O'Carroll D, Bidwell NJ, Laughlin SB and Warrant EJ.** Insect motion detectors matched to visual ecology. *Nature* 382: 63-66, 1996.
- Otsuna H and Ito K.** Systematic analysis of the visual projection neurons of *Drosophila melanogaster*. I. Lobula-specific pathways. *J Comp Neurol* 497: 928-958, 2006.
- Raghu SV, Joesch M, Borst A and Reiff DF.** Synaptic organization of lobula plate tangential cells in *Drosophila*: gamma-aminobutyric acid receptors and chemical release sites. *J Comp Neurol* 502: 598-610, 2007.

**Raghu SV, Joesch M, Sigrist SJ, Borst A and Reiff DF.** Synaptic Organization of Lobula Plate Tangential Cells in Drosophila: D $\alpha$ 7 Cholinergic Receptors. *J Neurogenet* DOI: 10.1080/01677060802471684: 2009.

**Reichardt W.** Autocorrelation, a principle for the evaluation of sensory information by the central nervous system. In: *Sensory Communication*, edited by Rosenblith WA. New York, London: The M.I.T. Press and John Wiley & Sons, 1961, p. 303-317.

**Reichardt W and Egelhaaf M.** Properties of individual movement detectors as derived from behavioural experiments on the visual system of the fly. *Biol Cybern* 58: 287-294, 1988.

**Rister J, Pauls D, Schnell B, Ting CY, Lee CH, Sinakevitch I, Morante J, Strausfeld NJ, Ito K and Heisenberg M.** Dissection of the peripheral motion channel in the visual system of *Drosophila melanogaster*. *neuron* 56: 155-170, 2007.

**Scott EK, Raabe T and Luo LQ.** Structure of the vertical and horizontal system neurons of the lobula plate in *Drosophila*. *Journal of Comparative Neurology* 454: 470-481, 2002.

**Single S and Borst A.** Dendritic integration and its role in computing image velocity. *Sci* 281: 1848-1850, 1998.

**Single S, Haag J and Borst A.** Dendritic computation of direction selectivity and gain control in visual interneurons. *J Neurosci* 17: 6023-6030, 1997.

**Strausfeld NJ.** *Atlas of an insect brain*. Berlin, Heidelberg: Springer, 1976.

**Strausfeld NJ.** Functional neuroanatomy of the blowfly's visual system. In: *Photoreception and vision in invertebrates*, edited by Ali MA. Plenum Publishing Corporation, 1984, p. 483-522.

**Tammero LF, Frye MA and Dickinson MH.** Spatial organization of visuomotor reflexes in *Drosophila*. *J Exp Biol* 207: 113-122, 2004.

**Warzecha AK, Egelhaaf M and Borst A.** Neural circuit tuning fly visual interneurons to motion of small objects. I. Dissection of the circuit by pharmacological and photoinactivation techniques. *J Neurophysiol* 69: 329-339, 1993.

**Wertz A, Haag J and Borst A.** Local and global motion preferences in descending neurons of the fly. *J Comp Physiol A Neuroethol Sens Neural Behav Physiol* 2009.

**Wilson RI and Laurent G.** Role of GABAergic inhibition in shaping odor-evoked spatiotemporal patterns in the *Drosophila* antennal lobe. *J Neurosci* 25: 9069-9079, 2005.

**Wilson RI, Turner GC and Laurent G.** Transformation of olfactory representations in the *Drosophila* antennal lobe. *Science* 303: 366-70, 2004.

**Zhu Y, Nern A, Zipursky SL and Frye MA.** Peripheral visual circuits functionally segregate motion and phototaxis behaviors in the fly. *Curr Biol* 19: 613-619, 2009.

## V. ON- and OFF-Pathways in *Drosophila* Motion Vision

Maximilian Joesch\*, Bettina Schnell\*, Shamprasad Varija Raghu, Dierk F. Reiff & Alexander Borst

\* equal contribution

This chapter is accepted for publication in Nature.

### 1. Summary

Motion vision is a major function of all visual systems, yet the underlying neural mechanisms and circuits are still elusive. In the lamina, the first optic neuropile of *Drosophila melanogaster*, photoreceptor signals split into five parallel pathways L1-5<sup>1</sup>. Here we examine how these pathways contribute to visual motion detection by combining genetic block and reconstitution of neural activity in different lamina cell types with whole cell recordings from downstream motion-sensitive neurons<sup>2,3</sup>. We find reduced responses to moving gratings if L1 or L2 is blocked. However, reconstitution of photoreceptor input to only L1 or L2 results in wild-type responses. Thus, the first experiment suggests necessity of both pathways, while the second indicates sufficiency of each single pathway. This contradiction can be explained by electrical coupling between L1 and L2, allowing for activation of both pathways even when only one of them receives photoreceptor input. A fundamental difference between the L1- and L2-pathway is uncovered when blocking L1 or L2 output while presenting moving edges of positive (ON) or negative (OFF) contrast polarity: blocking L1 eliminates the response to moving ON-edges, blocking L2 the response to moving OFF-edges. Thus, similar to the segregation of photoreceptor signals in ON- and OFF-bipolar cell pathways in the vertebrate retina<sup>4</sup>, photoreceptor signals segregate into ON-L1- and OFF-L2-channels in the lamina of *Drosophila*.

### **2. Results and Discussion**

Neurons responding to visual motion in a directionally selective way are found in a vast number of animals and brain regions, ranging from the retina of rabbits<sup>5</sup> to the visual cortex of macaques<sup>6</sup>. In flies, large-field motion-sensitive neurons are located in the third neuropile layer, the lobula plate (Fig.1a), and are thought to be involved in visual flight control<sup>7</sup>. These lobula plate tangential cells are preferentially sensitive to vertical (VS-cells) and horizontal (HS-cells) motion, respectively. They depolarize when stimulated by motion along their preferred direction ('PD-motion') and hyperpolarize during motion along the opposite, so-called null direction ('ND-motion'). In the first neuropile, the lamina, photoreceptors R1-6 provide input, directly or indirectly, onto five different monopolar cells L1-L5<sup>1,8</sup>, using histamine as their transmitter<sup>9</sup>. L1-5 send their axons into the medulla where neurons compute the direction of motion in accordance with the Reichardt model<sup>10</sup>. Such motion detectors then provide excitatory and inhibitory input onto the dendrites of lobula plate tangential cells<sup>2,3,7</sup>. However, the neural circuitry presynaptic to the tangential cells represented by the Reichardt detectors has so far escaped a detailed analysis, because of the small size of the columnar neurons. We set out to elucidate the cellular implementation of the Reichardt model of visual motion detection starting from the lamina, asking which of the various neurons provide input to the motion detection circuitry. Previous studies addressing this question in *Drosophila* used behavioral read-outs to test for effects of blocking and rescuing of specific lamina cells<sup>11-13</sup>. In order to get closer to the circuit in question, we combined genetic intervention in different lamina neurons with electrophysiological recordings of lobula plate tangential cells.

We used the Gal4/UAS-system<sup>14</sup> and intersectional expression strategies (Split-Gal4<sup>15</sup>) to specifically impair different lamina cells (Fig.1b). We tested necessity of L1 and L2 by blocking their output via targeted expression of a temperature-sensitive ('ts'), dominant-negative allele of *shibire*, a gene which codes for the GTPase dynamin needed for vesicle recycling<sup>16</sup>. In these experiments (Fig.2a-d; Fig.4), control flies had the same genotype as experimental flies, but were kept at permissive temperature throughout, while experimental flies were put to restrictive

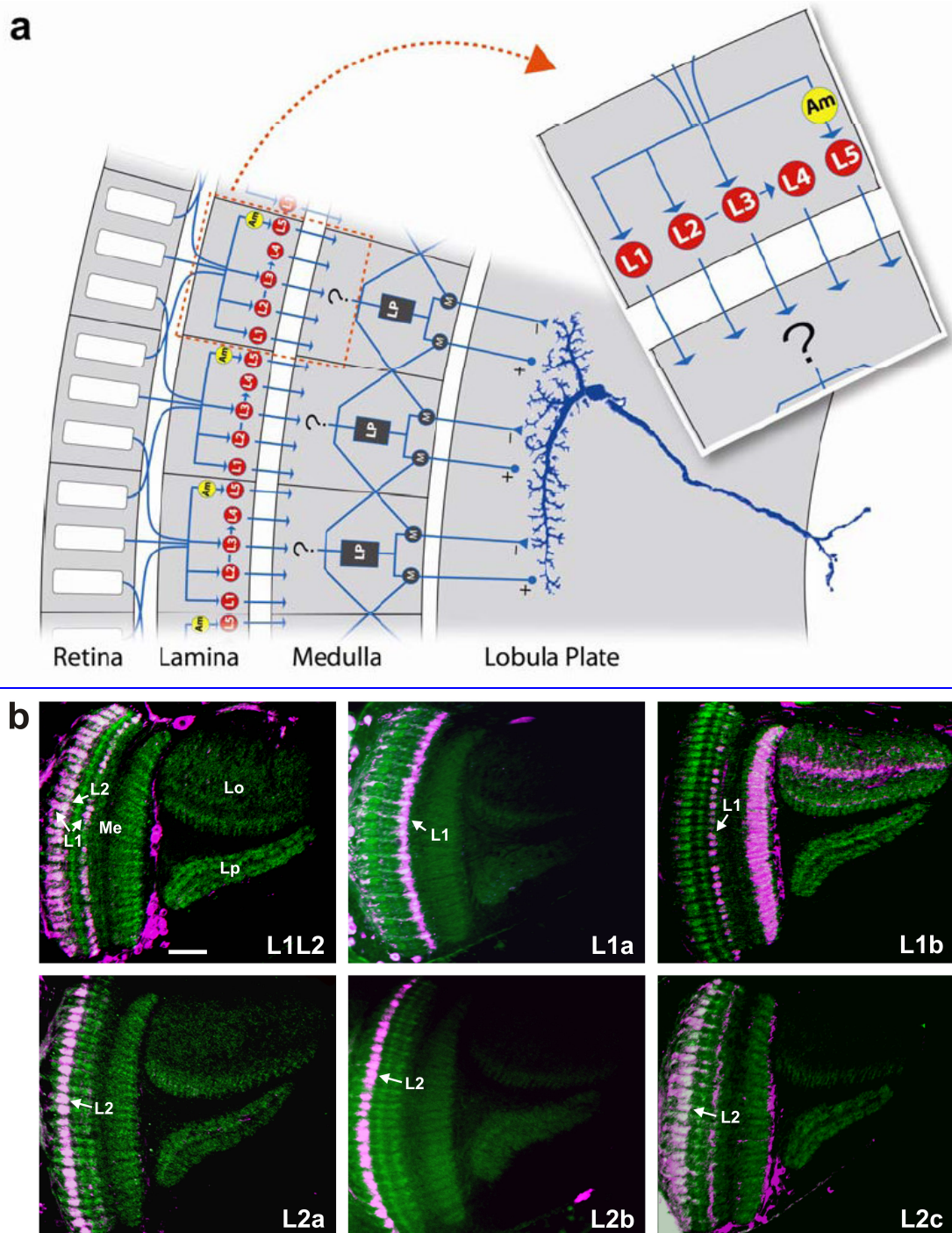


**Fig. 1: (a)** Schematic of the fly optic lobe (frontal view). Via neural superposition, photoreceptors R1-6 (only 3 are shown) connect to five different lamina cells. L1-3 and the amacrine cell receive direct input from the photoreceptors, while L4 and L5 receive indirect input via L2 and the amacrine cell, respectively (simplified after data in ref.1). Within the medulla, a circuit specified only in algorithmic form ('Reichardt detector'<sup>10</sup>) transforms signals from adjacent sampling points into directionally selective output signals. Each such detector consists of two mirror-symmetrical subunits the output signals of which provide excitatory and inhibitory input to lobula plate tangential cells, respectively. In each subunit, the signal derived from one sampling point is low-pass filtered (LP) and subsequently multiplied (M) with the instantaneous signal derived from the neighboring point. Which of the lamina cells

feed into the motion detection circuit and what signals they provide is the central question of this study. **(b)** Expression pattern in the optic lobes of the Gal4 and Split-Gal4 driver lines used in this study. Cells targeted by the driver line were visualized by expression of membrane-tagged DsRed (magenta). The neuropile was labeled using antisera against Dlg, a postsynaptic marker protein (green). Besides the lamina neurons indicated, all lines label, though less intensely, additional cells. For driver lines L1a, L2a and L2c, see ref. 19. For driver line L1b we found co-expression in some Pm-, Mt-, Lt- and Tlp-cells, for driver line L2b co-expression in Tm4-cells, and for driver line L1L2 co-expression in Tm5-, Tlp- and T3-cells. The genotype of each driver line is given in Methods. Scale bar = 20  $\mu$ m. Horizontal optical sections, Me=Medulla, Lo=Lobula, Lp=Lobula plate.

temperature 1h prior to the experiment (see Methods). Alternatively, L1 and L2 were silenced by targeted expression of an inward-rectifying potassium channel<sup>17</sup> ('*Kir2.1*'). In a complementary approach, we tested for sufficiency of L1 and L2 by rescuing a single lamina pathway via targeted expression of the wild-type histamine receptor, encoded by the *ort*-gene<sup>18</sup>, in an *ort*-null mutant background<sup>11,19</sup>. Surprisingly, contradictory results were obtained depending on the type of genetic intervention.

### **Blocking and Rescuing Experiments do not Complement Each Other**

We recorded from HS- and VS-cells and blocked the output of lamina neurons L1 and L2 by targeted expression of *shibire*<sup>ts</sup>. Control flies (black traces in Figs.2a-d) always revealed strong and reliable responses to a moving grating, saturating for increasing contrast levels. The responses to PD-motion (solid lines) were about twice or three times as large as those to ND-motion (dashed lines). Blocking both L1 and L2 led to a complete block of the motion responses even at the highest pattern contrast (Fig.2a, driver line L1L2, blue traces). Blocking only L1 strongly reduced PD and ND responses for all contrasts tested (Fig.2b, driver line L1a, green traces). Blocking L2 using two different driver lines moderately reduced the responses at all contrast levels (L2a, Fig.2c; L2b, Fig.2d; red traces). To test whether the temperature shift alone could lead to altered motion responses, flies that had the same genotype as experimental flies except for the Gal4-driver gene were put to restrictive temperature 1h prior to the experiment. The responses of these flies were indistinguishable from the ones of



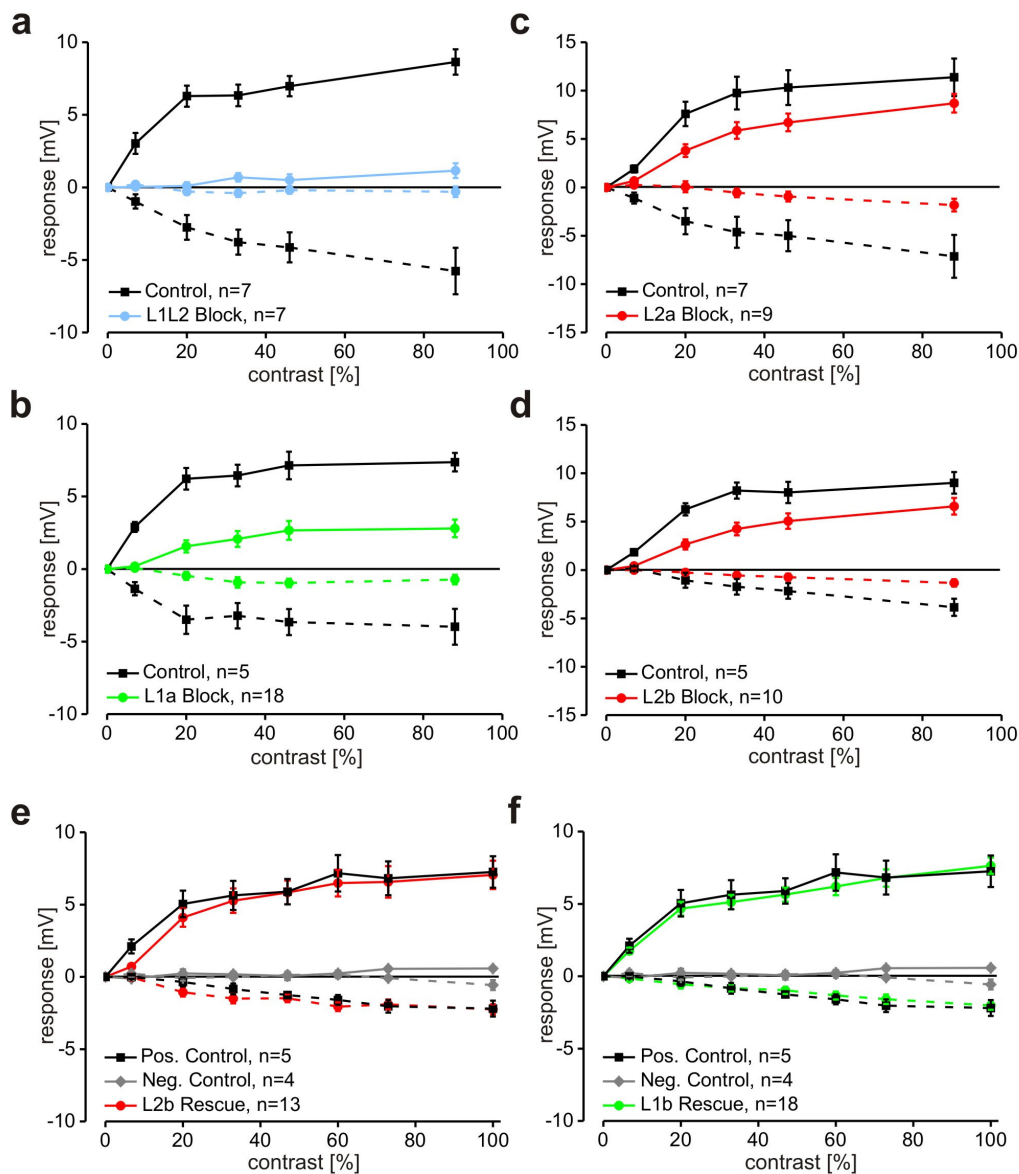


**Fig. 2:** Tangential cell responses to moving large field gratings of various contrasts. **(a-d)** Lamina neurons L1 and L2 **(a)**, only L1 **(b)** and only L2 **(c,d)** were blocked by cell-specific expression of *shibire<sup>ts</sup>*. Control flies (in black) had the same genotype as experimental flies, but were kept at permissive temperature throughout, while experimental flies (in color) were put to restrictive temperature 1h prior to the experiment. **(e,f)** L1- **(e)** and L2- **(f)** pathways were rescued by cell-specific expression of the wild-type histamine receptor ('*ort*') in an *ort*-null mutant. Data from positive control flies (heterozygous wild-type background) are shown in black, data from negative control flies (*ort*-null mutants) in grey, data from rescue flies in color. Data from positive and negative control flies are identical in e and f. Responses to grating motion along the preferred direction are shown as solid lines, to motion along the null direction as dashed lines. Data represent the mean  $\pm$  SEM obtained from n animals (n indicated in each panel). Since recordings from HS- and VS-cells revealed no difference, both groups were pooled. Blocking L1 or L2 significantly reduces the motion response (b-d), thus each pathway appears necessary. However, rescuing either one of them fully restores the wild-type response (e,f). Thus, each pathway appears sufficient.

the other control flies (n=5, data not shown). Together, these results suggest that L1 and L2 are necessary for wild-type responses to grating motion. In a complementary approach, we selectively rescued photoreceptor input to lamina cells L1 and L2<sup>11,19</sup>. Given the complete loss of motion responses after blocking L1 and L2, and the strong reduction in the response to grating motion when blocking L1, rescuing the L2-pathway should lead to only small motion responses at best. Rescuing the L1-pathway should result in larger motion responses, but still significantly reduced compared to wild-type. However, rescuing L2 led to wild-type motion responses at all contrasts tested, for PD- as well as for ND-motion (Fig.2e; driver line L2b; red traces). The same was true when lamina cells L1 were rescued: again, motion responses were nearly indistinguishable from the ones of 'positive control' flies (Fig.2f; driver line L1b; green traces). In these 'positive control' flies, no L1- or L2-Gal4, but one wild-type *ort*-allele was present leading to wild-type motion responses as expected (Fig.2e,f; black traces). In 'negative control' flies, where either no L1- and L2-Gal4 or no UAS-*ort* was present in an *ort*-null mutant background, motion responses were literally zero (Fig.2e,f; gray traces). Thus, blocking L1 or L2 revealed that the output of both L1 and L2 is necessary for wild-type motion responses. Rescuing the pathway of either L1 or L2 suggests, however, that either L1 or L2 is sufficient for a wild-type motion response. This contradiction deserves further investigation.

### **L1 and L2 are Electrically Coupled**

The blocking and rescuing experiments presented above differ in one important aspect: in one case, the synaptic output of L1 and L2 was blocked, in the other case, the synaptic input to the same cells was rescued. If L1 and L2 receive their input in parallel without any further interactions, both procedures should yield complementary results, which we did not find. Thus, we examined the existence of electrical connections between L1 and L2 by immuno-labeling of the innexin protein 'Shaking B', a member of the gap-junction forming protein family in flies<sup>20,21</sup>. We found strong immuno-labeling within the entire optic lobe including the lamina (Fig.3a). In addition, the basal laminar processes of L1 and L2 appeared to co-localize with the Shaking B immuno-labeling (Fig.3a, insert).

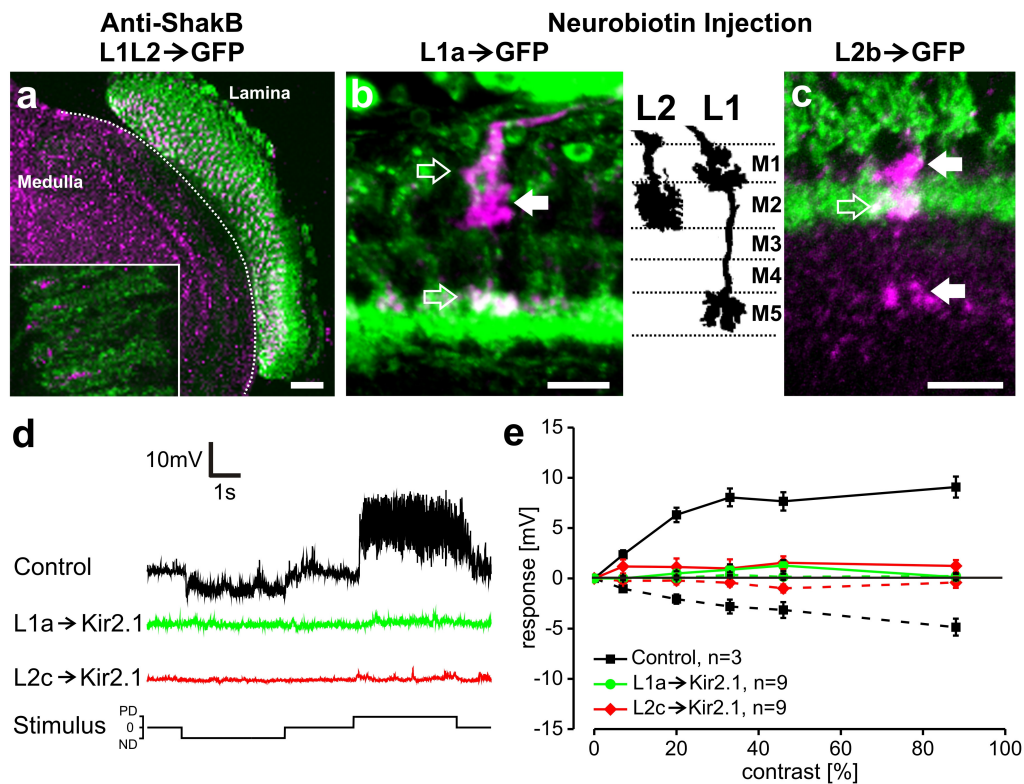


**Fig. 3:** Lamina cells L1 and L2 are electrically coupled. **(a)** Immuno-staining of the lamina, using the Shaking-B antibody (magenta), in an L1L2 line expressing GFP (green). The inset represents a 3-fold magnification of the large figure showing immuno-staining primarily in the proximal part of adjacent lamina cartridges. Scale bar = 25  $\mu\text{m}$ . **(b)** Dye-coupling between L1- and L2-cells. An L1-cell was injected with Neurobiotin in an L1a line expressing GFP (green). The terminals of a single L2-cell (magenta, white arrow) are visible in the medulla. The open arrows point towards the terminals of the injected L1-cell (white). Similar results were obtained in  $n=6$  flies. **(c)** An L2-cell was injected with Neurobiotin in an L2b line expressing GFP (green). The terminals of a single L1-cell (magenta, white arrows) are visible in the medulla. The open arrow points towards the injected L2-cell (white). Similar results were obtained in  $n=7$  flies. Scale bar in b and c = 5  $\mu\text{m}$ . The inset between b and c shows the terminals of Golgi-impregnated L1- and L2-cells (from ref.30). **(d,e)** Voltage responses of lobula plate tangential cells in flies expressing an inwardly rectifying potassium channel ('Kir2.1') in L1-cells via the driver line L1a, or in L2-cells via the line L2c. For each fly, a single response trace is shown in d, the average response in e. In e, data represent the mean  $\pm$  SEM of the data, obtained from  $n$  flies ( $n$  indicated in each panel). Data from control flies are shown in black, data from experimental flies are shown in color. Responses to grating motion along the preferred direction are shown as solid lines, to motion along the null direction as dashed lines. Since recordings from HS- and VS-cells revealed no difference, both groups were pooled. Motion responses are almost completely abolished, no matter whether *Kir2.1* was expressed in L1 or in L2.

Since some dipteran gap-junctions were demonstrated to be permeable for Neurobiotin<sup>2,22</sup>, we injected L1-cells with Neurobiotin and looked for co-staining in L2. When a single L1 was injected, a clear staining became visible in the adjacent L2-cell as well, identified by its characteristic terminal in medulla layer 2 (Fig.3b). Injecting L2 led to co-staining of the adjacent L1-cell, identified by its characteristic terminals in medulla layers 1 and 5 (Fig.3c). This was observed in a total of 13 experiments. We therefore suggest that L1 and L2 are electrically coupled via gap-junctions.

Gap-junctional coupling between L1 and L2 could in principle explain the contradictory results obtained in blocking and rescuing experiments: Through electrical coupling, rescuing the photoreceptor input to L1 restores the L2-pathway as well, and vice versa. This explanation, however, requires that the coupling between L1 and L2 provides a sufficiently large input to the respective partner cell. In order to investigate the strength of the coupling, we expressed an inwardly rectifying potassium channel in one of the two lamina cells. Given that the electrical coupling between L1 and L2 is large, the shunting action of the potassium channel expressed in one cell should affect the neighboring cell as well. When we expressed the potassium channel in L1 alone, motion responses were completely abolished (Fig.3d,e; driver line L1a, green traces), comparable to the situation when L1 and L2 were blocked by *shibire*<sup>ts</sup> (Fig.2a, blue traces). A similar finding was obtained when the potassium channel was expressed in L2-cells (Fig.3d,e; driver line L2c, red traces). These results argue for a strong electrical coupling between L1 and L2 and, thus, resolve the apparent discrepancy between blocking and rescuing experiments.

### **Evidence for Splitting into ON- and OFF Pathways**

So far, our data support the view that both L1 and L2 feed, with a somewhat different contribution, into the motion detection circuitry. However, no evidence is provided as to any functional specialization of each of the pathways. As one possibility, lamina cells L1 and L2 might be specifically involved in the analysis of either ON- or OFF-input signals, in analogy to the vertebrate retina<sup>4</sup>. Since a grating stimulus is composed of many simultaneously moving dark-to-bright (ON-edge) and bright-to-dark transitions (OFF-edge), this would have escaped our analysis

presented above. To investigate this possibility, we presented moving edges of a single polarity to flies in which we blocked the output of lamina cells L1 and L2 by *shibire*<sup>ts</sup>. In control flies, moving ON- and OFF-edges elicited strong and reliable voltage responses in lobula plate tangential cells during PD- and ND-motion (Fig.4a,b; black traces). When the output from L1 was blocked, the response to moving ON-edges was literally zero while the response to moving OFF-edges was still about 50 % of the wild-type response (Fig.4a,b, top row; driver line L1a, green traces).

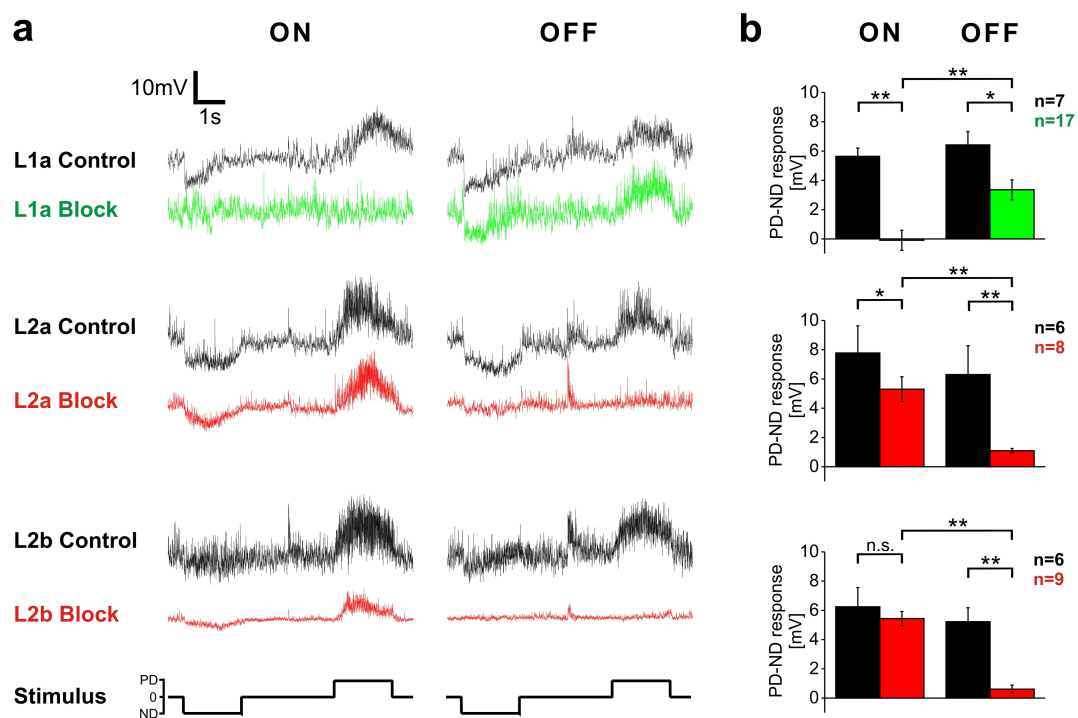


**Fig. 4:** Voltage responses of lobula plate tangential cells to moving edges of a single polarity (single example response in a, average in b). Lamina neurons L1 (top row) or L2 (2nd and 3rd row) were blocked by cell-specific expression of *shibire*<sup>ts</sup>. Control flies (in black) had the same genotype as experimental flies, but were kept and recorded at permissive temperature. Experimental flies (L1a in green, L2a and L2b in red) were shifted to restrictive temperature 1h prior to the experiment. Data in b represent the mean response (PD - ND)  $\pm$  SEM of the data obtained from n flies (n indicated in each panel). Asterisks indicate the significance level of the difference between the mean values: \* =  $p < 0.05$ , \*\* =  $p < 0.001$ . Since recordings from HS- and VS-cells revealed no difference, both groups were pooled. Blocking L1 abolishes the response to moving ON-edges completely, while blocking L2 mainly affects the response to moving OFF-edges.

The opposite was true when the output from L2 was blocked by expressing *shibire*<sup>ts</sup> using two different Gal4-driver lines: Then, the response to moving ON-edges was only mildly reduced while the response to moving OFF-edges was nearly abolished (Fig.4a,b, 2nd and 3rd row; driver lines L2a and L2b, red traces).

### Concluding Remarks

In their pioneering study and in line with our results, Rister and colleagues found that rescuing either the L1- or the L2-pathway led to wild-type optomotor responses at high pattern contrasts<sup>11</sup>. For low contrasts (5-10 %), a functional specialization of the L1- and L2-pathway for back-to-front and front-to-back motion was suggested<sup>11</sup>, which, however, does not match our data on tangential cell responses in that contrast range (Fig.2e,f). First evidence for a role of the L2-pathway in transmitting light-OFF signals was obtained in a study on freely walking flies, where blocking L2 impaired turning tendencies in response to contrast decrements<sup>12</sup>. However, our finding that photoreceptor signals in the fly segregate into ON- and OFF-pathways via L1 and L2 neurons is surprising in so far as, different from ON- and OFF-bipolar cells of the vertebrate retina<sup>4</sup>, both lamina cell types possess the same transmitter receptor<sup>9</sup> and produce similar light responses in their dendrite<sup>23</sup>. This similarity is likely to be increased even further by the gap-junctional coupling between dendritic compartments of L1 and L2, which might help to average out uncorrelated noise both cells receive from photoreceptor R1-6 input. Subsequently, however, these signals must become differentially rectified. For L2, this has been recently shown to occur already within the cell, as L2-axon terminals reveal pronounced calcium signals selectively in response to light-OFF stimuli<sup>24</sup>. Whether this also holds true for L1, or whether the selective responsiveness of the L1-pathway to light-ON stimuli is only acquired further downstream in its postsynaptic neurons<sup>25</sup> is currently not known. Based on co-stratification of columnar neurons<sup>26</sup> as well as 2-Deoxyglucose activity labeling<sup>27</sup>, L1 and L2 have been proposed for long to represent the entry points to two parallel motion pathways in the fly visual system, with L1 synapsing onto medulla intrinsic neuron Mi1 which in turn contacts T4 cells, L2 synapsing onto transmedullar neuron Tm1 which in turn contacts T5-cells, and T4- and T5-cells finally converging on the dendrites of the lobula plate tangential cells. Our results

provide evidence that these two pathways deal specifically with the processing of ON- and OFF-stimuli. Moreover, splitting a positively and negatively going signal into separate ON- and OFF-channels alleviates the neural implementation of a multiplication, as postulated by the Reichardt detector. While otherwise, the output signal of the multiplier had to increase in a supra-linear way when both inputs increase as well as when they decrease, dealing with positive signals only in separate multipliers seems to be less demanding with respect to the underlying biophysical mechanism<sup>28</sup>. Whatever this mechanism will turn out to be, our finding about the splitting of the photoreceptor signal into ON- and OFF-pathways adds to the already described commonalities between the invertebrate and the vertebrate visual system<sup>29</sup>. Obviously, the selection pressure for an energy-efficient way of encoding light increments and decrements led to rather similar implementations across distant phyla.

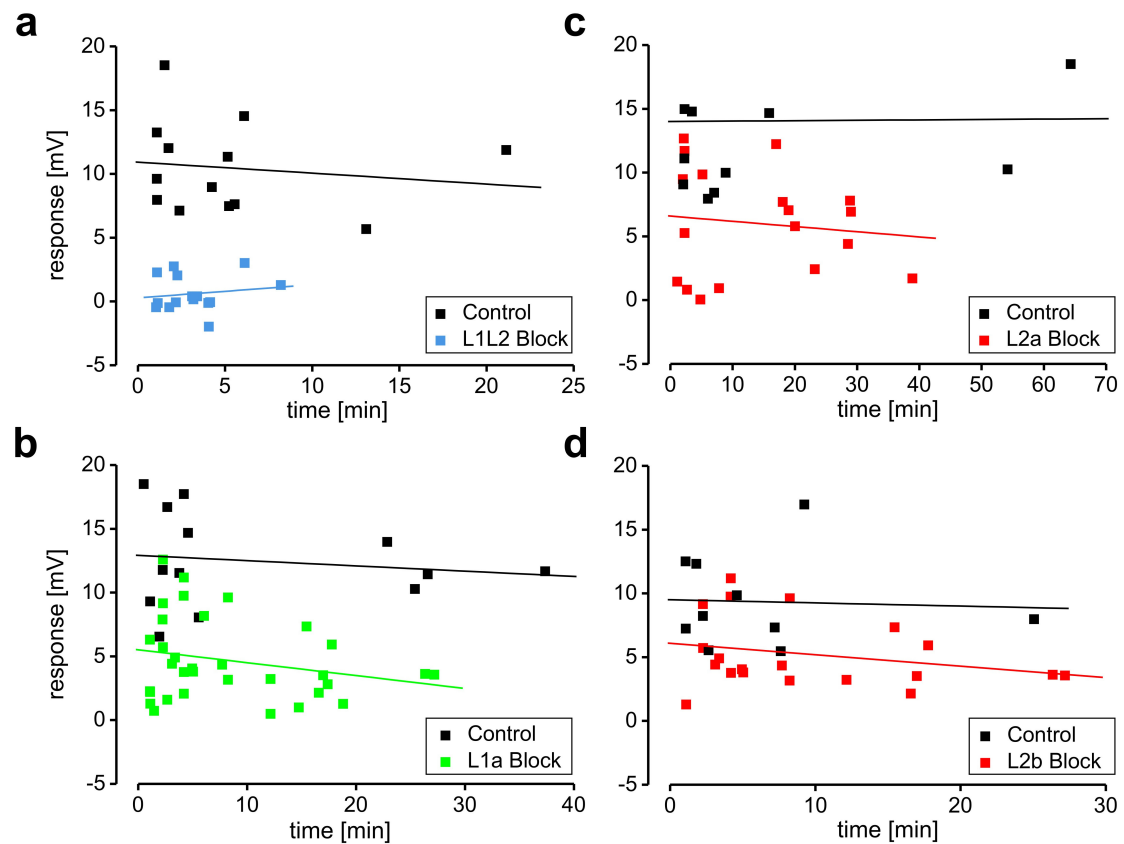
**Acknowledgements**

We thank Chi-Hon Lee, Jens Rister and Christopher Schnaitmann for kindly providing flies. Shaking B antibody was kindly provided by Jonathan Bacon. We thank Wolfgang Essbauer and Christian Theile for excellent technical assistance, and Robert Schorner for the artwork in Fig.1a.

**Author Contributions**

MJ performed the blocking experiments and Neurobiotin injections, BS did the rescue experiments, MJ and BS did all fly work and data analysis, VSR analyzed expression patterns of the driver lines, DFR and AB designed and supervised the study, AB wrote the manuscript with the help of all authors.

## 3. Supplement



**Supplementary Fig.:** Time course of motion responses of tangential cells in flies expressing *shibire*<sup>ts</sup> after temperature shift. Analysis was performed on the data obtained from the four types of flies the average of which is shown in Fig.2 a-d, i.e. L1/L2 block, L1 block, L2a block, L2b block as well as the respective control flies. Each data point is obtained from a single trial from a single fly, consisting of the response to a grating of 47 % contrast, moving along the preferred (PD) and null direction (ND) of the cell. The response plotted represents the absolute value (in mV) of the PD response minus the ND-response. Since all cells were tested with a variety of different contrasts, only 2 data points were obtained from each single cell for the 47% contrast condition in most cases. Solid lines represent the fit of a linear regression to the data. The x-axis indicates the time in minutes that have passed since a seal was established on the soma of the cell. About 15-20 minutes have to be added for the time at room temperature to account for the dissection procedure. All responses are stable over time, with no sign of recovery from the block during the experiment.



#### 4. Methods

**Flies.** Flies were raised on standard cornmeal-agar medium at a 12 h light / 12 h dark cycle, 25°C and 60 % humidity. We used female experimental flies, one day post-eclosion. Two effector strains carrying the *white*-gene with multiple insertions of *UAS-shi<sup>ts</sup>* on the third chromosome or a single insertion of *UAS-Kir2.1-GFP* on the second chromosome were used for blocking experiments. Heterozygous control and experimental flies were obtained by crossing the respective Gal4-driver and UAS-effector strains. For the *shibire* experiments, control and experimental flies were raised at 18°C (permissive temperature). Experimental flies were shifted for 1 h to 37°C (restrictive temperature) directly before the experiment and recorded at room temperature. No recovery of the block was detected within the time of recording (see supplement). For the *Kir2.1* experiments, experimental and control flies were raised at 30°C to boost the expression level of *Kir2.1*. Three sets of *white*<sup>+</sup> control flies were used for the experiments shown in Fig.3e: *UAS-Kir2.1-GFP* (n=3), L1a (n=5) and L2c (n=4). To restore photoreceptor input to L1 or L2 *DB331-Gal4*, *UAS-mCD8-TnXL-8aa* (for highlighting tangential cells<sup>2</sup>); *UAS-ort*; *ort<sup>US2515</sup>* was crossed to *c202a-Gal4* (L1b); *ninaE<sup>1</sup>*, *ort<sup>1</sup>* or *21D-Gal4* (L2b), *ort<sup>1</sup>* (ref.11). *DB331-Gal4*, *UAS-mCD8-TnXL-8aa/+*; *UAS-ort/+*; *ort<sup>US2515</sup>/+* served as positive control, *DB331-Gal4*, *UAS-mCD8-TnXL-8aa/+*; *UAS-ort/+*; *ort<sup>US2515</sup>/ninaE<sup>1</sup>*, *ort<sup>1</sup>* and *DB331-Gal4*, *UAS-mCD8-TnXL-8aa/+*; *c202a-Gal4* (L1b)/+; *ort<sup>US2515</sup>/ninaE<sup>1</sup>*, *ort<sup>1</sup>* served as negative controls. The driver lines had the following genotypes:

L1a: *vGlut-dVP16AD/CyO*; *ortC2-Gal4DBD/TM3*, ref.19, provided by Chi-Hon Lee.

L1b: *c202-Gal4*, ref.11, provided by J. Rister.

L2a: *ortC1-3-GAL4AD*; + ; *cha-Gal4DBD*, ref.19, provided by Chi-Hon Lee.

L2b: *21D-Gal4*. ref.11, provided by J. Rister.

L2c: *ortC3-Gal4*, ref.19, provided by Chi-Hon Lee.

L1L2: *6298-Gal4*, ref.11, provided by J. Rister.

**Preparation.** Flies were anesthetized on ice and waxed on a Plexiglas holder using bee wax. The dissection of the fly cuticle and exposure of the lobula plate was performed as in ref.2. A ringer-filled cleaning electrode (tip ~ 4 µm) was used to remove the extracellular matrix and to expose the somata of lobula plate tangential

cells for recording. These somata were recognized either by expression of a fluorescent marker (see above) or by their location next to a prominent tracheal branch.

**Whole cell recording.** VS- and HS-cell somata covered by ringer solution were approached with a patch electrode filled with a red fluorescent dye (intracellular solution as in ref.2). Recordings in rescue experiments were performed with fluorescently targeted neurons as in ref.3, recordings in blocking experiments were established under high-contrast optics using a 40X water immersion objective (LumplanF, Olympus), a Zeiss Microscope (AxioTech vario 100, Zeiss, Oberkochen, Germany), illumination (100 W fluorescence lamp, heat mirror, neutral density filter OD 0.3; all from Zeiss, Germany). To enhance tissue contrast, we used two polarization filters, one located as an excitation filter and the other as an emission filter, with slight deviation on their polarization plane. For eye protection, we additionally used a 420 nm LP filter on the light path. For further details of the setup, see ref.2.

**Neurobiotin dye fill and staining.** Flies expressing mCD8-GFP in L1 or L2 (L1a or L2b) were decapitated. The heads were fixed and lamina cells were injected with a 5 mM Alexa Fluor 568 (A10442; Invitrogen, Karlsruhe, Germany) and 2% Neurobiotin (Vector Labs) solution as described in ref.3. Access to the lamina monopolar cell somata was possible after removal of the fly's retina. A single lamina cell was injected per brain. Neurobiotin was detected by coupling to Streptavidin–Alexa568 conjugate (1:100, Invitrogen)<sup>2</sup>.

**Immunohistochemistry.** Female flies three to five days after eclosion were dissected. Their heads were fixed in freshly prepared 4 % paraformaldehyde in PBT (overnight at 4°C). Subsequently, the heads were washed for 45 - 60 minutes in PBT and mounted in 7 % agarose. Agarose blocks containing a single fly head were sectioned at 50 µm using a vibratome (Leica VT 1000S). The sections were immediately treated with 2% Sodium Borohydrate (806372, MERCK) for 20 minutes at room temperature to reduce the auto-fluorescence. After proper washing in PBT for 45-60 minutes, the sections were further incubated in PBT including 2 % normal goat serum (50-062Z, Invitrogen) and subsequently in primary antibodies (1: 200,

overnight at 4°C). Antibodies were removed by several washing steps (5 x 20 minutes in PBT) and secondary antibodies were added (1: 200, overnight at 4°C). A 5 x 20 minutes washing protocol (PBT) was followed by final washing steps in PBS (5 x 20 minutes). The stained tissues were mounted in Vectashield (Vector Laboratories, Burlingame) and analyzed by confocal microscopy. The following primary and secondary antibodies were used in the present study: rat anti-mCD8 (MCD0800, Caltag laboratories), mouse anti-Dlg (Developmental Studies Hybridoma Bank, University of Iowa, Iowa City), rabbit anti-shakB antibodies (Jonathan Bacon, University of Sussex), Alexa Fluor 568 goat anti-rat-IgG (A11077, Molecular Probes), Alexa Fluor 568 goat anti-rabbit-IgG (A11011, Molecular Probes) and Alexa Fluor 488 goat anti-mouse-IgG (A11001, Molecular Probes). Female experimental flies of the following genotypes were used for immuno-histochemistry: +/+; vGlut-dVP16AD/UAS-mCD8-DsRed; ortC2-Gal4DBD/TM3 (for L1a), +/+; c202-Gal4/UAS-mCD8-DsRed; +/+ (for L1b), ortC1-3-GAL4AD/+; UAS-mCD8-DsRed/+; cha-Gal4DBD/+ (for L2a), +/+; UAS-mCD8-DsRed/+; 21D-Gal4/+ (for L2b), +/+; UAS-mCD8-DsRed/+; ortC3-Gal4/+ (for L2c) and +/+; 6298-Gal4/UAS-mCD8-DsRed; +/+ (for L1L2).

**Confocal microscopy.** Serial optical sections were taken at 0.5  $\mu\text{m}$  intervals with 1024 x 1024 pixel resolution using a confocal microscope (Leica TCS-NT) and an oil-immersion 40X- (NA = 1.25) Plan-Apochromat objective or a 40X water-immersion objective (LUMPlanF, Olympus). The individual confocal stacks were analyzed using Image J (NIH, U.S.A). The size, contrast and brightness of the resulting images were adjusted with Photoshop® CS (Adobe Systems, San Jose, CA).

**Visual stimulation.** A custom-built LED arena covered  $\sim 170^\circ$  ( $1.9^\circ$  resolution) of the horizontal and  $\sim 100^\circ$  ( $1.8^\circ$  resolution) of the vertical visual field of the fly, allowing refresh rates of up to 600 Hz with 16 intensity levels. The spectral peak of the LEDs was at 568 nm and the luminance range of the stimuli were between 0.5 – 8  $\text{cd} / \text{m}^2$  (For further details see ref.2). Two types of visual stimuli were used: The moving grating consisted of either a square-wave (Fig.2) or a sine-wave (Fig.3) pattern with a spatial wavelength of  $22^\circ$  moving at  $22^\circ/\text{sec}$ . The moving ON- or OFF-edge (Fig.4) consisted of an edge of either polarity moving at  $44^\circ/\text{sec}$ .

**Data analysis.** Data was acquired and analyzed using the data acquisition and analysis toolboxes of Matlab (The Mathworks, USA). The contrast was calculated as  $(I_{\max} - I_{\min}) / (I_{\max} + I_{\min})$  with an absolute  $I_{\min}$  and  $I_{\max}$  of 0.5 and 8 cd / m<sup>2</sup>, respectively. The responses were defined as the difference between the average membrane voltage during the 2 s stimulation period and the 500 ms average potential prior to stimulation.

### 5. References

1. Meinertzhagen, I. A. & O'Neil, S. D. Synaptic organization of columnar elements in the lamina of the wild type in *Drosophila melanogaster*. *J. Comp. Neurol.* **305**, 232-263 (1991).
2. Joesch, M., Plett, J., Borst, A. & Reiff, D. F. Response properties of motion-sensitive visual interneurons in the lobula plate of *Drosophila melanogaster*. *Curr. Biol.* **18**, 368-374 (2008).
3. Schnell, B., Joesch, M., Foerstner, F., Raghu, S.V., Otsuna, H., Ito, K., Borst, A., Reiff, D.F. Processing of horizontal optic flow in three visual interneurons of the *Drosophila* brain. *J. Neurophysiol.* **103**, 1646-1657 (2010).
4. Waessle, H. Parallel processing in the mammalian retina. *Nat. Rev. Neurosci.* **5**, 747-757 (2004).
5. Barlow, H. B., Hill, R. M. & Levick, W. R. Retinal ganglion cells responding selectively to direction and speed of image motion in the rabbit. *J. Physiol.* **173**, 377-407 (1964).
6. Dubner, R. & Zeki, S. M. Response properties and receptive fields of cells in an anatomically defined region of superior temporal sulcus in monkey. *Brain Res.* **35**, 528-532 (1971).
7. Borst, A., Haag, J. & Reiff, D. F. Fly motion vision. *Annu. Rev. Neurosci.* **33**, 49-70 (2010).
8. Strausfeld, N. J. Atlas of an insect brain (Springer 1976).
9. Hardie, R. C. A histamine-activated chloride channel involved in neurotransmission at a photoreceptor synapse. *Nature* **339**, 704-706 (1989).
10. Reichardt, W. Autocorrelation, a principle for the evaluation of sensory information by the central nervous system. In *Sensory Communication*, ( ed.

Rosenblith, W. A.) 303-317 (New York, London: The M.I.T. Press and John Wiley & Sons 1961).

11. Rister, J., Pauls, D., Schnell, B., Ting, C. Y., Lee, C. H., Sinakevitch, I., Morante, J., Strausfeld, N. J., Ito, K. & Heisenberg, M. Dissection of the peripheral motion channel in the visual system of *Drosophila melanogaster*. *Neuron* **56**, 155-170 (2007).

12. Katsov, A. Y. & Clandinin, T. R. Motion processing streams in *Drosophila* are behaviorally specialized. *Neuron* **59**, 322-335 (2008).

13. Zhu, Y., Nern, A., Zipursky, S.L. & Frye, M.A. Peripheral visual circuits functionally segregate motion and phototaxis behaviors in the fly. *Current Biology* **19**, 613-619 (2009).

14. Brand, A. H. & Perrimon, N. Targeted gene expression as a means of altering cell fates and generating dominant phenotypes. *Development* **118**, 401-415 (1993).

15. Luan, H., Peabody, N.C., Vinson, C.R. & White, B.H. Refined spatial manipulation of neuronal function by combinatorial restriction of transgene expression. *Neuron* **52**, 425-436 (2006).

16. Kitamoto, T. Conditional modification of behavior in *Drosophila* by targeted expression of a temperature-sensitive shibire allele in defined neurons. *J. Neurobiol.* **47**, 81-92 (2001).

17. Johns, D. C., Marx, R., Mains, R. E., O'Rourke, B. & Marban E. Inducible genetic suppression of neuronal excitability. *J. Neurosci.* **19**, 1691-1697 (1999).

18. Gengs, C., Leung, H. T., Skingsley, D. R., Iovchev, M. I., Yin, Z., Semenov, E. P., Burg, M. G., Hardie, R. C. & Pak, W. L. The target of *Drosophila* photoreceptor synaptic transmission is a histamine-gated chloride channel encoded by *ort* (*hclA*). *J. Biol. Chem.* **277**, 42113-42120 (2002).

19. Gao, S., Takemura, S., Ting, C., Huang, S., Lu, Z., Luan, H., Rister, J., Thum, A.S., Yang, M., Hong, S., Wang, J.W., Odenwald, W.F., White, B.H., Meinertzhagen, I.A. & Lee, C. The neural substrate of spectral preference in *Drosophila*. *Neuron* **60**, 328-342 (2008).

20. Phelan, P., Bacon, J.P., Davies J.A., Stebbings, L.A. & Todman, M.G. Innexins: a family of invertebrate gap-junction proteins. *Trends in Genetics* **14**, 348-349 (1998).

21. Blagburn, J. M., Alexopoulos, H., Davies, J. A. & Bacon, J. P. Null mutation in shaking-B eliminates electrical, but not chemical, synapses in the *Drosophila* giant fiber system: a structural study. *J. Comp. Neurol.* **404**, 449-458 (1999).

22. Haag, J. & Borst, A. Dye-coupling visualizes networks of large-field motion-sensitive neurons in the fly. *J. Comp. Physiol. A* **191**, 445-454 (2005).

23. Laughlin, S. B. & Osorio, D. Mechanism for neural signal enhancement in the blowfly compound eye. *J. Exp. Biol.* **144**, 113-146 (1989).
24. Reiff, D. F., Plett, J., Mank, M., Griesbeck, O. & Borst, A. Visualizing retinotopic half-wave rectified input to the motion detection circuitry of *Drosophila*. *Nat. Neurosci.* **13**, 973-978 (2010).
25. Takemura, S. Y., Lu, Z. & Meinertzhagen, I. A. Synaptic circuits of the *Drosophila* optic lobe: the input terminals to the medulla. *J. Comp. Neurol.* **509**, 493-513 (2008).
26. Bausenwein, B., Dittrich, A.P.M. & Fischbach, K.-F. The optic lobe of *Drosophila melanogaster*. II. Sorting of retinotopic pathways in the medulla. *Cell Tiss. Res.* **267**, 17-28 (1992).
27. Bausenwein, B. & Fischbach, K.-F. Activity labeling patterns in the medulla of *Drosophila melanogaster* caused by motion stimuli. *Cell Tiss. Res.* **270**, 25-35 (1992).
28. Hassenstein, B. & Reichardt, W. Systemtheoretische Analyse der Zeit-, Reihenfolgen- und Vorzeichenbewertung bei der Bewegungspertzeption des Rüsselkaefers *Chlorophanus*. *Z. Naturforsch.* **11b**, 513-24 (1956).
29. Sanes, J. R. & Zipursky, L. Design principles of insect and vertebrate visual systems. *Neuron* **66**, 15-36 (2010).
30. Fischbach, K.F. & Dittrich, A.P.M. The optic lobe of *Drosophila melanogaster*. I. A Golgi analysis of wild-type structure. *Cell Tiss Res.* **258**, 441-475 (1989).

## **VI. Dscams affect dendritic shape, information processing and optomotor behavior in *Drosophila*.**

Jing Shi , Bettina Schnell, Väinö Haikala, Friedrich Forstner, Haihuai He, Maria-Luise Erfurth, Dietmar Schmucker, Alexander Borst and Dierk Frithjof Reiff.

This chapter will be submitted in the near future.

### **1. Summary**

Directionally selective lobula plate tangential cells (LPTCs) are key elements in the optomotor circuitry of flies. Their function relies on large dendrites that receive topographically organized input from presynaptic motion detectors. Down syndrome cell adhesion molecules (Dscams) mediate precise neuronal wiring in different animal species including flies and humans. Thousands of different Dscams establish a complex surface code in *Drosophila*, whose disruption leads to severe anatomical defects. Consistently, Dscam misexpression reduces the dendritic branching complexity and occupied territory of LPTCs. The anatomical defects were accompanied by gaps in the neural representation of the external world, i.e. the receptive field of identified LPTCs. Misexpression caused reduced yaw-turning responses in tethered flying flies. Thus, Dscams play an important role in the development and integration of LPTCs into the motion detection circuitry and enable LPTCs to efficiently control optomotor turning behavior of the fly.

### **2. Introduction**

Animals rely on precisely structured neural circuits for the integration of sensory information and the generation of motor commands. Dendrites that are specialized

in receiving signals are key elements of these circuits and their precise shape defines dendritic processing (Segev and London, 2000; London and Hausser, 2005; Rall, 1969; Rall, 1962). In the visual system of different animal species dendritic and axonal processes segregate and meet in distinct columns and layers and form a precise topographic map that ensures that there are no gaps in the neuronal representation of the visual world (Clandinin and Feldheim, 2009). Optimized wiring and efficient coverage of sensory space is ensured by self-avoidance of dendritic and axonal arborizations and Dscams play an important role in the underlying developmental processes (Schmucker and Chen, 2009; Hattori et al., 2007) in the vertebrate (Fuerst et al., 2008; Fuerst et al., 2009) and fly visual system (Millard et al., 2007; Millard et al., 2010).

The *Drosophila* visual system is a well established model system for the analysis of genes, development and behavior. However, the investigation of single cell physiology and activity in small neuronal circuits has been accomplished only very recently. Most of these studies concentrate on large directionally selective tangential cells in the lobula plate (LPTCs) of *Drosophila* (Joesch et al., 2008; Schnell et al., 2010; Reiff et al., 2010; Chiappe et al., 2010; Seelig et al., 2010; Maimon et al., 2010). Here we build on these studies and combine genetics, cellular physiology and behavior to address the role of Dscam (Schmucker et al., 2000) in establishing functional LPTCs. Furthermore, we use Dscam to address the contribution of horizontally sensitive (HS cells) cells in the control of optomotor behaviour of *Drosophila*. This study is facilitated by several aspects. First, most if not all visual interneurons have been identified based on their anatomy and position (Strausfeld, 1976; Fischbach and Dittrich, 1989). Furthermore, visual interneurons are embedded in a topographically organized circuitry. Thus, their sensory area can be inferred from their position and size. Second, for some neurons the synaptic connections have been revealed at the ultra-structural level (Braitenberg, 1970; Braitenberg and Hauser-Holschuh, 1972;



Meinertzhagen and O'Neil, 1991; Meinertzhagen, 1996; Takemura et al., 2008). Third, the constant dendritic anatomy, position and molecular key players in LPTCs are well characterized (Scott et al., 2002; Raghu et al., 2009; Raghu et al., 2007). Fourth, the functional properties of directionally selective HS cells in the lobula plate are extremely well characterized in big fly species (Hausen, 1982a; Hausen, 1982b) and *Drosophila* (Schnell et al., 2010; Chiappe et al., 2010). Fifth, HS cells are supposed to control well investigated compensatory optomotor behavior. We hypothesize that our methods are sensitive enough to detect even subtle alterations in the shape and function of HS cells in response to altered *Dscam* expression. Any alteration in tightly controlled flight maneuvers will instruct us (a) on the behavioral relevance of *Dscam*-mediated recognition events in neuronal wiring and (b) on the role of HS cells in the control of yaw-turning responses.

LPTCs are supposed to control optomotor behavior in dipteran flies. Presynaptic to LPTCs, large arrays of layered reiterated columns are formed that are supposed to differ only in the area of visual space to which they are devoted. These columns include local microcircuits that compute local motion vectors which indicate the direction of image motion at each sampled image point. In a second step, LPTCs spatially integrate the local motion vectors with their large dendrites in the lobula plate (Single and Borst, 1998) and process global image shift during self motion of the animal (Borst and Haag, 2002; Borst et al., 2010). Third, network interactions among different LPTCs establish receptive fields that are precisely tuned to optic flow patterns characteristic for specific flight maneuvers of the fly. However, in a first approximation, individual LPTCs are either tuned to vertical motion (vertical system, VS cells, Hengstenberg et al., 1982; Joesch et al., 2008) or horizontal motion (horizontal system, HS cells, Hausen, 1982a; Hausen, 1982b; Schnell et al., 2010) determined by the orientation tuning of the sampled local motion vectors (Borst and Egelhaaf, 1990). HS cells become excited by front to back motion in front of the

ipsilateral eye and inhibited by motion in the opposite direction (Hausen, 1982a; Hausen, 1982b; Krapp et al., 2001; Schnell et al., 2010). In addition, the HS cells of one hemisphere are coupled to each other and HSN and HSE receive input from neurons of the contralateral hemisphere that have opposite directional tuning (Schnell et al., 2010). Thus, optic flow during translation, head movement and yaw rotation generates the most effective pattern of image motion detected by HS cells. Furthermore, direct connections to descending neurons that control head, wing and haltere muscles (Chan et al., 1998; Gilbert et al., 1995; Gronenberg and Strausfeld, 1990) suggest an important role in the control and stabilization of the flight path (Hausen and Wehrhahn, 1989). Microsurgical lesions of HS cells (Hausen and Wehrhahn, 1983), the study of mutant flies (Heisenberg et al., 1978) and recordings from HS cells in head fixed walking fruit flies (Chiappe et al., 2010; Seelig et al., 2010) further suggest the involvement of HS cells in yaw-turning behavior.

HS cell responses during local visual stimulation suggest that their responses reflect precise connections of their dendrite to the topographically organized presynaptic circuitry (Schnell et al., 2010; Krapp et al., 1998). Dscams have been shown to control precise neuronal wiring in *Drosophila* (Chen et al., 2006; Schmucker et al., 2000; Hughes et al., 2007; Hummel et al., 2003; Zhu et al., 2006; Wang et al., 2004; Wang et al., 2002; Zhan et al., 2004), mice (Ly et al., 2008; Fuerst et al., 2008; Fuerst et al., 2009), *Aplysia* (Li et al., 2009) and humans (Yamakawa et al., 1998; Agarwala et al., 2001). In the chicken retina they control synapse specificity (Yamagata and Sanes, 2008). *Drosophila*, as other arthropods, has four Dscam genes. *Drosophila* Dscam1, hereafter called Dscam gives rise to an extraordinary molecular diversity that is generated by mutually exclusive alternative splicing of hypervariable exon clusters. 95 alternatively spliced exons encode parts of the extracellular and transmembrane domain and result in 38016 or even 152064 specific isoforms if two recently discovered exon clusters are included (Yu et al., 2009). This stunning diversity is

generated by mRNA splicing, and combinatorial expression of many different Dscam isoforms on the same cell (Wojtowicz et al., 2007; Wojtowicz et al., 2004) establishes a highly complex surface code. This code is essential for the development of proper neuronal anatomy in the fly. Dscams likely exhibit their function by mediating homophilic temporary interactions that trigger repulsion between sister-branches and avoidance of neighboring neurons that express the same Dscam isoform (Matthews et al., 2007; Chen et al., 2006; Hughes et al., 2007). Through its role in determining neuronal anatomy, Dscam is likely to be essential for neuronal information processing and behavior (Zipursky et al., 2006; Matthews et al., 2007; Hattori et al., 2007; Hattori et al., 2008; Schmucker and Chen, 2009). We hypothesize that Dscam mediated changes in the dendritic anatomy of HS cells alter dendritic information processing and the neural representation of the external world. Furthermore, if HS cells contribute to the stabilization and control of the flight path, the observed defects should affect visually driven optomotor behavior.

Here we show that HS cells express Dscam. Misexpression (Gal4/UAS-system, Brand and Perrimon, 1993) of a single Dscam isoform (11.31.25.1) in HS cells (hereafter called HS<sup>+</sup> cells) reduces the dendritic branching complexity and territory. Mostly terminal dendritic branches are lost that would normally cover the lateral lobula plate and that receive input from the frontal field of view of the fly. Local visual stimulation in this area during whole cell recording reveals local motion blindness. Furthermore, flies with misexpression of Dscam in HS cells (DSCAM<sup>+</sup> flies) exhibit only small behavioral yaw-turning responses when stimulated in the same area. In contrast, physiological and behavioral responses to large field motion stimuli were fully intact. Thus, Dscams execute a behaviorally relevant function in the fine wiring of the optomotor circuitry that allows HS cells to efficiently control yaw-turning behavior in *Drosophila*.

### **3. Results**

#### **Dscams are expressed broadly in the fly visual system including directionally delective HS cells.**

Three HS cells (HSN, HSE and HSS) elaborate their large, overlapping dendrites in constant areas stacked along the dorsal-ventral axis of the lobula plate (Heisenberg et al., 1978; Fischbach and Dittrich, 1989; Scott et al., 2002; Hausen, 1982a). The HS cells have correspondingly large, overlapping receptive fields centered at a dorsal, equatorial and ventral position of the field of view of the fly (Schnell et al., 2010; Hausen, 1982b). We investigated the expression pattern of Dscam in HS cells and the *Drosophila* brain by immunolabeling of a conserved intracellular domain (see methods). In accordance with previous reports (Wang et al., 2004; Hummel et al., 2003) Dscam is expressed broadly in the entire brain (Fig.1, magenta) including the lamina (not shown), medulla, lobula and lobula plate of the fly visual system (Fig.1). Moreover, immunoreactivity of Dscam labeled reiterative columns and layers in the medulla and lobula (Fig. 1A-C), and four neuropile layers (Fig.1C, D) can readily be identified in the lobula plate (Buchner et al., 1984; Fischbach and Dittrich, 1989).

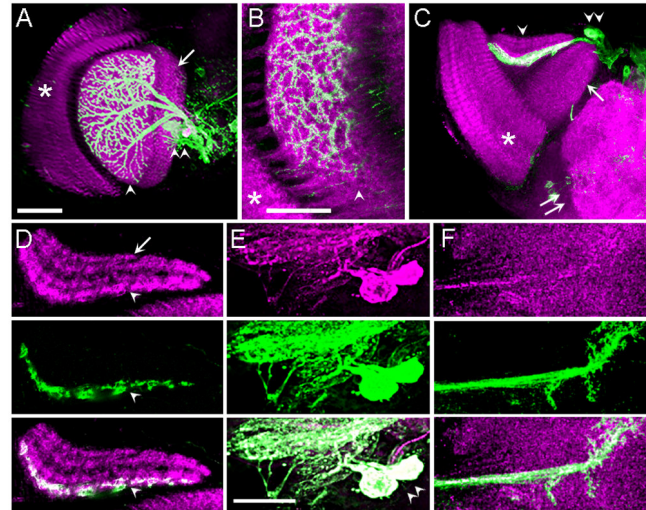
To investigate if HS cells express Dscam we performed co-immunolabeling of Dscam and GFP. Two different Gal4-driver lines, DB3331-Gal4 (DB331-Gal4, Joesch et al., 2008) and R27B03-Gal4 (Seelig et al., 2010) were used to drive GFP expression in LPTCs. R27B03-Gal4 is a highly specific driver for all three HS cells (Fig.1) in the lobula plate and has additional expression in the central brain. GFP expression labels the large overlapping dendrites of HSN, HSE and HSS that are confined in the anterior most layer of the lobula plate. HS dendrites cover the entire topographically organized neuropile of the lobula plate (Fig.1A,B, frontal sections) up to the outer border. GFP expression in HS cells co-localizes with Dscam immunolabeling (Fig.1C,D, horizontal sections) which is further corroborated by single confocal image sections

of the dendrite, soma and axon terminal (Fig.1D-F). Similar results were obtained in all experiments and using both Gal4-driver lines DB3331-Gal4 and R27B03-Gal4.

Misexpression of Dscam causes reduced branching complexity and loss of terminal branches.

**Fig. 1: Dscam is expressed in HS cells, the entire fly visual system and the central brain.** (A)

Frontal section. Double-Immunolabeling of Dscam (magenta) and GFP (green) shows Dscam expression in all neuropiles of the fly visual system and the central brain (double arrow). Dscam immunoreactivity labels columns and layers in the lamina (not shown), medulla (asterisk), lobula (arrow) and the lobula plate (arrowhead) of the fly visual system. Three giant neurons of the HS system (green) express GFP (R27B03-Gal4→UAS-mCD8-GFP) and show co-labeling of Dscam. Their large overlapping dendrites are stacked along the dorsal-ventral axis and cover the entire lobula plate. (B) Close up of the outer lobula plate (arrowhead) and inner medulla (asterisk) shown in A. GFP and Dscam co-localize in dendritic branches of HS cells. (C) Horizontal section. The dendritic arborizations of HS cells are restricted to the thin, most anterior layer of the lobula plate (double arrowhead indicate HS-somata, see also A and E). There is strong Dscam immunoreactivity in the central brain (double arrow). (D) Close up of the lobula plate. Dscam expression labels 4 layers of the lobula plate. The anterior most layer (arrowhead) co-localizes with GFP expressing dendrites of the three HS cells. The most posterior layer (arrow) is separated by two embedded layers and hosts the VS cells. Co-localization of Dscam and GFP in (E) HS cell somata (double arrowhead) and (F) HS axon terminals. Dscam was labeled with an antibody raised against the intracellular domain (Dscam IC, magenta). Confocal image stacks were taken with a z-increment of 0.3 μm, a 63X objective and minimized pinhole. Composite images in A, B and C were generated by collapsing 150, 29 and 40 images, respectively. Scale bar 50 μm in A,C and 30 μm in B. D-F are single confocal images, scale bar 30 μm.



So far we have shown that HS cells express Dscam (Fig.1). To analyze the role of Dscams in the development of HS cell dendrites (Fig.2 and 3) we used the Gal4-UAS system to perform gain of function experiments by misexpressing single Dscam isoforms in LPTCs. In a first series of experiments we investigated the dendritic branching patterns of HSN and HSE of control flies (Scott et al., 2002; Schnell et al., 2010) (Fig.1A,B, Fig.2A,B and Fig.3A). HS cells were chosen because their anatomy should allow us to infer their receptive field whereas the receptive fields of VS cells are widened by extensive electrical coupling of neighboring VS cells (see introduction). In these and in all other experiments (except Fig.1) throughout the manuscript we consistently used the driver line DB331-Gal4 to express GFP and to manipulate cells because of the early onset of Gal4 expression during development and availability of the line at the beginning of the study. R27B03-Gal4 became available only recently (Seelig et al., 2010) and has a late developmental onset of expression. DB331 labels 6 VS and 3 HS cells (Fig.2A,B) that ramify in the most posterior (Fig.1D, arrow) and most anterior layer (Fig.1D, arrowhead) respectively, of the lobula plate (Buchner et al., 1984; Fischbach and Dittrich, 1989). Thus, besides few branches in the dorsal area of the lobula plate (Scott et al., 2002), HS cells are completely separate from VS cells, receive input from different sets of elementary motion detectors and can be distinguished based on their different shape and position (Fischbach and Dittrich, 1989; Scott et al., 2002). The dendrites of HSS were not analyzed in depth as their ramifications are located deeper in the lobula plate and because DB331-Gal4 expresses only weakly in HSS. Both aspects caused fragmentary labeling and prevented a detailed and reproducible analysis. Immunolabeling of the postsynaptic scaffolding protein Discs large (Dlg) was used to visualize the outline and size of the neuropiles of the fly visual system and allowed us to evaluate the topological structure of dendritic arborization of GFP expressing HSN and HSE cells (Fig.2).

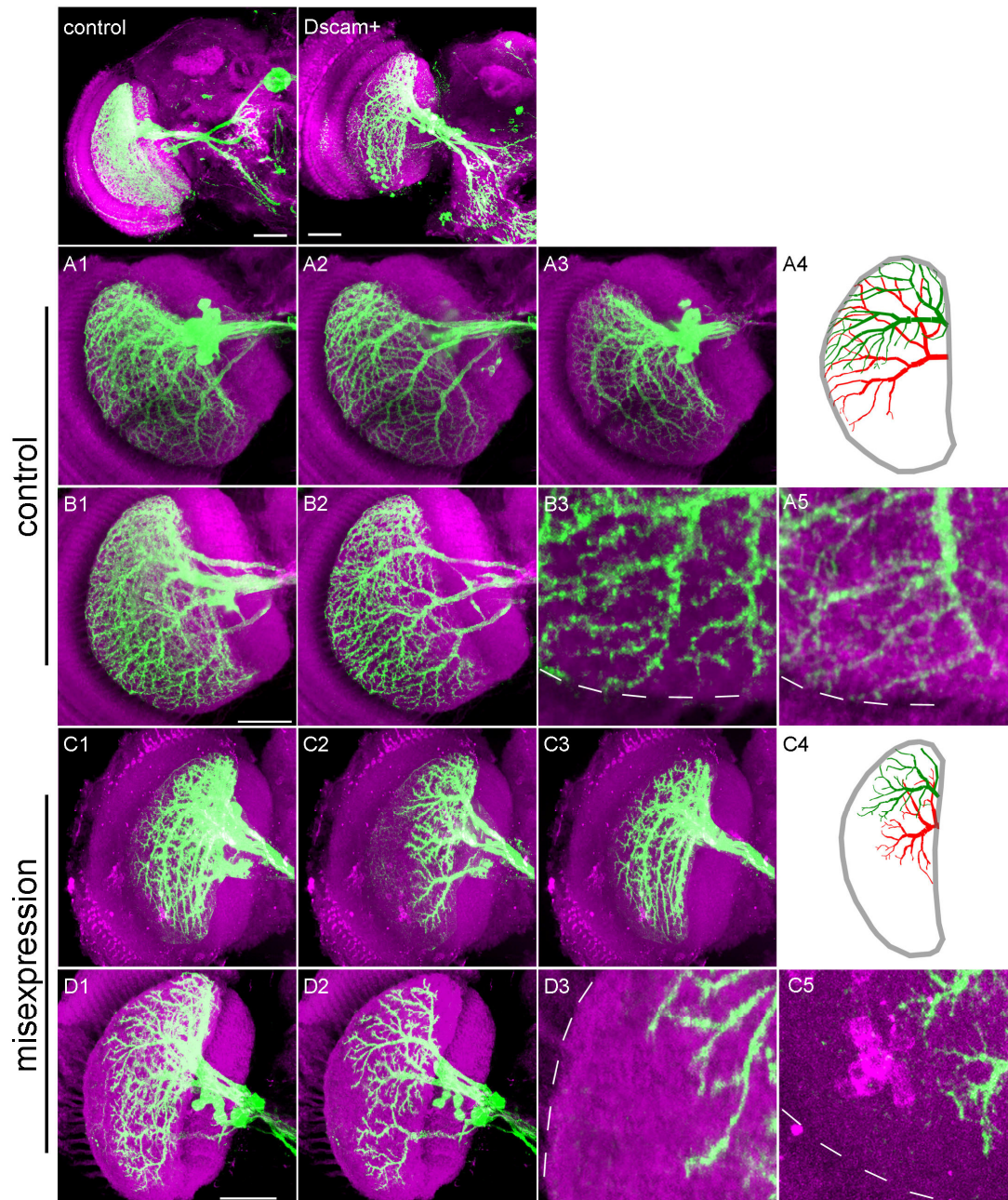


**Fig. 2: Dscam controls dendritic growth of directionally selective HS cells.**

Determination of the dendritic branching pattern of HS cells and coverage of the receptive area in the lobula plate. The neuropile is visualized by immunolabeling of *dlg* (magenta) and HS and VS cells express membrane tagged GFP (green; *DB331-Gal4*→*UAS-mCD8GFP*). Confocal image stacks were analyzed using the TREES software package (see methods). **(A,B)** Control. Close up of the lobula plate (collapsed image stack). 6VS and 3HS cells cover the entire lobula plate (A1,B1). The TREES software enables the separation and visualization of HS (A2,B2) and VS cells (A3). Dendritic sister branches of the same HS cell never cross, branches of different HS cells cross extensively and cause massive overlap of the dendrites. HS dendrites reach out to the outer boarder of the lobula plate (indicated by the dashed line) in which they are confined. (A5,B3; 5x close up of A2 and B2, respectively). (A4) Reconstruction of HSN (green) and HSE (red) including the outer boarder of the

lobula plate (grey line). (A) and (B) are taken from different animals. **(C,D)** Misexpression of a single Dscam isoform (11.31.25.1) in neighboring HS cells causes reduced dendritic branching complexity and reduced arbor size. Images in (C) and (D) are from different animals and were treated similar to (A) and (B). HS cell dendrites occupy much smaller areas in the lobula plate (C2, D2 and C4). The higher order and terminal dendritic branches are missing. The lateral area of the lobula plate is no more covered (D3 and C5; outer boarder indicated by the dashed line).

We used the open source software package “TREES toolbox” (Cuntz et al., 2010) for the manipulation and analysis of confocal image stacks. TREES enabled the tracing and reconstruction of individual neurons in 3D-space from fluorescence images and allowed us to separate the dendrites of the 6 VS from the dendrites of the 3 HS cells (Fig.2A). TREES in addition allowed us to untangle the dendrites and to generate morphological reconstructions of HSN and HSE from the fluorescent image stacks (Fig.2A4, 2C4 and Fig.3A). Collapsed confocal image stacks (frontal sections) show that the entire lobula plate is densely covered by the dendritic branches of VS and HS cells (Fig.2A1, B1). We analyzed the branching pattern, position along the dorsal-ventral axis, laminar position and coverage of HSN and HSE dendrites in the lobula plate based on the generated graphical representations of both cell types (Fig.3A). The dendrites of HSN and HSE show several characteristic arborization features. First, individual HS cell dendrites and dendritic branches strictly avoid self-crossing and occupy their territory in the lobula plate in the most efficient way. This finding suggests efficient self-recognition and repulsion between dendritic sister branches of the same cell, a feature that is widely controlled by Drosophila Dscams (Hattori et al., 2008). Second, their dendritic branching pattern is extraordinarily complex and the consecution of main, higher order and terminal branches densely covers the occupied territory reaching the outermost border of the lobula plate. Similar aspects have been shown to be regulated by Dscams (Chen et al., 2006). Third, the dendrites of HSN and HSE do not tile the occupied territory in the lobula plate, instead they show massive overlap. HSE covers about 90 % of the territory occupied by the HSN dendrite (Schnell et al., 2010). The dendrites of the different HS cells do not strictly



repel each other as has been shown for particular amacrine cells in the retina (Fuerst et al., 2008) or columnar neurons in the fly visual system (Millard et al., 2007). However, HSN and HSE strictly avoid fasciculation of their processes although they cross each other. Fourth, the dendritic arborizations of HS cells are restricted to a thin synaptic layer in the most anterior lobula plate (Fig.1D). The panels and close ups of GFP labeled dendrites exemplify these features (Fig.1, Fig.2A,B). A summary of the reconstructed dendritic arborizations of 8 HSN (green) - HSE (red) pairs (light grey outline indicates lobula plate) is shown in Figure 3A. To the left and to the right of the reconstructions are the dendritic spanning fields in the corresponding colors. The light red area indicates the dendritic overlap of both cell types. HSN and HSE cover the entire dorsal and equatorial lobula plate, only the ventral area that is covered by the dendrite of the HSS cell (not shown) is free (shaded grey area).

In the following series of experiments we misexpressed a single Dscam isoform in LPTCs in addition to the endogenously expressed Dscam compliment. Isoform 11.31.25.1 was chosen from a small collection of different UAS-Dscam constructs because its misexpression caused a reproducible dendritic phenotype. Ectopic expression of Dscam 11.31.25.1 caused severe defects in the elaboration of the HS<sup>+</sup> cell dendrites (Fig.2C,D). HS<sup>+</sup> dendrites were characterized using the TREES toolbox as described for control HS cells (Fig.2A4). Misexpression of Dscam caused a significant reduction in the size and complexity of the dendritic arbor (Fig.2C,D). The dendrites of both cells HSN<sup>+</sup> and HSE<sup>+</sup> were much smaller and in particular the small and terminal dendritic branches were missing. This was observed in all animals. However, it is important to note that we observed pronounced variability in the severity of the reduction in dendritic branching from animal to animal, between the hemispheres and between cells in the same hemisphere. These results are summarized in Figure 3A where we show 8 pairs of reconstructed HSN<sup>+</sup> and HSE<sup>+</sup> cells from different animals next to the HS cells of control flies.

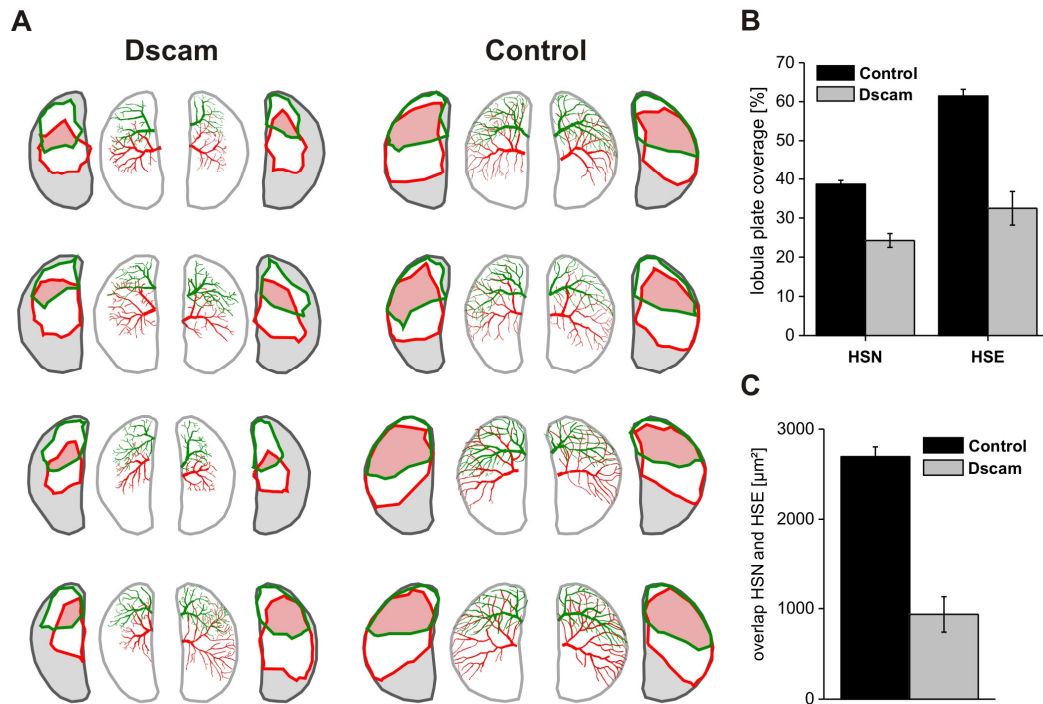


**Fig. 3: Misexpression of Dscam causes reduced dendritic branching and unoccupied territory in the lobula plate. (A)** Reconstruction of the dendritic arborizations of HSN (green) and HSE (red) cells in the lobula plate of control (right) and *Dscam*<sup>+</sup> (left) animals. The dendrites were reconstructed from confocal image stacks using the TREES software package. 8 hemispheres each including one pair of HSN and HSE are depicted for each genotype. The dendrites of control HS cells exhibit an extraordinarily complex branching pattern, strictly avoid self-crossing and occupy their territory in a most efficient way. The terminal branches end at the outer boarder (light grey line) of the lobula plate. The dendritic branches of HSN and HSE strictly avoid fasciculation, yet they cross and overlap extensively. Their occupied territory (the so called dendritic spanning fields) and overlapping area (light red) is depicted in the corresponding colors in the neighboring panels. The shaded grey area indicates the area of the lobula plate that is not occupied. In control animals HSN and HSE occupy the entire dorsal and equatorial lobula plate. Only the ventral territory that is occupied by the HSS cell is free because we failed to reliable reconstruct HSS cells. Misexpression of a single isoform and reconstruction of the dendrites reveals the absence of higher order branches and reduced size of the dendritic spanning field. Notably, the dendritic branching phenotype varies from animal to animal and between the hemispheres (compare lower left and right). **(B)** Misexpression causes a significant reduction of the occupied area of HSN and HSE in the lobula plate. HSN and HSE cover 38.6 % and 61.5 % (*n* = 10 each) of the lobula plate in control flies and 24.3 % and 32.5 % (*n* = 8 each), respectively, in *Dscam*<sup>+</sup> flies. **(C)** Misexpression causes a significant reduction in the area in which the dendrites of HSN and HSE overlap. The size of this area is 2695  $\mu\text{m}^2$  and 936  $\mu\text{m}^2$  in control and *Dscam*<sup>+</sup> flies, respectively.

The resulting reduction of their dendritic spanning field and overlap is shown in the corresponding panels on each side and quantified in the Figures 3B and C. The loss of mostly terminal branches causes a significant gap in the coverage of the lateral lobula plate (see Fig.3A) whereas the medial lobula plate is still occupied by the dendrites. Based on this phenotype and the topographic arrangement of the fly visual system and lobula plate we predicted that motion stimuli in the lateral field of view (corresponding to the medial lobula plate) should still be processed whereas motion processing in the frontal field of view (corresponding to the lateral lobula plate) should be impaired.

### **Misexpression of Dscam causes gaps in the receptive field of HS cells.**

To our best knowledge, there is no study so far that shows that Dscam mediated changes in the anatomy of identified neurons translate into altered information processing and behavior of an animal. We now address the functional implications of Dscam 11.31.25.1 misexpression by whole cell recording during visual stimulation of the fly. The recordings were done on control flies that express GFP in LPTCs and in flies that co-express Dscam 11.31.25.1, respectively. Recordings were established on the soma of *Drosophila* HS and HS<sup>+</sup> cells as described recently (Schnell et al., 2010) while flies were looking at a computer controlled LED display (Fig.4A). During the recording, the cells were perfused with a red dye which allowed us to identify cells and assign the recorded signals to a particular cell type (HSN, HSE or HSS). As reported recently, *Drosophila* HS cells become excited by front-to back motion in front of the ipsilateral eye and inhibited by motion in the opposite direction (Schnell et al., 2010). Typical recording traces during rotation of a large field periodic grating (extending 170 deg around the vertical body axis) are shown in Figure 4A. The recordings reveal similar directionally selective deflections of the membrane potential in HS and HS<sup>+</sup>. Thus, stimuli covering large areas of the field of view elicit

identical responses in both genotypes and there was no obvious defect in flies that misexpress Dscam 11.31.25.1. This result suggests that the basic response properties are largely intact in HS<sup>+</sup> cells and that they still receive input from (inhibitory and excitatory) local motion detectors (see discussion), yet more subtle defects might exist.

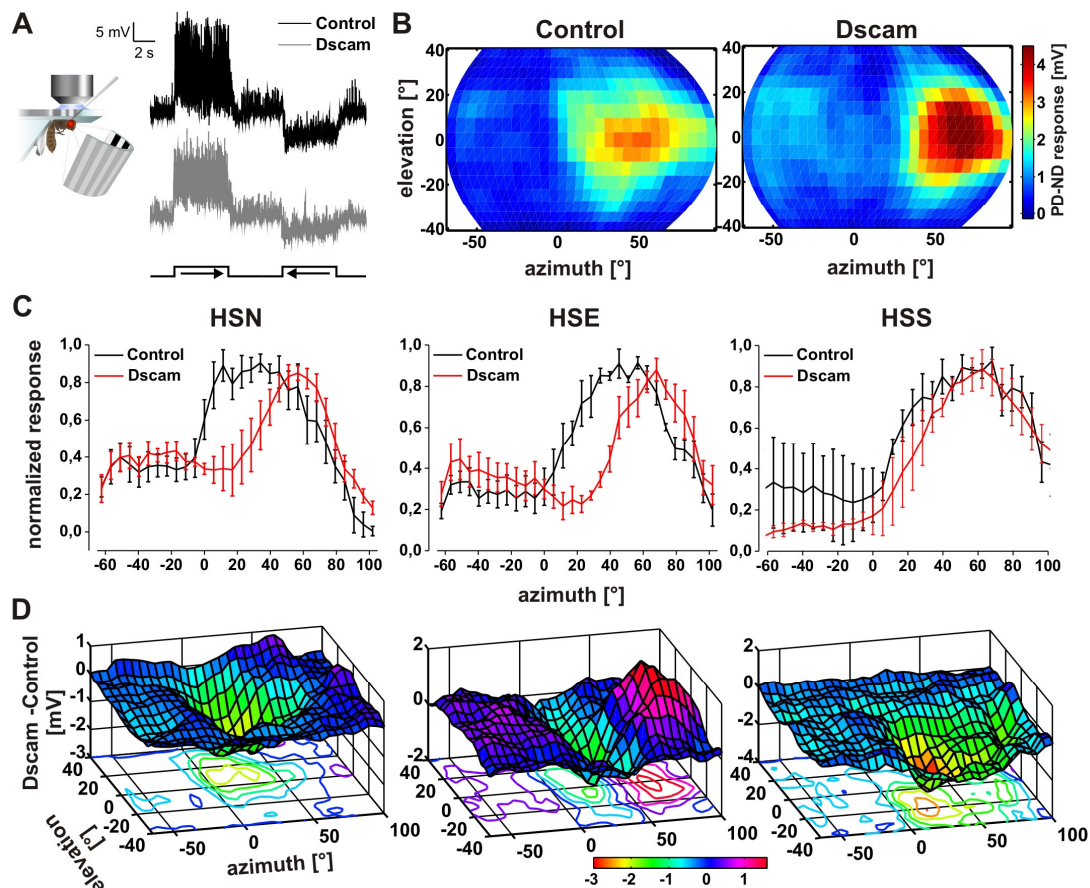


**Fig. 4: Misexpression of Dscam in HS cells causes a gap in the frontal receptive field.** (A) Voltage recordings from a control (black) and an HS cell misexpressing Dscam 11.31.25.1. (grey) in response to a drifting whole field sine grating moving at 1 Hz temporal frequency in preferred (PD, rightward) and null direction (ND, leftward). HS cells that misexpress Dscam exhibit depolarizing (PD) and hyperpolarizing (ND) changes of their membrane potential indistinguishable from control HS cells. The inset shows a scheme of the recording setup. (B) Receptive fields of control (n = 4) and Dscam misexpressing (n = 6) HSE cells. PD – ND responses elicited by a small, horizontally moving bar at different positions in the field of view are depicted in false color code. Along the dorsal-ventral axis, the receptive fields of HSE cells are centered at about 0° elevation. Control HSE cells have large receptive fields extending through the whole stimulated area on the ipsilateral side, including the frontal field of view. Misexpression of Dscam causes a massive reduction in sensitivity or complete motion blindness in the frontal area (ipsilateral side, from

frontal 0° to lateral 30-40°) corresponding well to the absence of dendritic branches in the corresponding lateral area of the lobula plate (Fig.2 and 3). The absolute response amplitudes of Dscam misexpressing HSE cells were increased at more lateral positions and on the contralateral side compared to control HSE cells. Similar experiments were performed for HSN ( $n = 4 / 6$  cells) and HSS ( $n = 3 / 5$  cells) (data not shown). **(C)** Response profiles of HSN, HSE (same data as in B) and HSS cells of control (black) and Dscam misexpressing (red) flies plotted against the azimuth. The mean of the responses (as depicted in B) along the elevation was calculated for each position along the azimuth and normalized to the maximal value. Plotted is the mean of 6 / 4 HSN, 6 / 4 HSE and 5 / 3 HSS cells of Dscam misexpressing / control flies. The normalized responses of Dscam misexpressing HSN and HSE cells are strongly reduced in the frontal area. In addition, their response profile is slightly shifted towards a more lateral position and responses to motion stimuli on the contralateral side are increased. The receptive fields of HSS cells show similar changes although less pronounced. **(D)** Differences in the receptive field of control and Dscam misexpressing HS cells displayed as false color coded contour plots. The differences between the local mean response amplitudes (mV) are visualized by subtracting the receptive fields (as depicted for HSE in B) of control HS cells from the ones of Dscam misexpressing HS cells (same data as in B and C). The difference is plotted along the z-axis in false color code at each position of the LED arena (x- and y-axis). Iso-response lines are projected to the bottom of the graphs. All three types of HS cells exhibit strongly reduced sensitivity in the frontal area of the ipsilateral field of view (downward deflection, green, between 0° and 50° along the azimuth). This deficit corresponds well to the lack of dendritic branches in the lateral medulla (Fig.2 and 3). In addition, HSE exhibits increased membrane potential fluctuations at more lateral positions and on the contralateral side (upward deflection, purple to red colors).

In a next step we mapped the receptive field of HS cells by moving a small bar (6 deg elevation and 1.4 deg width) left and right at all positions of the LED display. HS and HS<sup>+</sup> cells depolarize if the bar moves right (PD, preferred direction) and hyperpolarize if the bar moves left (ND, null direction) with respect to the right eye. We subtracted the ND from the PD response and plotted the obtained measure (PD-ND) at each position of the field of view of the fly (Fig. 4B). This protocol was repeated for several cells of each type (HSN, HSE and HSS) in both genotypes. The panels in Figure 4B show a heat map of the average sensitivity distribution (receptive field) of control (left panel) and HSE<sup>+</sup> cells (right panel). According to the position of their dendrite in mostly the equatorial area of the lobula plate, HSE is most sensitive to horizontal motion in the equatorial field of view in both genotypes (Fig.4B left panel). However,

control HS cells have a much broader receptive field compared to HS<sup>+</sup> cells. Normally, the receptive field includes the frontal field of view of the fly. Motion presented to this frontal area does not elicit significant responses in HSE<sup>+</sup> cells. Similar results were obtained for HSN and HSS in both genotypes (data not shown). In accordance with the position of their dendrite HSN and HSS are most sensitive in the dorsal and the ventral field of view (Schnell et al., 2010) and misexpression of Dscam 11.31.25.1 caused reduced or no responses if local motion stimuli are presented in the frontal field of view. However, responses to lateral stimuli tended to be larger compared to control HS cells (see discussion). These results are summarized in Figure 4C and D. In Fig. 4C, responses of individual cells exhibited at one position along the azimuth but different elevations were averaged and normalized to the maximum response. Plotting the mean response of all cells against the azimuth displays a pronounced gap in the frontal field of view of each HS<sup>+</sup> cell type compared to control cells (compare black and red traces in Fig.4C). A more detailed description of the change in the receptive fields of HSN, HSE and HSS induced by Dscam 11.31.25.1 misexpression is provided by subtracting the receptive field of control HS cells from the one of HS<sup>+</sup> cells. Plotting the difference in the absolute response amplitude as a heat colored 3D map (Fig.4D) provides a spatially resolved visualization of the exhibited reduction in motion responses in the frontal field of view of all three types of HS<sup>+</sup> cells (downward deflection, green in Fig.4D and see figure legend).

### **Misexpression of Dscam causes behaviorally relevant changes in the neuronal circuit.**

We analyzed visually guided, compensatory flight behavior to see if the so far reported changes in dendritic anatomy and physiology of HS<sup>+</sup> cells cause altered optomotor behavior. Periodic gratings that drift either clockwise or counter-clockwise around the vertical axis of a tethered flying fly were presented on a

panoramic LED display (Fig.5A). The drifting gratings elicit compensatory yaw-turning behavior that has been suggested to rely on visual processing in HS cells (Heisenberg et al., 1978; Heisenberg and Wolf, 1979). The strength of the yaw-turning response was analyzed by monitoring the stroke amplitude of the beating wings (Götz, 1987; Dickinson et al., 1993). Subtracting the amplitudes of both wings yields a reliable measure of the strength of the executed turning behavior. After the behavioral tests flies were sacrificed, GFP expression in HS cells was intensified by immunolabeling and the brains were analyzed by confocal microscopy and the TREES software as described above (Fig. 2 and 3).

Initial experiments in control flies showed that tethered flies exhibit compensatory responses of symmetrical strength for clockwise and counter-clockwise motion, respectively (not shown). Panoramic drifting gratings (360 deg) with maximum contrast (see below and methods) elicited nearly identical yaw-turning responses in *Dscam*<sup>+</sup> and control flies (Fig.5B). This finding is in line with the observed intact response properties of *HS*<sup>+</sup> under comparable stimulus conditions (Fig.4A).

Next, we presented monocular motion stimuli to the left or right eye of the fly. This stimulus excludes the zone of binocular overlap (+/- 15 deg) and excludes the additional input to HSN and HSE (see introduction) from cells of the contralateral brain (Schnell et al., 2010). We reasoned that both features might obscure the behavioral readout of deficient dendritic processing in *HS*<sup>+</sup> cells of one hemisphere. A likely disadvantage of this stimulus lies in the fact that the gap in dendritic coverage and receptive fields of *HS*<sup>+</sup> cells is most pronounced in the corresponding area. However, our whole cell recordings revealed that the reduction in the receptive fields of *HS*<sup>+</sup> cells extends across the frontal 40 – 50 deg. Thus, the area of deficient dendritic processing in *HS*<sup>+</sup> cells exceeds the spared 15 deg of our stimulus. Presentation of this monocular stimulus elicited strong yaw-turning responses in control flies and much weaker responses in *Dscam*<sup>+</sup> flies (Fig.5B).

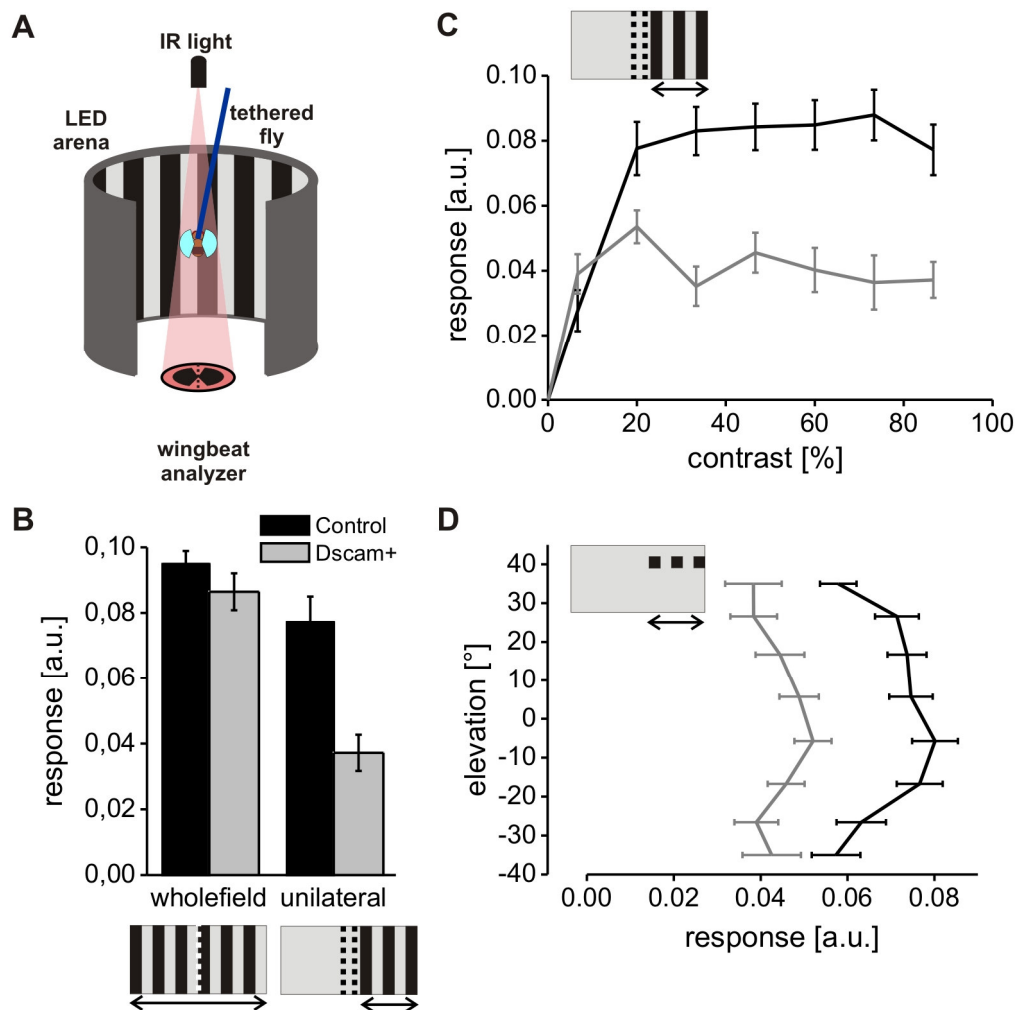


**Fig. 5: Misexpression of Dscam in HS cells causes reduced yaw-turning responses.** (A) Schematic drawing of a wing beat analyzer and recording setup. A tethered fly is surrounded by a 360 deg LED display. From above an infrared light source is directed at the fly. The beating wings cast a shadow on two detectors that are covered with an asymmetric slit. This design enables the readout of the wing beat amplitude from the detector current. Rotating stimuli elicit compensatory yaw-turning responses the strength of which can be quantified by subtracting the response during null direction from the response during preferred direction motion (see methods). (B) Panoramic (360 deg) drifting periodic gratings (see methods) with maximum contrast (86 %) elicited identical turning responses in control and *Dscam*<sup>+</sup> animals, indicating that *Dscam*<sup>+</sup> animals have no obvious weakness or physical deficit. Restriction of grating motion to the left or right 15 - 180 deg of the field of view (unilateral stimulus) revealed reduced responses in *Dscam*<sup>+</sup> animals. Symmetrical yaw-turning responses were recorded for clock- and counter- clockwise rotation in each genotype. (C) Contrast dependence of the yaw-turning response during unilateral stimulus presentation (see B). In both genotypes the response saturates and reaches a plateau with increasing contrast. *Dscam*<sup>+</sup> flies exhibit only 40 % of the response observed in control flies. (D) Further reduction of the monocular stimulus to a small horizontal stripe of about 10 deg elevation elicits robust compensatory yaw-turning responses in control flies and much weaker responses in *Dscam*<sup>+</sup> flies. This small field motion stimulus tends to fall into the receptive fields of the individual HS cells. In



both genotypes the biggest responses are elicited by motion in the equatorial plane where the dendrites of all three HS cells overlap.

In both genotypes yaw turning responses increased with increasing contrast and saturated (Fig.5C) at high contrast. However, saturated responses in *Dscam*<sup>+</sup> flies reached only about 40 % of the strength of the exhibited responses in control animals. Subsequent analysis of the anatomy of the HS<sup>+</sup> cells in each hemisphere revealed that their dendrites were always altered as described in Fig.2 and 3. Notably, these reduced responses can not be attributed to a general weakness or physical deficit as panoramic stimuli elicited identical responses in control and *Dscam*<sup>+</sup> flies.

Based on the observed physiological deficits in response to local motion stimuli (whole cell recording, Fig.4) we next analyzed yaw-turning behavior elicited by small field motion stimuli. However, identical local stimuli could not be used as a single moving bar elicits a different behavior (strong avoidance or fixation of the bar depending on its size and orientation). To avoid this problem, we presented a small horizontal grating extending about 10 deg in elevation and 100 deg along the azimuth (restricted to the monocular field of view as described above) moving at different elevations. This stimulus was sufficient to elicit robust compensatory yaw-turning responses in control flies (Fig. 5D). The biggest responses were elicited when stimuli were presented in the equatorial area which might be explained by the fact that this area is covered by the dendrites of all three HS cells (Schnell et al., 2010; Scott et al., 2002). However, *Dscam*<sup>+</sup> flies exhibited much weaker behavioral responses under similar stimulus conditions at each elevation tested. In summary, these results demonstrate that *Dscams* play a behaviorally relevant function in the development and local wiring of the optomotor circuitry. Moreover, we provide strong evidence that activity in HS cells critically contributes to flight control. Full coverage of the lobula plate by the dendrites of HS cells is required for the neuronal

representation of visual motion in all parts of the field of view. HS cells extract this information on horizontal image motion and participate in the control of compensatory, stabilizing flight maneuvers.

### **4. Discussion**

We show that *Drosophila* allows for combining a rigorous input-output analysis of optomotor behavior, cellular physiology and the underlying genes and molecules. We investigated directionally selective giant neurons, the HS cells, of the fly motion detection system that are involved in the processing of horizontal optic flow. Optic flow provides a rich source of information on self-motion and distance and can be described by the linear sum of two key components, rotation and translation (Koenderink and van Doorn, 1987). For motion in the horizontal plane, HS cells are involved in the processing of both parameters (Kern et al., 2005; van Hateren et al., 2005) and flies use this information to control visually driven behavior. Motion dependent behaviors in flies and other phyla including humans are very well described by the correlation-type model of motion detection (Reichardt, 1961; Nakayama, 1985; Borst and Egelhaaf, 1989; Emerson et al., 1992; Ibbotson et al., 1994). Yet, very little is known about the cellular implementation of the model and the molecules that mediate precise wiring in the motion detection circuitry (Borst et al., 2010).

Cellular responses of LPTCs in big flies and *Drosophila* display all characteristics of the behaviorally measured response and of the correlation-type model (Borst et al., 2010). Here we investigate HS cells that have a key role in the processing of horizontal optic flow and that have been suggested to have a primary role in the control of yaw-turning behavior including head movement and body rotation around the vertical axis of the fly. We provide solid evidence for the behavioral relevance of HS cells by interfering with their anatomy and function. HS cells were altered by

genetic manipulation of Dscam expression. We chose Dscams because Dscams have been shown to control the development and anatomy of numerous cell types in flies and vertebrates (Hattori et al., 2008; Schmucker and Chen, 2009). Furthermore, Dscams mediate important functions in the wiring of the early visual system of the fly (Millard et al., 2007; Millard et al., 2010). Yet, a definite link of Dscam to the physiology of identified cells and their role in behavior has not been established. We demonstrate for the first time that Dscam-mediated recognition events underlie the formation and physiology of HS cell dendrites. Furthermore, Dscam mediated recognition events help establishing functional dendrites that enable HS cells to efficiently control yaw-turning responses in *Drosophila*.

It is still largely unclear how dendritic growth, targeting and synapse formation are controlled in the development of HS cells and how these mechanisms affect dendritic information processing. Here, we show that the formation of the stereotyped features of dendritic arborization in HS cells relies on Dscam mediated recognition mechanisms (Schmucker and Chen, 2009; Hattori et al., 2008; Zipursky et al., 2006). Misexpression of a single Dscam isoform causes loss of terminal dendritic branches to a variable degree accompanied by motion blindness in the corresponding area of the receptive field. Small field stimuli that include this area elicit only weak yaw-turning responses. Thus, our data provide strong evidence for a definite link between Dscam, dendritic growth, physiology and behavior in *Drosophila*. Specifically, Dscam mediated recognition mechanisms seem to warrant efficient wiring and information processing in the motion detection circuitry and qualify HS cells for efficiently controlling visually guided yaw-turning behavior.

#### **Dscams mediate the characteristic branching and distribution of HS cell dendrites.**

The processes of different HS cells encounter each other frequently, cross extensively and the resulting dendrites overlap to a large degree. Yet, the branches

of different cells never fasciculate or run in parallel. Such phenomena are in line with numerous previous reports that suggest that surface interactions between the ectodomain of identical Dscam isoforms (Wojtowicz et al., 2007; Wojtowicz et al., 2004) induce a repulsive (Matthews et al., 2007; Hughes et al., 2007; Zhan et al., 2004; Soba et al., 2007) signal that might overwrite omnipresent adhesion (Petrovic and Hummel, 2008). This signal is communicated to the growing cells via the cytoplasmic domain of Dscam and causes the neurons to retract their neurites. We find that misexpression of a single Dscam isoform on the dendrites of neighboring HS cells causes a reduction in both dendritic branching and size of the dendritic arbor. Furthermore, the lateral part of the retinotopically organized lobula plate is no more occupied by the dendrites of manipulated HS cells. These findings were paralleled by a reduction in the overlap (Fig.3).

Several factors could account for these observations. Repulsion between neighboring HS cells might contribute to the observed anatomical phenotype. Yet, ectopic expression of Dscam 11.31.25.1 on neighboring HS cells did not force their dendrites to strictly tile the lobula plate. At least in our experiments misexpression of Dscam 11.31.25.1 is not sufficient to induce mosaic spacing of HSN and HSE. Misexpression of other isoforms and combinatorial misexpression will provide further insights into the role of Dscam in HS cell growth. Alternatively, functionally different neuronal populations might interact via Dscam expression (Chen et al., 2006). HS cells might encounter and be repelled by columnar neurons in the surrounding circuitry that express the same Dscam isoforms and that supply local motion input. We don't know which isoforms are expressed on LPTCs and columnar neurons. However, columnar elements massively express Dscam in the lobula plate (Fig.1). Moreover, four layers can be distinguished based on Dscam immunolabeling (Fig.1) and four similar layers were specifically marked by activity dependent uptake of radioactive 2-Desoxyglucose when visual motion was presented to the fly along

the four cardinal axis (front-to-back, back-to-front, up, down). Two large populations of neurons, the bushy T4- and T5-cells have been suggested to provide this input. Both classes of neurons likely exist in four different flavors per column and transmit motion information to each of the four layers in the lobula plate where LPTCs with similar preferred direction elaborate their dendrites. The neuropile in the anterior most layer was labeled by front-to-back motion (Buchner et al., 1984) which is the preferred direction of the here studied HS cells. We hypothesize that endogenous Dscam11.31.25.1 expression in T4, T5 or unknown cells causes repulsion and motion blindness in the frontal field of view. The observed lack of responses suggests that excitatory and inhibitory input is similarly repelled. The precise mechanisms that control Dscam splicing and neuronal wiring remain to be addressed. Constant dendritic spanning fields but highly variable dendritic arborization patterns of HS cells suggest a “random biased” Dscam expression mechanism that controls the development and wiring of columnar elements to LPTCs. Misexpression of 11.31.25.1 in HS cells would then lead to additional repulsion. The likelihood to receive an ectopic stop signal increases with increasing growth which could explain the pronounced lack of distal HS dendrites and lack of responses in the frontal field of view.

The strength of the generated repulsive signal might depend on the expression level of particular Dscam isoforms and the degree of overlap of the entire Dscam complement. This would explain why neurites of the same cell that express the exact same complement strictly avoid each other and never cross. Partial overlap of the Dscam complement in functionally related but different HS cells (HSN, HSE and HSS) would then be sufficient to prevent fasciculation but does not suppress crossing. Ectopic expression of a single isoform in all HS cells promoted growth away from each other (Fig.2,3). However, misexpression did not induce complete tiling of the dendrites. We did not rigorously investigate if some isoforms or misexpression of

small sets of Dscam isoforms can induce mosaic spacing of HS cell dendrites. Complete tiling of axonal processes in the fly visual system was suggested to depend on Dscam2 (Millard et al., 2007; Millard et al., 2010) which we did not manipulate. Two isoforms of *Drosophila* Dscam2 mediate isoform specific repulsion, proper tiling of axonal processes and stereotyped synapse formation in the lamina. A similar function has been reported for vertebrate DSCAM that controls neurite arborization and mosaic spacing in particular amacrine cells of the mouse visual system (Fuerst et al., 2008; Fuerst et al., 2009). To consolidate our hypothesis it would be great to know if Dscam expression in neighboring HS cells is regulated during development, if the full Dscam repertoire is required (Wang et al., 2004; Zhan et al., 2004; Wojtowicz et al., 2004) and if HS cells express Dscam2. Furthermore, the role of Dscam expression in the surrounding columnar network, in particular T4 and T5, need to be investigated. These important questions can now ideally be addressed in the here presented framework of *Drosophila* HS cells.

### **Dendritic arborization affects HS Cell function.**

The organization of neuronal dendrites that are specialized in receiving and processing input, and axons that provide input into complex circuits underlies information processing, decision making and behavior. The specific dendritic branching pattern and spanning field define their electrophysiological (Rall, 1962) and computational (Segev and London, 2000; London and Hausser, 2005) properties and differences in dendritic shape contribute most to the large anatomical diversity of neurons. However, dendrites of the same type of neurons, here directionally selective HS cells in *Drosophila*, tend to develop stereotypic characteristics (Hausen, 1982a; Fischbach and Dittrich, 1989; Schnell et al., 2010; Scott et al., 2002). The occupied territory and overlap of the dendrites of neighboring HS cells is highly stereotypic whereas the exact branching pattern of individual HS cells is variable.

Our approach relies on two assumptions. First, given that HS cell dendrites integrate local motion information in a retinotopic way, it should be possible to infer the size of the ipsilateral receptive field from the dendritic arborization pattern within the lobula plate (Hausen, 1982a; Hausen, 1982b; Krapp et al., 2001; Schnell et al., 2010). Second, changes in the physiological properties of HS cells should translate into altered optomotor behavior if HS cells control its execution.

HS cell dendritic shape reflects neural connectivity and information flow within the topographically organized motion detection circuitry (Schnell et al., 2010; Hausen, 1982b). HS cells are highly polarized neurons with a single axon and dendrite. Their axon projects centrally and connects a particular HS cell to neurons in the lateral protocerebrum. Furthermore, HS cells are electrically coupled to neighboring HS cells and other LPTCs. The elaborate and complex dendrites (Scott et al., 2002; Schnell et al., 2010) are specialized for the spatial integration and processing of local motion information from large arrays of elementary motion detectors in the field of view. Thus, the arborization pattern and occupied territory defines the area of synapse formation and the range of inputs that a particular HS cell receives. Hence, we must assume that the surrounding neuronal context represents a significant constraint in the determination of the shape of HS cell dendrites which is in line with a recent modeling study (Cuntz et al., 2010). We hypothesize that misexpression of a single *Dscam* isoform interferes with the molecular cues that normally mediate these constraints. According to this view, HS cells receive foreign signals that force their processes out of the usually occupied territory and they don't establish inhibitory and excitatory synaptic connections with presynaptic columnar neurons in this area anymore (Raghu et al., 2009; Raghu et al., 2007). This process should cause motion blindness in areas from which branches are repelled. The large gap in the frontal field of view of the fly can perfectly be explained this way (Fig.4). The dendritic branching deficit in this area causes the input from local motion detectors in the

stereotypic and hard-wired visual circuitry (Hiesinger et al., 2006; Fischbach and Hiesinger, 2008; Scott et al., 2003) to be no longer sampled.

Dipteran flies like *Drosophila* exhibit exquisite aerobatic maneuvers (Tammero and Dickinson, 2002; Heisenberg and Wolf, 1979; Mronz and Lehmann, 2008). When a fly moves, its entire visual field shifts in a manner specific to the maneuver being performed (Koenderink and van Doorn, 1987). Hard wiring of the circuitry warrants highly reproducible directionally selective responses in HS cells (Fig.4 and Schnell et al., 2010) and reliable optomotor behavior. Presentation of a drifting optic flow pattern to a tethered flying fly induces a particular, counteracting flight maneuver as if the fly would intend to keep its flight path straight (Heisenberg and Wolf, 1979). In our experiments, *Dscam* misexpressing flies exhibited saturating but only weak yaw turning responses (Fig.5C) if small field motion stimuli were presented in an area that includes most of the frontal 40-50 deg. HS cells were literally motion blind in this area and stimulation of the included more lateral field of view was obviously not sufficient to elicit optomotor responses of normal strength. However, the lateral field of view is still mapped on the medial lobula plate and the remaining dendrites of HS<sup>+</sup> cells. Local motion stimuli presented in this area tended to elicit stronger responses in HS<sup>+</sup> cells compared with control HS cells. However, responses to large field motion are about similar. Dendritic resistance and gain control can in principle explain these findings: Smaller dendrites in HS<sup>+</sup> cells should have a high input resistance and lower leak conductance. Thus, local stimuli and local neurotransmitter release would cause synaptic currents that elicit higher voltage changes - which we observed in the lateral field of view of the fly. However, large field stimuli cause about similar changes in small HS<sup>+</sup> and large HS cells. Dendritic gain control might explain this finding: In the large dendrites of HS cells the contribution of individual synaptic currents to dendritic potential changes drops steeply with increasing stimulus size. This is because of an increase in conductance



due to the opening of thousands of transmitter gated and voltage gated ion channels during the activation of not perfectly directionally selective input elements (Borst et al., 1995). Such gain control has first been observed in compensatory optomotor responses of flies (Reichardt et al., 1983) and recordings from LPTCs (Hausen, 1982b; Egelhaaf, 1985). These experiments show that the amplitude of the response saturates with increasing stimulus size and can thus explain why large field stimuli elicit about similar voltage changes and behavioral responses in our experiments. Thus, Dscam-mediated changes cause local defects in HS cell dendritic function whereas the encoding of panoramic motion is unaffected. However, medium size stimuli caused weaker behavioral responses in HS<sup>+</sup> flies which does not match the enhanced local responses. This discrepancy might be attributed to differences in the stimulus and the used read out. Whole cell recording reports the activity of the manipulated cell directly whereas behavior is the result of the activity in the whole network. Neurons other than the HS cells, like H1, H2 and small field motion detectors likely contribute to the control of yaw-turning behavior in *Drosophila*. Nevertheless, our results demonstrate an important role of HS cells in this behavior. Finally, Dscams (Schmucker et al., 2000) have been shown to regulate neuronal shape and connectivity in many different parts of the *Drosophila* brain (Schmucker and Chen, 2009; Hattori et al., 2008; Zipursky et al., 2006) and in many other invertebrate and vertebrate species including humans (Yamakawa et al., 1998; Agarwala et al., 2001). Our data show that this function of Dscam plays in addition a pivotal role in neuronal function and the execution of complex behavior.

## ***5. Experimental Procedures***

### **Fly Stocks and crossings**

*Drosophila melanogaster* were grown on standard corn medium at 25°C at 12 : 12 hours dark : light cycle and 60 % humidity. Flies were kept in 30 ml vials containing

10 ml food, 5-8 female virgin flies were crossed to 3-5 male flies. DB3331-Gal4 (Joesch et al., 2008) was used in all experiments, only for Dscam immunolabeling we used R27B03-Gal4 (Seelig et al., 2010, generously provided by Gerald Rubin). UAS-mCD8::GFP/CyO (Bloomington #5137) was used as marker. Ectopic Dscam expression: DB331-GAL4/x ; UAS-mCD8::GFP/BI ; UAS-Dscam11.31.25.1/+. Controls: DB331-GAL4/x ; UAS-mCD8::GFP/BI ; +/+. For the reconstruction of HS cell anatomy additional UAS-GFP (gift from Liquin Luo) facilitated the detection of the dendritic branches.

### **Immunohistochemistry**

3–5 days after eclosion brains of female flies were dissected according to standard procedures and brains from flies in whole cell recording and behavioral experiments were dissected following the experiments. In brief, brains were removed and fixed in 4 % paraformaldehyde for 30 minutes at room temperature. Brains were washed (3 x 20 minutes) in phosphate-buffered saline (PBS), pH 7.2, including 1 % Triton X-100 (PBT). For antibody staining, samples were further incubated in PBT including 4 % normal goat serum (Sigma Aldrich, St. Louis, MO; G9023) and primary antibodies were added overnight at 4°C. Antibodies were removed by several washing steps (3 x 20 minutes in PBT) and secondary antibodies were applied 1:200 overnight at 4°C. Antibodies were removed by several washing steps (PBT, 3 x 20-minutes). Subsequently, the brains were mounted in Ibidi Mounting Medium (Ibidi GmbH Martinsried, Munich) and prepared for confocal microscopy.

Primary and secondary antibodies: Alexa Fluor 488 conjugate rabbit IgG anti-GFP (catalog No. A-21311; Molecular Probes, Eugene, OR) and mouse anti-Dlg (4F3 anti-discs large; DSHB, Univ. of Iowa) were used in most experiments. Rat anti-mCD8 (catalog No. RM2200; Invitrogen Caltag) was used in combination with rabbit anti-DscamIC (generated in the Schmucker lab). As secondary antibodies we used Alexa

Fluor 488 goat anti-rat-IgG (catalog No. A11006; Molecular Probes), Alexa Fluor 568 goat anti-rabbit-IgG (catalog No. A11011; Molecular Probes) and Alexa Fluor 568 goat anti-mouse-IgG (catalog No. A11004; Molecular Probes).

### **Microscopy and data analysis**

Serial optical sections were taken every 0.3 - 0.5  $\mu\text{m}$  (1024x1024 pixels) using confocal microscopes (Leica TCSNT and Leica SP5), oil-immersion objectives 40x (n.a. 1.25) and 63x (n.a. 1.4) Plan-Apochromat (Zeiss, Oberkochen). Frontal image sections were taken by averaging four images at each z-position and starting from the posterior side of the brain. In few cases horizontal image sections were taken. Confocal image stacks were processed using Amira 4 (Zuse Institute Berlin (ZIB), Berlin) software. Figure were prepared using Photoshop CS3 (Adobe Systems, San Jose, CA).

### **Reconstruction**

The topological organization and dendritic spanning fields of HS cells were analyzed by reconstructing all clearly identifiable dendritic branches using previously described, custom written Matlab software (Cuntz et al., 2008). The outlines of the lobula plate were traced in ImageJ (ImageJ, <http://rsb.info.nih.gov/ij/>) and imported to Matlab. Statistical analysis and visualization was performed using Matlab and the TREES toolbox (Cuntz et al. 2010). Inkscape (Vector Graphics Editor, <http://inkscape.org/>) was used for post-processing of the plotted data and figure preparation.

### **Visually Guided Whole-Cell Recording and data analysis**

Patch-clamp recordings were performed as described previously (Joesch et al., 2008). Briefly, flies were anesthetized on ice and waxed on a Plexiglas holder with the head bent down. Aluminum foil separated the upper wet part (covered with

ringer solution (Wilson et al., 2004)) of the preparation from the lower dry compound eyes. A small window was cut into the backside of the head. Mild protease treatment (protease XIV, E.C.3.4.24.31, P-5147, Sigma Aldrich; 2 mg/ml, max 4 min) and a saline jet generated with a ringer-filled electrode was employed to remove the neurolemma. Genetically labeled green fluorescent HS cell somata were approached with a patch electrode filled with a red fluorescent dye (intracellular solution (Wilson and Laurent, 2005) containing additional 5 mM Spermine (S-2876, Sigma Aldrich) and 30 mM Alexa-Fluor-568-hydrazide-Na (A-10441, Molecular Probes) adjusted to pH = 7.3). Recordings were established under visual control with a 40x water-immersion objective (LumplanF, Olympus), a Zeiss Microscope (AxioTech Vario 100, Zeiss, Oberkochen, Germany), fluorescence excitation (100 W fluorescence lamp, heat filter, neutral-density filter OD 0.3; all from Zeiss, Germany) and a dual-band filter set (EGFP/DsRed, Chroma Technology, Vermont, USA).

Patch electrodes of 6-8 M $\Omega$  resistance (thin wall, filament, 1.5 mm, WPI, Florida, USA) were pulled on a Sutter- P97 (Sutter Instrument Company, California, USA). A reference electrode (Ag-AgCl) was immersed in the extracellular saline. Signals were recorded on a NPI BA-1S Bridge Amplifier (NPI Electronics GmbH, Tamm, Germany), low-pass filtered at 3 kHz, and digitized at 10 kHz via a digital-to-analog converter (PCI-DAS6025, Measurement Computing, Massachusetts, USA) with Matlab (Vers. 7.3.0.267, Mathworks, Massachusetts, USA).

After the recording, brains were dissected out and analyzed by confocal microscopy to reveal the anatomy of HS cells in flies that ectopically expressed Dscam 11.31.25.1.

Data were acquired and analyzed with the data acquisition and analysis toolboxes of Matlab. Receptive fields were calculated by binning the responses of single HS-cells to horizontal stimulation ( $\sim 5.6^\circ$  elevation and  $\sim 5.6^\circ$  azimuth) and subtracting the mean response during null direction from the mean response during preferred

direction motion. The receptive fields were smoothed by convolving them with a 3x3 kernel approximating an isotropic Gaussian function. Receptive fields were projected onto the azimuth by calculating the mean of the binned response across the elevation for each fly and normalizing it to the maximal value.

### **Visual Stimulation**

For visual stimulation during patch-clamp recordings a custom built LED arena was used based on the open-source information of the Dickinson Laboratory (<http://www.dickinson.caltech.edu/PanelsPage>) as described previously (Joesch et al., 2008). The arena consisted of 15 by 8 TA08-81GWA dot matrix displays (Kingbright, California, USA), each harboring 8 by 8 individual green (568 nm) LEDs, covering 170° in azimuth and 85° in elevation of the fly's visual field with an angular resolution of about 1.4° between adjacent LEDs. The arena is capable of frame rates above 600 fps with 16 intensity levels. Matlab was used for programming and generation of the patterns as well as for sending the serial command sequences via RS-232 to the main controller board and local buffering. The luminance range of the stimuli was 0-8 cd/m<sup>2</sup>. Large-field stimuli consisted of a sine grating (spatial wavelength 45°) covering the whole extent of the arena and moving horizontally in preferred or null direction with a temporal frequency of 1 Hz. The receptive fields of HS cells were determined as described previously (Schnell et al., 2010). HS cell responses were recorded during the movement of a small bar of 5.6° length and 1.4° width. The bar was moved horizontally from the contra- to the ipsilateral side and back again at different elevations.

### **Behavior**

One to five day old female flies were anesthetized on ice, placed on a Peltier stage (~5 °C) and glued (UV light-activated glue) to a thin wire placed between head and thorax. Animals were allowed to recover for at least 1 hour prior the experiments.

Tethered flies were placed into a panoramic LED display suspending 360 deg (otherwise see description above) and an IR light source (870 nm LED; JET-800-10, Roithner Lasertechnik, Austria) was mounted above the fly. The shadows cast by the beating wings of the fly hit two crescent shaped apertures placed above two photo detectors (UDT-555D, OSI Optoelectronics, US). Depending on the wing beat amplitude different portions of light were blocked by the wings. Due to the monotonically increasing area of the aperture, the measured photo-current at each detector is inversely proportional to the wing beat amplitude of each wing. The wing beat amplitude was calculated using the peak of each detector signal and normalized to its maximum. The strength of the turning response was quantified by subtracting the left wing beat amplitude from the right wing amplitude (“turning signal”).

Unless otherwise stated drifting gratings were presented to the eyes of the fly with 86 % contrast,  $\lambda = 24$  deg and  $f = 1.25$  Hz. At the beginning and end of each new stimulus protocol the performance of the fly was tested by presenting a whole field stimulus. In the individual experiments the visual stimuli moved for 2 seconds in one direction, changed direction and moved for 5 seconds and then moved in the opposite direction for 5 seconds.

Contrast dependence of the turning response: unilateral grating, presented on the left and right side, 15 – 180 deg in elevation, 86.7, 76.3, 60.0, 46.7, 33.3, 20.0 and 6.7 % contrast. Dependence on position along the azimuth: -38.6 to 38.6 deg in elevation (full arena elevation) and unilateral 33 deg along the azimuth, centered at left and right 31.5, 64.5, 97.5, 130.5 and 163.5 deg azimuth. Dependence on elevation: unilateral left and right 15 to 180 deg in azimuth and 38.6-30.9, 30.9-21.8, 21.8-11.3, 11.3-0 deg in elevation. After each trial the stimulus was stopped for 2 seconds and another trial was presented in random order. The strength of the turning response was calculated by subtracting the signals during front to back motion from the signals during back to front motion. For this calculation we took the

mean response that was exhibited during the last two seconds of the 5 second stimulus period. The response was defined positive if the fly followed the stimulus and negative otherwise.

## 6. References

1. Agarwala KL, Ganesh S, Tsutsumi Y, Suzuki T, Amano K, Yamakawa K (2001) Cloning and functional characterization of DSCAML1, a novel DSCAM-like cell adhesion molecule that mediates homophilic intercellular adhesion. *Biochem Biophys Res Commun* 285: 760-772.
2. Borst A, Egelhaaf M (1989) Principles of visual motion detection. *Trends Neurosci* 12: 297-306.
3. Borst A, Egelhaaf M (1990) Direction selectivity of fly motion-sensitive neurons is computed in a two-stage process. *Proc Natl Acad Sci USA* 87: 9363-9367.
4. Borst A, Egelhaaf M, Haag J (1995) Mechanisms of dendritic integration underlying gain control in fly motion-sensitive interneurons. *J Computat Neurosci* 2: 5-18.
5. Borst A, Haag J (2002) Neural networks in the cockpit of the fly. *J Comp Physiol A* 188: 419-437.
6. Borst A, Haag J, Reiff DF (2010) Fly motion vision. *Annu Rev Neurosci* 33: 49-70.
7. Braitenberg V (1970) Ordnung und Orientierung der Elemente im Sehsystem der Fliege. *Kybernetik* 7: 235-242.
8. Braitenberg V, Hauser-Holschuh H (1972) Patterns of projection in the visual system of the fly. II. Quantitative aspects of second order neurons in relation to models of movement perception. *Exp Brain Res* 16: 184-209.
9. Brand AH, Perrimon N (1993) Targeted gene expression as a means of altering cell fates and generating dominant phenotypes. *Development* 118: 401-15.
10. Buchner E, Buchner S, Bülthoff I (1984) Deoxyglucose mapping of nervous activity induced in *Drosophila* brain by visual movement. *J Comp Physiol A* 155: 471-483.
11. Chan WP, Prete F, Dickinson MH (1998) Visual input to the efferent control system of a fly's "gyroscope". *Sci* 280: 289-292.
12. Chen BE, Kondo M, Garnier A, Watson FL, Puettmann-Holgado R, Lamar DR, Schmucker D (2006) The molecular diversity of Dscam is functionally required for neuronal wiring specificity in *Drosophila*. *Cell* 125: 607-620.

13. Chiappe ME, Seelig JD, Reiser MB, Jayaraman V (2010) Walking Modulates Speed Sensitivity in *Drosophila* Motion Vision. *Curr Biol* 20: 1470-1475.
14. Clandinin TR, Feldheim DA (2009) Making a visual map: mechanisms and molecules. *Curr Opin Neurobiol* 19: 174-180.
15. Cuntz H, Forstner F, Borst A, Hausser M (2010) One rule to grow them all: a general theory of neuronal branching and its practical application. *PLoS Comput Biol* 6.
16. Dickinson MH, Lehmann FO, Gotz KG (1993) The active control of wing rotation by *Drosophila*. *J Exp Biol* 182: 173-189.
17. Egelhaaf M (1985) On the neuronal basis of figure-ground discrimination by relative motion in the visual system of the fly. I. Behavioural constraints imposed on the neuronal network and the role of the optomotor system. *Biol Cybern* 52: 123-140.
18. Emerson RC, Bergen JR, Adelson EH (1992) Directionally selective complex cells and the computation of motion energy in cat visual cortex. *Vision Res* 32: 203-218.
19. Fischbach KF, Dittrich APM (1989) The Optic Lobe of *Drosophila Melanogaster*. 1. A Golgi Analysis of Wild-Type Structure. *Cell and Tissue Research* 258: 441-475.
20. Fischbach KF, Hiesinger PR (2008) Optic lobe development. *Adv Exp Med Biol* 628: 115-136.
21. Fuerst PG, Bruce F, Tian M, Wei W, Elstrott J, Feller MB, Erskine L, Singer JH, Burgess RW (2009) DSCAM and DSCAML1 function in self-avoidance in multiple cell types in the developing mouse retina. *Neuron* 64: 484-497.
22. Fuerst PG, Koizumi A, Masland RH, Burgess RW (2008) Neurite arborization and mosaic spacing in the mouse retina require DSCAM. *Nature* 451: 470-474.
23. Gilbert C, Gronenberg W, Strausfeld NJ (1995) Oculomotor control in calliphorid flies: head movements during activation and inhibition of neck motor neurons corroborate neuroanatomical predictions. *J Comp Neurol* 361: 285-297.
24. Götz KG (1987) Course-control, metabolism and wing interference during ultralong tethered flight in *Drosophila melanogaster*. *J Exp Biol* 128: 35-46.
25. Gronenberg W, Strausfeld NJ (1990) Descending neurons supplying the neck and flight motor of diptera: Physiological and anatomical characteristics. *J Comp Neurol* 302: 973-991.
26. Hattori D, Demir E, Kim HW, Viragh E, Zipursky SL, Dickson BJ (2007) Dscam diversity is essential for neuronal wiring and self-recognition. *Nature* 449: 223-227.



27. Hattori D, Millard SS, Wojtowicz WM, Zipursky SL (2008) Dscam-mediated cell recognition regulates neural circuit formation. *Annu Rev Cell Dev Biol* 24: 597-620.
28. Hausen K (1982a) Motion sensitive interneurons in the optomotor system of the fly. I. The Horizontal Cells: Structure and signals. *Biol Cybern* 45: 143-156.
29. Hausen K (1982b) Motion sensitive interneurons in the optomotor system of the fly. II. The Horizontal Cells: Receptive field organization and response characteristics. *Biol Cybern* 46: 67-79.
30. Hausen K, Wehrhahn C (1983) Microsurgical lesion of horizontal cells changes optomotor yaw response in the blowfly *Calliphora erythrocephala*. *Proc R Soc Lond B* 219: 211-216.
31. Hausen K, Wehrhahn C (1989) Neural circuits mediating visual flight control in flies. I. Quantitative comparison of neural and behavioral response characteristics. *J Neurosci* 9: 3828-3836.
32. Heisenberg M, Wolf R (1979) On the structure of yaw torque in visual flight orientation of *Drosophila melanogaster*. *J Comp Physiol* 130: 113-130.
33. Heisenberg M, Wonneberger R, Wolf R (1978) Optomotor-blind (H31) - a *Drosophila* mutant of the lobula plate giant neurons. *J Comp Physiol* 124: 287-296.
34. Hengstenberg R, Hausen K, Hengstenberg B (1982) The number and structure of giant vertical cells (VS) in the lobula plate of the blowfly *Calliphora erythrocephala*. *J Comp Physiol A* 149: 163-177.
35. Hiesinger PR, Zhai RG, Zhou Y, Koh TW, Mehta SQ, Schulze KL, Cao Y, Verstreken P, Clandinin TR, Fischbach KF, Meinertzhagen IA, Bellen HJ (2006) Activity-independent prespecification of synaptic partners in the visual map of *Drosophila*. *Curr Biol* 16: 1835-1843.
36. Hughes ME, Bortnick R, Tsubouchi A, Baumer P, Kondo M, Uemura T, Schmucker D (2007) Homophilic Dscam interactions control complex dendrite morphogenesis. *Neuron* 54: 417-427.
37. Hummel T, Vasconcelos ML, Clemens JC, Fishilevich Y, Vosshall L, Zipursky SL (2003) Axonal targeting of receptor neurons in *Drosophila* is controlled by Dscam. *Neuron* 37: 221-231.
38. Ibbotson MR, Mark RF, Maddess TL (1994) Spatiotemporal response properties of direction-selective neurons in the nucleus of the optic tract and dorsal terminal nucleus of the wallaby, *Macropus eugenii*. *J Neurophysiol* 72: 2927-2943.
39. Joesch M, Plett J, Borst A, Reiff DF (2008) Response properties of motion-sensitive visual interneurons in the lobula plate of *Drosophila melanogaster*. *Current Biology* 18: 1-7.

40. Kern R, van Hateren JH, Michaelis C, Lindemann JP, Egelhaaf M (2005) Function of a fly motion-sensitive neuron matches eye movements during free flight. *PLoS Biol* 3: e171.
41. Koenderink JJ, van Doorn AJ (1987) Facts on optic flow. *Biol Cybern* 56: 247-254.
42. Krapp HG, Hengstenberg B, Hengstenberg R (1998) Dendritic structure and receptive-field organization of optic flow processing interneurons in the fly. *J Neurophysiol* 79: 1902-1917.
43. Krapp HG, Hengstenberg R, Egelhaaf M (2001) Binocular contributions to optic flow processing in the fly visual system. *J Neurophysiol* 85: 724-734.
44. Li HL, Huang BS, Vishwasrao H, Sutedja N, Chen W, Jin I, Hawkins RD, Bailey CH, Kandel ER (2009) Dscam mediates remodeling of glutamate receptors in *Aplysia* during de novo and learning-related synapse formation. *Neuron* 61: 527-540.
45. London M, Hausser M (2005) Dendritic computation. *Annu Rev Neurosci* 28: 503-532.
46. Ly A, Nikolaev A, Suresh G, Zheng Y, Tessier-Lavigne M, Stein E (2008) DSCAM is a netrin receptor that collaborates with DCC in mediating turning responses to netrin-1. *Cell* 133: 1241-1254.
47. Maimon G, Straw AD, Dickinson MH (2010) Active flight increases the gain of visual motion processing in *Drosophila*. *Nat Neurosci* 13: 393-399.
48. Matthews BJ, Kim ME, Flanagan JJ, Hattori D, Clemens JC, Zipursky SL, Grueber WB (2007) Dendrite self-avoidance is controlled by Dscam. *Cell* 129: 593-604.
49. Meinertzhagen IA (1996) Ultrastructure and quantification of synapses in the insect nervous system. *J Neurosci Meth* 69: 59-73.
50. Meinertzhagen IA, O'Neil SD (1991) Synaptic organization of columnar elements in the lamina of the wild type in *Drosophila melanogaster*. *J Comp Neurol* 305: 232-263.
51. Millard SS, Flanagan JJ, Pappu KS, Wu W, Zipursky SL (2007) Dscam2 mediates axonal tiling in the *Drosophila* visual system. *Nature* 447: 720-724.
52. Millard SS, Lu Z, Zipursky SL, Meinertzhagen IA (2010) *Drosophila* Dscam proteins regulate postsynaptic specificity at multiple-contact synapses. *Neuron* 67: 761-768.
53. Mronz M, Lehmann FO (2008) The free-flight response of *Drosophila* to motion of the visual environment. *J Exp Biol* 211: 2026-2045.
54. Nakayama K (1985) Biological image motion processing: a review. *Vision Res* 25: 625-660.

55. Petrovic M, Hummel T (2008) Temporal identity in axonal target layer recognition. *Nature* 456: 800-803.
56. Raghu SV, Joesch M, Borst A, Reiff DF (2007) Synaptic organization of lobula plate tangential cells in *Drosophila*: gamma-aminobutyric acid receptors and chemical release sites. *J Comp Neurol* 502: 598-610.
57. Raghu SV, Joesch M, Sigrist SJ, Borst A, Reiff DF (2009) Synaptic Organization of Lobula Plate Tangential Cells in *Drosophila*: Dalpha7 Cholinergic Receptors. *J Neurogenet* 23: 200-209.
58. Rall W (1962) Electrophysiology of a dendritic neuron model. *Biophys J* 2: 145-167.
59. Rall W (1969) Time constants and electrotonic length of membrane cylinders and neurons. *Biophys J* 9: 1483-1508.
60. Reichardt W (1961) Autocorrelation, a principle for the evaluation of sensory information by the central nervous system. In: *Sensory Communication* (Rosenblith WA, ed), pp 303-317. New York, London: The M.I.T. Press and John Wiley & Sons.
61. Reichardt W, Poggio T, Hausen K (1983) Figure-ground discrimination by relative movement in the visual system of the fly. Part II: Towards the neural circuitry. *Biol Cybern* 46: 1-30.
62. Reiff DF, Plett J, Mank M, Griesbeck O, Borst A (2010) Visualizing retinotopic half-wave rectified input to the motion detection circuitry of *Drosophila*. *Nat Neurosci* 13: 973-978.
63. Schmucker D, Chen B (2009) Dscam and DSCAM: complex genes in simple animals, complex animals yet simple genes. *Genes Dev* 23: 147-156.
64. Schmucker D, Clemens JC, Shu H, Worby CA, Xiao J, Muda M, Dixon JE, Zipursky SL (2000) *Drosophila* Dscam is an axon guidance receptor exhibiting extraordinary molecular diversity. *Cell* 101: 671-684.
65. Schnell B, Joesch M, Forstner F, Raghu SV, Otsuna H, Ito K, Borst A, Reiff DF (2010) Processing of horizontal optic flow in three visual interneurons of the *Drosophila* brain. *J Neurophysiol* 103: 1646-1657.
66. Scott EK, Raabe T, Luo LQ (2002) Structure of the vertical and horizontal system neurons of the lobula plate in *Drosophila*. *J Comp Neurol* 454: 470-481.
67. Scott EK, Reuter JE, Luo L (2003) Dendritic development of *Drosophila* high order visual system neurons is independent of sensory experience. *BMC Neurosci* 4: 14.

68. Seelig JD, Chiappe ME, Lott GK, Dutta A, Osborne JE, Reiser MB, Jayaraman V (2010) Two-photon calcium imaging from head-fixed *Drosophila* during optomotor walking behavior. *Nat Methods* 7: 535-540.
69. Segev I, London M (2000) Untangling dendrites with quantitative models. *Sci* 290: 744-750.
70. Single S, Borst A (1998) Dendritic integration and its role in computing image velocity. *Sci* 281: 1848-1850.
71. Soba P, Zhu S, Emoto K, Younger S, Yang SJ, Yu HH, Lee T, Jan LY, Jan YN (2007) *Drosophila* sensory neurons require Dscam for dendritic self-avoidance and proper dendritic field organization. *Neuron* 54: 403-416.
72. Strausfeld NJ (1976) Atlas of an insect brain. Berlin, Heidelberg: Springer.
73. Takemura SY, Lu Z, Meinertzhagen IA (2008) Synaptic circuits of the *Drosophila* optic lobe: the input terminals to the medulla. *J Comp Neurol* 509: 493-513.
74. Tammero LF, Dickinson MH (2002) The influence of visual landscape on the free flight behavior of the fruit fly *Drosophila melanogaster*. *J Exp Biol* 205: 327-343.
75. van Hateren JH, Kern R, Schwerdtfeger G, Egelhaaf M (2005) Function and coding in the blowfly H1 neuron during naturalistic optic flow. *J Neurosci* 25: 4343-4352.
76. Wang J, Ma X, Yang JS, Zheng X, Zugates CT, Lee CH, Lee T (2004) Transmembrane/juxtamembrane domain-dependent Dscam distribution and function during mushroom body neuronal morphogenesis. *Neuron* 43: 663-672.
77. Wang J, Zugates CT, Liang IH, Lee CH, Lee T (2002) *Drosophila* Dscam is required for divergent segregation of sister branches and suppresses ectopic bifurcation of axons. *Neuron* 33: 559-571.
78. Wilson RI, Laurent G (2005) Role of GABAergic inhibition in shaping odor-evoked spatiotemporal patterns in the *Drosophila* antennal lobe. *J Neurosci* 25: 9069-9079.
79. Wilson RI, Turner GC, Laurent G (2004) Transformation of olfactory representations in the *Drosophila* antennal lobe. *Sci* 303: 366-70.
80. Wojtowicz WM, Flanagan JJ, Millard SS, Zipursky SL, Clemens JC (2004) Alternative splicing of *Drosophila* Dscam generates axon guidance receptors that exhibit isoform-specific homophilic binding. *Cell* 118: 619-633.
81. Wojtowicz WM, Wu W, Andre I, Qian B, Baker D, Zipursky SL (2007) A vast repertoire of Dscam binding specificities arises from modular interactions of variable Ig domains. *Cell* 130: 1134-1145.
82. Yamagata M, Sanes JR (2008) Dscam and Sidekick proteins direct lamina-specific synaptic connections in vertebrate retina. *Nature* 451: 465-469.

83. Yamakawa K, Huot YK, Haendelt MA, Hubert R, Chen XN, Lyons GE, Korenberg JR (1998) DSCAM: a novel member of the immunoglobulin superfamily maps in a Down syndrome region and is involved in the development of the nervous system. *Hum Mol Genet* 7: 227-237.
84. Yu HH, Yang JS, Wang J, Huang Y, Lee T (2009) Endodomain diversity in the *Drosophila* Dscam and its roles in neuronal morphogenesis. *J Neurosci* 29: 1904-1914.
85. Zhan XL, Clemens JC, Neves G, Hattori D, Flanagan JJ, Hummel T, Vasconcelos ML, Chess A, Zipursky SL (2004) Analysis of Dscam diversity in regulating axon guidance in *Drosophila* mushroom bodies. *Neuron* 43: 673-686.
86. Zhu H, Hummel T, Clemens JC, Berdnik D, Zipursky SL, Luo L (2006) Dendritic patterning by Dscam and synaptic partner matching in the *Drosophila* antennal lobe. *Nature Neuroscience* 9: 349-355.
87. Zipursky SL, Wojtowicz WM, Hattori D (2006) Got diversity? Wiring the fly brain with Dscam. *Trends Biochem Sci* 31: 581-588.



## VII. Discussion

The huge advantage of *Drosophila* as a model organism for studying visual information processing is that it allows bridging the gap between a defined sensory stimulus and a well-described behavioral reaction. By combining genetic and physiological techniques in the fruit fly the intermediary neural circuits can hopefully be unraveled. This work provides important steps into that direction, first, by testing physiological tools for studying neuronal function (Chapter III), second, by characterizing the response properties of motion-sensitive HS cells thought to control important parts of optomotor behavior (Chapter IV), third, by using electrophysiological recordings of HS cells as direct readout for the effects of genetically manipulating the presynaptic circuitry in the lamina (Chapter V), and finally, by studying the functional consequences of an altered dendritic morphology in HS cells overexpressing a single Dscam isoform (Chapter VI).

### **1. Calcium imaging vs. electrophysiology**

Calcium imaging (e.g. Fiala et al., 2002; Wang et al., 2003; Wang et al., 2004; Shang et al., 2007) and whole-cell recordings (e.g. Wilson et al., 2004; Wilson and Laurent, 2005; Olsen et al., 2007; Olsen et al., 2010) are already well-established in the olfactory system of *Drosophila*, but they are only beginning to be used in the visual system (Joesch et al., 2008; Maimon et al., 2010; Seelig et al., 2010; Reiff et al., 2010; Chiappe et al., 2010). Whereas electrophysiological recordings are mainly hampered by the small size of most *Drosophila* neurons, Calcium imaging in the visual system faces two other problems. First, one has to make sure that the laser used to excite the fluorophore does not stimulate photoreceptors, which can be largely excluded by using two-photon microscopy. Second, the light from the visual stimulus must be prevented from reaching the highly sensitive photomultipliers used for capturing the emitted fluorescence light, which can be achieved by different means (Reiff et al., 2010; Seelig et al., 2010). With these problems solved, Calcium imaging is mainly limited by the properties of the available Calcium indicators. Whereas the first study

(Chapter III, Fig. 7) showed that all the indicators are in principle functional in the visual system, especially their temporal resolution is still very low. Since then, two new indicators have become available that turned out to be better suited for measuring signals in the visual system. These indicators are TN-XXL (Mank et al., 2008) and GCaMP3 (Tian et al., 2009).

Whereas genetically encoded Calcium indicators allow for simultaneously recording the activity of a population of cells, they have several drawbacks compared to patch-clamp recordings. Their temporal resolution and sensitivity are still much lower and not sufficient for resolving single action potentials or EPSPs at high frequencies (above 6Hz for GCaMP3). Thus, it is not clear how well a change in the intracellular Calcium concentration reflects the electrical activity of a neuron. In addition, hyperpolarizing signals might not be reported at all, which is a problem as many neurons of the visual system respond with graded depolarizing and hyperpolarizing membrane potential changes (Chiappe et al., 2010; Haag and Borst, 2000; Egelhaaf and Borst, 1995).

On the other hand, Calcium imaging can be used for measuring signals in different compartments of a neuron allowing for example to compare responses in the dendrites with those in the axon terminal (Elyada et al., 2009). In contrast, electrophysiological recordings in *Drosophila* are mainly performed from the cell somata, as this allows for more stable and long-lasting recordings. The somata of insect neurons, however, are usually distant and only connected by a thin process to the rest of the cell, so that only attenuated signals can be measured there (Gouwens and Wilson, 2009). In addition, no recordings from the tiny columnar neurons of the medulla in *Drosophila* were reported as yet. Thus, for characterizing their responses Calcium imaging seems to be the most promising technique at the moment.

In combination with genetic manipulations both techniques show great promise for enabling the dissection of the complete motion detection circuitry.

## **2. LPTCs and behavior**

Optomotor behavior in the fruit fly has been studied extensively (for review see Heisenberg and Wolf, 1984; Frye and Dickinson, 2004). However, not much is known about the underlying neural circuits. Based on anatomical similarities between



neurons of different species, these circuits were mainly inferred from physiological studies on larger flies, like *Calliphora* and *Musca*. A pioneering electrophysiological study on VS cells in *Drosophila* revealed that this anatomical similarity indeed goes along with similar response properties and connectivity (Joesch et al., 2008). However, it was also claimed that LPTCs of different fly species are well adapted to different behavioral needs (Buschbeck and Strausfeld, 1997). For the analysis of the neuronal circuits underlying a certain behavior it is therefore necessary to study both in the same species. Horizontally sensitive cells are ideal to address this problem as horizontal motion has been extensively used to analyze yaw-turning behavior of the fly.

Concerning their basic response properties, HS cells in *Drosophila* appear to be very similar to their counterparts in *Calliphora* (Chapter IV). They receive input from both the ipsi- and the contralateral eye tuning them to rotational motion around the vertical body axis.

Analyzing the structure and connectivity of HS cells in *Drosophila*, however, revealed interesting differences to the blowfly (Chapter IV). First, their dendrites overlap to a much larger degree with HSE covering nearly the whole lobula plate in *Drosophila*. Second, the close association with CH cells known from the blowfly seems to be lacking in *Drosophila*. CH cells in *Calliphora* play an important role in figure detection by transmitting smoothed inhibitory information about global motion from HS cells to FD cells thereby making the latter selective for small moving objects (Warzecha et al., 1993; Cuntz et al., 2003). *Drosophila* performs a similar behavior. It reacts to moving objects and stabilizes them in the frontal position, a behavior that is depended on inhibitory signaling (Fei et al., 2010). The underlying circuits, however, still have to be revealed in the small fly.

It is generally assumed that HS cells play a crucial role in optomotor behavior although conclusive evidence is still lacking. In *Drosophila* their involvement was mainly inferred from behavioral studies on mutant flies, like *omb*, with missing LPTCs (Heisenberg et al., 1978). However, it cannot be ruled out that other cells also affected in the mutant are the key players.

Here, further support is provided for the assumption that HS cells are central to optomotor yaw torque by showing that their response properties very well match

## Discussion

---

behavioral data obtained in tethered flying (Götz, 1972) or walking flies (Buchner, 1984). For example, they are tuned to a rotational optic flow field and exhibit a temporal frequency optimum of 1 Hz as well as a saturating contrast dependency (Chapter IV, Fig. 2). In addition, altering the morphology and receptive fields of HS cells leads to reduced optomotor responses (chapter VI, Fig. 5, behavioral experiments performed by V. Haikala).

Along these lines, a recent Calcium imaging study in tethered walking flies found a correlation between Calcium signals in HS cell and optomotor turning behavior (Seelig et al., 2010). However, the time lag of up to four seconds between these two events was surprisingly large. Whether this delay is biologically relevant or can be attributed to technical limitations remains to be analyzed.

In a subsequent study (Chiappe et al., 2010), Calcium imaging from HS cells in stationary flies revealed a temporal frequency optimum of 1Hz, which corresponds well to the findings presented here. However, a shift of this optimum to higher temporal frequencies as well as a higher response gain at high frequencies occurred when the fly was walking. This shift could explain findings from behavioral studies where the temporal frequency optimum was found to be significantly higher than 1 Hz (Duistermars et al., 2007; Fry et al., 2009). However, the results from these studies are not in line with earlier behavioral results (Götz, 1964; Buchner, 1984). Whether this discrepancy is due to different experimental conditions (like the presentation of the visual stimulus) or a different analysis of the behavioral data remains to be investigated.

In addition, it would be interesting to know, how the Calcium signals measured in HS cells in behaving fruit flies (Chiappe et al., 2010) translate into membrane potential changes. One study in *Calliphora* reported that Calcium and voltage signals in LPTCs differ in their dependence on the temporal frequency (Egelhaaf and Borst, 1995). Especially at high frequencies Calcium signals were relatively higher than the actual voltage responses, a finding that was explained by the different temporal characteristics of the two signals.

To reveal the dependence of the temporal frequency optimum on the behavioral state it would be beneficial to measure electrical signals and optomotor responses in the same fly using the same stimulus. Recently a paradigm was established that

allows for whole-cell recordings from LPTCs in tethered flying fruit flies (Maimon et al., 2010). In this study, responses of VS cells had a larger gain during flight than during rest. A similar change can be elicited by applying octopamine agonists, as was shown in *Calliphora* (Longden and Krapp, 2009), pinpointing at an important role of this neuromodulator in adjusting LPTC responses. At which level and how octopamine acts, however, is still unclear. Also, the velocity dependence of the response has not been analyzed in this study.

In any case, boosting responses to fast stimuli in cases where they are most likely to occur, i.e. during self-motion of the fly, would be an elegant mechanism for a cost-efficient processing of motion information.

Whereas care has to be taken when relating neuronal responses obtained in fixed animals to behavioral output obtained in moving flies, the former approach is still suitable for analyzing the circuitry underlying motion detection. This holds especially true for the columnar neurons presynaptic to LPTCs that represent the correlation-type motion detector and that are largely undescribed so far. Once these circuits are established, one can proceed to studying how their properties are modified during behavior.

### **3. Manipulating neuronal circuits**

There are a lot of genetic tools available for manipulating the function of neurons (for review see Luo et al., 2008). However, their performance has never been comprehensively validated and might depend on the types of neurons in which they are expressed (Thum et al., 2006; Rister and Heisenberg, 2006). Furthermore, neurons are usually embedded in a complex circuitry, which has to be taken into account when interpreting results obtained by interfering with their function. For example, blocking the input or the output of one neuron that is transmitted via chemical synapses is expected to lead to the same result only as long as this neuron does not make connections via electrical synapses. As shown here (Chapter V, Fig. 2), rescuing the *ort* gene in only L1 in an *ort*-null mutant background not only restored the input to L1, but via electrical synapses also to L2 and vice versa. Although this intervention has the advantage of being highly specific to the lamina, it led to

unexpected results, as not all connections of L1 and L2 were known. Nevertheless, the chemical connections in the lamina are very well described (Meinertzhagen and O'Neil, 1991). Much less is known about the connectivity of cells in the medulla, which has hampered an analysis of their function. However, EM studies are underway (e.g. Takemura et al., 2008) that hopefully provide this information in the near future.

Other genetic tools can only be employed in a meaningful way if Gal4 lines of high specificity are available. Otherwise their expression can lead to lethality during development in case vital cells are affected. Using *shibire<sup>ts</sup>* developmental problems can largely be circumvented as its effect of blocking synaptic output is temperature-inducible in adult flies. However, also *shibire<sup>ts</sup>* requires specific Gal4 lines to allow for attributing a certain function to a certain type of neuron. Combinatorial expression systems like split-Gal4 are a promising approach in that regard (Chapter V, Gao et al., 2008).

### **4. Gap-junctions in the fly visual system**

#### **4.1 Functional role**

Gap junctions were first described in invertebrates already in the 1950s (for review see Bauer et al., 2005). The results presented here (Chapters IV and V) provide further support for the accumulating evidence of their abundance and importance in the fly visual system (e.g. Curtin et al., 2002; Haag and Borst, 2005; Cuntz et al., 2007; Elyada et al., 2009). Using the spread of neurobiotin as evidence for gap junctions between two cells (Haag and Borst, 2005; Fan et al., 2005) revealed not only electrical coupling between the two lamina monopolar cells L1 and L2 (Chapter V, Fig. 3, experiments performed by M. Joesch), but also between HS cells themselves and between HS cells and descending neurons (Chapter IV, Fig. 6).

Gap junctions between the photoreceptor terminals in the lamina have been described for long and there was even some evidence for gap junctions between the somata of LMCs (Shaw, 1984; Meinertzhagen and O'Neil, 1991). Nevertheless, the finding that L1 and L2 are strongly coupled via electrical synapses most likely via their dendrites was unexpected. The strength of the coupling suggests that it plays

an important functional role. As the electrical responses measured in the dendrites of L1 and L2 seem to be rather similar this further interaction most likely aids in noise reduction and a more reliable and temporally precise encoding of light signals. Even more surprising was the finding that LPTCs make abundant electrical connections with each other, because in contrast to L1 and L2, they have different response properties and different input elements. As presented here, HS cells in *Drosophila* are coupled via electrical synapses probably in a chain-like manner (see Chapter IV). This organization is highly similar to the coupling of VS cells realized in *Calliphora* (Haag and Borst, 2004) as well as in *Drosophila* (Joesch et al., 2008). Modeling studies provided evidence that this coupling leads to a more reliable encoding of rotational axes by the VS cell ensemble if natural stimuli are presented (Cuntz et al., 2007). Concerning HS cells in *Calliphora*, electrical synapses there transmit information about horizontal motion to neighboring CH cells (Farrow et al., 2003) that in turn play a role in figure detection. CH cells could, however, not be found in *Drosophila* so far (see Chapter IV). Instead, all three HS cells have highly overlapping dendritic trees in the fruit fly, thus conveying partially redundant information (Chapter IV, Fig. 3). Maybe this organization serves a similar function as the coupling of VS cells, leading to more reliable and robust encoding of horizontal motion. This interpretation is also supported by the Dscam study (Chapter VI). Here, flies in which dendritic trees and receptive fields of HS cells are considerably reduced in size also have reduced optomotor responses to stimuli that are restricted to parts of the visual field (behavioral experiments performed by V. Haikala).

In any case, the broadening of responses in higher order neurons seems to be a common principle in sensory processing in the fly. Projection neurons in the olfactory system e.g. typically respond to more odors than do their directly presynaptic olfactory receptor neurons (Wilson et al., 2004; Olsen et al., 2007; Shang et al., 2007). There, however, the additional input seems to be conveyed by local interneurons interconnecting different glomeruli instead of a direct coupling of projection neurons.

HS cells were also found to be extensively coupled to descending neurons that relay motion information to motoneurons in the cervical connective and the thoracic ganglion (Chapter IV, Fig. 6). Most likely, electrical synapses serve a fast and reliable

information transfer necessary for rapid steering maneuvers of the fly. Another well-described case of gap-junctional coupling in *Drosophila* is the giant fiber system mediating a fast escape response (Thomas and Wyman, 1984; Phelan et al., 1996) for which speed and reliability are essential.

### 4.2 Molecular composition

Gap-junctional proteins in invertebrates are encoded by genes called 'innexins'. Whereas the primary amino acid sequence of innexins differs considerably from that of vertebrate connexins, their structure is rather similar (Bauer et al., 2005).

Two of the innexin genes, *ogre* (innexin 1) and *shaking B* (innexin 8) play a role in the development of the fly visual system being necessary for the proper formation of chemical synapses between photoreceptors and LMCs (Curtin et al., 2002). Mutations in *shaking B* mutants also reduce the number of gap junctions between photoreceptor terminals (Shimohigashi and Meinertzhagen, 1998). Furthermore, *shaking B* is involved in the formation of electrical connections in the giant fiber system (Phelan et al., 1996; Blagburn et al., 1999). Evidence suggests that pre- and postsynaptic neurons express two different splice variants leading to rectifying properties of the electrical synapses between them. Expression studies in oocytes revealed that depolarizing current preferentially spreads in one direction (correspondingly from the presynaptic to the postsynaptic cell) and hyperpolarizing current in the opposite direction (Phelan et al., 2008). Whether similar mechanisms are realized in the visual system of *Drosophila* is unclear as no double recordings could be performed so far. In addition, the molecular composition of electrical synapses there is still unknown. The *ort*-rescue experiments suggest that the information flow between LMCs is bidirectional, because both, restoring *ort* in L1 or in L2, led to normal motion responses (Chapter V, Fig. 2). An antibody against *shaking B* labeled the proximal parts of lamina cartridges (Chapter V, Fig. 3, experiments done by S.V. Raghu), making this innexin a good candidate for forming gap junctions between L1 and L2.

The function of most of the other innexin genes in the nervous system, however, is not well described. It remains to be studied which of the innexins are expressed in LPTCs and whether and how their function is regulated.

## **5. Implementation of the correlation-type motion detector**

### **5.1 Physiological evidence**

In flies, the correlation-type motion detector is now a well-established model backed by a vast amount of experimental data from behavioral as well as physiological studies (for review see Borst et al., 2010). The findings presented here provide further evidence as the responses of HS cells in *Drosophila* exhibit the characteristic fingerprints of presynaptic computations according to this motion detector model (Chapter IV, Fig. 2). One property is the independence of the response of the sign of contrast, which will be discussed in detail below. The most important prediction, however, is the characteristic dependence of the response on the velocity of the stimulus. Depending on the spatial layout of the pattern, responses are maximal for those velocities that result in a certain temporal frequency independent on the exact combination of pattern speed and spatial wavelength. This computational structure, however, makes responses ambiguous with respect to the velocity of the stimulus. This ambiguity is further enhanced by the contrast dependency of the response, which in theory should be quadratic, but in reality saturates for high contrasts (Buchner, 1984).

The temporal frequency optimum is usually determined by presenting gratings of a single spatial wavelength, which is, however, a rather artificial situation not usually occurring in nature. By presenting natural images it could be shown that response properties of LPTCs indeed reflect the velocity independent of the particular image and contrast (Straw et al., 2008). Thus, the tuning of EMDs seems to be optimally matched to features of the predominating visual input. A possible mechanism behind this effect was suggested based on the finding that responses to low-contrast stimuli increase and those to high-contrast stimuli decrease over time (Barnett et al., 2010). This adaptation process was speculated to lead to a response normalization and thus to reduce ambiguity caused by image contrast.

### **5.2 On- and Off-detectors**

Whereas there is vast evidence that computations described by the correlation-type motion detector are performed in the fly brain, not much is known about the

underlying cellular mechanisms. An especially intriguing question is how a sign-correct multiplication of two signals might be achieved. In its most basic form, the correlation-type motion detector requires that two signals of either positive or negative sign both lead to a positive output signal after multiplication. As it is hard to imagine how this can be achieved by single neurons, it was proposed that motion detection might be split into two different channels dealing only with brightness increments or decrements. However, interactions between light-on and light-off signals that lead to sign-inverted motion responses in LPTCs supported the original version of only one single motion detector (Egelhaaf and Borst, 1992). These interactions could, however, not be found when only photoreceptors of one ommatidium were stimulated with small light flashes (Franceschini et al., 1989).

A recent Calcium imaging study provides evidence for half-wave-rectification of the signal conveyed by L2, which exhibits large Calcium transients upon light-off (Reiff et al., 2010). This finding corroborates the results presented here (Chapter V, Fig. 4, experiments performed by M. Joesch) that light signals are split into two different channels dealing separately with light-on and light-off and fed by L1 and L2, respectively. A possible solution for the discrepancy between the apparent separation and interaction of on- and off-signals is the four-quadrant multiplier (Hassenstein and Reichardt, 1956). In this extended motion detector version, four types of interactions take place, namely on-on and off-off leading both to positive output signals and on-off and off-on leading to a sign-inverted output after the multiplication. This model, however, requires four times the number of channels per column compared to the original Reichardt detector. Although this is anatomically possible, it still raises the question why a visual system should waste energy for computing interactions between light-on and light-off that are unlikely to signal motion in nature. Either these interactions are just a by-product caused by incomplete rectification of on- and off-signals (Reiff et al., 2010; H. Eichner, unpublished) or they have another as yet undiscovered biological function.

### 5.3 Cellular implementation

Whereas it is now clear that L1 and L2 provide the major input to local motion detectors (Rister et al., 2007), nothing is known about the medulla cells performing



the actual computations postulated by the Reichardt model. Based on anatomical findings, two pathways were proposed to provide input to LPTCs, the first transmitting information from L1 via Mi1 and T4, the second from L2 via Tm1 and T5 (Bausenwein and Fischbach, 1992; Bausenwein et al., 1992). Already then, it was speculated that these two pathways might separately process on- and off-signals.

Based on few electrophysiological recording, T5 was reported to be fully and T4 to be only weakly directional selective (Douglass and Strausfeld, 1995; Douglass and Strausfeld, 1996) lending some support for their involvement in motion detection. However, whether they respond preferentially to either on- or off-signals was not analyzed and due to the scarceness of recordings their role remains inconclusive. In addition, both T4 and T5 come in four different variants projecting to the four different layers of the lobula plate (Fischbach and Dittrich, 1989). A recent MARCM study using a *cha*-Gal4 line suggests that T4 cells are cholinergic (Raghu et al., 2010). How many T4 and T5 cell variants there are per column, whether they use different neurotransmitters, excitatory or inhibitory ones, and whether they are specialized for signaling different motion directions and/or contrast polarities are all open questions.

## **6. Similarities to vertebrates**

In vertebrates, a separation of light-on and light-off signals occurs already at the synapse between cone photoreceptors and bipolar cells in the retina (for review see Wässle, 2004). On and off cone bipolar cells express different glutamate receptors and thus either depolarize or hyperpolarize in response to light. Whereas the underlying mechanism is not yet revealed in the fly, a separation into channels specialized for encoding either brightness increments or decrements seems to be common between flies and vertebrates (see Chapter V). This coding principle appears to be most efficient, because it does not require a tonically active synapse, whose transmitter release is either up- or downregulated (Laughlin, 1989). An interesting question is why the half-wave-rectification in the fly visual system does not already occur between photoreceptors and LMCs, which would be equivalent to the cone pathways in vertebrates. Probably the most important task of the lamina is to enhance signal-to-noise ratios and to increase sensitivity for low light intensities,

## Discussion

---

which is achieved by neuronal superposition (Kirschfeld, 1973) and a further electrical coupling of lamina neurons. Only at the next stage, i.e. at the level of synaptic output of LMCs (Reiff et al., 2010) or postsynaptic neurons in the medulla, light signals might then become half-wave rectified. In that regard the system is more similar to the vertebrate rod pathway, which is specialized for vision at low light intensities. Rods mainly provide input to one type of rod bipolar cell, which depolarizes in response to light-on and slightly hyperpolarizes to light-off stimuli (Euler and Masland, 2000). This bipolar cell in turn transmits information to on and off cone bipolar cells via All amacrine cells (Famiglietti and Kolb, 1975). However, there are also alternative routes and the information flow in the retina seems to be dependent on the lighting conditions (Münch et al., 2009).

Motion detection and its underlying mechanisms have also been studied extensively in vertebrates (for a comparison between flies and vertebrates see Clifford and Ibbotson, 2002). In primates, neurons of a visual cortical area called MST (medial superior temporal area) seem to subserve similar functions as do LPTCs. MST neurons were found to have large receptive fields and to be tuned to specific motion patterns (Tanaka et al., 1986; Duffy and Wurtz, 1991b; Duffy and Wurtz, 1991a). Based on that they are speculated to play a role in analyzing the optic flow fields caused by self-motion. MST receives input via an area called MT that predominantly contains direction-selective cells and receives input from the primary visual cortex area V1 (Born and Bradley, 2005). Whereas in primates V1 is the first area known to contain directionally selective neurons, in other vertebrates like rabbits and mice they already occur at the level of the retina. There, directional-selective ganglion cells and starburst amacrine cells and the mechanism underlying motion detection are well-described (Demb, 2007). Direction-selectivity in the vertebrate retina is achieved by a spatially-offset and prolonged inhibitory signal that suppresses responses to null-direction motion and not by a multiplication-like interaction as postulated by the Reichardt model.

## 7. LPTCs and Dscam

Cell types of the lobula plate in *Drosophila* are anatomically and physiologically well-described. Therefore, this system is ideally suited for studying the consequences of manipulating the Dscam system on a functional level.

By using Dscam as a tool for changing the morphology of HS cells, a striking correspondence between anatomy and function could be revealed (Chapter VI). Overexpression of a single Dscam isoform in HS cells led to cells with reduced dendritic coverage of the lobula plate (Chapter VI, Figs. 2 and 3, experiments performed by J. Shi and F. Förstner). In most cases, the dendrites especially of HSE did not reach the lateral border of the lobula plate anymore, an area corresponding to the frontal visual field. Concomitantly, HS cells had smaller receptive fields being less or not responsive to frontal stimuli (Chapter VI, Fig. 4).

Their receptive fields, thus, very well reflect their coverage of the lobula plate. Obviously no compensatory growth of the presynaptic, retinotopically organized elements occurs, suggesting that the system is rather hard-wired.

Whereas overexpression of single Dscam isoforms is useful for analyzing structure-function relationships, it allows only indirectly drawing conclusions about the function of Dscam in wild-type cells. Findings from other systems suggest that Dscam1 is used for providing cells with a unique molecular cell surface code (Schmucker, 2007). This code allows neurons to discriminate between themselves and others. Dscam2, however, which gives rise to only two isoforms, is thought to mediate tiling between neighboring neurons of the same type (Millard and Zipursky, 2008). This assumption is based on the finding that terminals of Dscam-null mutant L1 neurons in the medulla are no longer restricted to their own column, but overlap with neighboring L1 neurons (Millard et al., 2007).

A similar function is performed by DSCAM in the vertebrate retina, where it is necessary for tiling between retinal ganglion and amacrine cells of the same type (Fuerst et al., 2008; Fuerst et al., 2009).

Antibody stainings revealed that Dscam is expressed in LPTCs of wild-type flies (Chapter VI, Fig. 1, experiments done by J. Shi). However, it is not yet clear how a complete lack of Dscam or a reduction in isoform variability affects their structure

and function. More refined genetic tools will hopefully allow answering that question in the near future and provide further insights into the role of Dscams in wiring the neurons of the visual system of *Drosophila*.

### **8. Outlook**

While the circuits in the lobula plate and in the lamina are relatively well-described, the medulla still remains more or less a black box. T4 and T5 cells are promising candidates for providing the direct synaptic input to LPTCs. However, assumptions about the neurons presynaptic to them and postsynaptic to L1 and L2 are still rather speculative. Even if the cell types and synaptic connections in the medulla are uncovered by EM studies (e.g. Takemura et al., 2008), it remains to be revealed how the computations postulated by the Reichardt detector, i.e. the temporal filtering and the non-linear interaction, are biophysically achieved and by what cells.

Several approaches promise to elucidate the function of medulla neurons in the future. Firstly, as outlined in this work, combining physiological recordings from LPTCs with a genetic block of medulla neurons can reveal their function provided that specific Gal4-lines are available. While this approach tests the necessity of a neuron for a certain computation, their sufficiency can, secondly, be studied by optically stimulating cells expressing the newly developed light-sensitive ion channels or pumps like channelrhodopsin or halorhodopsin (for review see Szobota and Isacoff, 2010). Thirdly, Calcium imaging makes it possible to directly monitor the activity of the small columnar cells although not with the high temporal resolution of electrophysiological recordings (Reiff et al., 2010). To complement these analyses, functional neuroanatomy can provide hints to the neurotransmitters and receptors expressed by the cell types of interest (Raghu et al., 2007; Raghu et al., 2009).

While all of these approaches have their drawbacks, in combination they will allow to elucidate the neuronal correlates of the elementary motion detector.

## VIII. References

Anderson JC, Laughlin SB (2000) Photoreceptor performance and the co-ordination of achromatic and chromatic inputs in the fly visual system. *Vision Research* 40: 13-31.

Arnett DW (1972) Spatial and Temporal Integration Properties of Units in First Optic Ganglion of Dipterans. *J Neurophysiol* 35: 429-&.

Barnett PD, Nordstrom K, O'Carroll DC (2010) Motion Adaptation and the Velocity Coding of Natural Scenes. *Current Biology* 20: 994-999.

Bauer R, Loer B, Ostrowski K, Martini J, Weimbs A, Lechner H, Hoch M (2005) Intercellular Communication: the *Drosophila* Innexin Multiprotein Family of Gap Junction Proteins. *Chemistry & Biology* 12: 515-526.

Bausenwein B, Dittrich APM, Fischbach KF (1992) The optic lobe of *Drosophila melanogaster*. 2. Sorting of retinotopic pathways in the medulla. *Cell Tissue Res* 267: 17-28.

Bausenwein B, Fischbach KF (1992) Activity labeling patterns in the medulla of *Drosophila melanogaster* caused by motion stimuli. *Cell Tissue Res* 270: 25-35.

Blagburn JM, Alexopoulos H, Davies JA, Bacon JP (1999) Null mutation in shaking-B eliminates electrical, but not chemical, synapses in the *Drosophila* giant fiber system: A structural study. *J Comp Neurol* 404: 449-458.

Born RT, Bradley DC (2005) Structure and function of visual area MT. *Annual Review of Neuroscience* 28: 157-189.

Borst A (1986) Time Course of the Houseflies' Landing Response. *Biological Cybernetics* 54: 379-383.

Borst A, Egelhaaf M (1989) Principles of visual motion detection. *Trends Neurosci* 12: 297-306.

Borst A, Egelhaaf M (1990) Direction selectivity of blowfly motion-sensitive neurons is computed in a two-stage process. *Proc Natl Acad Sci USA* 87: 9363-9367.

Borst A, Haag J (2002) Neural networks in the cockpit of the fly. *J Comp Physiol A* 188: 419-437.

Borst A, Haag J, Reiff DF (2010) Fly motion vision. *Annu Rev Neurosci* 33.

Braitenberg V (1967) Patterns of Projection in Visual System of Fly. I. Retina-Lamina Projections. *Exp Brain Res* 3: 271-&.

## References

---

Braitenberg V, Hauser-Holschuh H (1972) Patterns of Projection in Visual System of Fly. 2. Quantitative Aspects of Second-Order Neurons in Relation to Models of Movement Perception. *Exp Brain Res* 16: 184-209.

Brand A (1995) Gfp in *Drosophila*. *Trends in Genetics* 11: 324-325.

Brand AH, Perrimon N (1993) Targeted gene expression as a means of altering cell fates and generating dominant phenotypes. *Dev* 118: 401-415.

Brotz TM, Borst A (1996) Cholinergic and GABAergic receptors on fly tangential cells and their role in visual motion detection. *J Neurophysiol* 76: 1786-1799.

Buchner E (1976) Elementary Movement Detectors in an Insect Visual-System. *Biological Cybernetics* 24: 85-101.

Buchner E (1984) Behavioural analysis of spatial vision in insects. In: *Photoreception and vision in invertebrates* (Ali MA, ed), pp 561-621. New York, London: Plenum Press.

Buchner E, Buchner S, Bulthoff I (1984) Deoxyglucose Mapping of Nervous Activity Induced in *Drosophila* Brain by Visual Movement. 1. Wildtype. *J Comp Physiol* 155: 471-483.

Buschbeck EK, Strausfeld NJ (1997) The relevance of neural architecture to visual performance: Phylogenetic conservation and variation in dipteran visual systems. *J Comp Neurol* 383: 282-304.

Card G, Dickinson MH (2008) Visually mediated motor planning in the escape response of *Drosophila*. *Current Biology* 18: 1300-1307.

Chen BE, Kondo M, Garnier A, Watson FL, Puettmann-Holgado R, Lamar DR, Schmucker D (2006) The molecular diversity of Dscam is functionally required for neuronal wiring specificity in *Drosophila*. *Cell* 125: 607-620.

Chen MS, Obar RA, Schroeder CC, Austin TW, Poodry CA, Wadsworth SC, Vallee RB (1991) Multiple forms of dynamin are encoded by *shibire*, a *Drosophila* gene Involved in endocytosis. *Nature* 351: 583-586.

Chiappe ME, Seelig JD, Reiser MB, Jayaraman V (2010) Walking Modulates Speed Sensitivity in *Drosophila* Motion Vision. *Current Biology* 20: 1470-1475.

Clifford CWG, Ibbotson MR (2002) Fundamental mechanisms of visual motion detection: models, cells and functions. *Progress in Neurobiology* 68: 409-437.

Cook T, Desplan C (2001) Photoreceptor subtype specification: from flies to humans. *Semin Cell Dev Biol* 12: 509-518.

Coombe PE, Srinivasan MV, Guy RG (1989) Are the Large Monopolar Cells of the Insect Lamina on the Optomotor Pathway? *J Comp Physiol A* 166: 23-35.

Cuntz H, Haag J, Borst A (2003) Neural image processing by dendritic networks. Proc Natl Acad Sci USA 100: 11082-11085.

Cuntz H, Haag J, Forstner F, Segev I, Borst A (2007) Robust coding of flow-field parameters by axo-axonal gap junctions between fly visual interneurons. Proc Natl Acad Sci USA 104: 10229-10233.

Curtin KD, Zhang Z, Wyman RJ (2002) Gap junction proteins expressed during development are required for adult neural function in the *Drosophila* optic lamina. J Neurosci 22: 7088-7096.

Demb JB (2007) Cellular mechanisms for direction selectivity in the retina. Neuron 55: 179-186.

Devoe RD, Ockleford EM (1976) Intracellular responses from cells of the medulla of the fly, *Calliphora erythrocephala*. Biological Cybernetics 23: 13-24.

Douglass JK, Strausfeld NJ (1995) Visual motion detection circuits in flies: peripheral motion computation by identified small-field retinotopic neurons. J Neurosci 15: 5596-5611.

Douglass JK, Strausfeld NJ (1996) Visual motion-detection circuits in flies: parallel direction- and non-direction-sensitive pathways between the medulla and lobula plate. J Neurosci 16: 4551-4562.

Duffy CJ, Wurtz RH (1991a) Sensitivity of MST neurons to optic flow stimuli. 2. Mechanisms of response selectivity revealed by small-field stimuli. J Neurophysiol 65: 1346-1359.

Duffy CJ, Wurtz RH (1991b) Sensitivity of MST neurons to optic flow stimuli. 1. A continuum of response selectivity to large-field stimuli. J Neurophysiol 65: 1329-1345.

Duistermars BJ, Chow DM, Condro M, Frye MA (2007) The spatial, temporal and contrast properties of expansion and rotation flight optomotor responses in *Drosophila*. J Exp Biol 210: 3218-3227.

Egelhaaf M (1985) On the Neuronal Basis of Figure-Ground Discrimination by Relative Motion in the Visual-System of the Fly. 2. Figure-Detection Cells, A New Class of Visual Interneurones. Biological Cybernetics 52: 195-209.

Egelhaaf M, Borst A (1992) Are There Separate On and Off Channels in Fly Motion Vision? Vis Neurosci 8: 151-164.

Egelhaaf M, Borst A (1995) Calcium Accumulation in Visual Interneurons of the Fly - Stimulus Dependence and Relationship to Membrane Potential. J Neurophysiol 73: 2540-2552.

## References

---

- Elyada YM, Haag J, Borst A (2009) Different receptive fields in axons and dendrites underlie robust coding in motion-sensitive neurons. *Nature Neuroscience* 12: 327-332.
- Euler T, Masland RH (2000) Light-Evoked Responses of Bipolar Cells in a Mammalian Retina. *J Neurophysiol* 83: 1817-1829.
- Famiglietti J, Kolb H (1975) A bistratified amacrine cell and synaptic circuitry in the inner plexiform layer of the retina. *Brain Research* 84: 293-300.
- Fan RJ, Marin-Burgin A, French KA, Friesen WO (2005) A dye mixture (Neurobiotin and Alexa 488) reveals extensive dye-coupling among neurons in leeches; physiology confirms the connections. *J Comp Physiol A* 191: 1157-1171.
- Farrow K, Borst A, Haag J (2005) Sharing receptive fields with your neighbors: Tuning the vertical system cells to wide field motion. *J Neurosci* 25: 3985-3993.
- Farrow K, Haag J, Borst A (2003) Input organization of multifunctional motion-sensitive neurons in the blowfly. *J Neurosci* 23: 9805-9811.
- Fei H, Chow DM, Chen A, Romero-Calderon R, Ong WS, Ackerson LC, Maidment NT, Simpson JH, Frye MA, Krantz DE (2010) Mutation of the *Drosophila* vesicular GABA transporter disrupts visual figure detection. *J Exp Biol* 213: 1717-1730.
- Fermi G, Reichardt W (1963) Optomotor reactions of *Musca domestica* flies - Dependence of the reaction on wavelength, speed, contrast, and average brightness of moving periodic patterns. *Kybernetik* 2: 15-28.
- Fiala A, Spall T, Diegelmann S, Eisermann B, Sachse S, Devaud JM, Buchner E, Galizia CG (2002) Genetically expressed cameleon in *Drosophila melanogaster* is used to visualize olfactory information in projection neurons. *Current Biology* 12: 1877-1884.
- Fischbach KF, Dittrich APM (1989) The Optic Lobe of *Drosophila melanogaster*. 1. A Golgi Analysis of Wild-Type Structure. *Cell and Tissue Research* 258: 441-475.
- Franceschini N, Riehle A, le Nestour A (1989) Directionally selective motion detection by insect neurons. *Facets of vision: Ch. 17, 360-390* (eds. Stavenga, D.G. & Hardie, R.C.; Springer-Verlag, Berlin).
- Fry SN, Rohrseitz N, Straw AD, Dickinson MH (2009) Visual control of flight speed in *Drosophila melanogaster*. *J Exp Biol* 212: 1120-1130.
- Frye MA, Dickinson MH (2004) Closing the loop between neurobiology and flight behavior in *Drosophila*. *Current Opinion in Neurobiology* 14: 729-736.
- Fuerst PG, Koizumi A, Masland RH, Burgess RW (2008) Neurite arborization and mosaic spacing in the mouse retina require DSCAM. *Nature* 451: 470-474.



- Fuerst PG, Bruce F, Tian M, Wei W, Elstrott J, Feller MB, Erskine L, Singer JH, Burgess RW (2009) DSCAM and DSCAML1 Function in Self-Avoidance in Multiple Cell Types in the Developing Mouse Retina. *Neuron* 64: 484-497.
- Gao S, Takemura SY, Ting CY, Huang S, Lu Z, Luan H., Rister J, Thum AS, Yang M, Hong S-T, Wang JW, Odenwald WF, White BH, Meinertzhagen IA, Lee C-H (2008) The neural substrate of spectral preference in *Drosophila*. *Neuron* 60: 328-342.
- Gengs CX, Leung HT, Skingsley DR, Iovchev MI, Yin Z, Semenov EP, Burg MG, Hardie RC, Pak WL (2002) The target of *Drosophila* photoreceptor synaptic transmission is a histamine-gated chloride channel encoded by *ort* (*hclA*). *Journal of Biological Chemistry* 277: 42113-42120.
- Gilbert C, Penisten DK, Devoe RD (1991) Discrimination of visual motion from flicker by identified neurons in the medulla of the fleshfly *Sarcophaga bullata*. *J Comp Physiol A* 168: 653-673.
- Gonzalez-Bellido PT, Wardill TJ, Kostyleva R, Meinertzhagen IA, Juusola M (2009) Overexpressing Temperature-Sensitive Dynamin Decelerates Phototransduction and Bundles Microtubules in *Drosophila* Photoreceptors. *J Neurosci* 29: 14199-14210.
- Goodman LJ (1960) The Landing Responses of Insects. 1. The Landing Response of the Fly, *Lucilia Sericata*, and Other Calliphoridae. *J Exp Biol* 37: 854-878.
- Götz KG (1964) Optomotorische Untersuchungen des visuellen Systems einiger Augenmutanten der Fruchtfliege *Drosophila*. *Kybernetik* 2: 77-91.
- Götz KG (1968) Flight control in *Drosophila* by visual perception of motion. *Kybernetik* 4: 199-&.
- Götz KG (1972) Principles of optomotor reactions in insects. *Bibl Ophthal* 82: 251-259.
- Götz KG (1987) Course-Control, Metabolism and Wing Interference During Ultralong Tethered Flight in *Drosophila Melanogaster*. *J Exp Biol* 128: 35-46.
- Gouwens NW, Wilson RI (2009) Signal Propagation in *Drosophila* Central Neurons. *J Neurosci* 29: 6239-6249.
- Haag J, Borst A (2000) Spatial distribution and characteristics of voltage-gated calcium signals within visual interneurons. *J Neurophysiol* 83: 1039-1051.
- Haag J, Borst A (2004) Neural mechanism underlying complex receptive field properties of motion-sensitive interneurons. *Nature Neuroscience* 7: 628-634.
- Haag J, Borst A (2005) Dye-coupling visualizes networks of large-field motion-sensitive neurons in the fly. *J Comp Physiol A* 191: 445-454.
- Haag J, Borst A (2008) Electrical Coupling of Lobula Plate Tangential Cells to a Heterolateral Motion-Sensitive Neuron in the Fly. *J Neurosci* 28: 14435-14442.

## References

---

Hardie RC (1989) A histamine-activated chloride channel involved in neurotransmission at a photoreceptor synapse. *Nature* 339: 704-706.

Hardie RC (2001) Phototransduction in *Drosophila melanogaster*. *J Exp Biol* 204: 3403-3409.

Hardie RC, Weckström M (1990) Three classes of potassium channels in large monopolar cells of the blowfly *Calliphora vicina*. *J Comp Physiol A* 167: 723-736.

Hassenstein B, Reichardt W (1956) Systemtheoretische Analyse der Zeit-, Reihenfolgen- und Vorzeichenbewertung bei der Bewegungspertzeption des Rüsselkäfers *Chlorophanus*. *Z Naturforsch* 11b: 513-524.

Hattori D, Chen Y, Matthews BJ, Salwinski L, Sabatti C, Grueber WB, Zipursky SL (2009) Robust discrimination between self and non-self neurites requires thousands of *Dscam1* isoforms. *Nature* 461: 644-U87.

Hattori D, Demir E, Kim HW, Viragh E, Zipursky SL, Dickson BJ (2007) *Dscam* diversity is essential for neuronal wiring and self-recognition. *Nature* 449: 223-227.

Hattori D, Millard SS, Wojtowicz WM, Zipursky SL (2008) *Dscam*-Mediated Cell Recognition Regulates Neural Circuit Formation. *Annual Review of Cell and Developmental Biology* 24: 597-620.

Hausen K (1976) Functional characterization and anatomical identification of motion sensitive neurons in the lobula plate of the blowfly *Calliphora erythrocephala*. *Zeitschrift für Naturforschung C* 31: 629-633.

Hausen K (1982) Motion Sensitive Interneurons in the Optomotor System of the Fly. 1. the Horizontal Cells - Structure and Signals. *Biological Cybernetics* 45: 143-156.

Hausen K (1984) Photoreception and vision in invertebrates. The lobula-complex of the fly: structure, function and significance in visual behaviour. NATO ASI (Advanced Science Institutes) Series Series A Life Sciences 74.

Hayashi S, Ito K, Sado Y, Taniguchi M, Akimoto A, Takeuchi H, Aigaki T, Matsuzaki F, Nakagoshi H, Tanimura T, Ueda R, Uemura T, Yoshihara M, Goto S (2002) GETDB, a database compiling expression patterns and molecular locations of a collection of *Gal4* enhancer traps. *Genesis* 34: 58-61.

Heim N, Garaschuk O, Friedrich MW, Mank M, Milos RI, Kovalchuk Y, Konnerth A, Griesbeck O (2007) Improved calcium imaging in transgenic mice expressing a troponin C-based biosensor. *Nature Methods* 4: 127-129.

Heisenberg M, Buchner E (1977) Role of Retinula Cell-Types in Visual Behavior of *Drosophila-Melanogaster*. *Journal of Comparative Physiology* 117: 127-162.

Heisenberg M, Wolf R (1984) *Vision in Drosophila*. Springer Press, New York.

- Heisenberg M, Wonneberger R, Wolf R (1978) Optomotor-blind<sup>H31</sup> – a *Drosophila* mutant of lobula plate giant neurons. *Journal of Comparative Physiology* 124: 287-296.
- Hengstenberg R, Hausen K, Hengstenberg B (1982) The number and structure of giant vertical cells (VS) in the lobula plate of the blowfly *Calliphora erythrocephala*. *Journal of Comparative Physiology* 149: 163-177.
- Hughes ME, Bortnick R, Tsubouchi A, Baumer P, Kondo M, Uemura T, Schmucker D (2007) Homophilic Dscam interactions control complex dendrite morphogenesis. *Neuron* 54: 417-427.
- Järvilehto M, Zettler F (1973) Electrophysiological-histological studies on some functional properties of visual cells and second-order neurons of an insect retina. *Z Zellforsch* 136: 291-306.
- Joesch M, Plett J, Borst A, Reiff DF (2008) Response properties of motion-sensitive visual interneurons in the lobula plate of *Drosophila melanogaster*. *Current Biology* 18: 368-374.
- Johns DC, Marx R, Mains RE, O'Rourke B, Marban E (1999) Inducible genetic suppression of neuronal excitability. *J Neurosci* 19: 1691-1697.
- Katsov AY, Clandinin TR (2008) Motion processing streams in *Drosophila* are behaviorally specialized. *Neuron* 59: 322-335.
- Kirschfeld K (1967) Die Projektion der optischen Umwelt auf das Raster der Rhabdomere im Komplexauge von MUSCA. *Exp Brain Res* 3: 248-270.
- Kirschfeld K (1972) The visual system of Musca: studies on optics, structure and function. In: *Information Processing in the Visual Systems of Arthropods* (Wehner R, ed), pp 61-74. Berlin, Heidelberg, New York: Springer.
- Kirschfeld K (1973) Das neuronale Superpositionsauge. *Fortschritte der Zoologie* 21: 228-257.
- Kitamoto T (2001) Conditional modification of behavior in *Drosophila* by targeted expression of a temperature-sensitive *shibire* allele in defined neurons. *J Neurobiol* 47: 81-92.
- Krapp HG, Hengstenberg R (1996) Estimation of self-motion by optic flow processing in single visual interneurons. *Nature* 384: 463-466.
- Kunes S, Steller H (1991) Ablation of *Drosophila* Photoreceptor Cells by Conditional Expression of A Toxin Gene. *Genes & Development* 5: 970-983.
- Laughlin S (1989) Coding efficiency and design in visual processing. *Facets of vision: 213-234*, Springer Verlag, Berlin.

## References

---

Laughlin SB, Osorio D (1989) Mechanisms for Neural Signal Enhancement in the Blowfly Compound Eye. *J Exp Biol* 144: 113-146.

Lee T, Luo LQ (1999) Mosaic analysis with a repressible cell marker for studies of gene function in neuronal morphogenesis. *Neuron* 22: 451-461.

Longden KD, Krapp HG (2009) State-Dependent Performance of Optic-Flow Processing Interneurons. *J Neurophysiol* 102: 3606-3618.

Luan HJ, Peabody NC, Vinson CR, White BH (2006) Refined spatial manipulation of neuronal function by combinatorial restriction of transgene expression. *Neuron* 52: 425-436.

Luo L, Callaway EM, Svoboda K (2008) Genetic Dissection of Neural Circuits. *Neuron* 57: 634-660.

Maimon G, Straw AD, Dickinson MH (2010) Active flight increases the gain of visual motion processing in *Drosophila*. *Nature Neuroscience* 13: 393-399.

Mank M, Griesbeck O (2008) Genetically encoded calcium indicators. *Chemical Reviews* 108: 1550-1564.

Mank M, Santos AF, Drenth S, Mrcic-Flogel TD, Hofer SB, Stein V, Hendel T, Reiff DF, Levelt C, Borst A, Bonhoeffer T, Hubener M, Griesbeck O (2008) A genetically encoded calcium indicator for chronic in vivo two-photon imaging. *Nature Methods* 5: 805-811.

Matthews BJ, Kim ME, Flanagan JJ, Hattori D, Clemens JC, Zipursky Sá, Grueber WB (2007) Dendrite Self-Avoidance Is Controlled by Dscam. *Cell* 129: 593-604.

McGuire SE, Le PT, Osborn AJ, Matsumoto K, Davis RL (2003) Spatiotemporal rescue of memory dysfunction in *Drosophila*. *Science* 302: 1765-1768.

Meijers R, Puettmann-Holgado R, Skiniotis G, Liu JH, Walz T, Wang JH, Schmucker D (2007) Structural basis of Dscam isoform specificity. *Nature* 449: 487-491.

Meinertzhagen IA, O'Neil SD (1991) Synaptic organization of columnar elements in the lamina of the wild type in *Drosophila melanogaster*. *J Comp Neurol* 305: 232-263.

Meinertzhagen IA, Sorra KE (2001) Synaptic organization in the fly's optic lamina: few cells, many synapses and divergent microcircuits. *Prog Brain Res* 131.

Millard SS, Flanagan JJ, Pappu KS, Wu W, Zipursky SL (2007) Dscam2 mediates axonal tiling in the *Drosophila* visual system. *Nature* 447: 720-724.

Millard SS, Zipursky SL (2008) Dscam-mediated repulsion controls tiling and self-avoidance. *Current Opinion in Neurobiology* 18: 84-89.

- Miyawaki A, Llopis J, Heim R, McCaffery JM, Adams JA, Ikura M, Tsien RY (1997) Fluorescent indicators for Ca<sup>2+</sup> based on green fluorescent proteins and calmodulin. *Nature* 388: 882-887.
- Moffat KG, Gould JH, Smith HK, Okane CJ (1992) Inducible Cell Ablation in *Drosophila* by Cold-Sensitive Ricin-A Chain. *Dev* 114: 681-687.
- Münch TA, da Silveira RA, Siegert S, Viney TJ, Awatramani GB, Roska B (2009) Approach sensitivity in the retina processed by a multifunctional neural circuit. *Nature Neuroscience* 12: 1308-1316.
- Nakai J, Ohkura M, Imoto K (2001) A high signal-to-noise Ca<sup>2+</sup> probe composed of a single green fluorescent protein. *Nat Biotech* 19: 137-141.
- Neves G, Zucker J, Daly M, Chess A (2004) Stochastic yet biased expression of multiple Dscam splice variants by individual cells. *Nat Genet* 36: 240-246.
- Nikolaev A, Zheng L, Wardill TJ, O'Kane CJ, de Polavieja GG, Juusola M (2009) Network Adaptation Improves Temporal Representation of Naturalistic Stimuli in *Drosophila* Eye: II Mechanisms. *Plos One* 4 (1): e4306.
- O'Tousa JE, Baehr W, Martin RL, Hirsh J, Pak WL, Applebury ML (1985) The *Drosophila ninaE* gene encodes an opsin. *Cell* 40: 839-850.
- Olsen SR, Bhandawat V, Wilson RI (2007) Excitatory interactions between olfactory processing channels in the *Drosophila* antennal lobe. *Neuron* 54: 89-103.
- Olsen SR, Bhandawat V, Wilson RI (2010) Divisive Normalization in Olfactory Population Codes. *Neuron* 66: 287-299.
- Pantazis A, Segaran A, Liu CH, Nikolaev A, Rister J, Thum AS, Roeder T, Semenov E, Juusola M, Hardie RC (2008) Distinct roles for two histamine receptors (hclA and hclB) at the *Drosophila* photoreceptor synapse. *J Neurosci* 28: 7250-7259.
- Pfeiffer BD, Jenett A, Hammonds AS, Ngo TTB, Misra S, Murphy C, Scully A, Carlson JW, Wan KH, Laverty TR, Mungall C, Svirskas R, Kadonaga JT, Doe CQ, Eisen MB, Celniker SE, Rubin GM (2008) Tools for neuroanatomy and neurogenetics in *Drosophila*. *Proc Natl Acad Sci USA* 105: 9715-9720.
- Phelan P, Goulding LA, Tam JLY, Allen MJ, Dawber RJ, Davies JA, Bacon JP (2008) Molecular Mechanism of Rectification at Identified Electrical Synapses in the *Drosophila* Giant Fiber System. *Current Biology* 18: 1955-1960.
- Phelan P, Nakagawa M, Wilkin MB, Moffat KG, Okane CJ, Davies JA, Bacon JP (1996) Mutations in shaking-B prevent electrical synapse formation in the *Drosophila* giant fiber system. *J Neurosci* 16: 1101-1113.
- Raghu SV, Joesch M, Borst A, Reiff DF (2007) Synaptic organization of lobula plate tangential cells in *Drosophila*: gamma-aminobutyric acid receptors and chemical release sites. *Journal of Comparative Neurology* 502: 598-610.

## References

---

- Raghu SV, Joesch M, Sigrist SJ, Borst A, Reiff DF (2009) Synaptic Organization of Lobula Plate Tangential Cells in *Drosophila*: D7 Cholinergic Receptors. *Journal of Neurogenetics* 23: 200-209.
- Raghu SV, Reiff DF, Borst A (2010) Neurons with cholinergic phenotype in the visual system of *Drosophila*. *J Comp Neurol*, in press.
- Reichardt W (1961) Autocorrelation, a principle for the evaluation of sensory information by the central nervous system. In: *Sensory Communication* (Rosenblith WA, ed), pp 303-317. New York, London: The M.I.T. Press and John Wiley & Sons.
- Reichardt W, Wenking H (1969) Optical Detection and Fixation of Objects by Fixed Flying Flies. *Naturwissenschaften* 56: 424.
- Reiff DF, Ihring A, Guerrero G, Isacoff EY, Joesch M, Nakai J, Borst A (2005) In vivo performance of genetically encoded indicators of neural activity in flies. *J Neurosci* 25: 4766-4778.
- Reiff DF, Plett J, Mank M, Griesbeck O, Borst A (2010) Visualizing retinotopic half-wave rectified input to the motion detection circuitry of *Drosophila*. *Nat Neurosci* 13: 973-978.
- Riehle A, Franceschini N (1984) Motion detection in flies: parametric control over ON-OFF pathways. *Exp Brain Res* 54: 390-394.
- Rister J, Heisenberg M (2006) Distinct functions of neuronal synaptobrevin in developing and mature fly photoreceptors. *J Neurobiol* 66: 1271-1284.
- Rister J, Pauls D, Schnell B, Ting CY, Lee CH, Sinakevitch I, Morante J, Strausfeld NJ, Ito K, Heisenberg M (2007) Dissection of the peripheral motion channel in the visual system of *Drosophila melanogaster*. *Neuron* 56: 155-170.
- Rubin GM, Spradling AC (1982) Genetic-Transformation of *Drosophila* with Transposable Element Vectors. *Science* 218: 348-353.
- Schmucker D (2007) Molecular diversity of Dscam: recognition of molecular identity in neuronal wiring. *Nat Rev Neurosci* 8: 915-920.
- Schmucker D, Clemens JC, Shu H, Worby CA, Xiao J, Muda M, Dixon JE, Zipursky SL (2000) *Drosophila* Dscam Is an Axon Guidance Receptor Exhibiting Extraordinary Molecular Diversity. *Cell* 101: 671-684.
- Schümperli RA (1973) Evidence for colour vision in *Drosophila melanogaster* through spontaneous phototactic choice behaviour. *J Comp Physiol A* 86: 77-94.
- Scott EK, Raabe T, Luo LQ (2002) Structure of the vertical and horizontal system neurons of the lobula plate in *Drosophila*. *Journal of Comparative Neurology* 454: 470-481.

- Seelig JD, Chiappe ME, Lott GK, Dutta A, Osborne JE, Reiser MB, Jayaraman V (2010) Two-photon calcium imaging from head-fixed *Drosophila* during optomotor walking behavior. *Nature Methods* 7: 535-540.
- Shang YH, Claridge-Chang A, Sjulson L, Pypaert M, Miesenbock G (2007) Excitatory local circuits and their implications for olfactory processing in the fly antennal lobe. *Cell* 128: 601-612.
- Shaw SR (1984) Early Visual Processing in Insects. *J Exp Biol* 112: 225-251.
- Shimohigashi M, Meinertzhagen IA (1998) The *shaking B* gene in *Drosophila* regulates the number of gap junctions between photoreceptor terminals in the lamina. *J Neurobiol* 35: 105-117.
- Soba P, Zhu S, Emoto K, Younger S, Yang SJ, Yu HH, Lee T, Jan LY, Jan YN (2007) *Drosophila* sensory neurons require Dscam for dendritic self-avoidance and proper dendritic field organization. *Neuron* 54: 403-416.
- Strausfeld NJ (1976) Atlas of an Insect Brain. Springer Verlag, Berlin, Heidelberg.
- Strausfeld NJ, Lee JK (1991) Neuronal Basis for Parallel Visual Processing in the Fly. *Visual Neuroscience* 7: 13-33.
- Strauss R, Renner M, Gotz K (2001) Task-specific association of photoreceptor systems and steering parameters in *Drosophila*. *J Comp Physiol A* 187: 617-632.
- Straw AD, Rainsford T, O'Carroll DC (2008) Contrast sensitivity of insect motion detectors to natural images. *Journal of Vision* 8: 32, 1-9.
- Sweeney ST, Broadie K, Keane J, Niemann H, Okane CJ (1995) Targeted Expression of Tetanus Toxin Light-Chain in *Drosophila* Specifically Eliminates Synaptic Transmission and Causes Behavioral Defects. *Neuron* 14: 341-351.
- Szobota S, Isacoff EY (2010) Optical Control of Neuronal Activity. *Annual Reviews of Biophysics* 39: 329-348.
- Takemura SY, Lu Z, Meinertzhagen IA (2008) Synaptic circuits of the *Drosophila* optic lobe: the input terminals to the medulla. *J Comp Neurol* 509: 493-513.
- Tanaka K, Hikosaka K, Saito H, Yukie M, Fukada Y, Iwai E (1986) Analysis of Local and Wide-Field Movements in the Superior Temporal Visual Areas of the Macaque Monkey. *J Neurosci* 6: 134-144.
- Thomas JB, Wyman RJ (1984) Mutations altering synaptic connectivity between identified neurons in *Drosophila*. *J Neurosci* 4: 530-538.
- Thum AS, Knapek S, Rister J, Dierichs-Schmitt E, Heisenberg M, Tanimoto H (2006) Differential potencies of effector genes in adult *Drosophila*. *J Comp Neurol* 498: 194-203.

## References

---

Tian L, Hires SA, Mao T, Huber D, Chiappe ME, Chalasani SH, Petreanu L, Akerboom J, McKinney SA, Schreiter ER, Bargmann CI, Jayaraman V, Svoboda K, Looger LL (2009) Imaging neural activity in worms, flies and mice with improved GCaMP calcium indicators. *Nature Methods* 6: 875-881.

Wang J, Zugates CT, Liang IH, Lee CHJ, Lee TM (2002) *Drosophila* Dscam is required for divergent segregation of sister branches and suppresses ectopic bifurcation of axons. *Neuron* 33: 559-571.

Wang JW, Wong AM, Flores J, Vosshall LB, Axel R (2003) Two-photon calcium imaging reveals an odor-evoked map of activity in the fly brain. *Cell* 112: 271-282.

Wang YL, Guo HF, Pologruto TA, Hannan F, Hakker I, Svoboda K, Zhong Y (2004) Stereotyped odor-evoked activity in the mushroom body of *Drosophila* revealed by green fluorescent protein-based Ca<sup>2+</sup> imaging. *J Neurosci* 24: 6507-6514.

Warzecha AK, Egelhaaf M, Borst A (1993) Neural Circuit Tuning Fly Visual Interneurons to Motion of Small Objects. 1. Dissection of the Circuit by Pharmacological and Photoinactivation Techniques. *J Neurophysiol* 69: 329-339.

Wässle H (2004) Parallel processing in the mammalian retina. *Nature Reviews Neuroscience* 5: 747-757.

Wehner R (1972) Spontaneous pattern preferences of *Drosophila melanogaster* to black areas in various parts of the visual field. *Journal of Insect Physiology* 18: 1531-1543.

Wertz A, Gaub B, Plett J, Haag J, Borst A (2009) Robust Coding of Ego-Motion in Descending Neurons of the Fly. *J Neurosci* 29: 14993-15000.

Wilson RI, Laurent G (2005) Role of GABAergic inhibition in shaping odor-evoked spatiotemporal patterns in the *Drosophila* antennal lobe. *J Neurosci* 25: 9069-9079.

Wilson RI, Turner GC, Laurent G (2004) Transformation of olfactory representations in the *Drosophila* antennal lobe. *Science* 303: 366-370.

Witte I, Kreienkamp HJ, Gewecke M, Roeder T (2002) Putative histamine-gated chloride channel subunits of the insect visual system and thoracic ganglion. *Journal of Neurochemistry* 83: 504-514.

Wojtowicz WM, Flanagan JJ, Millard SS, Zipursky SL (2004) Alternative splicing of *Drosophila* Dscam generates axon guidance receptors that exhibit isoform-specific homophilic binding. *Cell* 118: 619-633.

Wojtowicz WM, Wu W, Andre I, Qian B, Baker D, Zipursky SL (2007) A vast repertoire of Dscam binding specificities arises from modular interactions of variable Ig domains. *Cell* 130: 1134-1145.



Yamaguchi S, Desplan C, Heisenberg M (2010) Contribution of photoreceptor subtypes to spectral wavelength preference in *Drosophila*. *Proc Natl Acad Sci USA* 107: 5634-5639.

Yamaguchi S, Wolf R, Desplan C, Heisenberg M (2008) Motion vision is independent of color in *Drosophila*. *Proc Natl Acad Sci USA* 105: 4910-4915.

Yasuyama K, Meinertzhagen IA (1999) Extraretinal photoreceptors at the compound eye's posterior margin in *Drosophila melanogaster*. *Journal of Comparative Neurology* 412: 193-202.

Zheng L, Polavieja GG, Wolfram V, Asyali MH, Hardie RC, Juusola M (2006) Feedback network controls photoreceptor output at the layer of first visual synapses in *Drosophila*. *Journal of General Physiology* 127: 495-510.

Zheng YC, Hirschberg B, Yuan J, Wang AP, Hunt DC, Ludmerer SW, Schmatz DM, Cully DF (2002) Identification of two novel *Drosophila melanogaster* histamine-gated chloride channel subunits expressed in the eye. *Journal of Biological Chemistry* 277: 2000-2005.

Zhu Y, Nern A, Zipursky SL, Frye MA (2009) Peripheral Visual Circuits Functionally Segregate Motion and Phototaxis Behaviors in the Fly. *Current Biology* 19: 613-619.

## IX. Abbreviations

ACh	acetylcholine
CFP	cyan fluorescent protein
CH	centrifugal horizontal
Dscam	Down syndrome cell adhesion molecule
FD	figure detection
GABA	$\gamma$ -Aminobutyric acid
GECI	genetically encoded Calcium indicator
GFP	green fluorescent protein
HSE	horizontal system equatorial
HSN	horizontal system northern
HSS	horizontal system southern
Kir	Potassium inward rectifier
LMC	lamina monopolar cell
LPTC	lobula plate tangential cell
MARCM	mosaic analysis with a repressible cell marker
MST	medial superior temporal
MT	middle temporal
<i>omb</i>	optomotor blind
VS	vertical system
YFP	yellow fluorescent protein

## X. Curriculum Vitae

### Personal information

---

Name Bettina Schnell  
Date of birth 3<sup>rd</sup> May 1982  
Nationality German

### Education

---

since 09/2006 **PhD Thesis**  
Max-Planck-Institute of Neurobiology, Munich, Germany  
Department of Systems and Computational Neurobiology  
Supervisors: Prof. Dr. Alexander Borst and Dr. Dierk Reiff

06/2006-08/2006 **Research assistant**  
University of Würzburg, Germany  
Department of Genetics and Neurobiology

07/2005-05/2006 **Diploma thesis**  
University of Würzburg, Germany  
Department of Genetics and Neurobiology  
Title: Genetic Intervention in the Periphery of the Visual System of *Drosophila melanogaster*  
Supervisor: Prof. Dr. Martin Heisenberg

10/2001-05/2006: **Studies in Biology**  
University of Würzburg, Germany  
Degree: Diplom

1992-2001 **High School**  
Wirsberg-Gymnasium, Würzburg, Germany  
Degree: Abitur

### Teaching experience

---

2007-2009 Teaching assistant in the practical course of animal physiology at the LMU, Munich

2006 Teaching assistant in the practical course of neurobiology at the University of Würzburg, Germany

## Conferences

---

### **Visual Processing in Insects: From Anatomy to Behavior II**

Conference

Janelia Farm Research Campus, Ashburn, Virginia, USA, May 2009

Poster presentation

### **12th Göttingen Meeting of the German Neuroscience Society**

Göttingen, Germany, March 2009

Poster presentation

### **12th European Drosophila Neurobiology Conference**

Würzburg, Germany, September 2008

Poster presentation

### **11th Göttingen Meeting of the German Neuroscience Society**

Göttingen, Germany, April 2007

## Publications

---

Joesch, M., **Schnell, B.**, Raghu, S.V., Reiff, D.F., and Borst A. ON and OFF Pathways in Drosophila Motion Vision, Nature, accepted for publication.

**Schnell, B.**, Joesch, M., Foerstner, F., Raghu, S.V., Otsuna, H., Ito, K., Borst, A., Reiff, D.F. Processing of horizontal optic flow in three visual interneurons of the *Drosophila* brain. J. Neurophysiol. 103, 1646-1657 (2010).

Hendel, T., Mank, M., **Schnell, B.**, Griesbeck, O., Borst, A., and Reiff, D.F. Fluorescence changes of genetic calcium indicators and OGB-1 correlated with neural activity and calcium in vivo and in vitro. J. Neurosci. 28, 7399-7411 (2008).

Rister, J., Pauls, D., **Schnell, B.**, Ting, C. Y., Lee, C. H., Sinakevitch, I., Morante, J., Strausfeld, N. J., Ito, K. & Heisenberg, M. Dissection of the peripheral motion channel in the visual system of *Drosophila melanogaster*. Neuron 56, 155-170 (2007).

## **XI. Acknowledgments**

First and foremost I want to thank my “Doktorvater” Axel Borst for continuous support, trust and stimulating discussions during my PhD and also for letting me go to New York, which I highly appreciate.

I want to thank my direct supervisor Dierk Reiff for a lot of support, advice and technical help that made this work successful and for all the things I learned from him.

I am also much indebted to my colleague Max Jösch, who taught me patch-clamp recordings and who always helped with whatever problems I had.

I want to thank all other co-workers on the various projects, Thomas Hendel, Sham V. Raghu, Jing Shi, Friedrich Förstner and Väinö Haikala for a fruitful collaboration. Thanks to Johannes Plett for building the LED arena and always helping with technical problems.

Thanks to our technicians Wolfgang Essbauer and Christian Theile for taking care of flies and all the other work they did. Thanks also to the MPI workshop and all the other staff for making working at the MPI easy.

I want to further thank my former supervisor Jens Rister, now at the NYU, for providing flies and continuous advice and support. Thanks to Chi-Hon Lee from the NIH for always readily providing flies and reagents. Thanks to Prof. Erich Buchner for being a member of my Thesis Committee and for bringing me in contact with the visual system of the fly.

I want to thank the whole Borst department and the whole Griesbeck group for a great working atmosphere, for all the activities outside the institute and for all the discussions about scientific and non-scientific questions.

Finally I want to thank my parents for raising my interest in nature and for supporting me in whatever I am doing.